UNIVERSITY OF PARMA

Department of Chemistry, Life Sciences and Environmental Sustainability

Ph.D. in Biotechnologies

XXIX COURSE

Functional characterization of yeast mutants carrying disease-causing mutations in panthotenate kinase and CoA synthase encoding genes and identification of chemical suppressors

Coordinator of the Ph.D. Program:
Prof. Simone Ottonello

Scientific Tutor:
Prof.ssa Paola Goffrini

Ph.D. Student : **Camilla Ceccatelli Berti**

2014/2017

SSD: [BIO/18]

Thesis performed at Laboratory of Molecular Genetics and Biotechnology, Department of Chemistry, Life Sciences and Environmental Sustainability, University of Parma, Italy

To my family

To Tommaso and Milla

"The Warrior knows that he is free to choose his desires, and he makes these decisions with courage, detachment and sometimes, with just a touch of madness"

-Paulo Coehlo-

"You do not do your duty because someone will thank you for it... you do it as a matter of principle, for yourself, for your own dignity."

-Oriana Fallaci-

Index

Introduction

Aim of the research **27**

Results

Section 1. Yeast model of PKAN disease

Introduction

1.1 Coenzyme A: structure, function and biosynthesis

Coenzyme A (CoA), identified more than 70 years ago (Baddiley et al., 1953), is an essential cofactor in all living organisms where it functions as an acyl group carrier and as a carbonyl-activating group. About 9% of known enzymes utilize CoA as an obligate cofactor (Strauss et al., 2010) and it is involved in over 100 different reactions in intermediary metabolism. More specifically CoA is a key molecule in the metabolism of fatty acids, carbohydrates, amino acids and ketone bodies. It consists of 3'-phosphoadenosine linked through the 5' position of the ribose, to pantothenic acid via pyrophosphate linkage. The carboxyl end of pantothenic acid is linked through a peptidic bond to 2-mercaptoethanol amine (Fig 1.1).

Thanks to its sulfhydryl group (-SH), it acts as a carrier of acyl groups through the formation of thioesters (Nelson et al., 2010).

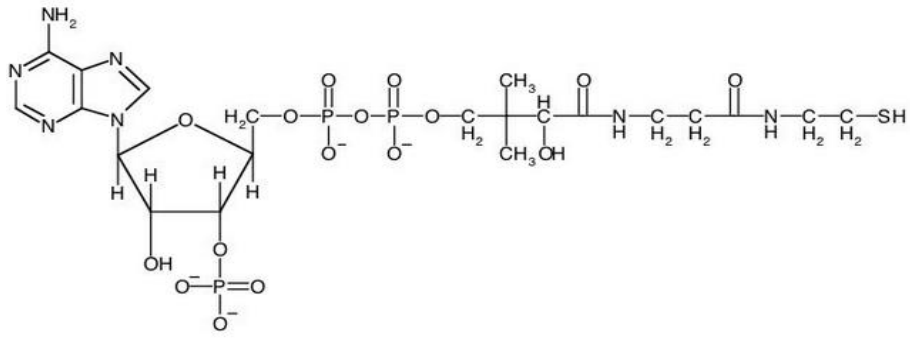

Figure 1.1 Structure of CoA

The biosynthesis *de novo* of CoA from pantothenic acid is an essential and universal pathway in prokaryotes and eukaryotes and proceeds through five enzymatic steps starting from pantothenate or Vitamin B5 (Fig 1.2). In the first step, pantothenate is phosphorylated to 4'-phosphopantothenate by pantothenate kinase ATP dependent (PANK); this reaction is the primary rate-limiting step in CoA biosynthesis and it is controlled by the end-products of the pathway, CoA and CoA thioesters. Condensation of 4'-phosphopantothenate with cysteine catalyzed by 4'-phospho-pantothenoylcysteine synthase (PPCS), is followed by a decarboxylation reaction to yield 4'-phosphopantetheine with 4'-phosphopantothenoylcysteine decarboxylase (PPCDC) acting as the catalytic enzyme. Next, the AMP moiety of ATP is added to form dephospho-CoA by 4'-phosphopantetheine adenylyltransferaase (PPAT), which is subsequently phosphorylated on the 3'-hydroxyl to form CoA thanks to the dephospho-CoA kinase (DPCK) enzyme.

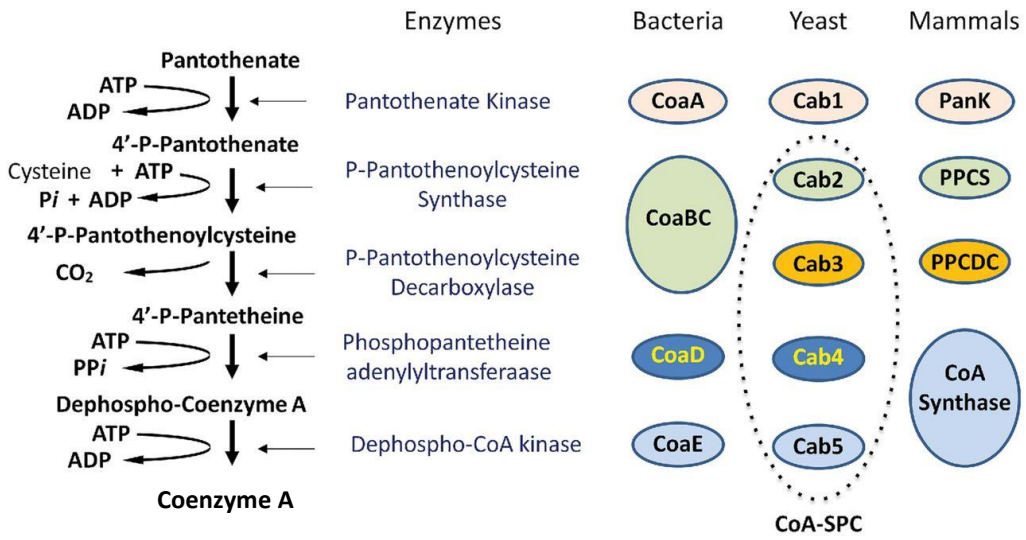

Fig 1.2 Biosynthesis of CoA. On the right are the enzymes that are involved in this pathway in different organisms. From Martinez et al., 2014

In *Escherichia coli*, pantothenate could be formed *de novo* or taken up from outside the cell. The uptake is mediated by pantothenate permease, also termed PanF protein, encoded by the *panF* gene (Leonardi et al., 2005). In the majority of bacteria the biosynthesis of CoA is catalyzed by five enzymes: CoaA, CoaB, CoaC, CoaD and CoaE (Song et al., 1992; Geerlof et al., 1999; Mishra et al., 2001; Kupke et al., 2002); the two reactions generally catalyzed by PPCS and PPCDC are carried out by one bifunctional enzyme CoaBC (Strauss et al., 2001) (Fig 1.2). In mammals the genes encoding enzymes involved in the biosynthesis of CoA are *PANK* (pantothenate kinase), *PPCS* (phosphopantothenoylcysteine synthase), *PPCDC* (phosphopantotenoylcysteine decarboxylase) and *COASY* (CoA synthase) that encodes a bifunctional enzyme that has both PPAT and DPCK activity. In humans there are three splice variants of COASY: COASY alpha expressed ubiquitously, COASY beta expressed predominantly in the brain and COASY gamma predicted to encode for the C-terminal region of CoA synthase corresponding to the DPCK domain. CoA synthase alpha and beta are anchored to the outer mitochondrial membrane by the N-terminal region (Zhyvoloup et al., 2003) or localized to the mitochondrial matrix (Dusi et al., 2014).

Furthermore, different isoforms have been identified for the enzyme PANK: PANK1, PANK2, PANK3 and PANK4. The first three share the same function in mammalians' cells and tissues but show important differences in terms of sub-cellular compartmentalization, regulation and expression. More specifically, PANK2 is ubiquitous but widely expressed in the brain (Zhou et al., 2001), localized in the mitochondrial inner membrane space (Hörtnagel et al., 2003; Johnson et al., 2004; Kotzbauer et al., 2005) and possibly in the nucleus (Alfonso-Pecchio et al., 2012), whereas PANK1 and PANK3 are predominantly found in the cytosol (Alfonso-Pecchio et al., 2012). PANK4 is

probably not active as pantothenate kinase in fact it lacks an essential catalytic residue for enzyme activity (Hortnagel et al., 2003).

In the yeast *Saccharomyces cerevisiae,* like *E. coli*, pantothenate could be synthesized *de novo* or taken up from outside thanks to Fen2p transporter (Stolz et al., 1999). The enzymes involved in this pathway are encoded by the five essential genes: *CAB1*, *CAB2*, *CAB3*, *CAB4* (PPAT activity) and *CAB5* (DPCK activity) (Fig 1.2). The sub-cellular compartmentalization of this pathway is still under investigation. A protein complex CoA-SPC (400 kDa) formed by the four proteins Cab2, Cab3, Cab4 and Cab5 has been identified. However the complex formation is not essential for the activity of the single enzymes since the substitution of yeast proteins with homologues bacterial proteins that do not possess the ability to form a complex do not compromise the biosynthesis of CoA (Olzhausen et al., 2013).

1.2 NBIA (Neurodegeneration with brain iron accumulation)

Neurodegeneration with brain iron accumulation (NBIA) are a group of progressive neurological disorders characterized by excess iron accumulation in the globus pallidus and to a lesser degree in the substantia nigra (Gregory et al., 2005; Gregory et al., 2009). Iron accumulates in the brain gives rise to a progressive dystonia, spasticity, parkinsonism, neuropsychiatric abnormalities and retinal degeneration. NBIA diseases are inherited in an autosomal recessive or dominant mode, are X-linked and generally begin in childhood or adolescence. The frequency of NBIA in the general population is estimated to be between one to three people per one million individuals (Aoun et al., 2015). To date, ten genes causative genes underlying NBIA have been identified: *PANK2*, *PLA2G6*, *FA2H, ATP13A2*, *C19orf12*, *FTL*, *CP*, *C2orf37/DCAF17*, *WDR45* (Rouault 2013) and *COASY* (Dusi et al., 2014). Nonetheless, in a many patients, 20 % of cases no genetic alteration has been found (Colombelli et al., 2014; Arber et al., 2016). Among the known disease genes, only two encode proteins directly involved in iron metabolism: ceruloplasmin (*CP*) and ferritin light chain (*FTL*) (Rouault 2013). The other eight genes code for proteins with different functions. For example, *WDR45* and *ATP13A2* genes are implicated in autophagosome and lysosomal activity respectively, while the *C2orf37* gene encodes a nucleolar protein of unknown function. Pantothenate kinase 2 (*PANK2)* and CoA synthase (*COASY*) are implicated in biosynthesis of CoA while phospholipase A2 group VI (*PLA2G6*), fatty acid-2-hydroxylase (*FA2H*), and *C19orf12* genes seem to be involved in lipid metabolism, membrane integrity and mitochondrial function. *PLA2G6, PANK2, COASY* and *C19orf12* encode proteins localized in mitochondria. Since many of these genes

encode for proteins involved in lipid metabolism, it has been recently proposed that the iron accumulation is not likely the primary cause of neurodegeneration in NBIA but rather defects in lipid metabolism and mitochondrial function underline shared pathological mechanisms in these diseases (Aoun et al., 2015).

1.2.1 Pantothenate kinase-associated neurodegeneration (PKAN)

Mutations in pantothenate kinase encoding gene (*PANK2*), mapped to chromosome 20p13 (OMIM 234200), lead to pantothenate kinase-associated neurodegeneration (PKAN) and account approximately for 50% of all NBIA cases (Leoni et al., 2012).

The majority of PKAN patients suffer from a combination of dystonia, parkinsonism, dysarthria, spasticity, mental retardation and pigmentary retinopathy (Hayflick et al., 2006). There are two distinct manifestations of this disease: classical and atypical. Classic PKAN patients develop the disease in the first ten years of life, starting at an average age of three and a half and die before the age of twenty. The onset of the atypical form of PKAN occurs after the age of ten and within the first three decades of life. The disease progresses more slowly than classic PKAN with a predominant neuropsychiatric syndrome characterized by obsessive–compulsive disorder, schizophrenia-like psychosis and depression (Kruer et al., 2011). The main diagnostic criterion is the observation of the typical magnetic resonance imaging (MRI) pattern known as “eye of tiger” (Fig 1.3) (Hayflick, 2006; Kruer et al., 2011).

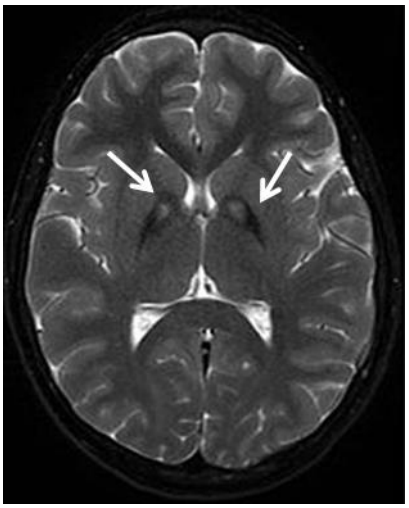

Fig 1.3 MRI of PKAN patient. Classical ‘eye of the tiger’ sign. From Hayflick et al,, 2006

So far more than 80 mutations have been identified that spread throughout the whole *PANK2* gene. About 50 are missense mutations, while the remaining are frameshift and nonsense mutations, stop codons, splicing errors or deletions/insertions. Insertions, deletions and frameshift mutations are clinically linked to early onset disease indicating that null mutants of Pank2 lead to rapidly progressive PKAN. In contrast, the missense mutations have mixed early and late onset patterns (Zhou et al., 2001; Hayflick et al., 2003).

Subramanian and collaborators in 2016, demonstrated that all pantothenate kinases operate by a compulsory ordered mechanism with ATP as the leading substrate followed by pantothenate (Fig 1.4). The principal mechanism for controlling mammalian pantothenate kinase activity is through feedback inhibition by acetyl-CoA. More specifically they observed that PANK3 exists as a dimer in two distinct conformations. The inactive conformation has an "open" carboxyl-terminal nucleotide binding domain that is stabilized by the binding of the acetyl-CoA (red). The active conformation has a "closed" nucleotide-binding domain that is stabilized by the binding of ATP (green). The binding of acetyl-CoA and ATP to PANK3 is competitive. Pantothenate binds to the PANK3•ATP•Mg^{2+} complex and, following catalysis, 4-phosphopantothenate is released, followed by ADP. 4-Phosphopantothenate is rapidly converted to CoA.

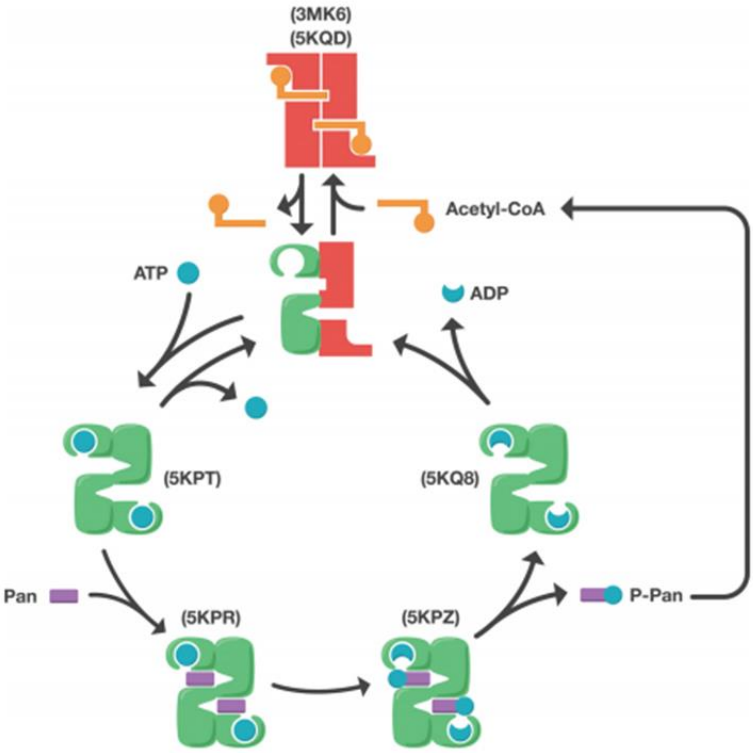

1.4 Catalytic cycle and acyl-CoA inhibition of PANK3. From Subramanian et al., 2016

The same mechanism has been proposed for PANK2 the structure of which is not yet available. Moreover the high degree of similarity between human Pank3 and Pank2 protein (highly homologous catalytic core e.g. the identity of 83%) allowed Hong and collaborator in 2007 to analyze 28 missense mutations associated with PKAN. They obtained the crystal structure of human pantothenate kinases 3 and classified the mutations on the basis of their localization. The human Panks contains two domains (Fig 1.5 A and B): the A domain consists of a six-stranded β-sheet (strands Ab1–Ab6) flanked by five helices (Ah1–Ah3 on one side and Ah4 and Ah11 on the other side) and a glycine-rich loop, probably involved in ATP binding site. The B domain consists of nine β-sheet (strands Bb7-Bb15) and contains the extensive dimerization interface.

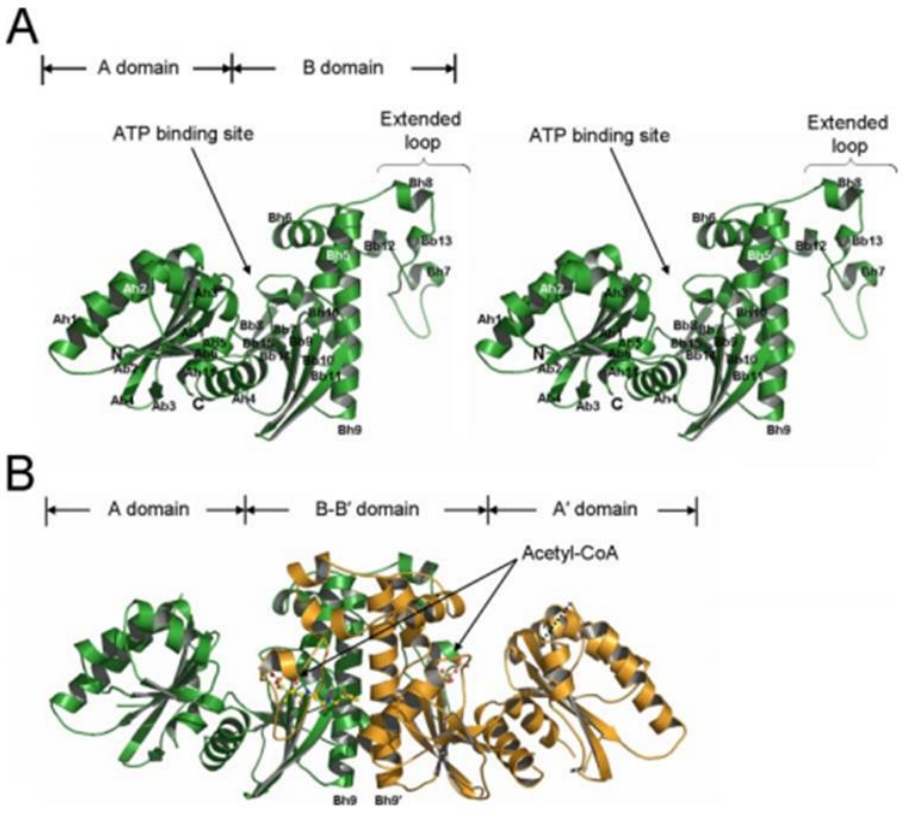

Fig 1.5 Structure of human Pank3. A) structure of monomer with indicated A and B domains B) Pank3 dimeric structure. From Hong et al., 2007

On the basis of these observations they grouped the mutations into three categories: active site mutations, mutations at the dimer interface and protein interior and mutations on the surface of Pank (Table 1.1). They also investigated *in vitro* the effect of these mutations on activity and stability of the protein (Table 1.1), showing that mutations at the ATP binding site and dimer interface compromise the enzyme activities and stabilities and are mostly associated with the early onset of the PKAN phenotype. In fact these mutations could destabilize the monomer

structure reducing the formation of dimers. On the contrary the surface mutations are catalytically active but show slight instabilities relative to the wild type and are linked to the mixed onset of disease phenotype.

Mutations		Tag	ΔΔG	Relative activity		Number of patient[a]	
PanK3	PanK2			PanK3	PanK2[b]	Early onset	Late onset
		°C	*Kcal/mol*	%			
WT		45.4	0.0	100 ± 2.3	100		
ATP binding							
G19V	G219V	36.7	−2.46	1.4 ± 1.2	0.4		1
G321R[c]	G521R	ND[d]	ND	ND	<0.2	24	7
Dimerization domain							
L213P	L413P	36.9	−3.32	2.0 ± 0.4	ND	1	
D247N	D447N	36.6	−4.11	5.2 ± 0.5	ND	1	
S271N	S471N	36.1	−4.36	2.6 ± 0.3	16	3	
N300I	N500I	36.6	−1.84	3.5 ± 0.9	3.9	2	
I297T	I497T	37.7	−3.0	14.5 ± 4.4	ND	1	
I301T	I501T	41.1	−1.23	82.9 ± 2.8	ND		1
A309V	A509V	42.2	−0.77	62.4 ± 0.7	105	2	
N311D	N511D	40.5	−1.71	164.9 ± 5.0	ND	1	
Interior							
L82V	L282V	42	−0.81	141.9 ± 3.1	ND	1	
A198T[e]	A398T	ND	ND	ND	ND	1	
L363P[c]	L563P	ND	ND	ND	<0.2	1	
Surface							
T34A	T234A	46.2	0.12	153.5 ± 2.0	112		2
R49P	R249P	45.8	0.07	122.9 ± 0.4	ND	1	
R64W	R264W	46	0.16	35.7 ± 0.7	58	2	
R78L	R278L	42.6	−0.83	172.5 ± 4.3	ND	1	
R78C	R278C	43	−0.74	184.9 ± 0.8	ND		1
R86C	R286C	40.6	−1.41	154.9 ± 1.7	176	2	2
E122G	E322G	43.8	−0.26	138 ± 6.6	ND	1	
E122D	E322D	43.2	−0.59	149.6 ± 3.4	ND		1
T127I	T327I	42.3	−0.60	112 ± 3.1	91	2	
S151P	S351P	39.8	−1.57	103.7 ± 8.1	78		2
N155S	N355S	45	−0.06	138.5 ± 7.0	ND		1
N204I	N404I	42.4	−0.65	159.4 ± 7.9	83		3
C228Y	C428Y	44.7	−0.14	147.4 ± 11	ND	1	
T328M	T528M	46.2	0.11	162.1 ± 7.9	146	3	7
K332W[f]	R532W	40.9	−0.90	79.7 ± 1.7	95	2	

Table 1.1 Enzyme activities and thermostabilities of Pank3 and Pank2 mutant proteins. From Hong et al., 2007

1.2.2 CoPAN (COASY protein-Associated Neurodegeneration)

Mutations in the *COASY* gene, mapped to chromosome 17q21 (MIM 615643), lead to CoPan or COASY Protein-Associated Neurodegeneration which occurs in childhood with spasticity and dystonia of the lower limbs occurring early on, while dystonia of the mouth and jaw appears later as the disease progresses. The patients also suffer from speech difficulties and dysarthria.

As previously mentioned *COASY* encodes for a bifunctional enzyme containing an import signal in the mitochondria, a regulatory domain and two catalytic domains: adenyl-transferase (PPAT) and dephospho-CoA kinase (DPCK). The few mutations associated to this rare form of NBIA mapped in both PPAT and DPCK domain (Fig 1.6). In 2014 Dusi and collaborators found a patient that carried a homozygous nucleotide substitution- c.1495 C > T that affected a conserved arginine residue (p.Arg499Cys) in the nucleotide binding site of the dephospho-CoA kinase (DPCK) domain (Fig 1.7B). The other patient was a compound heterozygous carrying the same c.1495 C > T transition

and the c.175 C > T variation leading to a premature p.Gln59* stop codon in the N-terminal regulatory region of the protein. Recently others two patients carrying the missense mutation p.Arg214Val in the phosphopantetheine adenylyltransferaase (PPAT) domain were found (Evers et al., 2017).

Fig 1.6 Schematic domain structure of Coenzyme A synthase. From Evers et al., 2017

In order to evaluate the pathogenic role of the mutation R499C, functional studies have been performed in patient fibroblasts and in the yeast model (Dusi et al., 2014). As depicted in the sequence alignment (Fig 1.7A) Arg499 is conserved from yeast to human and corresponds to Arg146 in the yeast Cab5p. The pathogenic role of the mutation was assessed using either the homologous and heterologous complementation since the Δ*cab5* lethal phenotype was rescued by the expression of *COASY* human gene.

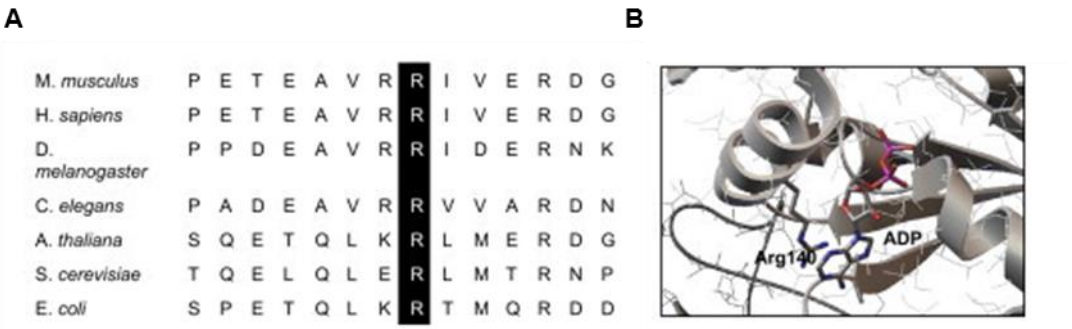

Fig 1.7 (A) Amino acid sequence alignment showing conservation of Arg499 across specie; (B) Crystal structure of *E. coli* DPCK (CoaE) (PDB ID 1VHL) showing the position of Arg140 (equivalent to Arg499 in human DPCK) in the nucleotide-binding site. From Dusi et al., 2014

In the absence of pantothenate in the medium, the strains expressing the mutated allele *COASY*^{R499C} or *cab5*^{R146C} showed a severe growth defect at 37°C and an impairment of growth at 28°C (Fig 1.8A and Fig 1.8B). This result supported the pathogenicity of the substitution p.Arg499Cys and suggested that the mutant enzyme requires a higher concentration of pantothenate to produce enough CoA to sustain yeast growth.

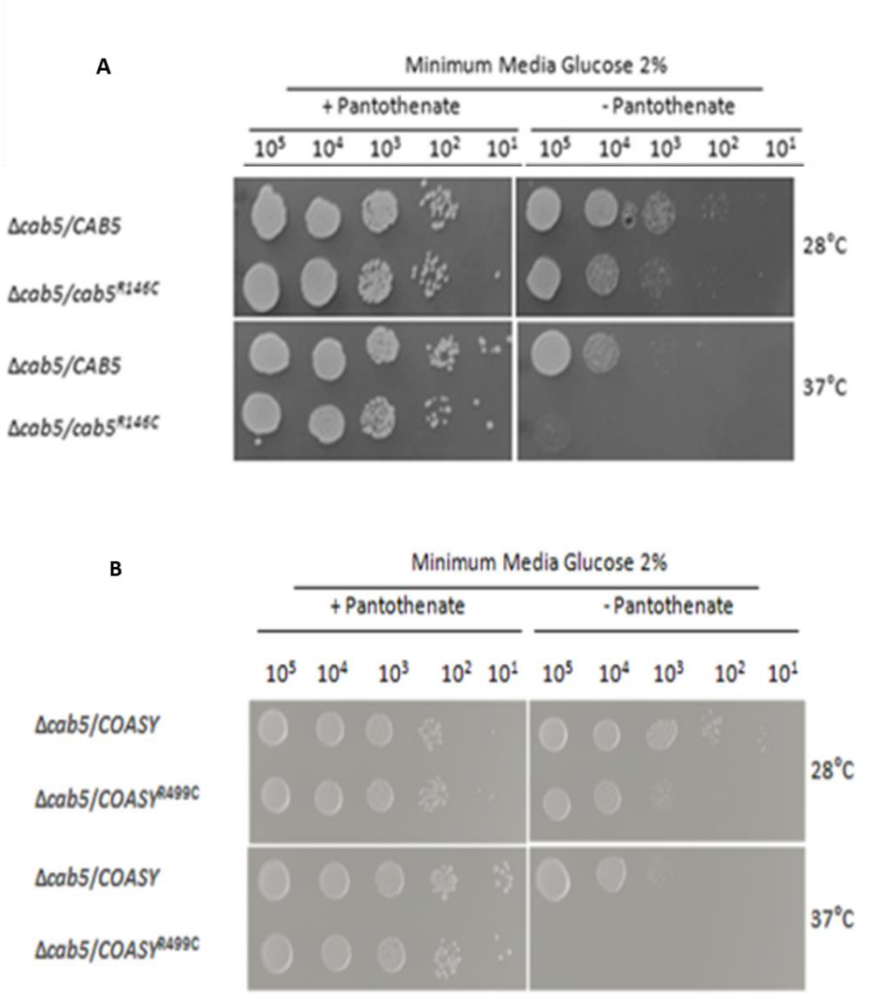

Fig 1.8 A/B Spot assay of Δ*cab5*/CAB5 and Δ*cab5*/*cab5*^{R499C} (A) or Δ*cab5*/*COASY* and Δ*cab5*/*COASY*^{R499C} (B) at 28°C and 37°C on glucose in the presence or absence of pantothenate in the medium. From Dusi et al., 2014

Furthermore the authors measured the level of CoA in mitochondria isolated from the mutant strains Δ*cab5/COASY*^{R499C} and Δ*cab5/cab5*^{R499C} showing a reduction of CoA content by about 40% respect to parental strain (Fig 1.9). According to these results, the same analysis on the derived fibroblast of patients showed a reduction of total CoA level.

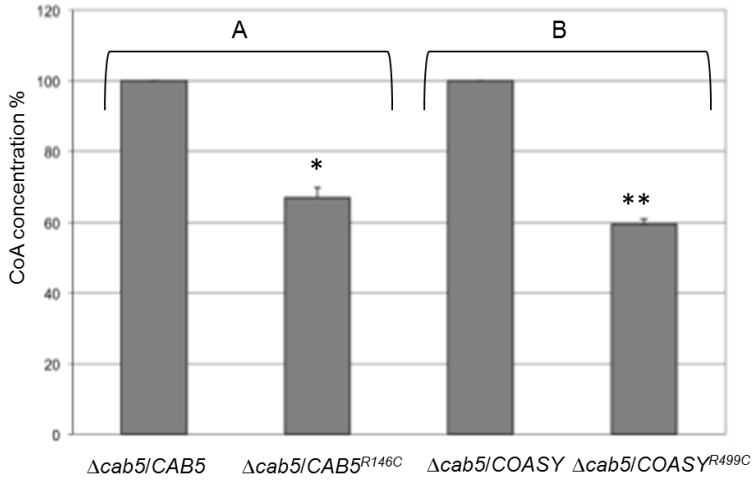

Fig 1.9 Percentage of CoA concentration in yeast strains obtained by HPLC analysis. Values of mutant samples are expressed as percentage of values obtained in wild-type samples, taken as 100%. Statistically significant differences were determined by the Student's t-test; *p<0.05; **<0.02. From Dusi et al., 2014

1.3 Pathogenesis of NBIA

Mitochondrial dysfunction, iron accumulation and oxidative stress are hallmarks of several neurodegenerative diseases, although the relationship between these events in the development of the disorders is not yet clear (Mena et al., 2015). A cause-effect relationship between iron accumulation and oxidative damage has been established and it is namely through the Fenton reaction in which the iron reacts with H_2O_2 to generate the highly reactive hydroxyl free radical (ROS). Neurons are particularly sensitive to ROS and in fact it has been demonstrated that iron accumulation leads to neuronal death (Halliwell 1992; Halliwell 1996). The neurodegenerative disorders associated with iron homeostasis alteration could be due to its accumulation in specific areas of the brain or to a defect in its metabolism, although still today it is not yet clear whether the iron accumulation process is the primary cause of the disorders or not.

Concerning the PKAN and CoPAN disorders, the reason for iron accumulation is still unclear.

It has been hypothesized that enzyme deficiency due to mutations in *PANK2*, lead to a reduction of the final product and accumulation of substrates synthesized upstream in the metabolic pathway, such as N-pantothenoyl-cysteine and pantetheine which are potentially toxic (Leoni et al., 2012). In fact cysteine is a potent iron chelator therefore, high local levels of cysteine could be the basis of the subsequent accumulation of iron, resulting in increased oxidative stress (Perry et al., 1985). However the fact that in other NBIA disorders, such as COPAN, a similar pattern of iron overload has been observed without increased cysteine levels, does not support this hypothesis. It has been proposed that alterations in phospholipid metabolism due to CoA-deficiency both in

PKAN and CoPAN may affect membrane integrity, with consequent oxidative stress that leads to an alteration of iron homeostasis (Leonardi et al. 2007; Santambrogio et al., 2015; Aoun et al., 2015). Another hypothesis links the CoA deficiency to altered gene regulation, DNA stability and cellular homeostasis. This is because Acetyl-CoA, a CoA derivative, is involved in histone protein acetylation a post-translational modification that compromises the affinity between histone and DNA. Low CoA levels could determine a histone hypoacetylation and contribute to neurological phenotype of PKAN and COPAN (Nakamura et al., 2012; Brunetti et al., 2012).

1.4 Model organisms for PKAN and COPAN

In order to explain the relationship between iron accumulation and CoA deficiency and identify therapeutic compounds for PKAN and COPAN diseases, different models *in vivo* and *in vitro* have been created.

1.4.1 *Drosophila melanogaster*

Drosophila melanogaster, *fumble* mutant was obtained by the insertion of the *P*-element near the *PANK* locus that encodes different pantothenate kinase isoforms including mitochondrial isoform (Afshar et al., 2001). The *fumble* flies showed locomotor dysfunction, lower pupation efficiency and reduced adult survival. Moreover d*PANK*/*fbl* mutant flies displayed reduced levels of CoA and impaired mitochondrial integrity (swollen mitochondria, aberrant cristae and ruptured membranes), increased levels of oxidized proteins (increased oxidative stress), increased loss of locomotor function, neurodegeneration, and decreased lifespan (Bosveld et al., 2008; Wu et al., 2009; Rana et al., 2010). The neurodegeneration observed was probably due to an increased number of vacuoles in the brains and not to iron overload. It has been demonstrated that d*PANK*/*fbl* phenotypes were rescued by the addition of the compound pantethine to the food (Rana et al., 2010). The same study also showed that the mechanism underlying pantethine rescue is specific and not general; in fact other neurodegenerative *Drosophila* models are not sensitive to pantethine treatment. This result suggest the existence of an alternative pathway to the canonical *de novo* CoA biosynthesis starting from pantethine that allow to bypass the first step of the pathway: pantethine could be reduced into pantetheine that could be converted into 4'-phospopantetheine, an intermediate substrate synthesized upstream of the PPAT (Rana et al., 2010).

1.4.2 *Mus musculus*

Another animal model for PKAN disorder is *Mus musculus* that presents four isoforms of pantothenate kinase similar to what found in humans. In 2005 Kuo and collaborators constructed and characterized the knock-out *pank2* mouse model. The *pank2*$^{-/-}$ mice partially recapitulate the pantothenate kinase associated neurodegeneration disease phenotype: growth retardation, azoospermia and retinal degeneration but they did not develop brain iron accumulation or apparent neurological difficulties (Kuo et al., 2005). In a further study, the removal of pantothenic acid from the diet lead to a severe phenotype characterized by motor dysfunctions, neurological impairment with feet-clasping and weight loss (Kuo et al., 2007). Upon the re-introduction of the pantothenic acid, the mice were able to restore the locomotor defects and weight loss within four weeks. The pantothenic acid deficiency could therefore represent a useful phenocopy of PKAN and could be used to test pharmacological strategies for the treatment of this disease.

On the basis of the role of CoA in several crucial metabolic pathways and considering the impairment of lipid metabolism in PKAN patients, Brunetti and collaborators in 2014 decided to characterize the *pank2*$^{-/-}$ mice fed to a ketogenic diet, thus stimulating lipid utilization by mitochondrial β-oxidation and ketone body production in the liver. In this way they demonstrated that the introduction of the ketogenic diet resulted in the onset of a severe phenotype in *pank2*$^{-/-}$ mice characterized by motor dysfunctions, neuronal cytoplasmic inclusion and exacerbated mitochondrial alterations such as aberrant cristae and defects of mitochondrial membrane potential. Moreover, this diet showed cytoplasmic accumulation of abnormal ubiquinated proteins as observed in the brains of PKAN patients (Brunetti et al., 2014). On the basis of the results obtained in the *Drosophila* model where it was shown that pantethine could work as a precursor of CoA, they administer pantethine to mice under ketogenic diet and they demonstrated that pantethine restored the movement disorder and ameliorated the mitochondrial dysfunction and the lifespan of *pank2*$^{-/-}$ mice on a ketogenic diet. The mechanism of action of pantethine is not clear, in humans and rodents pantethine is readily metabolized to cysteamine and pantothenate compounds that cannot provide a biochemical bypass for the blockage of CoA biosynthesis (Zizioli et al., 2015). Since cysteamine was shown to have important neuroprotective effects in different models of neurodegenerative disorders, it has been proposed that the pantetheine effect in mice is at least in part mediated by this metabolite.

1.4.3 Zebrafish

Another important model to study the pathophysiology of PKAN disease is Zebrafish with a vertebrate biology, easy methods of genetic manipulation and specific brain regions that are conserved and comparable to human counterparts. Zebrafish possess a single ortholog of *PANK2* together with three other paralogs (*pank1*α, *pank1*b and *pank4*). This gene is expressed at high levels in the brain and particularly in neurons in the adult animals similar to what happens for the human gene (Zizioli et al., 2015). The morphological investigation of the phenotype induced by *pank2* down regulation showed abnormal head development with smaller eyes, perturbation of brain morphology (clear loss of neural cells in telencephalon and diencephalon), a reduction of the antero-posterior axis and the presence of edema in the cardiac region. Furthermore, a defect in vascular integrity has been observed. The wild type phenotype is restored by feeding *pank2* zebrafish to pantethine or CoA. The latter compound fully prevented the development of the abnormal phenotype. On the basis of these results Khatri and collaborators in 2016 extended their analysis to the *COASY* gene. In *Danio rerio* there is a single *COASY* gene with a high level of similarity to the human homolog. The apparently complete down-regulation of *COASY* expression lead to a severe alteration of development with early death, alteration of tissue of the ventral origin and a poorly defined brain. Moreover *coasy* morphants showed an altered vasculature structure particularly in the brain and trunk as showed in *pank2* morphants. With regards to the iron homeostasis, the study showed a reduced Bmp expression (the Bmp- signaling is the main regulator of hepcidin expression the master regulator of systemic and cerebral iron balance). These phenotypes were associated with the storage of CoA availability; indeed CoA supplementation to fish water or overexpression of the human wild type *COASY* mRNA could prevent the abnormal phenotype (Khatri et al., 2016).

However neither *pank2* nor *coasy* morphants displayed any iron accumulation.

1.4.4 PKAN fibroblasts

In order to clarify the mechanism of iron accumulation, Campanella and collaborators (2012) examined iron metabolism in *PKAN* fibroblasts and demonstrated an abnormal behavior of *PANK2* deficient cells in response to treatment with iron. In these cells it was observed a defect in IRPs (*iron regulatory proteins*) activity that lead to an up-regulation of Ft (ferritins- proteins involved in iron storage) and a down-regulation of Tfr1 (transferrin receptor 1- protein involved in cellular iron uptake). The inaccurate quantity of these proteins increased the carbonylated proteins and ROS

generation. To investigate whether iron mishandling could occur in the mitochondria, affecting organelle functionality, Santambrogio and collaborators in 2015 further analyzed PKAN fibroblasts. They observed several mitochondria dysfunctions: altered mitochondrial morphology and mitochondrial membrane potential suggesting a global organelle impairment. Moreover, there was an increase in carbonylated proteins levels suggesting an alteration of oxidative status. The content of iron in mitochondria do not appear to be properly utilized in ISC (*Iron Sulfur Cluster*) and heme biosynthesis. In fact, the activity of Fe-S enzymes like cytosolic/mitochondrial aconitase was reduced in PKAN fibroblasts and the heme content was about 25% less when compared to control fibroblasts (Santambrogio et al., 2015). The reason why these phenotypes occur is not yet clear. The researchers proposed that the impairment of the Krebs cycle due to an altered CoA metabolism leads to a lower production of GTP and NADH factors also required for ISC synthesis. So they suggested that the reduction of aconitase activity could be due to the higher oxidative stress produced by ROS or by the diminished production of ISC, thus compromising ATP production (mACO role) and iron homeostasis (cACO role). They also proposed that the cell could respond to this affected ISC synthesis by increasing cellular iron uptake. This could lead to iron accumulation and consequent oxidative stress.

1.4.5 hiPSC-derived neuronal model

Taking advantage of the technology (Amamoto et al., 2014; Caiazzo et al., 2011) that allows neurons to be directly transdifferentiated from fibroblasts, induced neurons (iNs) from PKAN patients were created. This innovative model could represent a suitable model to study the consequences of *PANK2* dysfunction. The initial studies conducted by Santambrogio and collaborators in 2015 showed a higher ROS levels and significantly lower membrane potentials in PKAN iNs. Further studies demonstrated that *PANK2* deficiency lead to mitochondrial dysfunction and altered ISC and heme biosynthesis in PKAN iNs (Orellana et al., 2016). More specifically, the latter study showed morphological alterations of mitochondria which appear aberrant, enlarged and swollen with damaged cristae. These were accompanied by a decreased respiratory activity. ISC cluster and heme biosynthesis were compromised with the aconitase activity (mACO and cACO) and the heme content reduced in PKAN iNs and NPCs respectively. By measuring the level of two iron proteins, they revealed an increased level of Tfr1 and a decrease level of Ft in these neuronal precursors cells (NPCs). The addition of CoA to the neuronal culture medium during

differentiation restores the ROS levels, the mitochondria respiratory activity and the amount of heme in PKAN iNs and NPCs.

The PKAN iNs characterized by Arber and collaborators in 2017 showed similar phenotypes to those previously described by Orellana; decreased respiratory activity and increased ROS content that in this model lead to a higher lipid peroxidation. However, they did not observe a different expression level of TfR whilst the Ft expression was increased. Moreover, an increased expression of Ferroportin (iron protein exporter) and MTFT (Mitochondrial Ferritin- stored mitochondrial iron) was observed in *PANK2* knockout cell lines. They speculated that the mitochondrial defect could lead to altered iron storage in the mitochondrial matrix and increased iron export, leading to iron dyshomeostasis and a potential accumulation over time (Arber et al., 2017).

None of the models described by Orellana and Arber showed iron accumulation.

1.5 *Saccharomyces cerevisiae* as a model organism for the study of iron-related disorders and lipid metabolism

The yeast *S. cerevisiae*, defined as an "honorary mammal" (Resnick and Cox, 2000), has been extensively used to study several mechanisms and pathways existing in higher eukaryotes and is one of the most useful model organisms to investigate the molecular and genetic basis of human diseases.

S. cerevisiae was the first eukaryote organism to have its genome fully sequenced, published and annotated (Goffeau et al., 1996). Remarkably, about 46% of human-known proteins have homologs in yeast including proteins involved in DNA replication, recombination, transcription and translation, cellular trafficking and mitochondrial biogenesis (Venter et al., 2001). Moreover, about 40% of human genes which have mutations leading to diseases, have an orthologue in yeast (Bassett et al., 1996). Many genetic tools are available including the complete collection of gene deletions and the possibility to duplicate as haploid or diploid makes this organism a flexible tool to determine whether a nuclear mutation is recessive or dominant and, in the latter case, which kind of dominance (Baruffini et al., 2010).

When a homolog of the gene involved in the disease is present in the yeast genome, the mutation can be introduced in the yeast gene and its effects can be evaluated both at a physiological and molecular level. On the other hand, when the disease-associated gene does not have the counterpart in yeast the transgene can be heterologously expressed in yeast and the resulting strain, named "humanized yeast", can be subjected to functional analysis (Khurana et al., 2010).

Moreover, the heterologous or homologous complementation approach can be used to assess the pathogenic role of a substitution. In both cases the collection of *S. cerevisiae* gene deletions strains is exploited: in the first case the human wild type or mutant cDNA are used to transform the null yeast strain to determine the possible relationship between genotype/phenotype. Through this strategy we can confirm the role of human gene and we also can assess the pathogenic role of a mutation. When human cDNA is unable to complement the yeast null strain, we use the homologous complementation approach. In this case we use site-specific mutagenesis to insert the pathological substitutions in orthologous yeast genes to genes that, when mutated, give rise to diseases. On the basis of phenotypic analyses we can thus confirm the pathogenic role of a mutation and also study the molecular basis of the disease.

The yeast *S. cerevisiae* is the only eukaryote able to survive large deletions or total loss of mtDNA (*petite* mutants) provided it is supplied with a fermentative substrate. For this reason it has been largely used for the study of mitochondrial biogenesis and of mitochondria related pathologies (Rinaldi et al., 2010).

In the last decade *S. cerevisiae* has been widely used to decipher molecular mechanisms of neurodegenerative disorders such as Alzheimer's, Huntington's, Friedreich's ataxia and Parkinson's and to investigate the key proteins involved in the etiology and/or pathology of these diseases (Tenreiro et al., 2010). A high degree of similarity of the iron homeostasis pathway between yeast and humans makes yeast an ideal model organism for studying iron-related disorders (Bleackley et al., 2011) (as described in paragraph 1.6 of Introduction).

A good example of this is the study of iron accumulation in the neurodegenerative disorder Friedreich's ataxia (FRDA an autosomal recessive mitochondrial disease characterized by progressive cardiological and neurological degeneration. FRDA is caused by GAA triplet expansion in the first intron of the frataxin gene (*FA*) (Campuzano et al., 1996). The yeast frataxin homologue, *YFH1*, encodes a protein localized in the mitochondria like the FA. The *YFH1* knockout strain leads to an excessive iron accumulation in the mitochondria resulting in the generation of ROS and consequently oxidative damage (Lodi et al., 1999). The yeast model provided the evidence that FRDA is a mitochondrial disorder and allowed a better understanding of its pathophysiology and also provided a tool for the search of therapeutic targets.

With regards to the study of lipid metabolism, the budding yeast *S. cerevisiae* offers an exceptional advantage to understand the lipid-protein interactions since lipid metabolism and homeostasis are relatively simple and well characterized when compared to other eukaryotes (Singh 2017).

Yeast deletion collections have been employed in a number of high-throughputs to determine and understand the role of a particular lipid in various lipid metabolic disorders (Daum et al., 1999; Proszynski et al., 2005; Hancock et al., 2006; Bozaquel-Morais et al., 2010; Villa-Garcia et al., 2011). The biochemistry and molecular biology of lipid metabolism in yeast have been discussed extensively in literature to establish a good model for the study of lipid synthesis and lipid cellular transport (Daum et al., 1998). The yeast diverges from humans for the biosynthesis of phosphatidylserine, of ergosterol and for the sphingolipid composition. As happens in higher eukaryotes, acetyl-CoA is the precursor of lipid synthesis in yeast. In *S. cerevisiae*, acetyl-CoA metabolism takes place in at least four subcellular compartments: nucleus, mitochondria, cytosol and peroxisomes (Chen et al., 2012). Nuclear acetyl-CoA serves as an acetyl donor for histone acetylation but besides this role in chromatin regulation, acetyl-CoA is mainly important for the central carbon metabolism. Depending on the supply of substrate to the cell, various mechanisms may lead to the formation and utilization of acetyl-CoA. In the presence of glucose as carbon source, acetyl-CoA arises from pyruvate in a reaction catalyzed by the pyruvate dehydrogenase complex (PDH) in the mitochondria. Alternatively, acetyl-CoA generates pyruvate decarboxylase and acetaldehyde dehydrogenase via direct activation of acetate in an ATP-dependent reaction catalyzed by acetyl-CoA synthetase. This is the only source for fatty acid and sterol biosynthesis in the cytosol. Acetyl-CoA is also the end product of β-oxidation of straight chain fatty acids which in yeast takes place exclusively in the peroxisomes.

Since the membranes of organelles are impermeable for acetyl-CoA (Van Roermund et al., 1995), this molecule must either be synthesized within each subcellular compartment where it is required or imported using specific transport mechanisms. Two transport systems have been identified. In the first system the carnitine/acetyl-carnitine shuttle acetyl-CoA produced in the peroxisomes or the cytosol is converted into acetylcarnitine which is subsequently transported into the mitochondria. However, it has been shown that *S. cerevisiae* is not capable of *de novo* synthesis of carnitine and unless carnitine is supplied with the medium, this transport system does not function (Van Roermund et al., 1999). The second pathway is the synthesis of C_4 dicarboxylic acids from acetyl-CoA via the glyoxylate shunt, followed by transport of the C_4 dicarboxylic acids to the mitochondria or the cytosol where they can serve as precursor for formation of pyruvate or phosphoenolpyruvate required for either the TCA cycle or gluconeogenesis.

In acetyl-CoA metabolism, the acetyl-CoA synthase carries out a fundamental role ,converting the acetaldehyde derived from the decarboxylation of pyruvate to acetate and acetyl-CoA. Two

structural genes, *ACS1* and *ACS2*, encoding this enzyme have been characterized in *S. cerevisiae* (Van den Berg et al., 1995). They differ in such kinetics property, specificity of substrate and cellular localization. At high concentrations of glucose, *ACS1* is transcriptionally repressed whereas a severe de-repression occurs under glucose limitation or supplementation with non-fermentable carbon sources such as ethanol or acetate. It is located in the mitochondria (Klein et al., 1979; Kumar et al., 2002) and possibly also in the peroxisome (De Virgilio et al., 1992) and it is required for the histone acetylation and for the biology of the endoplasmic reticulum (ER), the Golgi apparatus and the vacuole. *ACS2* is constitutively expressed, is predicted to be cytosolic but may also be present in the nucleus and possibly in the ER. It is involved in histone acetylation and global transcriptional regulation (Pronk et al., 1996; Takahashi et al., 2006).

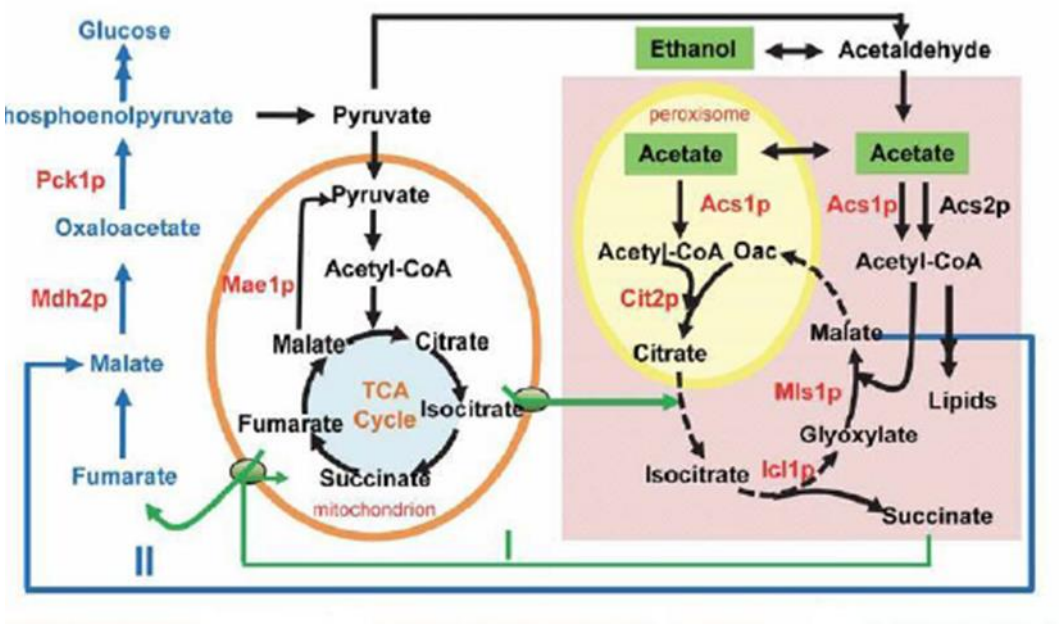

Fig 1.10 Schematic representing cytosolic and peroxisomal acetyl-CoA metabolism in *S. cerevisiae*. From Chen et al., 2012

1.6 Iron homeostasis in human and in yeast

Iron is an essential cofactor in different fundamental biological processes, including DNA synthesis and repair, oxygen transport, cellular respiration, metabolism of xenobiotics and hormonal synthesis (Gutteridge et al., 2000). The mitochondrion plays a key role in iron metabolism and, in fact, is the cellular compartment where iron-sulfur clusters, the prosthetic group that are essential for cell functioning, are synthesized (Stehling et al., 2013). Normally, Fe appears to be widely distributed by cell-type and accumulates progressively during aging and neurodegenerative processes. Organisms have evolved a number of systems for the efficient uptake, intracellular

transport, protein loading and storage of iron and to ensure that the needs of the cells are met whilst minimizing the associated toxic effects. Alteration in iron handling is associated to several diseases. In a variety of eukaryotes the Fe metabolism is mainly regulated at the level of uptake. In fact, changes in gene expression in response to iron overload have been observed either in mammals or yeast (Romney et al., 2008; Li et al., 2008). Iron uptake in *S. cerevisiae* occurs through four distinct pathways, three of these depend on the reduction of iron present in the environment as Fe^{3+} to soluble Fe^{2+} by membrane-bound reductases Fre1p and Fre2p (Georgatsou et al., 1994) (Fig 1.11).

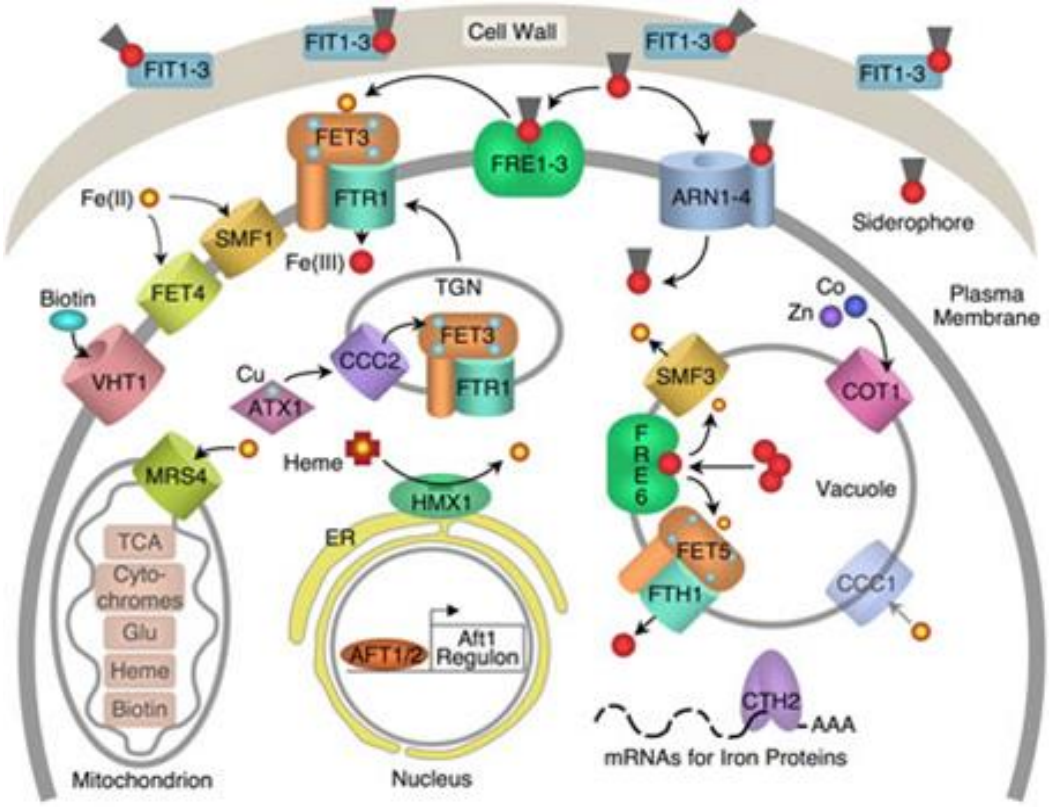

Fig 1.11 Iron homeostasis in *S. cerevisiae*. From Caroline et al., 2006

Fet4p is a low affinity iron transporter in the yeast plasma membrane but it has also been shown to transport other metals such as copper and zinc (Hasset et al., 2000; Waters and Eide2002). Alternatively, iron enters inside the cell though Smf1p a broad specificity divalent metal transporter that drives the transport on the basis of a proton gradient (Chen et al., 1999).

The third reductive system is represented by the Fet3-Ftr1 complex. Fet3p oxidizes $Fe2^{+}$, itself reduced by Fre1/2p, to give rise to Fe^{3+} for subsequent cellular uptake by the permease Ftr1p. Ftr1p only accept Fe^{3+} directly from the ferroxidase Fet3p in a process known as iron channelling

(Kwork et al., 2006). The nonreductive Fe uptake system is mediated by the ARN family (Arn1-4) of membrane permease that transport siderophore-Fe^{3+} complexes (Philpott and Protchenko, 2008; Nevitt 2011). Siderophores are small organic molecules produced by bacteria, fungi and grasses under iron-limiting conditions and are among the strongest Fe^{3+} chelating molecules (Neilands 1995). The yeast does not produce any endogenous siderophores but it does express the necessary transporter to scavenge siderophores secreted by other organisms (Kosman 2003). In addition to the siderophores transporters, a FIT family on cell wall mannoproteins (Fit1-3) retain siderophores-bound iron in the cell wall (Philpott et al., 2002). Inside the cell, the iron overload is sequestered into the vacuole by the Ccc1 transporters. The *CCC1* knockout strain displayed a growth sensitivity to iron addition in the medium, showing the protective role of vacuole and of Ccc1 transporter in this process (Li et al., 2001). On the other hand, during Fe limitation, the Fet5/Fthh1 complex mobilizes Fe out of the vacuole for use (Urbanowski and Piper 1999). During Fe deprivation, the transcription factor Aft1p is translocated from cytosol to the nucleus where it induces the expression of the iron regulon. This translocation is dependent on an interaction with a complex consisting of Fra1p and Fra2p which senses the Fe/S cluster levels in the cell. Aft1p targets approximately 20 genes including genes encoding siderophore uptake proteins, the high affinity iron transport complex and other proteins that function in intracellular iron metabolism (Shakoury-Elizeh et al., 2004). When the iron levels are low, the mRNAs encoding for proteins that bind the iron are degradated, thus allowing the cell to use the resources of this ion (Puig et al., 2005).

The iron homeostasis in also regulated by the mitochondrial machinery ISC (Iron sulfur cluster) it has been proposed that this machinery synthetizes a regulatory component that is then exported to the cytosol by the ISC export component Atm1 that prevents the iron responsive transcription factor Aft1 from entering the nucleus and turning on the iron regulon (Lill et al., 2008).

Functional impairment of the ISC assembly and/or exporter machinery leads to a decrease of the regulatory component in the cytosol, translocation of Aft1 in the nucleus and, consequently, the activation of the iron regulon. This leads to an increase in iron uptake and translocation to the mitochondria where it is accumulated (Lill et al., 2008). The mitochondrial iron uptake is mediated by two homologous membrane transporters Mrs3/Mrs4 (Muhlenhoff et al., 2003). Inside this organelle, the yeast frataxin homolog Yfh1p binds iron and acts as a mitochondrial iron chaperone, delivering iron to sites where it is required (Bulteau et al., 2004).

A high degree of conservation for genes of iron metabolism exists between yeast and humans (Bleackley et al., 2011). The major differences are in the mechanisms of iron exporter and of storage of excessive iron (Fig 1.12). In the mammalian mechanisms, there is a membrane Fe exporter, Ferroportin (Fpn) and the excess iron is stored in the lumen of the ubiquitous multimeric protein ferritin (Torti et al., 2002). More specifically, ferroportin mediates the release of Fe in conjunction with ceruloplasmin (Cp) which must oxidize the Fe^{2+} transported by Fpn to Fe^{3+} before its release into the extracellular medium (Harris et al., 1999). Fpn expression is also detected in the blood-brain barrier (BBB) endothelial cells, neurons, oligodendrocytes, astrocytes, the choroid plexus and ependymal cells (Batista-Nascimento et al., 2012). Cp is essential for the stabilization of Fpn and is the yeast Fet3 homologue. The Fe uptake pathway starts in the intestines where Fe^{3+} is reduced to Fe^{2+} which is then transported to the blood by Fpn and oxidized by Cp that, in turn, promotes the binding of Fe^{3+} to the serum iron carrier transferrin (Tf). The circulating Fe bound to Tf is captured by TfR, enters the cell by endocytosis and translocated across the endosomal membrane through the divalent metal transporter 1 (DMT1). Fe^{2+} in the cytoplasm is then transported inside the mitochondria by mitoferrin (mitochondrial membrane iron transporter).

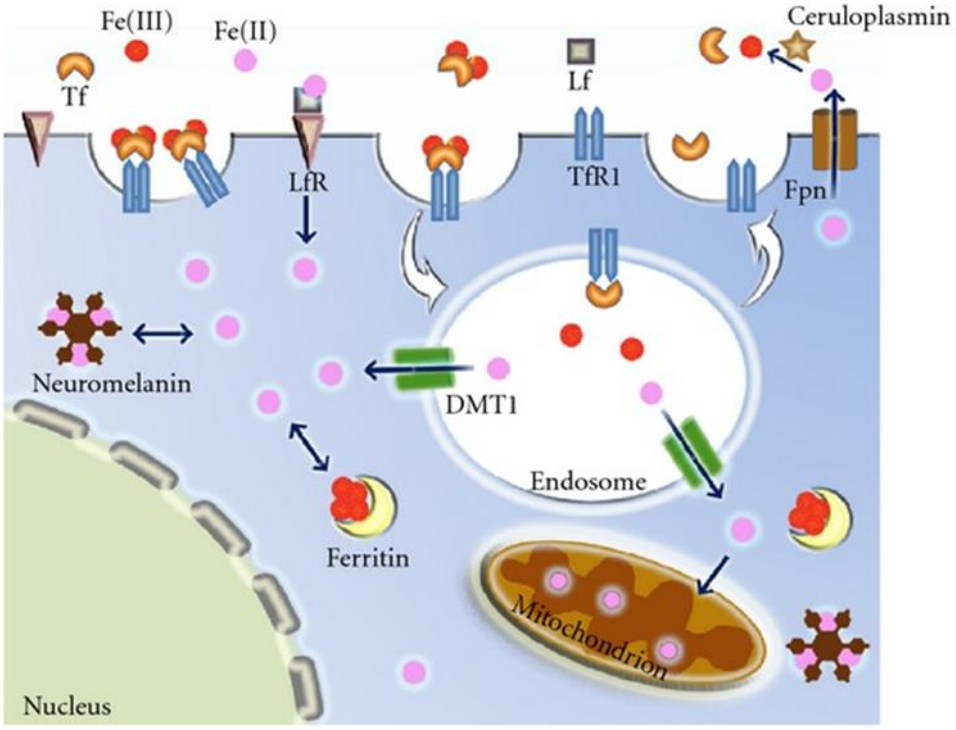

Fig 1.12 Iron homeostasis in humans. From Batista-Nascimento et al., 2012

In mammals, the regulatory mechanism for Fe homeostasis is mediated by the iron-regulatory proteins IRP1 and IRP2, which post-transcriptionally modulate the expression of specific mRNA in response to intracellular iron transferrin and ferritin. In iron depleted cells, IRPs bind to the IREs' (iron responsive elements) cis-elements present in ferritin and transferrin mRNA, preventing ferritin translation and protecting the TfR1 transcript from degradation (Wilczynska et al., 2005). In Fe-replete cells, IRPs do not bind to IREs and ferritin is freely translated whereas TfR1 undergoes cleavage and subsequently degradation (Rouault et al., 2006; Galy et al., 2004; Theil et al., 2000).

1.7 *Saccharomyces cerevisiae* as a model organism for drug discovery

Drug discovery is a highly complex and multidisciplinary process with a goal to identify compounds with therapeutic effects, i.e. molecules able to modulate the function of either a protein or a cellular pathway involved in a human disease. The current paradigm for *de novo* drug discovery begins with the identification of a potential target (usually a protein) and proceeds through the validation of the target in animal and/or cell culture models. Once the target is validated, the process proceeds with the development and execution of a screening system to obtain small molecules that modulate the activity of the target, followed by the characterization and optimization of these small molecules. Active compounds are subsequently tested for their efficacy, toxicity and side effects in animals and/or cell culture models and, finally, a series of FDA-supervised clinical trials are performed to evaluate safety, pharmacology and efficacy in comparison to existing treatments for the same indications (Hughes 2002). The entire progression typically lasts a decade and costs millions of dollars for every molecule reaching the market. Improvement and acceleration of the drug discovery and development process at virtually any step is therefore of interest from commercial, economic and medical viewpoints.

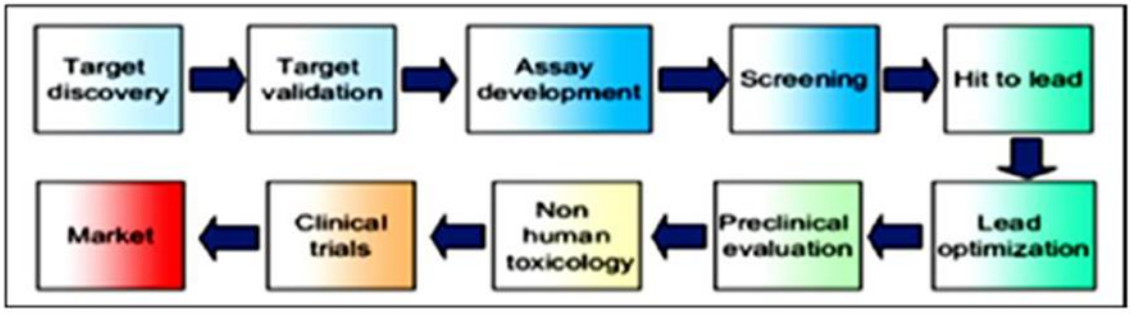

Fig 1.13 Diagram of de novo drug discovery process. From Carnero 2006

For this reason current approaches to drug discovery require an assay that can simultaneously test hundreds of thousands of compounds and hence high throughput screenings (HTS) have become the major tools in this emerging field. HTS allow the isolation of dozens to thousands of molecules to be further tested and ranked for development priority. On such a scale it is fundamental that HTS assays can be performed in small volumes, high density (i.e. 384- and 1536-well microplates) and with the help of robotic processing. In general HTS assay formats can be classified into two types *in vitro* target-based biochemical assays and cell-based assays. *In vitro* target-based biochemical screening is an effective approach with a well-defined pathology and highly validated target. Its biggest advantage is that the exact target and mechanism of action are known. However, many of the most commonly used drugs function through unknown mechanisms and target-based approaches have a few drawbacks. First, the success of target-centric approaches hinges on correctly predicting the link between the chosen target and disease pathogenesis. Second, this biased approach may not actually target the best or most "druggable" protein to provide optimal rescue. Third, it is not always possible to accurately predict the activity of compounds *in vivo*. Finally, the small molecules obtained *in vitro* may have chemical liabilities that preclude efficacy *in vivo*, including entry into cells, solubility, metabolism, distribution, excretion and off-target effects (Tardiff and Lindquist 2013). These potential pitfalls can hinder validation of a compound within the context of a cellular or animal model. In contrast, cell-based assays do not require purified target proteins and can be engineered to produce a simple, measurable readout of cellular processes for HTS (Barberis et al. 2005). Furthermore, in these formats the activity of any compound against a specific target is analyzed in a cellular context that more closely resembles the in vivo scenario. The most significant barrier in cell-based screens is determining a mechanism of action of the compound and protein target. However, the genetic tractability of model organisms offers new approaches for target discovery, although this is often difficult. Of course, a limiting factor for cell-based screening is that a compound potential is only as valid as the model from which it was derived. Cellular screens should ideally be performed with cells of human origin, which evidently provide the most physiologically relevant model system. However, human cells are expensive to culture and sometimes difficult to propagate in automated systems used for HTS. Moreover, the genetic manipulation of mammalian cells is generally problematic and time-consuming. The high degree of conservation of basic molecular and cellular mechanisms between yeast and human cells underscores the value of *S. cerevisiae* as a tool for drug discovery. In yeast cells the function of human proteins can often be reconstituted and aspects of some human

physiological processes can be recapitulated. Thus, yeast represents an inexpensive and simple alternative system to mammalian culture cells for the analysis of drug targets and for the screening of compounds in a heterologous yet cellular, eukaryotic environment. Despite its numerous advantages, yeast assays are not without limitations for the purposes of drug discovery. Principal among these is the high concentration of compound often required to produce a biological response, likely due to the barrier presented by the cell wall, and the presence of numerous active efflux pumps and detoxification mechanisms (Smith et al., 2010).

Couplan and colleagues developed a two-step yeast phenotype-based assay, called "Drug drop test", to identify active drugs against human mitochondrial diseases affecting ATP synthase, in particular NARP (neuropathy, ataxia, and retinitis pigmentosa) syndrome. An appropriate yeast model of such disorders is the deletion mutant for the nuclear gene *FMC1* that encodes a protein required at high temperatures (35-37°C) for the assembly of the F1 sector of ATP synthase. Indeed when the *fmc1Δ* mutant is grown at high temperatures, its mitochondria contain fewer assembled ATP synthase complexes than a wild-type strain. The Drug drop test was performed in a solid medium and it was composed of a primary screening in which ~12.000 compounds from various chemical libraries were tested for their ability to suppress the respiratory growth defect of the *fmc1Δ* mutant. Some of the tested compounds were from the Prestwick Chemical Library, a collection of drugs for which bioavailability and toxicity studies have already been carried out in humans and therefore, active compounds from this library can directly enter drug optimization programs. Experimentally, *fmc1Δ* cells were spread on solid glycerol medium and exposed to filters spotted with the compounds. After incubation at 35°C, active compounds were then identified by a halo of enhanced growth around a filter (example in Fig 1.14).

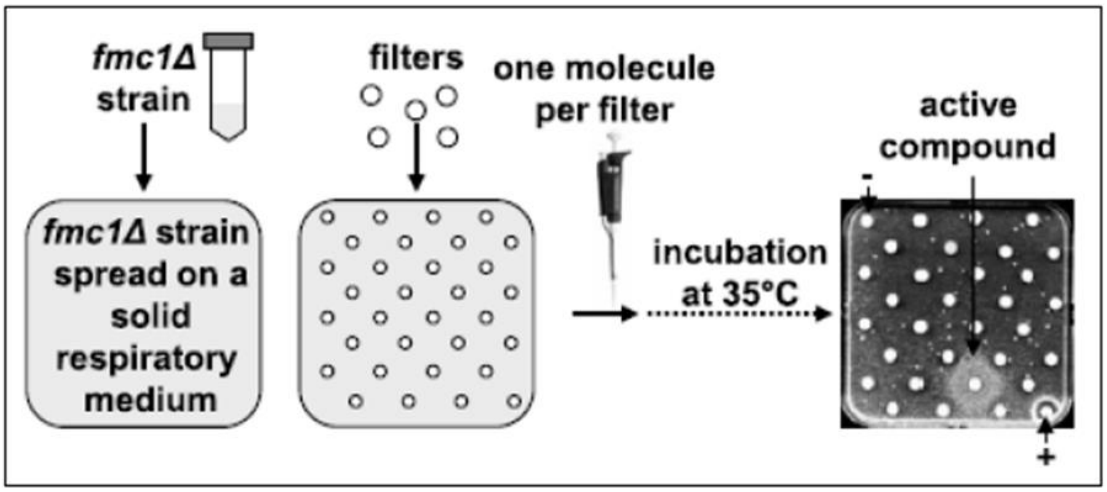

Fig 1.14 Schematic representation of the "Drug Drop Test" technique. From Couplan et al., 2011

Using the same experimental procedure, active compounds isolated from the primary screening were tested (in a secondary screening) on the five yeast *atp6*-NARP mutants which are the yeast models of the five most common mutations in *ATP6* related to NARP syndrome,. The advantage of this method is that, in one simple experiment, it allows numerous compounds to be tested across a large range of concentrations due to diffusion of the drugs in the growth medium. Two compounds were identified as active. Further studies demonstrated that both these molecules were active also on human cells (Couplan et al., 2011). A similar approach has been recently used in our laboratory for the search of active molecules against mitochondrial disorders caused by mutations in *POLG* which encodes for the catalytic subunit of the DNA polymerase γ. In this study, *mip1* mutated yeast strains carrying different thermo-sensitive mutations which led to a high frequency of *petite* mutants at 37°C, were used. Using the "Drug drop test" method previously described, six molecules, named MRS1-6, were proven to be able to rescue the mutant phenotypes of the *mip1* yeast strains. Interestingly, one of these molecules, MRS3, was also active on *C. elegans* and human fibroblasts. This finding can lead the way, for a clinical trial for this molecule in the search for treatments of human mitochondrial diseases related to POLG (Pitayou et al., 2016). In summary, one can state that these results demonstrate that *S. cerevisiae* is a useful model for drug discovery approaches. Furthermore, as yeast models of inherited mitochondrial disorders continue to be developed, the high-throughput screening approach described here will continue to yield both promising chemical therapeutics and insights into disease mechanisms.

Aim of the research

The specific aims of my PhD project were:

1. **Localization of Cab1 and Cab5 proteins**

   In *S. cerevisiae* the sub-cellular compartmentalization of the CoA biosynthetic pathway is not established. Therefore, the Cab1p and Cab5p localization was investigated.

2. **Construction and characterization of yeast models of CoPAN and PKAN diseases**

   PKAN and CoPAN diseases are forms of neurodegeneration with brain iron accumulation (NBIA) associated to mutations in panthotenate kinase (*PANK2*) and coenzyme A synthase (*COASY*), both involved in CoA biosynthesis. Although iron overload is a hallmark of PKAN and CoPAN, its relationship with CoA dysfunction is not yet clear. In particular whether iron accumulation is the primary cause of the diseases or not has not been established.

   In order to investigate the connection between CoA deficiency and iron overload, yeast models of both PKAN and CoPAN were constructed and characterized. To this aim strains expressing pathological variants in the corresponding yeast proteins were generated.

3. **Identification of chemical suppressor for PKAN treatment**

   In order to identify molecules that could represent therapeutic drugs active against these diseases, a screening of Selleck-FDA approved chemical library was performed, taking advantage of the growth defective phenotype of PKAN yeast model.

Results

1. Yeast model of PKAN disease

1.1 Strains construction

In order to study *PANK2* pathological mutations in the yeast model associated with PKAN, we created a haploid strain deleted in the *CAB1* gene the *PANK2* yeast orthologue. As previously mentioned, *CAB1* in an essential gene, i.e. *cab1Δ* is unviable. For this reason, the *CAB1* gene was disrupted in the presence of a plasmid-borne wild type allele. Firstly we cloned *CAB1* gene in the centromeric pFL38 plasmid (*URA3* marker). The gene and its upstream and downstream regulatory regions were PCR amplified using genomic DNA of the W303-1B strain as template and *CAB1*Fw*Hind*III and *CAB1*Rv*Bam*HI as primers. The amplicon was then digested with *Hin*dIII and *Bam*HI and cloned in pFL38, digested with the same enzymes to obtain the construct pFL38*CAB1*. The gene was also inserted in the pFL39 vector (*TRP1* marker). pFL38*CAB1* was then transformed into the W303-1B strain. In the strain obtained, *CAB1* gene was then disrupted by "one step gene disruption" (Rothstein et al, 1983), modified according to Wach et al. (Wach et al., 1994) as described in Materials and Methods. With this technique, the gene of interest is disrupted at the chromosomal locus by the KanMX4 cassette conferring geneticin resistance to the transformed yeast strain. The cab1::KanMX4 cassette was amplified using the pFA6a-*KanMX4* plasmid (Wach et al., 1994) as template and *CAB1*FwKan and *CAB1*RvKan as primers. These primers contain 40bp identical to the sequence of *CAB1* gene and 18-20bp homologues to the *KanMX4* cassette. The cassette was then inserted into the W303-1B/pFL38*CAB1* strain through "high efficiency yeast transformation protocol" (Gietz et la., 2002). The cab1::KanMX4 cassette could recombine either at the *CAB1* gene present on the vector or at the chromosomal locus. To distinguish between these two cases, plasmid shuffling on 5-FOA was performed and the viability on glucose was checked. Cells in which the genomic *CAB1* locus was disrupted were unviable and vice-versa, cells in which the cab1::KanMX4 cassette recombined at the *CAB1* plasmid borne locus were viable maintaining the genomic *CAB1* copy.

In order to study the human *PANK2* mutations we first investigated if human *PANK2* was able to complement the *CAB1* deletion. For this purpose the *PANK2* cDNA (kindly supplied by Dr. V. Tiranti, *Istitito Neurologico Besta*, Milan) was cloned in two different multicopy yeast expression vectors, under the control of either the strong promoter *CUP1* (pYEX-BX) (Clontech Laboratories) or of the inducible *GAL1* promoter (pSH63) and the recombinant constructs were then introduced into the *cab1*Δ/pFL38*CAB1* or into the *cab1*Δ/pFL39*CAB1*. To obtain a strain containing only the human *PANK2*, plasmid shuffling was performed on 5-FOA or in YNB DO-TRP depending on the combination of plasmids carried by the strains. In no cases were viable cells (*cab1*Δ/*PANK2*)

obtained when the vector containing the *CAB1* yeast gene was lost, indicating that the human *PANK2* failed to complement *CAB1* deletion. If the lack of complementation of the *cab1*Δ lethal phenotype by h*PANK2* can be the consequence of an incorrect or a different localization of Cab1 protein remains to be clarified. Cab1 protein shows high sequence identity with the PANK2 human counterpart lacking the stretch of about 120 amino acids present at the N-terminus of the human sequence that was shown to contain the mitochondrial targeting signal (Alfonso-Pecchio et al., 2012) suggesting a cytosolic localization for the yeast protein. Alternatively, although *in vitro* assay in yeast suggests a mitochondrial sub-localization for hPANK2 protein (Hortnagel et al., 2003) we can hypothesize that, *in vivo,* the import of hPANK2p in the heterologous mitochondria could not happen thus explaining the inability to complement.

In order to clarify the lack of complementation of the *cab1*Δ lethal phenotype by h*PANK2* we performed some experiments to investigate the Cab1p localization (section 4).

1.2 Analysis on the conservation between human and yeast of mutated *PANK2* residues and in silico pathogenicity prediction

PKAN or Pantothenate Kinase-Associated Neurodegeneration, is the most common form of NBIA. Indeed between 35 and 50 percent of the NBIA patients have PKAN caused by mutations in the *PANK2* gene (Hartig et al.,2006; Leoni et al., 2012). So far more than 80 mutations have been identified that spread throughout the whole *PANK2* gene. About 50 are missense mutations while the remaining are frameshift and nonsense mutations, stop codons, splicing errors or deletions/insertions. In order to decide which mutation/s express in yeast to create the PKAN model, the identification of the mutations which affect the conserved amino acid residues between human and yeast protein was performed. As shown by the alignment in Fig 1.1, 13 missense mutations were regarded as conserved residues between Cab1/PANK2 protein (green color) with the remaining ones not conserved (purple color) or regarded as residues in parts of sequences that do not overlap the yeast sequence (yellow color).

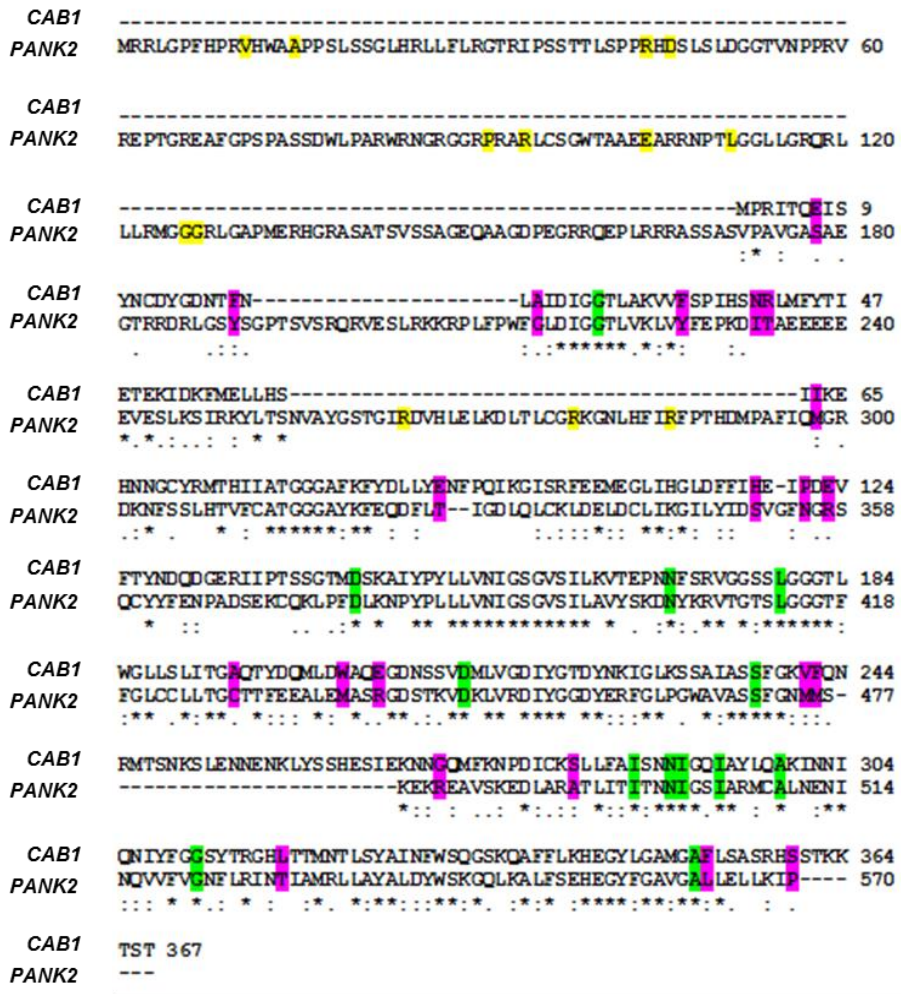

Fig 1.1 Alignment of cab1 and Pank2 protein sequences obtained with ClustalW. In green are represented the conserved residues between Cab1/PANK2 protein, in purple the residues not conserved and in yellow residues in parts of sequences that do not overlap the yeast sequence.(http://www.ebi.ac.uk/Tools/clustalw).

As previously described in the Introduction, the hPANK2 protein functions as a dimer and the 13 missense conserved mutations are classified on the basis of their localization. In particular two mutations (G219V and G521R of PANK2) were mapped to the ATP binding site, two (N404I and D378G of PANK2) were located on the surface of the protein while the remaining were located in the dimerization domain. When deciding which mutations express in yeast, one must keep in mind that it is important to understand how these mutations could affect the protein activity. To attain this information we performed *in silico* analysis of pathogenic prediction using 3 different bioinformatics tools. The residual activity was measured for only six of them (table 1.1 Introduction).

Through these bioinformatics software, each of which uses a different prediction algorithm, we were able to predict the effect of each amino acid substitution on the protein function. Here is a list of the 3 bioinformatics tools employed:

- SIFT (http://sift.jcvi.org) Range from 0 to 1. The amino acid substitution is predicted as damaging if the score is <=0.05 and tolerated if the score is >0.05.
- PolyPhen-2 (http://genetics.bwh.harvard.edu/pph2/) Range from 0.00 (benign) to 1.00 (probably damaging). The amino acid substitution is predicted as benign- possibly damaging- probably damaging.
- PANTHER (http://www-pantherdb.org) Range from 0 (neutral) to 1 (pathological).

The output results are different depending on which program is used. In order to homogenize the results obtained by the 3 bioinformatics programs, a score and a color-code were given to each of the 3 outputs predicted for each mutation according to the following rules: score 0 and color green if the mutation was predicted as "neutral," score 1 and color yellow if the output was "tolerated,", score 2 and color red if the mutation was predicted "damaging" or "probably damaging". So for each mutation 3 scores were defined and a single "Consensus score" was obtained by summing the 3 scores and by dividing the sum by 3 (that corresponds to the number of bioinformatics tools used). On the basis of these "Consensus score" we classified the mutations in three different groups:

1. 0-0.66: mutations were predicted as "neutral" and colored in green
2. 0.66-1.32: mutations were predicted as "tolerated" and colored in yellow
3. 1.32-2: mutations were predicted as "damaging" or "probably damaging" and colored red

In this way, out of the 13 mutations analyzed, 2 were classified as "neutral", 3 as "tolerated" and 8 as "damaging" (Table 1.1).

Human Protein	Yeast Protein	SIFT[1]	Polyphen[2]	Panther[3]	Consensus
Gly219Val	Gly26Val	0.00 AFFECT PROTEIN FUNCTION	1 Probably damaging	0.98	2
Asp378Gly	Asp144Gly	0.14 TOLERATED	0.025 Benign	0.20	0
Asn404Ile	Asn170Ile	0.03 AFFECT PROTEIN FUNCTION	0.14 Benign	0.65	1
Leu413Phe	Leu179Phe	0.01 AFFECT PROTEIN FUNCTION	1 Probably damaging	0.83	2
Asp447Asn	Asp213Asn	0.00 AFFECT PROTEIN FUNCTION	1 Probably damaging	0.87	2
Ser471Asn	Ser237Asn	0.37 TOLERATED	1 Probably damaging	0.78	1
Ile497Thr	Ile287Thr	0.00 AFFECT PROTEIN FUNCTION	0.993 Possibly damaging	0.58	1.33
Asn500Ile	Asn290Ile	0.24 TOLERATED	1 Probably damaging	0.76	1
Ile501Thr	Ile291Thr	0.00 AFFECT PROTEIN FUNCTION	1 Probably damaging	0.76	1.66
Ile504Val	Ile294Val	0.26 TOLERATED	0.025 Benign	0.12	0
Ala509Val	Ala299Val	0.00 AFFECT PROTEIN FUNCTION	1 Probably damaging	0.54	1.66
Gly521Arg	Gly311Arg	0.00 AFFECT PROTEIN FUNCTION	1 Probably damaging	0.94	2
Ala562Thr	Ala352Thr	0.37 TOLERATED	0,999 Probably damaging	0,91	1.33

Table 1.1 Analyses of pathogenicity prediction using three bioinformatics tools

[1] http://sift.jcvi.org

[2] http://genetics.bwh.harvard.edu/pph2/

[3] http://www.pantherdb.org

On the basis of this result we decided to construct 5 mutant alleles with different consensus value and mapping in different domains. More specifically, we chose Gly219Val (Gly26 in yeast) and Gly521Arg (Gly 311 in yeast) that map in ATP binding domain and present a consensus value = 2; Asn404Ile (Asn170 in yeast) that localizes on the surface and presents a consensus value =1; and Leu413Phe (Leu 179 in yeast) and Asn500Ile (Asn290 in yeast) that map in the dimerization domain and present a consensus value= 2 or 1 respectively.

Starting with the hypothesis that these mutations could determine a complete loss of function, we decided to construct a yeast strain expressing the known thermosensitive allele Gly351Ser (Olzhausen et al., 2009).

cab1 mutant alleles were constructed using mutagenic overlap PCR with the oligonucleotides reported in Table 1.5 in Materials and Methods, digested with *Hin*dIII and *Bam*HI and sub-cloned in pFL39 centromeric vector (*TRP1* marker).

The recombinant plasmids pFL39*cab1*^{G26V}, pFL39*cab1*^{G311R}, pFL39*cab1*^{L179P}, pFL39*cab1*^{N170I}, pFL39*cab1*^{N290I} and pFL39*cab1*^{G351S} were transformed into the *cab1*Δ/pFL38*CAB1* strain. To obtain strains containing only the mutated alleles, we then counter-selected the pFL38*CAB1* through plasmid shuffling on 5-FOA, as described in Materials and Methods. If the mutant allele was able to complement the *cab1* deletion, cells would be capable of losing the wild type allele and would be viable in 5-FOA whilst the cells would be unviable in 5-FOA.

As expected, the three mutant alleles *cab1*^{G26V}, *cab1*^{G311R} and *cab1*^{L179P} were unable to rescue the lethal phenotype of *cab1*Δ. The null *cab1* lethal phenotype was rescued by the expression of mutant alleles *cab1*^{N170I}, *cab1*^{N290I} and as expected of *cab1*^{G351S} .

These mutants were further characterized.

1.3 Phenotypic characterization of *cab1*Δ/pFL39*cab1*^{N170I}, *cab1*Δ/pFL39*cab1*^{N290I} and *cab1*Δ/pFL39*cab1*^{G351S}

1.3.1 Analysis of OXPHOS metabolism

Due to the fundamental role of Coenzyme A in a variety of cellular processes, a defect in its biosynthesis could lead to a variety of metabolic alterations. In particular we focused on energy metabolism by investigating mitochondrial function. We first evaluated the ability of the mutant strain to utilize respiratory vs fermentable carbon sources both at 28 and 37°C. Serial dilutions of

the different mutant strains were spotted on YNB DO-TRP supplemented with either ethanol or glycerol. The strain *cab1*Δ/pFL39*cab1*^{G351S}, besides a thermosensitive phenotype (ts) on glucose (Olzhausen et al., 2009), exibits a clear growth defect on respiratory source both at 37°C and 28°C (Fig 1.2A). The same phenotype, ts on glucose and a growth defect on oxidative carbon source was shown by the mutant strain *cab1*Δ/pFL39*cab1*^{N290I} (Fig 1.2B). On the contrary, the mutant strain *cab1*Δ/pFL39*cab1*^{N170I} did not exhibit any evident growth defect (Fig. 1.2B)

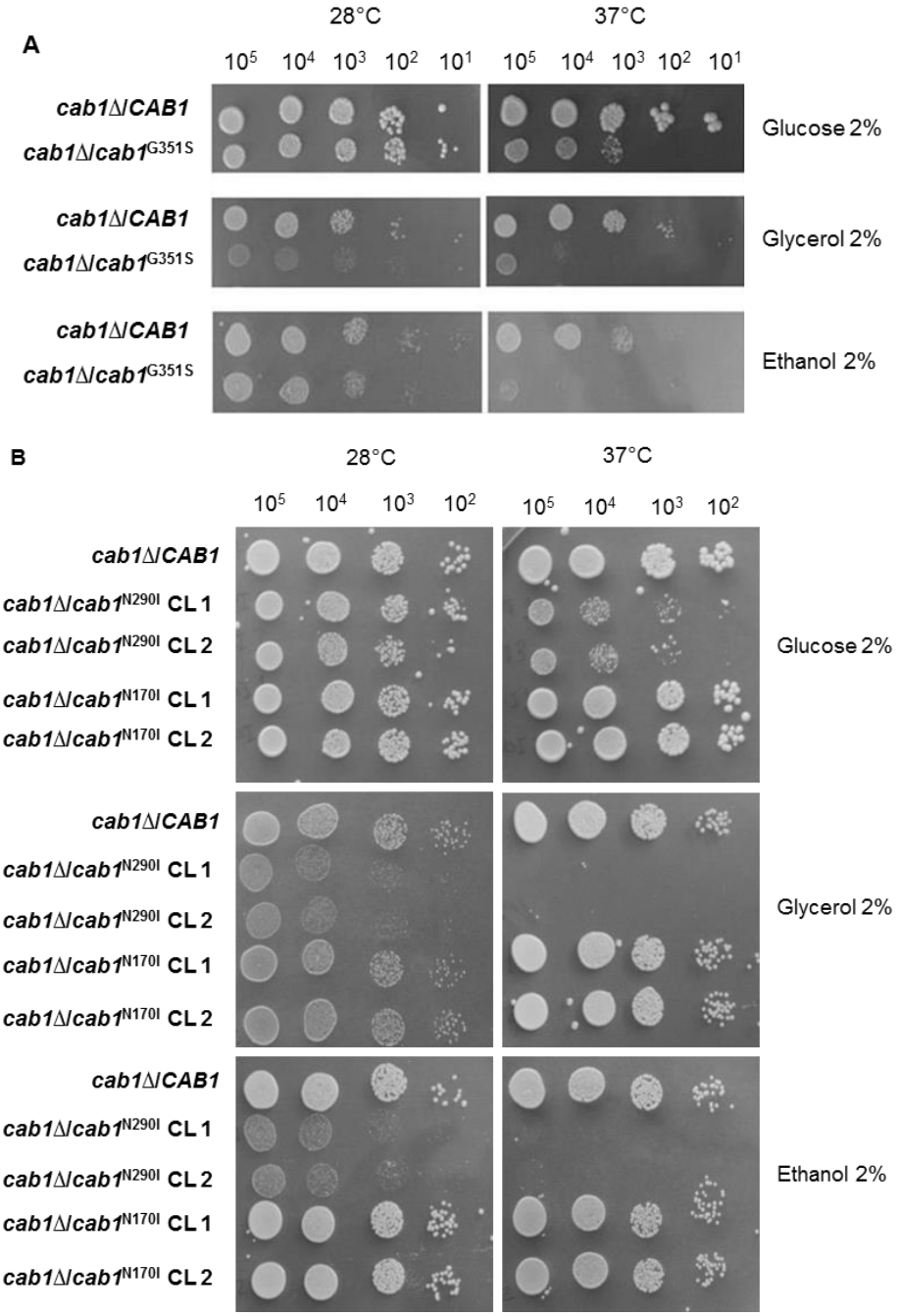

Fig 1.2 Spot assay of *cab1*Δ strain harbouring the pFL39*CAB1* or pFL39*cab1*^{G351S} (Fig. 1.2A), pFL39*cab1*^{N290I} and pFL39*cab1*^{N170I} (Fig 1.2B) on YNB DO-TRP medium plus 2% glucose, 2% glycerol or 2% ethanol. The growth was scored after 3 days of incubation at 28°C and 37°C.

To better define the oxidative growth deficiency, we measured oxygen consumption of whole cells, as described in Materials and Methods. Based on their growth we can state that the phenotype *cab1*Δ/*cab1*^{N170I} mutant strain did not exhibit a respiratory defect while *cab1*Δ/pFL39*cab1*^{G351S} and *cab1*Δ/pFL39*cab1*^{N290I} show a decreased respiratory ability compared to the wild type by about 33% and 27% respectively (Fig 1.3).

On the basis of the results obtained, further analyses were performed only on the strains expressing the variants Asn290Ile and Gly351Ser.

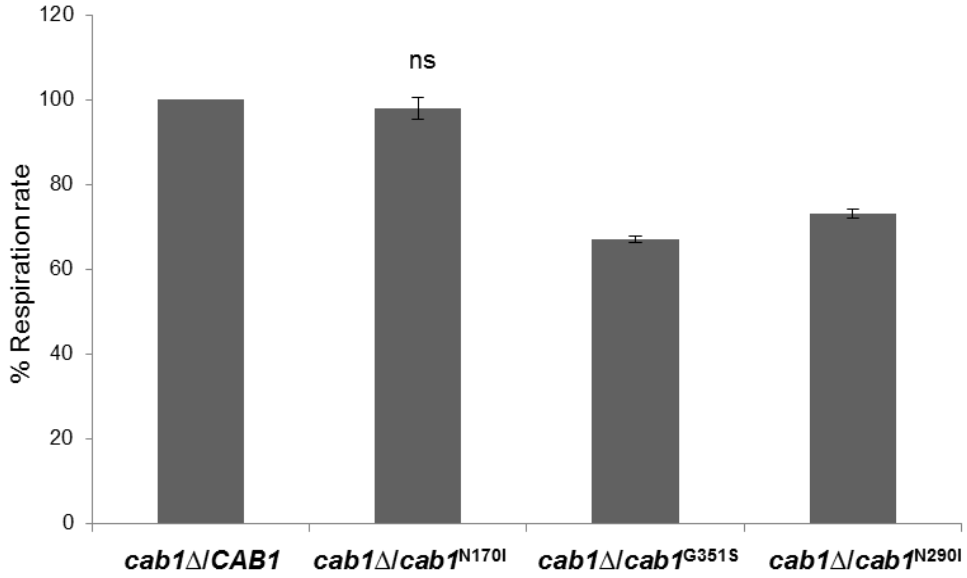

Fig 1.3 Oxygen consumption of *cab1*Δ harbouring the plasmid pFL39*CAB1*, pFL39*cab1*^{N170I}, pFL39*cab1*^{G351S} and pFL39*cab1*^{N290I} at 28°C grown in YNB DO-TRP medium supplemented with 0,2% glucose and 2% galactose.

In both mutant strains the activity of the respiratory complexes NADH-cytochrome c reductase (NCCR, NADH reductase + CIII) and the cytochrome c oxidase (COX, CIV) were then measured on a mitochondrial-enriched fraction as described in Materials and Methods. These activities were likewise significantly reduced in both mutant strains though to different extents, ranging from 40% and 50% for NCCR activity and from 67% and 40% for COX activity as shown in Fig 1.4.

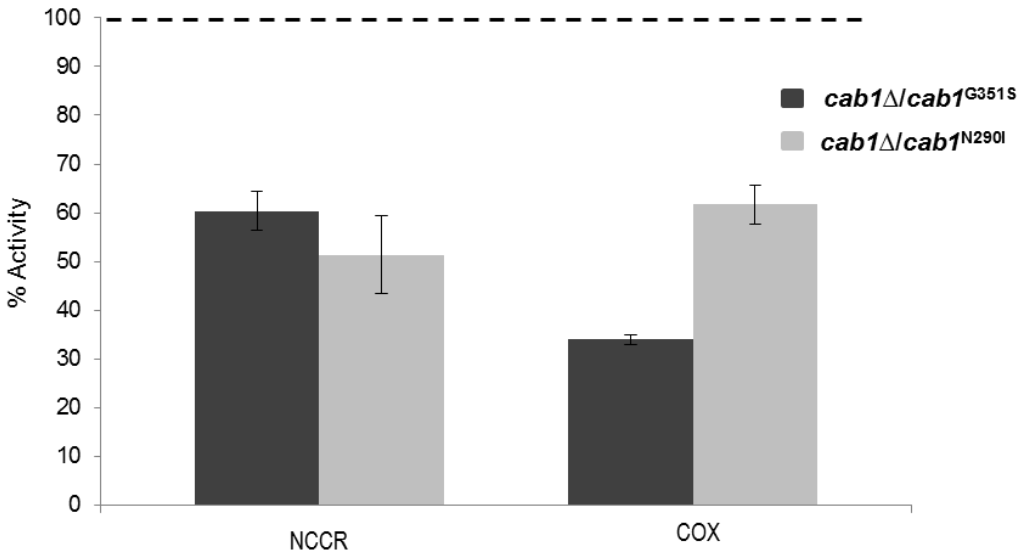

Fig 1.4 NCCR and COX activities were measured in mitochondria extracted from cells grown exponentially at 28°C in YNB DO-TRP medium plus 0,2% glucose and 2% galactose. Each activity was normalized to 100% for the strain containing pFL39*CAB1* .

1.3.2 Analysis of mtDNA mutability

S. cerevisiae has the unique property to produce cells with homoplasmic-deleted mtDNA molecules, referred to as *petite* mutants. Yeast *petite* colonies are compromised to different extents in their mtDNA which, in turn, results in loss of respiratory activity and complete dependence on fermentative metabolism. Analysis of mtDNA mutability was performed at 28°C as described in Materials and Methods. As shown in Fig 1.5, *cab1*Δ/pFL39*cab1*^{G351S} and *cab1*Δ/pFL39*cab1*^{N290I} mutants display a *petite* frequency of about 8% more than the wild type.

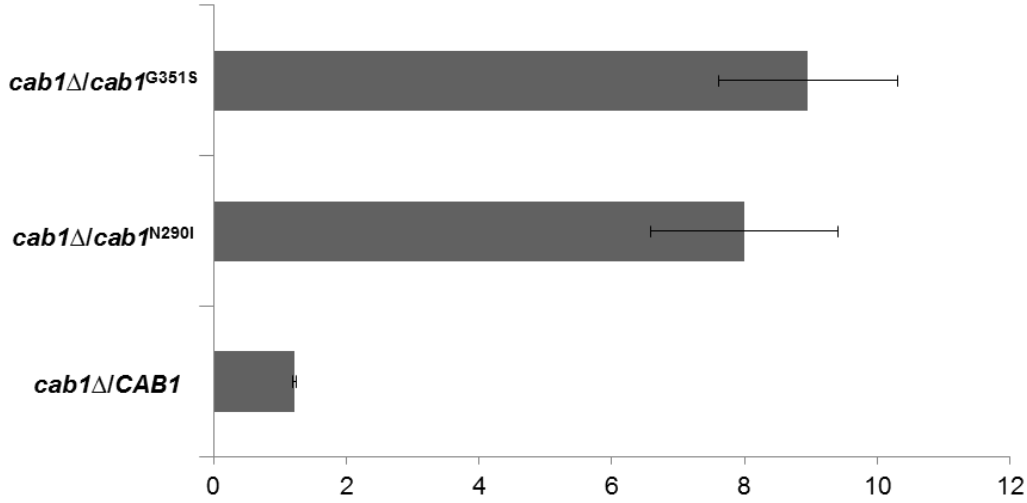

Fig 1.5 Analysis of mtDNA mutability was performed on respiratory sufficient *cab1*Δ/pFL39*CAB1*, *cab1*Δ/pFL39*cab1*^{G351S} and *cab1*Δ/pFL39*cab1*^{N290I} strains at 28°C in YNB DO-TRP supplemented with ethanol 2% and then shifted to 2% glucose.

1.3.3 Perturbation of iron homeostasis in *cab1* mutant cells

As previously said, PKAN disorder is characterized by iron deposition in the brain but the relationship between CoA deficiency and iron accumulation is still poorly understood. Animal models so far characterized fail to display iron accumulation and it has been recently demonstrated that in patient-derived neuronal cultures total iron content was also unchanged (Arber et al., 2017). In order to investigate if panthotenate kinase mutations perturb iron homeostasis in our model, the cellular response to iron was first evaluated. In particular, the inhibition of cellular growth by the addition of $FeSO_4$ to the medium was tested since it has been reported that an excessive iron accumulation in the mitochondria led to an increased sensitivity to this ion (Foury and Cazzalini 1997; Patil et al., 2012). As shown in Fig 1.6A and B, *cab1*Δ/pFL39*cab1*^{G351S} cells show growth sensitivity to $FeSO_4$ both in glucose (fermentable) and galactose (respiro-fermentable) media. The sensitivity to iron in galactose-containing medium was observed at lower $FeSO_4$ concentration (7 and 9mM $FeSO_4$) with respect to glucose (9 and 12 mM $FeSO_4$). This is most likely due to the fact that cells have a greater demand for iron in respiratory and respiro-fermentable media (Kaplan et al., 2006; Garber Morales et al., 2010).

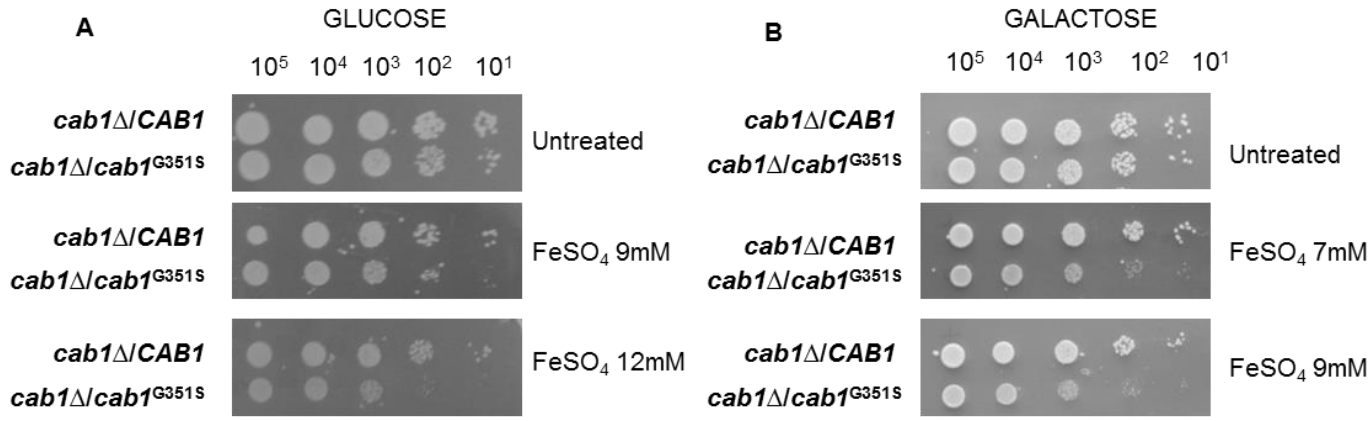

Fig 1.6 Spot assay of *cab1*Δ strain harbouring the pFL39*CAB1* or pFL39*cab1*^{G351S} on YNB DO-TRP 2% glucose (A) or 2% galactose (B), with the addition of 9 and 12mM $FeSO_4$ or 7 and 9mM $FeSO_4$. The growth was scored after 3 days of incubation at 28°C.

As shown in Fig 1.7A and B the mutant strain *cab1*Δ/pFL39*cab1*^{N290I} also showed a higher sensitivity to iron with respect to the wild-type strain.

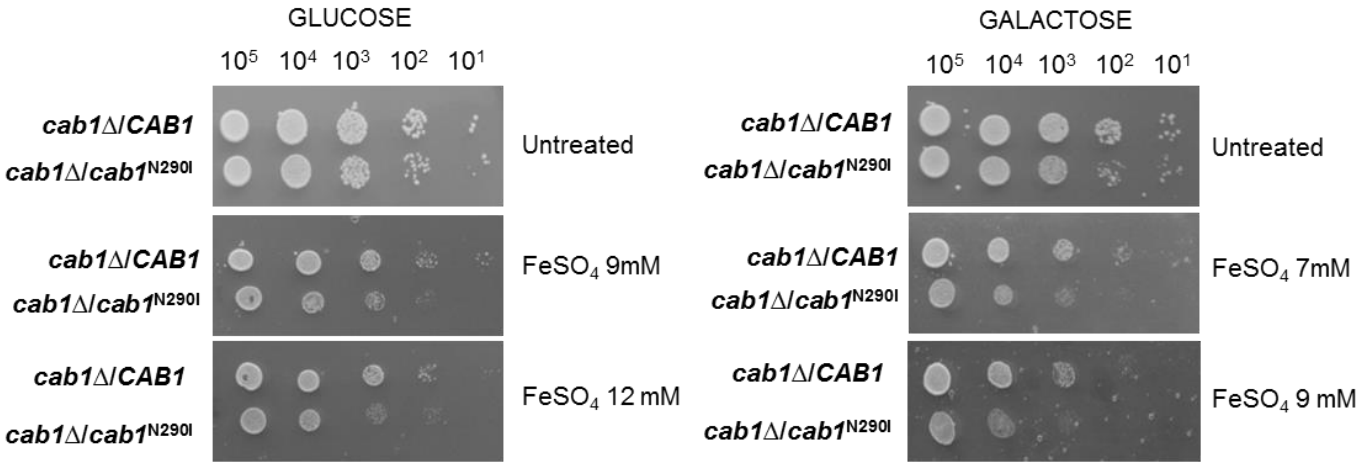

Fig 1.7 Spot assay of *cab1*Δ strain harbouring the pFL39*CAB1* or pFL39*cab1*^{N290I} on YNB DO-TRP 2% glucose (A) or 2% galactose (B), with the addition of 9 and 12mM $FeSO_4$ or 7 and 9mM $FeSO_4$. The growth was scored after 3 days of incubation at 28°C.

To investigate whether the differences observed in response to iron addition were due to an increased content of this ion, we performed a quantitative determination of cellular iron by using a colorimetric assay that relies on the formation of colored iron complexes with BPS after nitric acid digestion of yeast cells. As shown in Fig 1.8 both mutant strains *cab1*Δ/pFL39*cab1*^{G351S} and *cab1*Δ/pFL39*cab1*^{N290I} showed a two-fold increase in iron content with respect to the parental strain.

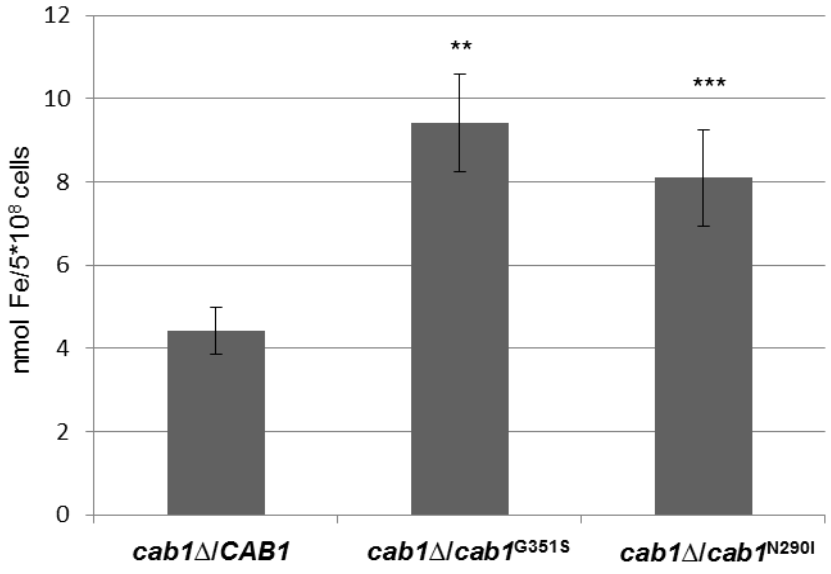

Fig 1.8 Cellular iron levels

It is known that there is a relationship between iron accumulation and the biosynthesis of the cluster Fe-S- a marker of mitochondrial functionality linked to iron metabolism.

For this reason we assayed the activities of the Fe-S enzymes succinate dehydrogenase and aconitase in both mutant strains. The activities, measured on a mitochondrial-enriched fraction and on whole-cell extracts (described in Material and Methods) decreased; in particular in the mutants the decrease of SDH was by 44 and 50%, while for aconitase it was by 26% and 25% , with respect to the wild type (Fig 1.9).

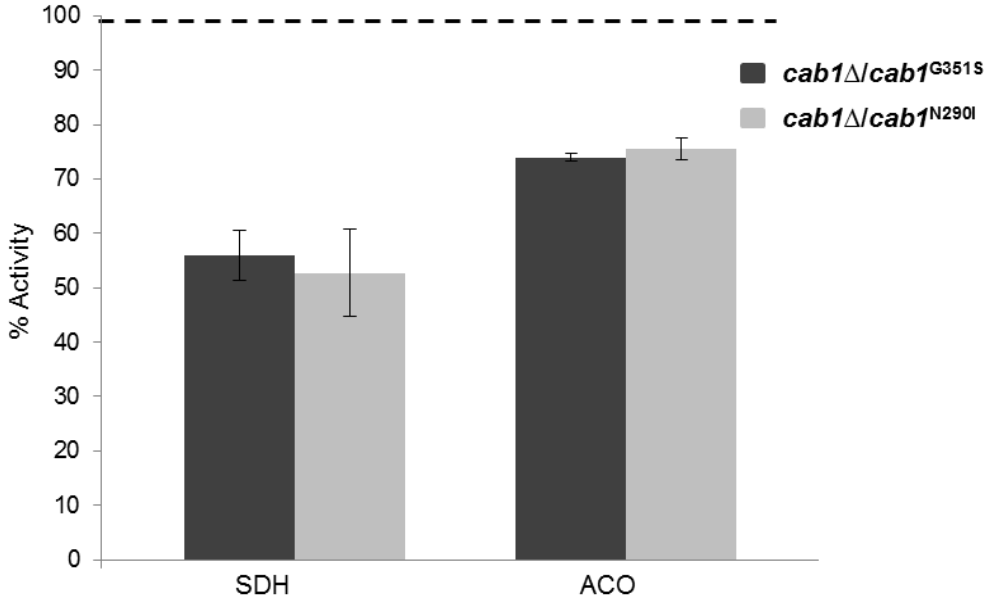

Fig 1.9 SDH and aconitase activities were measured in mitochondrial-enriched fraction and whole-cell extracts from cells grown exponentially at 28°C in YNB DO-TRP medium plus 0,2% glucose and 2% galactose. Each activity was normalized to 100% for the strain transformed with pFL39*CAB1*.

1.3.4 Increased ROS production and oxidative stress in *cab1* mutants

High iron content causes hypersensitivity to oxidative stress (Schilke et al., 1999; Mühlenhoff et al., 2002; Patil et al., 2012), which may cause greater sensitivity to ROS-inducing agents. Using a viability assay, we tested the survival of yeast cells exposed to oxidative stress with hydrogen peroxide. As shown in Fig 1.10 and 1.11 the *cab1*Δ/pFL39*cab1*^{G351S} mutant exhibits increased sensitivity to the ROS-inducing agent H_2O_2, a result consistent with increased oxidative stress.

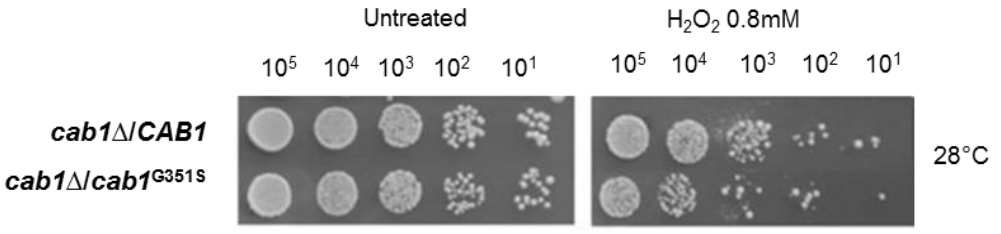

Fig 1.10 Spot assay of *cab1*Δ strain harbouring the pFL39*CAB1* or pFL39*cab1*^{G351S} on YP 2% glucose media after the treatment with 0.8mM H_2O_2 for 4 hours.

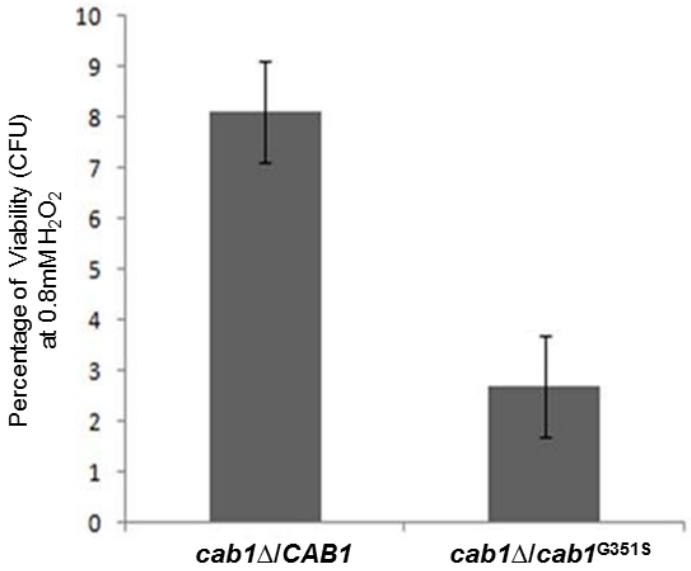

Fig 1.11 Percentage of viability after exposure of cell to 0.8mM H_2O_2.

Quantification of ROS was then performed in the *cab1*Δ/pFL39*cab1*^{G351S} and *cab1*Δ/pFL39*cab1*^{N290I} mutant strains using the dichlorofluorescein diacetate (DCFDA) assay (Marchetti et al., 2006). Inside the cells DCFDA can be oxidized by ROS to dichlorofluorescein (DCF) a fluorescent molecule. 1x 10^7 cells grown up to stationary phase were incubated with DCFDA (20µM) for 30 minutes at 28°C, washed two time, suspended in lysis buffer and broken with glass beads (see Materials and Methods). The fluorescence of the cell extract was measured by the "Tecan SPECTRAR Fluor Plus" system as an indirect read-out of the ROS amount. As shown in Fig 1.12, both the mutant strains show a 3,5 fold increase of ROS with respect to the parental strain.

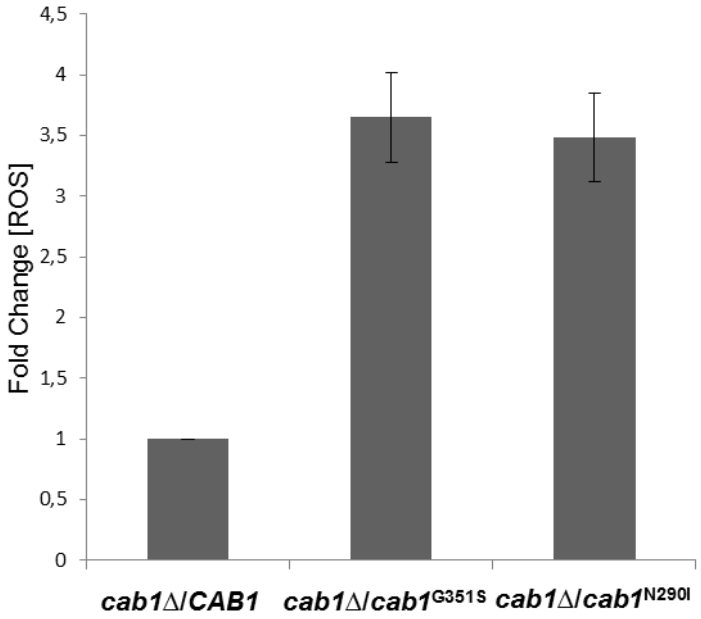

Fig 1.12 Evaluation of ROS content in *cab1*Δ/pFL39*CAB1, cab1*Δ/pFL39*cab1*^{G351S} and *cab1*Δ/pFL39*cab1*^{N290I} grown in YNB DO-TRP 2% galactose media.

One of the consequences of high levels of free radicals or reactive oxygen species is a direct damage to lipids thus leading to impairment of the membrane function. Generally, ROS attack lipids containing carbon-carbon double bond(s) especially polyunsaturated fatty acid (PUFAs), or other targets such as glycolipids, phospolipids and cholesterol (Ayala et al., 2014). When oxidizing agents target lipids, they can initiate the lipid peroxidation process a chain reaction that produces multipe breakdown molecules such as malondialdehyde (MDA) and 4-hydroxynonenal (HNE). MDA is widely used as a convenient biomarker for lipid peroxidation (Boominathan et al., 2003) because of its reaction with thiobarbituric acid (TBA) that produces of a pink pigment with a peak of absorption at 532-535 nm, easly measurable (Esterbauer et al., 1991). To investigated the "lipid status", we therefore measured MDA content in yeast mutant strains after a total cellular extract mixed in TBA containing buffer was incubated for 30 minutes at 95°C of.

The results obtained show a 1,6 and 1,8 fold increase respectively in MDA content in *cab1*Δ/pFL39*cab1*^{G351S} and *cab1*Δ/pFL39*cab1*^{N290I} with respect to the parental strain (Fig 1.13)

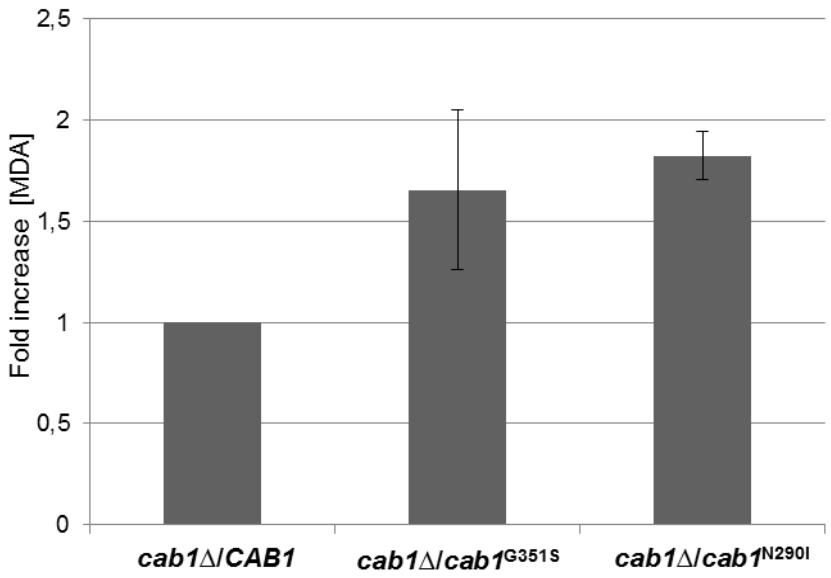

Fig 1.13 The MDA content was measured spectrophotometrically. Values are reported as fold change in content over WT

1.3.5 Content of lipid droplets

Acetyl-Coenzyme A is necessary for the production of a large chemical variety of lipids including neutral lipids which serve as energy reserves and are stored in lipid droplets. We evaluated the content of intracellular lipid droplets in *cab1* mutants by fluorimetric analysis using the fluorescent lipophilic dye Nile Red. The measurements, performed in triplicate, highlighted a reduction of lipid droplets of 49% and 46% in mutant strains when compared to the wild type (Fig. 1.14) suggesting that at least lipid droplet homeostasis is impaired when CoA biosynthesis is impaired.

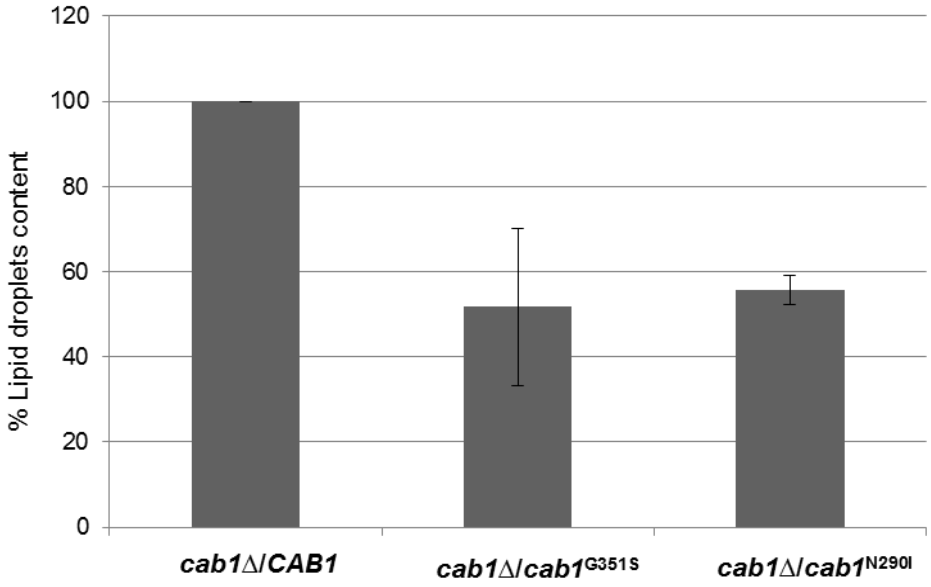

Fig 1.14 The intracellular lipid droplets content has been detected by fluorimetric analysis after incubation of wild type and mutants cells with the fluorescent lipophilic dye Nile Red (4ug/ml).The values corresponding to mutants are expressed as percentage of the content obtained in the wild type strain.

The result obtained in yeast is in agreement with what observed in the *Drosophila* PKAN model (Bosveld et al., 2008) and with the studies of global metabolic profiling in patient-derived fibroblasts revealing an altered lipid metabolism.

1.3.6 Transcriptional analysis of genes involved in lipid and iron metabolism

To better understand the molecular basis of NBIA diseases, Bettencourt and collaborators (2015) investigated NBIA-enriched gene networks. They used whole-transcriptome gene expression data from human brain samples originating from 101 neuropathologically normal individuals (10 brain regions) to generate weighted gene co-expression networks and cluster the 10 known NBIA genes. In this way they found NBIA gene networks enriched in iron-related genes and also in genes involved in lipid metabolism.

The results we obtained from the characterization of pantothenate kinase deficient mutant strains, according to what was observed in the Drosophila PKAN model (Bosveld et al., 2008) and the global metabolic profiling studies in fibroblasts derived from patients (Leoni et al., 2012), showed impaired iron and lipid homeostasis.

Therefore, Real Time transcriptional analysis of genes involved in iron homeostasis and fatty acid metabolism was performed. These experiments were performed only in the strain expressing the pathological variant N290I found in PKAN patients. The wild type and the mutant strain were grown to exponential or stationary phase in YNB DO-TRP medium supplemented with 2% galactose or 0,6% glucose and total RNA was isolated and quantified as described in Materials and Methods. The cDNAs were synthesized and quantitative PCRs were performed (described in Materials and Methods). As internal control we used *ACT1* that encodes structural protein involved in cell polarization. The RNA level of the gene of interest was normalized to *ACT1* levels (described in Materials and Methods).

With regards to the genes involved in lipid metabolism biosynthesis, the expression of *ACS2* and *HFA1* were analyzed. *ACS2* encodes acetyl-CoA synthase, a key enzyme in the pathway leading to cytosolic acetyl-CoA- a key carbon precursor for the synthesis of a large variety of lipids. Pyruvate is first decarboxylated to acetaldehyde which is then converted to acetate and acetyl-CoA by acetyl-CoA synthases.

HFA1 encodes the mitochondrial acetyl-coenzyme A carboxylase which catalyzes production of malonyl-CoA in mitochondrial fatty acid biosynthesis.

As shown in Fig 1.15 the mRNA levels of *ACS2* and *HFA1* in *cab1*Δ/pFL39*cab1* ^{N290I} are about 2,16 and 1.46 fold higher respectively.

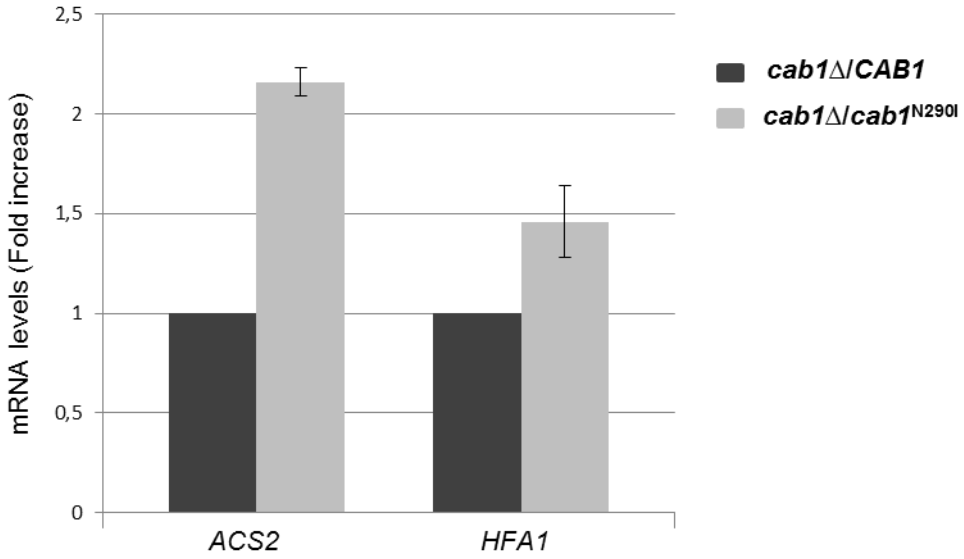

Fig 1.15 The mRNA levels of *ACS2* and *HFA1* genes were quantified by qPCR. Values are reported as fold change in expression over WT. Expression was normalized to the mRNA levels of the internal control *ACT1*.

This result suggests that to counteract the altered lipid content/damage, the mutant cells try to increase the synthesis of the fundamental precursor Acetyl CoA.

It is known that *S. cerevisiae* responds to reduced iron sulfur cluster synthesis by increasing cellular iron uptake and changing intracellular iron re-distribution. To investigate if iron accumulation observed in *cab1*Δ/pFL39*cab1*^{N290I} was due to transcriptional activation of "iron regulon genes" and thus to an increased iron uptake, we investigated the expression level of three key genes: *FET3*, *FTR1* and *FIT3* by RT-qPCR analysis. Fet3p is a Ferro-O_2-oxidoreductase that oxidizes ferrous (Fe2+) to ferric iron (Fe3+) for subsequent cellular uptake by the high affinity iron transporter Ftr1p (Stearman et al., 1996). Ftr1, a transmembrane permease (Bonaccorsi di Patti et al., 2005), accepts Fe^{3+} only from the ferroxidase activity of Fet3p in a process known as iron channeling (Kwork et al. 2006). *FIT3* (facilitator of iron transport) encodes for a cell wall mannoprotein that plays a role in the uptake or utilization of siderophore-iron (Protchenko et al., 2001 and Philpott et al., 2002).

As depicted in Fig 1.16 and 1.17, *FET3*, *FTR1* and *FIT3* are down-regulated both in the exponential and the stationary growth phase. In particular, *FET3* and *FIT3* are down-regulated by about 0,35 and 0,34 fold in the exponential phase. In the stationary phase all three genes are down-regulated by about 0,66 0,41 and 0,99 fold respectively.

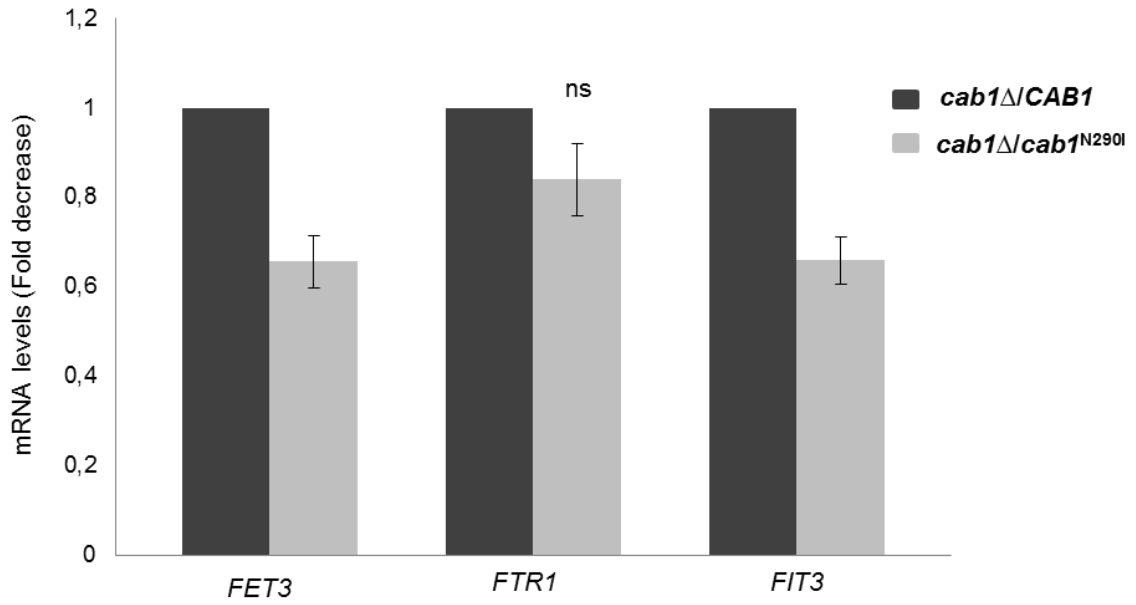

Fig 1.16 The mRNA levels of iron regulon genes were quantified by qPCR from cells grown up to exponential phase. Values are reported as fold change in expression over WT. Expression was normalized to the mRNA levels of the internal control *ACT1*.

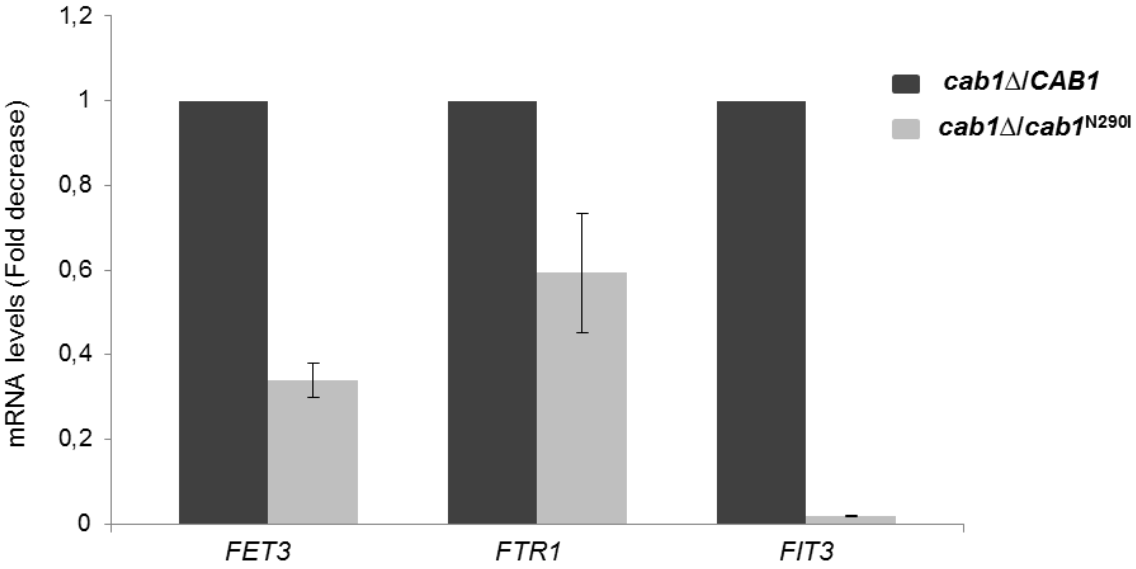

Fig 1.17 The mRNA levels of iron regulon genes were quantified by qPCR from cells grown up to stationary phase. Values are reported as fold change in expression over WT. Expression was normalized to the mRNA levels of the internal control *ACT1*.

This result suggests that iron accumulation in PKAN yeast is not due to an increase in iron uptake. We can hypothesize that the iron which is not correctly utilized for the ISC biosynthesis is then accumulated. The cell responds to this accumulation, limiting the iron uptake thus minimizing its overload.

Results

2. Yeast model of CoPAN disease

2.1 Phenotypic characterization of *cab5*Δ/*COASY*^{R499C}

A yeast model for disease associated to *COASY* mutation, namely CoPAN, has been previously generated. In yeast, the DPCK activity is encoded by *CAB5* gene whose deletion is lethal; both human wt *COASY* or human *COASY* ^{R499C} were able to rescue the Δ*cab5* lethal phenotype. However the mutant strain *COASY* ^{R499C} showed a severe growth defect in the absence of pantothenate, the precursor of the biosynthetic pathway, at the restrictive temperature of 37°C. The results obtained in yeast validated the pathogenicity of the substitution p.Arg499Cys suggesting that the mutant enzyme requires a higher concentration of pantothenate to produce enough CoA to sustain yeast growth. Moreover the CoA level in mitochondria isolated from mutant strain was reduced to 40% respect to wild-type (Dusi et al., 2014).

The evaluation of metabolic consequences of CoA deficiency in this mutant strain was further investigated.

2.1.1 Analysis of OXPHOS metabolism

Given that defective CoA biosynthesis could lead to a variety of metabolic defects including energy metabolism we first looked to mitochondrial function.

In order to reveal a possible respiratory growth defect, serial dilutions of the strains were spotted on mineral medium (40) without pantothenate supplemented with either ethanol or glycerol, at 28°C. As shown in Fig. 2.1A the OXPHOS growth of the *cab5*Δ/*COASY*^{R499C} mutant was partially affected compared to *COASY* wild type expressing strain. To better evaluate the growth delay we determined the cell yield for each yeast strain grown on ethanol or glycerol Fig 2.1B.

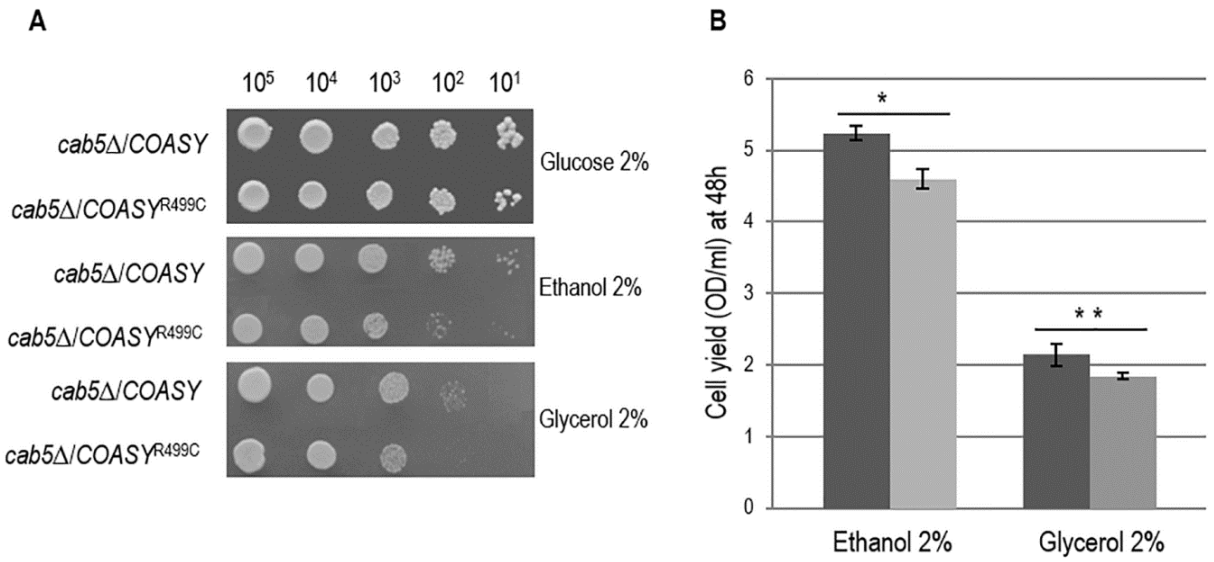

Fig 2.1 (A)Spot assay of *cab5*Δ strain harbouring the pYEX-BX*COASY* or pYEX-BXpFL39*COASY*^{R499C} on mineral medium (40) plus 2% glucose, 2% ethanol or 2% glycerol without pantothenate. The growth was scored after 5 days of incubation at 28°C. (B) Cell yield (OD/ml) at 48H for *COASY* (black columns) and *COASY*^{R499C} (grey columns) grown on ethanol and glycerol. *: p< 0,05 and **<0,01.

To further analyze the respiratory deficiency we measured the oxygen consumption of the mutant strain grown in mineral medium (40) without pantothenate supplemented with either 0,2% glucose and 2% galactose at 28°C. Accordingly to the OXPHOS growth phenotype the oxygen consumption rate of the *cab5*Δ/*COASY*^{R499C} was 25% less than that of *cab5*Δ/*COASY* (Fig 2.2).

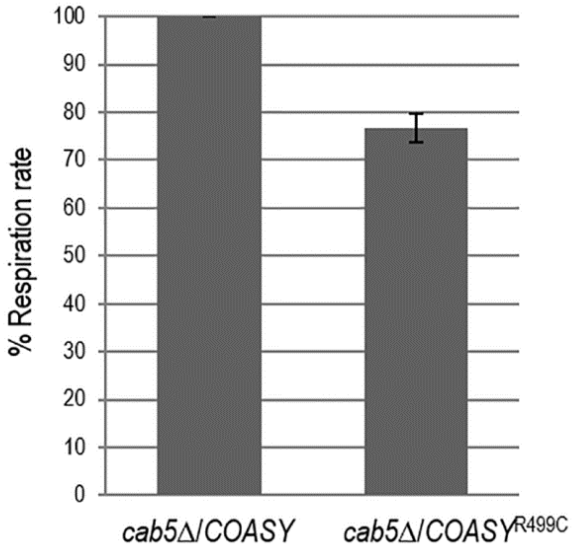

Fig 2.2 Respiratory activity of *cab5*Δ strain harbouring the pYEX-BX plasmid carrying the wild type *COASY* or the mutant *COASY*^{R499C}. Respiratory activity was normalized to 100% for strain transformed with pYEX-BX*COASY*.

On a mitochondrial-enriched fraction of proteins we then measured the enzyme activities of NADH-cytochrome c reductase (NCCR, NADH reductase + CIII) and cytochrome c oxidase (COX, CIV). As shown in Fig 2.3 all the enzyme activities were reduced in the mutant strain respectively to 26% and 42% as compared to wild type. Accordingly, the steady state levels of complex III and IV subunits are decreased (Fig. 2.3). Altogether these results indicate a mitochondrial dysfunction associated to the reduced CoA level.

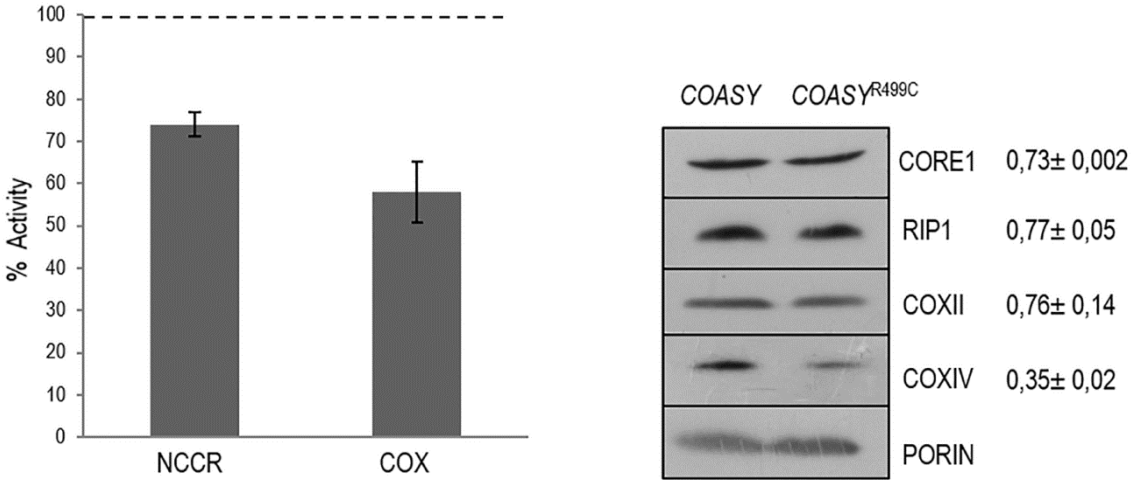

Fig 2.3 Left panel: NCCR and COX activities were measured in mitochondria extracted from cell grown exponentially at 28°C in mineral medium (40) plus 0,2% glucose and 2% galactose without pantothenate. Each activity was normalized to 100% for strain carrying pYEX-BX*COASY*. Right panel: Steady state level of cIII and cIV subunits in cells carrying the wild type *COASY* and the mutant allele. The filter was incubated with specific antibodies against Core1 and Rip1 cIII subunits, CoxII and CoxIV cIV subunits and Porin. The signals were normalized according to the control signal (porin) and taken as 1.00 the signal of the *cab5Δ*/*COASY* (wild type) strain.

2.1.2 Perturbation of iron homeostasis in *COASY* mutant

To assess whether a reduction of CoA in yeast was associated to iron overload we performed some experiments. Since in yeast excessive iron accumulation in the mitochondria led to an increased sensitivity to this ion (Foury and Cazzalini, 1997; Patil et al., 2012) we first evaluated the inhibition of cellular growth of the *COASY*^{R499C} mutant strain by the addition of 5mM and 7mM $FeSO_4$ to the medium. As depicted in Fig. 2.4, the mutant strain showed a clear growth defect when compared to wild type strain indicating, although indirectly, a higher iron content.

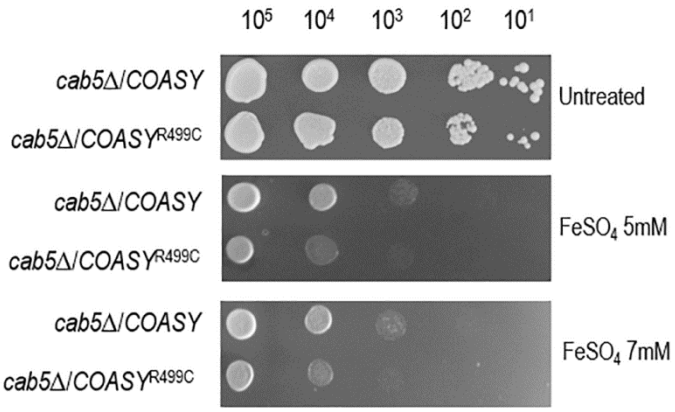

Fig 2.4 Spot assay on *cab5*Δ strain harbouring the pYEX-BX *COASY* or pYEX-BX *COASY*^{R499C} on mineral medium (40) without pantothenate plus 2% glucose, added of 5mM and 7mM $FeSO_4$. The growth was scored after 5 days of incubation at 28°C

To quantify the intracellular iron content we performed the colorimetric assay proposed by Tamarit et al. (2006). 5X10^8 cells of wild type or mutant strains were suspended in nitric acid and incubated over night at 95°C. After incubation, samples were centrifuged and the supernatant was mixed in buffer added of BPS. Non-specific absorbance was measured at 680nm and subtracted from the specific absorbance of the iron-BPS complex (535nm). The results obtained showed a two-fold increase in iron content in the *COASY*^{R499C} mutant respect to the parental strain (Fig 2.5).

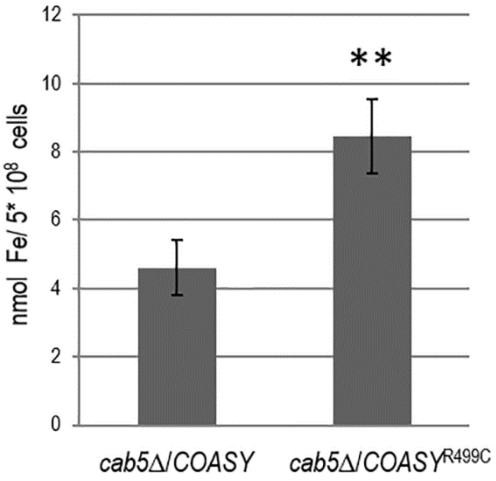

Fig 2.5 Cellular iron levels of cells grown up to early stationary phase in YNB glucose (0,6%) medium. **<0.01 (unpaired two-tailed t-test)

We then investigated whether the biosynthesis of the Fe-S cluster, a marker of mitochondrial functionality linked to iron metabolism (Moreno Cermeño et al., 2010), was affected by COASY deficiency. The activities of two Fe-S cluster enzymes, aconitase and succinate dehydrogenase,

were measured on whole-cell extracts and on mitochondrial-enriched protein fraction (described in Materials and Methods). As shown in Fig 2.6 both the activities were decreased in the mutant as compared to wild type strain; in particular SDH activity was decreased by about 50% and aconitase activity by about 25%.

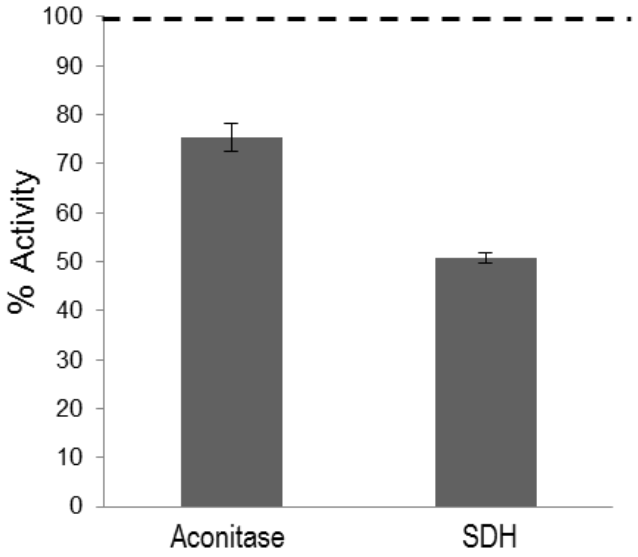

Fig 2.6 Aconitase ad SDH activities were measured on whole cell extracts and on mitochondria extracted from cells grown exponentially at 28°C in mineral medium (40) plus 0,2% glucose and 2% galactose without pantothenate. Each activity was normalized to 100% for strain carrying pYEX-BX*COASY*

2.1.3 Sensitivity to oxidative stress

It is known that an excess of iron increase the oxidative stress (Schilke et al., 1999; Mühlenhoff et al., 2002; Patil et al., 2012) another key feature of disease associated to CoA deficiency (Campanella et al., 2012; Wu et al., 2009; Rana et al., 2010), which may be reflected in hypersensitivity to oxidative stress-induced cell death. To test this hypothesis cells derived from cultures in exponential phase were exposed to 1mM and 2mM H_2O_2 for 4 hours and cell viability was determined by spot assay analysis and by counting the formation of colonies (C.F.U.). After the treatment 10^5, 10^4, 10^3, 10^2, 10^1 cells/spot were plated on YP media plus 2% glucose and the plates were incubated at 28 °C and 37°C. The growth was scored after 48h; as shown in fig 2.7. the mutant showed greater sensitivity to treatment compared to wild type strain at both concentrations tested.

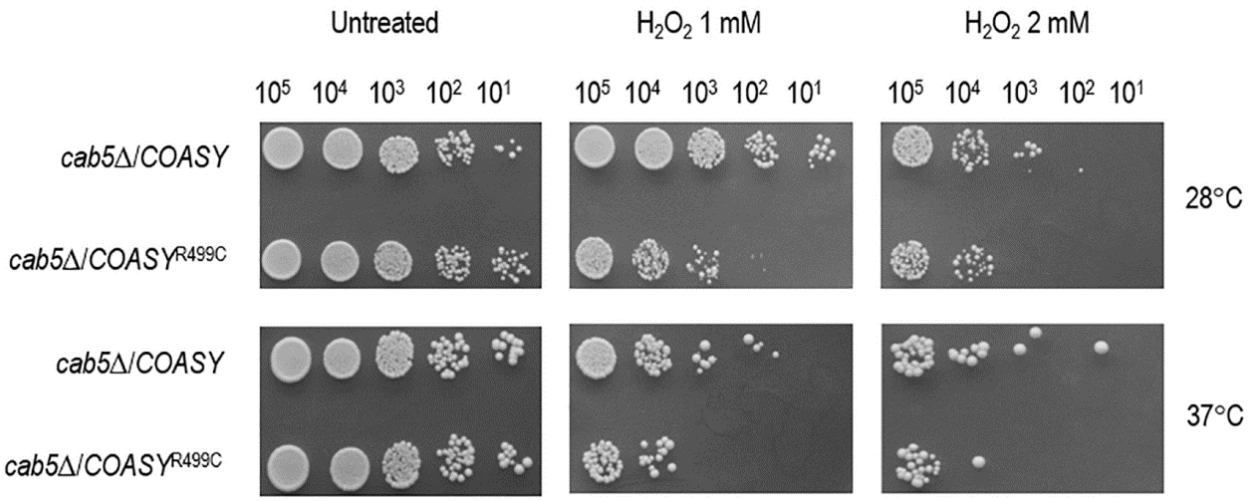

Fig 2.7 Spot assay on *cab5*Δ strain harbouring pYEX-BX*COASY* or pYEX-BX *COASY*^{R499C} on YP 2% glucose media after the treatment with 1mM and 2mM H_2O_2 for 4 hours.

To better quantify H_2O_2 sensitivity, after the treatment with 2mM H_2O_2, an equal amount of cells derived from mutant and wild type strain were plated on YP media and incubated at 28 °C. The cell survival was determined by counting the formation of colonies. At the tested concentration wild type cells showed a viability of 10%, while mutant cells showed a viability of 2% demonstrating that a COASY defect leads to oxidative stress susceptibility (Fig 2.8).

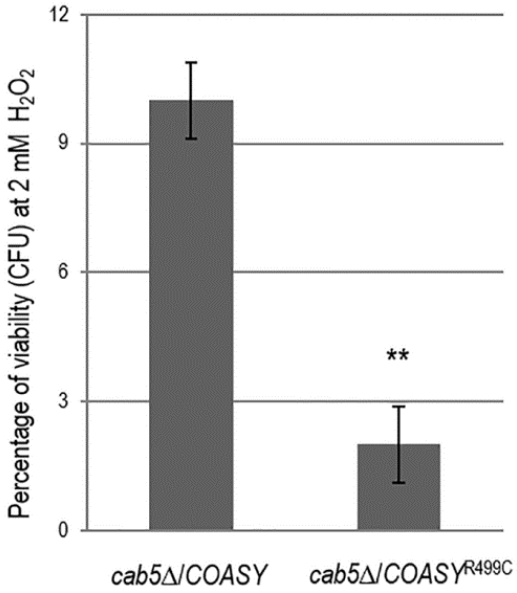

Fig 2.8 Percentage of viability after exposure of cell to 2mM H_2O_2. Count the formation of colonies after three days. **<0.01 (unpaired two-tailed t-test).

2.1.4 Content of lipid droplets

Acetyl-CoA is necessary for the production of neutral lipids, which serve as power reserve for the cell and are stored in lipid droplets. In man and in model organisms has been observed that a deficiency of CoA leads to alterations in lipid metabolism (Bosveld et al., 2008; Leoni et al., 2012; Brunetti et al., 2014). Since it is known that the mutant *cab5*Δ/*COASY*^{R499C} shows a 40% reduction of coenzyme A (Dusi et al., 2014) we evaluated the content of intracellular lipid droplets in the mutant compared to the wild type by fluorescence microscopy and fluorimetric analysis. These analysis were performed using the fluorescent lipophilic dye Nile Red. As shown in Fig. 2.9 the content of lipid droplets is decreased in the mutant expressing the *COASY*^{R499C}. To better quantify this reduction the fluorescence of cells stained with Nile Red was measured using a fluorescence spectrometer. The measures, performed in triplicate, highlighted a reduction of lipid droplets of 25% in mutant strain compared to wild type (Fig. 2.9).

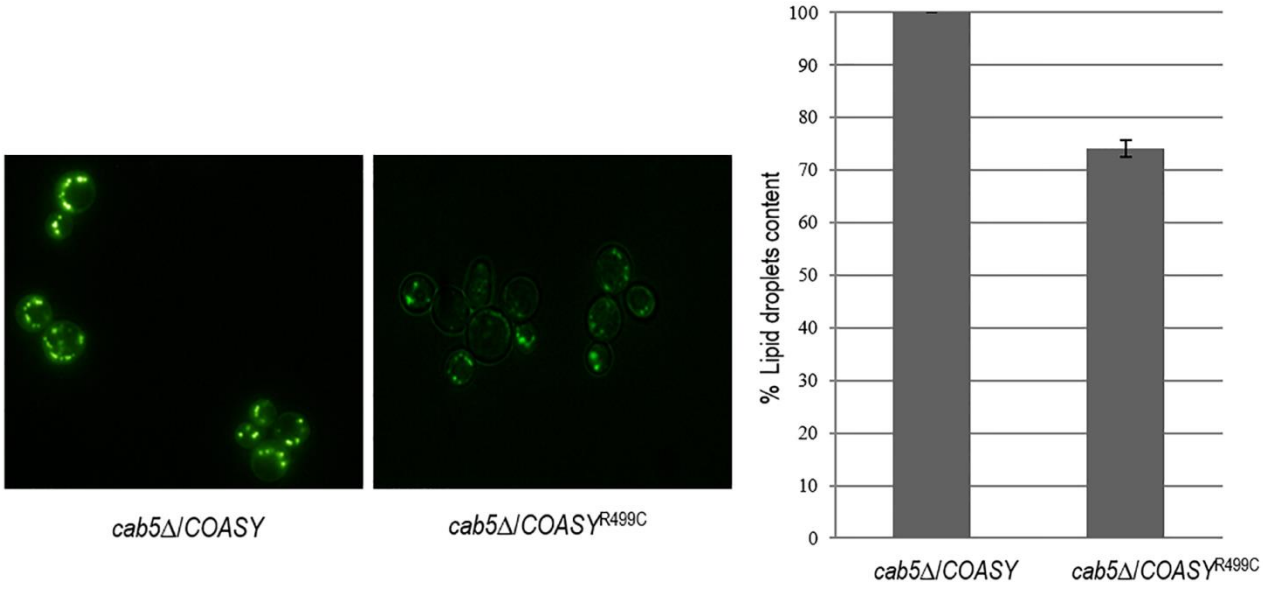

Fig 2.9 The intracellular lipid droplets content has been detected by fluorescence microscopy (left panel) and fluorimetric analysis (right panel) after incubation of wild type and mutant cells with the fluorescent lipophilic dye Nile Red (4ug/ml).The values corresponding to mutant *COASY* are expressed as percentage of the content obtained in the wild type strain.

2.1.5 Treatment with lipoic acid

Schonauer et al., suggested that a low availability of acetyl-CoA causes a deficit in mitochondrial fatty acid (mtFAS) synthesis lipoic acid (LA) included. This would contribute to the deficit of mitochondrial function, particularly of the respiratory activity (Schonauer et al., 2009). In fact, lipoic acid is a sulfur-containing cofactor required for the function of several multienzyme

complexes including the pyruvate dehydrogenase (PDH), the α-ketoglutarate dehydrogenase (α-KDH) and the glycine cleavage system (GC). We wondered whether the addition of lipoic acid to the growth medium could have beneficial effect on the growth of *COASY*^{R499C} mutant. As previously demonstrated this mutant shows a "growth retarded" phenotype in the absence of pantothenate at 28°C; therefore the growth in the same condition with the addition of 30 µM lipoic acid in the medium was tested. As show in Fig 2.10 the lipoic acid rescues the mutant defect.

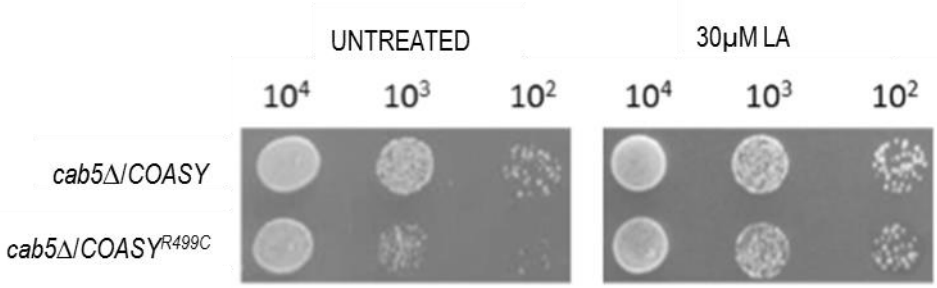

Fig 2.10 Spot assay on *cab5*Δ strain harbouring the pYEX-BX*COASY* or pYEX-BX *COASY*^{R499C} on mineral medium (40) plus 2% glucose without pantothenate added of 30µM acid lipoic (LA). The growth was scored after 2 days of incubation at 28°C

Then we measured the oxygen consumption of the mutant grown in the presence of lipoic acid. In this condition the respiratory activity of the mutant strain was similar to that of the wild type strain (Fig 2.11).

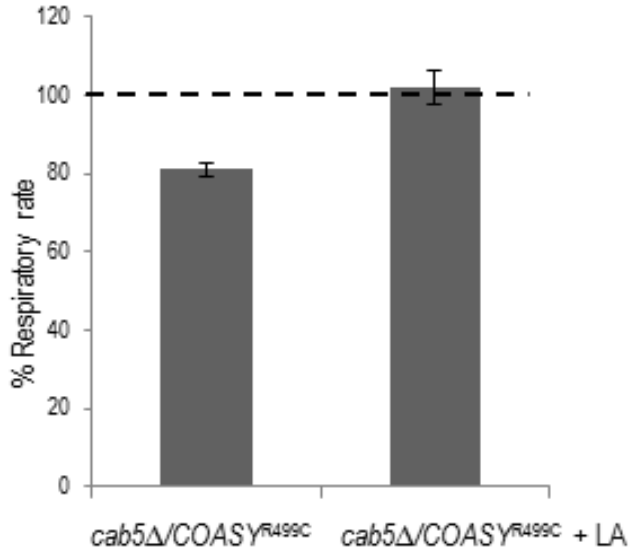

Fig. 2.11 Respiratory activity of *cab5*Δ/*COASY*^{R499C} grown in absence or presence of acid lipoic (LA) . Respiratory activity was normalized to 100% for strain carrying pYEX-BX*COASY*.

Although the mechanism by which lipoic acid is able to "rescue" the respiratory activity is not clear we can hypothesize that the increase of respiratory activity after the addition in the medium of LA could be due to the lipoylation of the E2 subunits of PDH complex and α-KDH. Moreover since it is known that lipoic acid could act as an antioxidant and chelating metal ion (Petersen Shay et al., 2008), the "rescue" could be ascribed to a decreased oxidative stress.

Results described in this section have been published in:

Ceccatelli Berti C, Dallabona C, Lazzaretti M, Dusi S, Tosi E, Tiranti V, Goffrini P. Modeling human Coenzyme A synthase mutation in yeast reveals altered mitochondrial function, lipid content and iron metabolism. Microbial Cell 2015, Vol. 2, No. 4, pp. 126 - 135.

Results

3. Search for chemical suppressors of *PANK* mutations

3.1 Search for chemical suppressors of *PANK* mutations

As reported in the Introduction, Pantothenate kinase-associated neurodegeneration is a very severe disorder for which only symptomatic treatments were available, although the therapeutic effect of exogenous CoA administration in reverting pathological phenotypes in PKAN-derived neurons has been very recently demonstrated (Orellana et al., 2016).

In the last years, yeast has proved to be a good model for high-throughput screening (HTS) in drug discovery. HTS has been defined as "the process of assaying a large number of potential effectors of biological activity against targets (a biological event)" (Armstrong J.W, 1999) ant its goal is to accelerate drug discovery by screening large libraries often composed of thousands of compounds. The results obtained in this work demonstrated that both yeast mutant strains *cab1*Δ/pFL39*cab1*^{G351S} and *cab1*Δ/pFL39*cab1*^{N290I} give rise to the most important phenotypes found in PKAN patients: mitochondrial dysfunction, altered lipid metabolism, iron overload and oxidative damage.

In order to find molecules with a potential therapeutic activity for PKAN treatment, a screening of the Selleck chemical library (http://www.selleckchem.com/screening/fda-approved-drug-library.html) has been performed taking advantage of the OXPHOS negative phenotype of the strains expressing pathological alleles Gly351Ser and Asn290Ile. The "Drug drop test" technique (Couplan et al., 2011) as described in Material and Methods was used.

3.1.1 Determination of optimal screening conditions and choice of the strain

The screening was performed on YP medium in fact it is known that, in general, the molecules appear to be less bio-available in synthetic medium, maybe due to their interaction with the saline components of the medium. In order to evaluate the ability of the drugs to rescue the respiratory defect of the mutant strain and to avoid a great number of false-positives, it is fundamental to define the optimal conditions by which the screening has to be performed. For this reason all the preliminary analyses were performed in both mutant strains characterized, focusing on three different parameters: the carbon source, the incubation temperature and the number of cells to spread on the plates. With regards to the oxidative carbon source, glycerol and ethanol were tested and, after several experiments (data not shown), we decided to use ethanol because of the lowest background growth observed. When different cell concentrations (1-2-4-8*10^5 cell/plate) were plated we observed that the 4*10^5 cell/plate an intermediate concentration between 2*10^5 cell/plate (low cells number for rescue visualization) and 8*10^5 cell/plate (elevated background

growth) was the best one. Finally we tested two temperatures 36°C and 37°C and we fixed 37°C as the optimal incubation temperature. On the basis of all the results obtained we decided to perform the screening in the mutant strain *cab1*Δ/pFL39*cab1*^{G351S} and to observe the following parameters:

Cells/plate	$4*10^5$
Temperature	37°C
Carbon source	Ethanol
Positive control	*cab1*Δ/*CAB1*

Table 3.1 Scheme of the condition chosen for the screening

3.1.2 Screening of *Selleck FDA-approved Drug Library*

Selleck FDA-approved Drug Library is a collection of 1018 FDA-approved drugs. These molecules are structurally diverse, medicinally active and cell permeable. All compounds have been approved by the FDA and their bioactivity and safety were confirmed by clinical trials. Every compounds is also accompanied by a rich documentation concerning its chemical structure, IC50 and customer reviews. In addition, NMR and HPLC have been performed for each drug to ensure high purity. This *chemical library* contains drugs related to oncology, cardiology, anti-inflammatory, immunology, neuropsychiatry, analgesia, etc. (http://www.selleckchem.com/screening/fda-approved-drug-library.html)

Compounds are solubilized in DMSO at the final concentration of 10mM and organized in 96well plates. In each plate set up for the screening (seed with $4*10^5$ cells of *cab1*Δ/pFL39*cab1*^{G351S} mutant) 31 filters were placed, one was used for the negative control (DMSO) and a central spot for the positive control (*cab1*Δ/pFL39*CAB1).* 2.5 µl of every molecules of the chemical library (at a final concentration of 10mM in DMSO) were spotted onto the remaining 30 filters. In this way we could test 30 different molecules in each plate. The plates were incubated at 37°C and the growth of the *cab1*Δ/pFL39*cab1*^{G351SI} mutant was monitored for 7 days.

Out of 1018 compounds tested about 21 were classified as active and were tested in a secondary screening in order to counter-select false positive compounds. In the secondary screening we used the same conditions described for the primary screening except for the number of filters placed on

each plate. In this screening each plate contained only three equidistant filters: one of them was used for the negative control (DMSO) and the others were spotted with two different compounds to test. Molecules of class 1, leading to an enhanced halo of growth were spotted at the same concentration used in primary screening (2.5µl). Molecules of class 2, leading to a halo of no growth plus a halo of growth were tested at a lower concentration (1-1.5 µl), depending on the size of the halo of no growth observed in the primary screening. In fig 3.1 an example of secondary screening is reported.

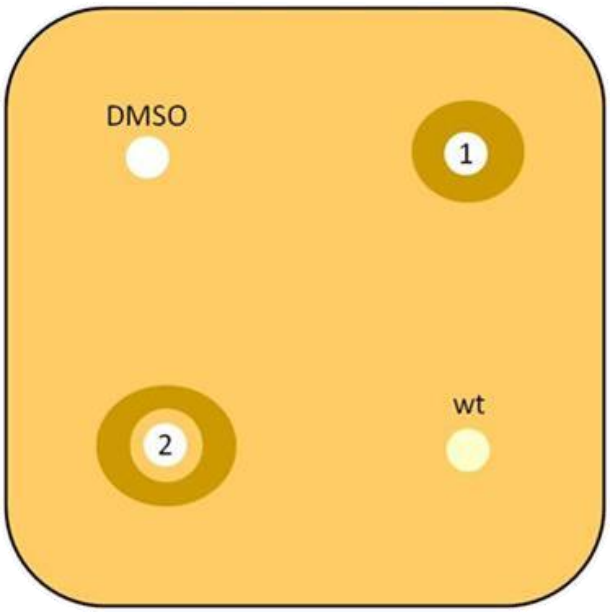

Fig 3.1 Graphic representation of a plate set up for secondary screening.

In this secondary screening 8 molecules re-confirmed their ability to rescue the growth defect of *cab1*Δ/pFL39*cab1*^{G351SI} mutant strain and were classified as active (Fig 3.2). The compounds found to be inactive were classified as false-positives.

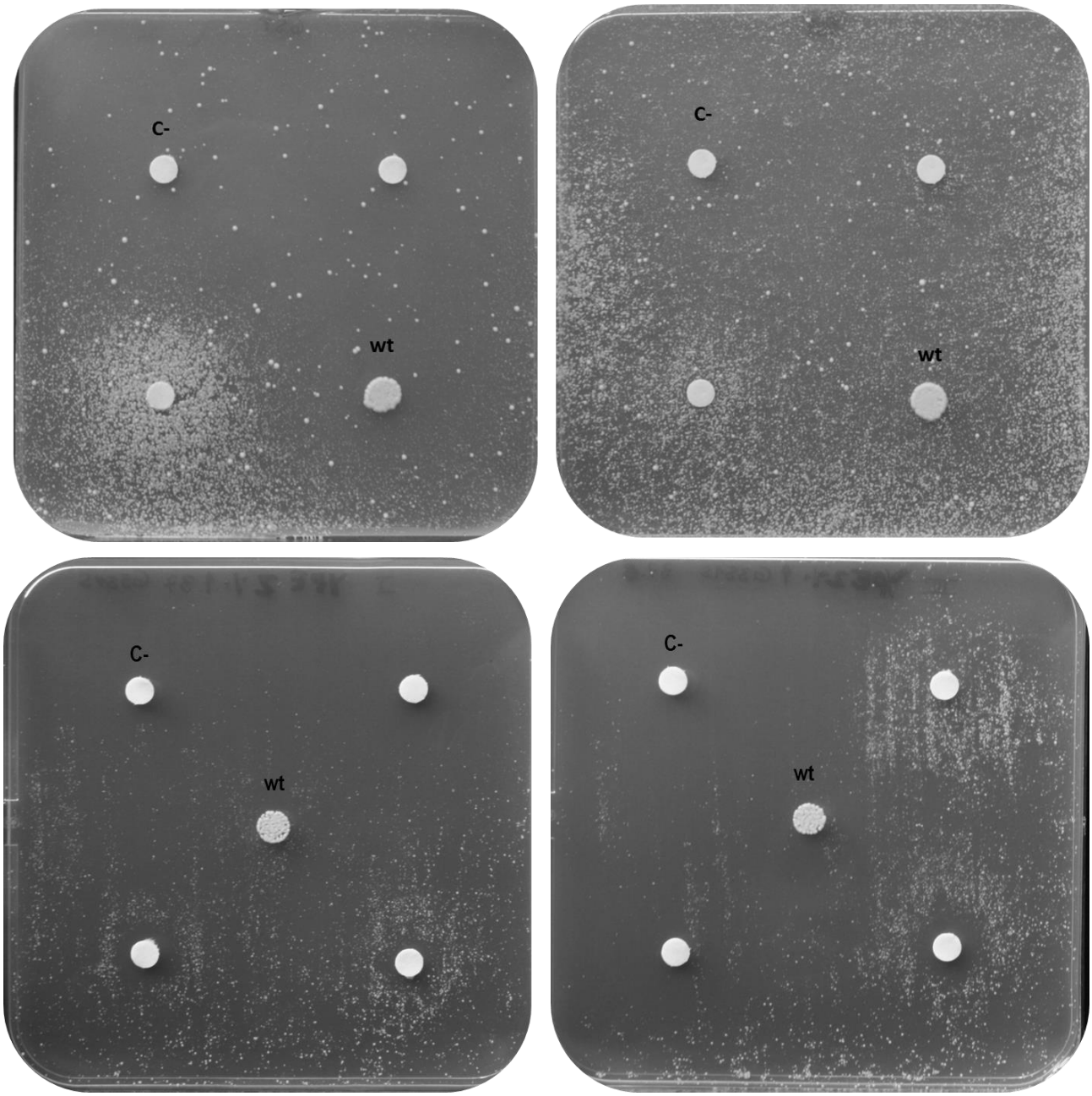

Fig 3.2 Photo of some molecules that re-confirmed their beneficial effect while others, classified as a false-positive, did not re-confirm their activity. C-:DMSO. The growth was scored after 5 days of incubation at 37°C.

These 8 drugs were then tested for their ability to rescue the growth defect of *cab1*Δ/pFL39*cab1*^{N290I} and we identified 4 active molecules named with the conventional name *Selleck* CRM (**C**AB1 **R**escue **M**olecules) 1-4. In table 3.2 a summary of the 4 molecules with their action and a small description was reported.

Drugs	Phenotype	Growth Intesity	Description
CRM1	Inhibition+ Growth	+	It is an antibiotic agent. Primarily inhibits the growth of Gram-positive and some Gram-negative bacteria. Shows bacteriostatic, fungistatic and antiprotozoal effects *in vivo.* It is use as antiseptic or disinfectant.
CRM2	Growth	+++	It is effective primarily against gram-negative bacteria, with minor anti-gram-positive activity. It has historically been used for treating urinary tract infections, caused, for example, by *Escherichia coli*. It selectively and reversibly blocks DNA replication inhibit a subunit of DNA gyrase and topoisomerase IV and induce formation of cleavage complexes.
CRM7	Inhibition+ Growth	+	It is a typical antipsychotic drug belonging to the phenothiazine drug group and was previously widely used in the treatment of schizophrenia and psychosis.
CRM8	Growth	+	It is a dopamine (D_2) receptor antagonist that belongs to the phenothiazine class of antipsychotic agents that are used for the antiemetic treatment of nausea and vertigo.

Table 3.2 Summary of the active molecules

The CRM1 and CRM2 drugs were further evaluated for their ability to rescue the other phenotypes associated to CoA deficiency since they were found to be the most effective in both mutant strains and at both 28 and 37° C.

3.1.3 Research of drugs optimal concentration able to revert OXPHOS defect

To identify the CRM-optimal concentration able to rescue the growth defect of *cab1*Δ/*cab1*^{N290I} we performed a growth test in liquid medium. The same cell concentrations of mutant and wild type strains were inoculated in YNB DO-TRP medium plus ethanol 2% and containing different concentrations of each molecule. We monitored the growth for four days at 28°C by measuring the increase of the optical density OD_{600}. For both molecules the initial concentration was chosen in relation to their solubility. For CRM1 we used 10 different concentrations starting from the highest 1µM while for CRM2 we used 20 different concentrations starting from 128 µM. Since the compounds are solubilized in DMSO, we also ensured that this solvent does not affect the growth. The cell yield at 48h showed that CMR1 was able to reduce the growth defect starting from the concentration of 0,0625 µM and was able to cancel it at 1 µM (Fig 3.3). For this reason, we used 1 µM CRM1 for the subsequent analyses.

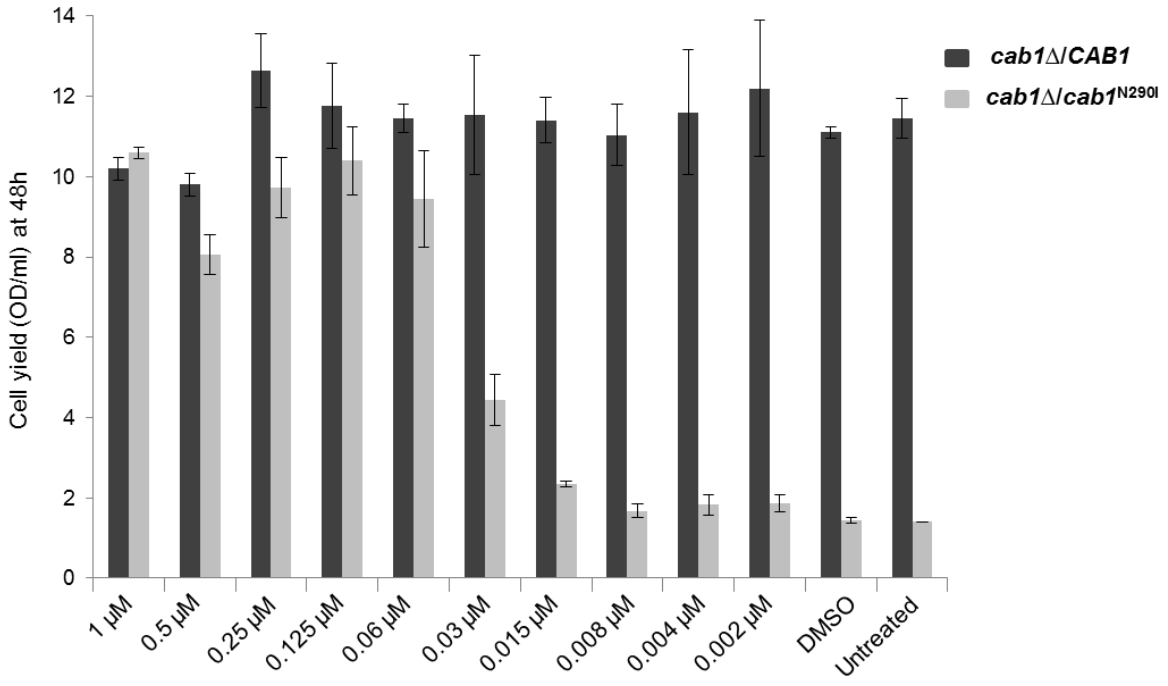

Fig 3.3 Cell yield (OD/ml) at 48h of *cab1*Δ/pFL39*CAB1* (black columns) and *cab1*Δ/pFL39*cab1*^{N290I} (grey columns) grown in YNB DO-TRP medium plus 2% ethanol and DMSO or 10 different concentration of CRM1.

In the presence of CRM2 the mutant growth defect was reduced in the range of concentrations between 0,5 µM and 32 µM (Fig 3.4). For the subsequent analyses we chose the intermediate concentration of 4 µM.

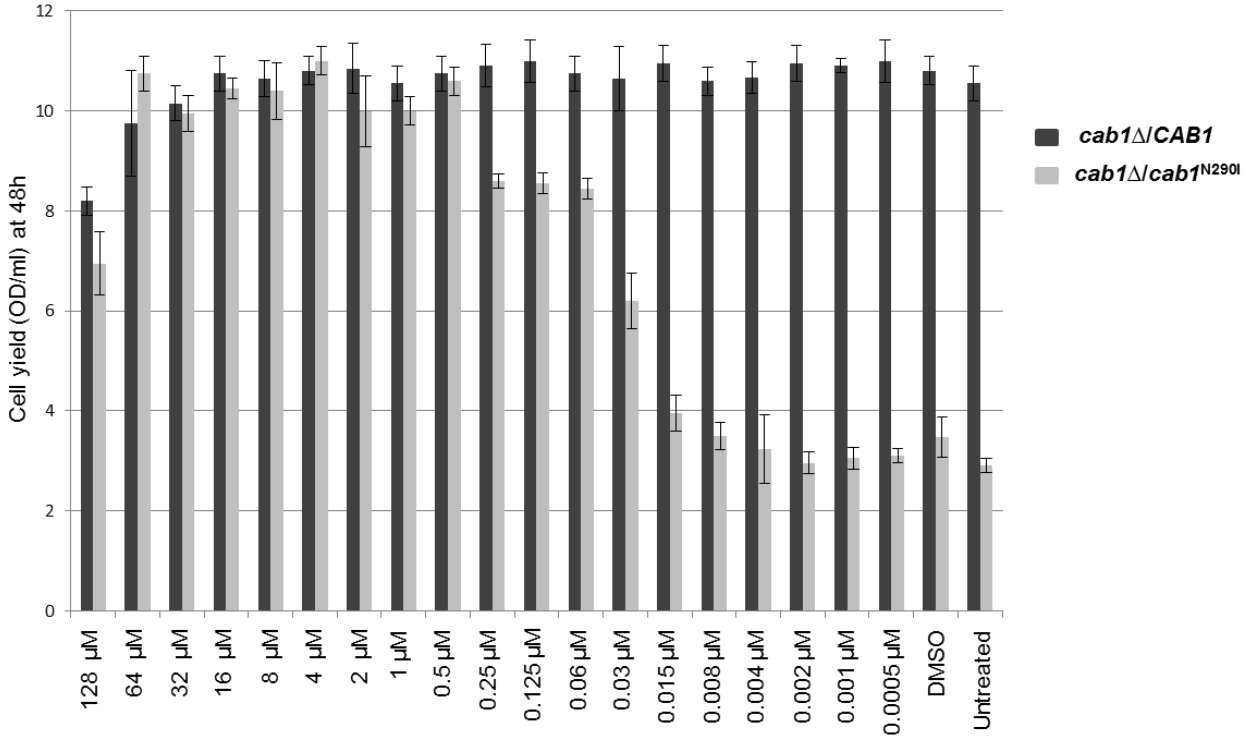

Fig 3.4 Cell yield (OD/ml) at 48h of *cab1*Δ/pFL39*CAB1* (black columns) and *cab1*Δ/pFL39*cab1*^{N290I} (grey columns) grown in YNB DO-TRP medium plus 2% ethanol and DMSO or 19 different concentration of CRM2.

3.2 Analysis of CRM-rescuing effects on the *cab1*Δ/*cab1*^{N290I} mutant strain

3.2.1 Mitochondrial function

We further investigated whether the rescue of *cab1*Δ/*cab1*^{N290I} OXPHOS growth defect by CRM1 and CRM2 was related to an improved mitochondrial function. We then measured the oxygen consumption rate of *cab1*Δ/*cab1*^{N290I} grown in galactose 2% at 28°C with or without 1µM CRM1 or 4µM CRM2. The respiratory activity of mutant strain grown in presence of both CRM drugs was similar to the wild type strain (Fig 3.5).

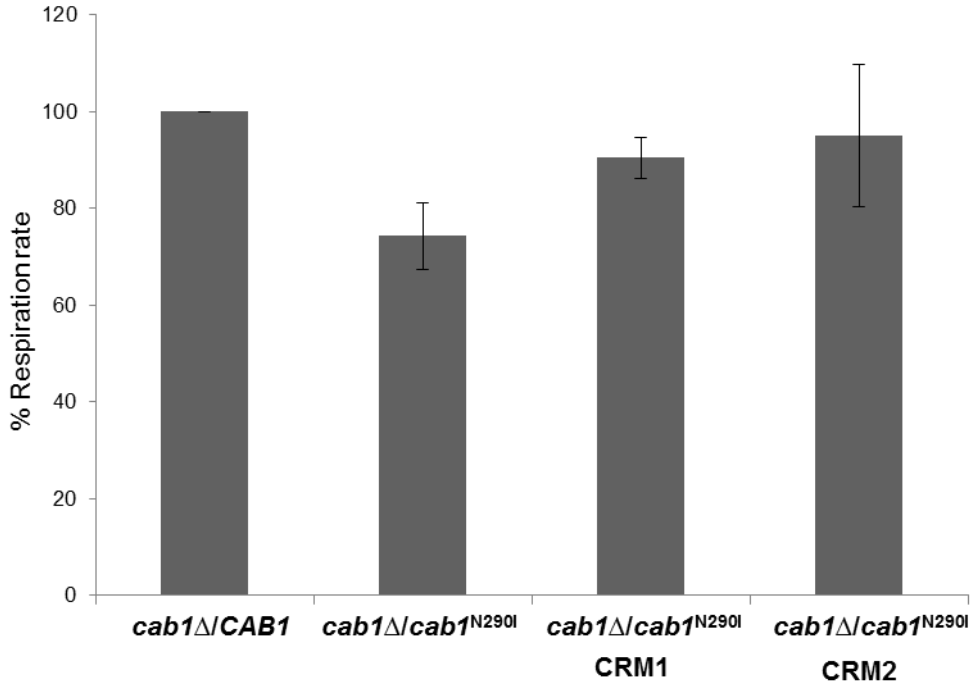

Fig 3.5 Oxygen consumption of *cab1*Δ/pFL39*CAB1* and *cab1*Δ/pFL39*cab1*^{N290I} mutant strain grown in the presence or absence of CRM1 or CRM2 at 28°C in YNB DO-TRP medium plus 2% galactose.

We later analyzed the activities of mitochondrial respiratory complexes (NCCR, SQDR and COX) in cells grown in 0,2% glucose and 2% galactose with or without CRM1/CRM2. As shown in Fig 3.6, 3.7 and 3.8 the addition of CRM1 or CRM2 in the growth medium increased the activity of mitochondrial complexes.

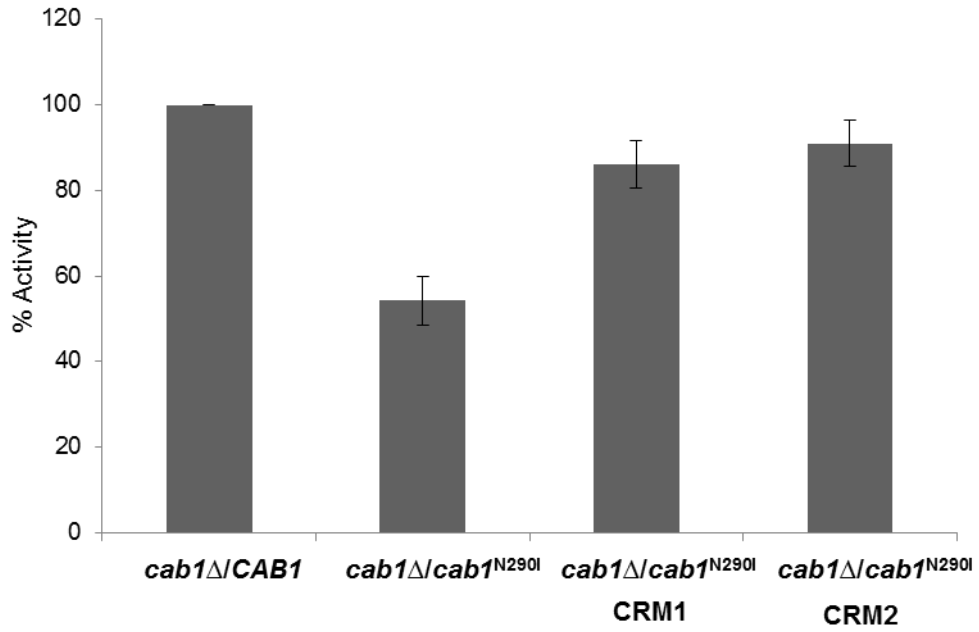

Fig 3.6 NCCR activity was measured in mitochondria extracted from cells grown exponentially at 28°C in YNB DO-TRP medium plus 0,2% glucose and 2% galactose with or without CRM1/CRM2. Each activity was normalized to 100% for strains containing pFL39*CAB1*

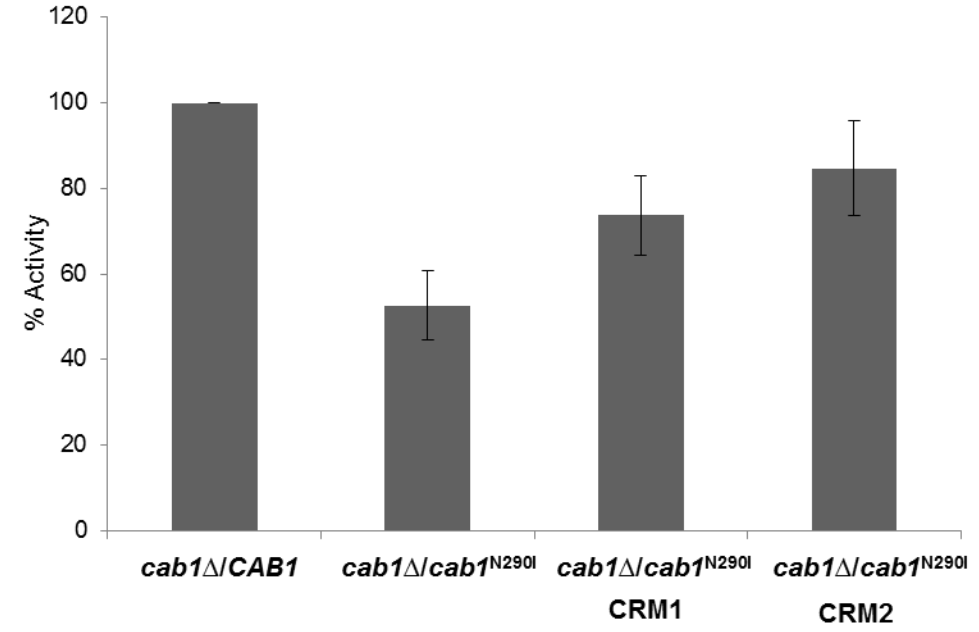

.

Fig 3.7 SDH activity was measured in mitochondria extracted from cells grown exponentially at 28°C in YNB DO-TRP medium plus 0,2% glucose and 2% galactose with or without CRM1/CRM2. Each activity was normalized to 100% for strains containing pFL39*CAB1*

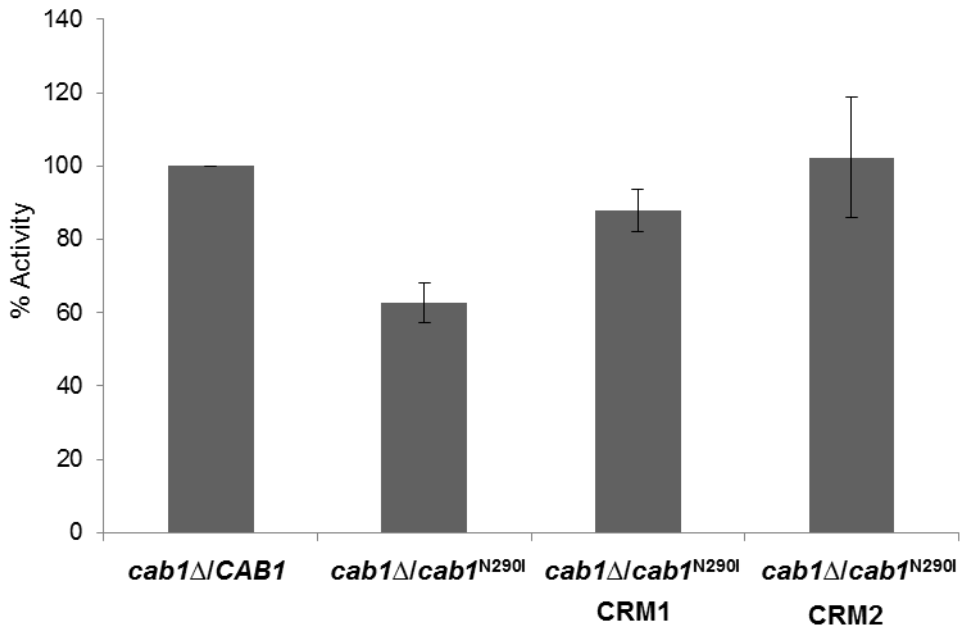

Fig 3.8 COX activity was measured in mitochondria extracted from cells grown exponentially at 28°C in YNB DO-TRP medium plus 0,2% glucose and 2% galactose with or without CRM1/CRM2. Each activity was normalized to 100% for strains containing pFL39*CAB1*

3.2.2 CRM1

CRM1 is 5,7 dichloro-8 hydroxyquinoline (CQ_{Cl}) (Fig 3.9), a heterocycle compound belonging to the quinoline family with 8-hydroxyquinoline (8HQ) being its precursor. This latter lipophilic compound has several bioactivity: antimicrobial activity, anticancer activity, anti-inflammatory activity, antioxidant activity, antineurodegenerative activity, etc.. Most bioactivities of 8HQ and its derivatives are due to their metal chelating ability; for example the antimicrobial activity is dependent on the concentration and lipophilicity of the compound (to penetrate bacterial cell membranes) and hence, on its ability to bind metals of bacterial enzymes (Prachayasittikul et al.,2013).

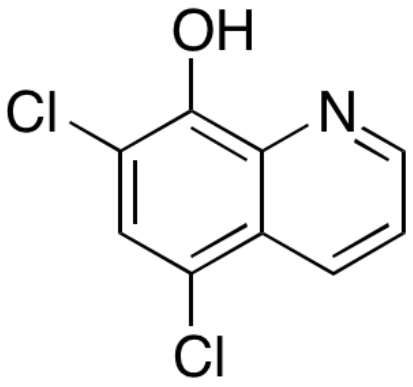

Fig 3.9 Structure of 5,7 dichloro-8 hydroxyquinoline

CQ_{CL} has also been reported to have an antimicrobial activity as well as anti-dental plaque activity. This compound could be used via a polyethylene glycol vehicle as an ointment or additive ingredient in dentifrice to control dental disease (Tanzer et al., 1978). In addition, it is able to bind metals such as copper, zinc and iron (Matlack et al., 2014).

3.2.3 CRM2

CRM2 is nalidixic acid (nalH) the first of the synthetic quinolone antibiotics, a large group of synthetic antibacterials very active against aerobic Gram-negative microorganism. Since the introduction of nalH into clinical practice in the early 1960s, a number of structurally related, highly potent, broad-spectrum anti-bacterial agents have been isolated (Turel 2002). Nalidixic acid is based on a 4-oxo-1,8-naphthyridin-3-carboxylic acid nucleus (Fig 3.10) and the derived new compounds retain several structural features of this nucleus.

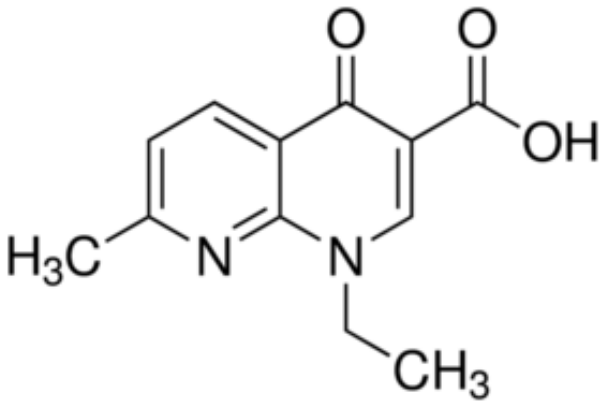

Fig 3.10 Structure of nalidixic acid

These antibiotics block DNA replication in a selective and reversible mode. They inhibit a sub-unit of DNA gyrase and.topoisomerase IV and induce formation of cleavage complexes (Pommier et al., 2010). In addition, the quinolones are able to assemble a complex with various metal cations together with iron, copper, zinc, aluminum, calcium and magnesium. These molecules can coordinate the metals through carboxylic oxygen and an adjacent 4-keto oxygen.

3.2.4 Iron level, ROS content and lipid peroxidation

The characteristic shared by both molecules, CQ_{CL}/nalH, is the ability to bind bivalent ions including iron (Turel 2002; Matlack et al., 2014). Therefore we hypothesize that their rescuing ability could be due to this ability and for this reason intracellular iron content was determined by means of the colorimetric BPS assay. As shown in Fig. 3.11 and 3.12 both molecules reduced the

iron content and in fact the mutant strain showed an iron level similar to wild type grown under the same conditions.

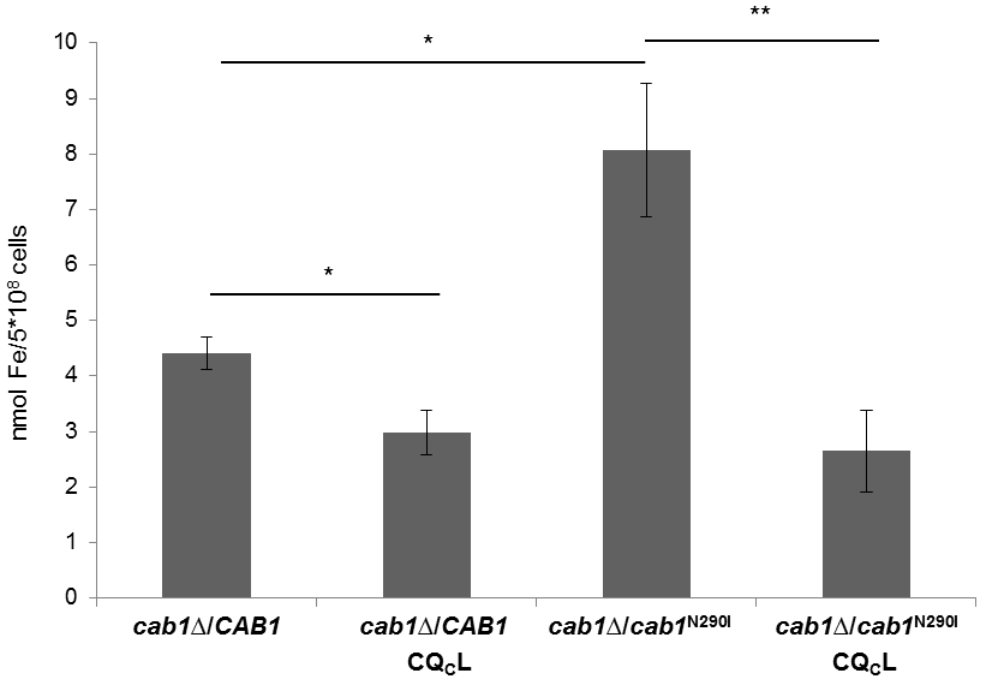

Fig 3.11 Cellular iron levels in *cab1*Δ/pFL39*CAB1* and *cab1*Δ/pFL39*cab1*^{N290I} mutant strain grown with CQ_{CL} at 28°C in YNB DO-TRP medium plus 2% galactose.

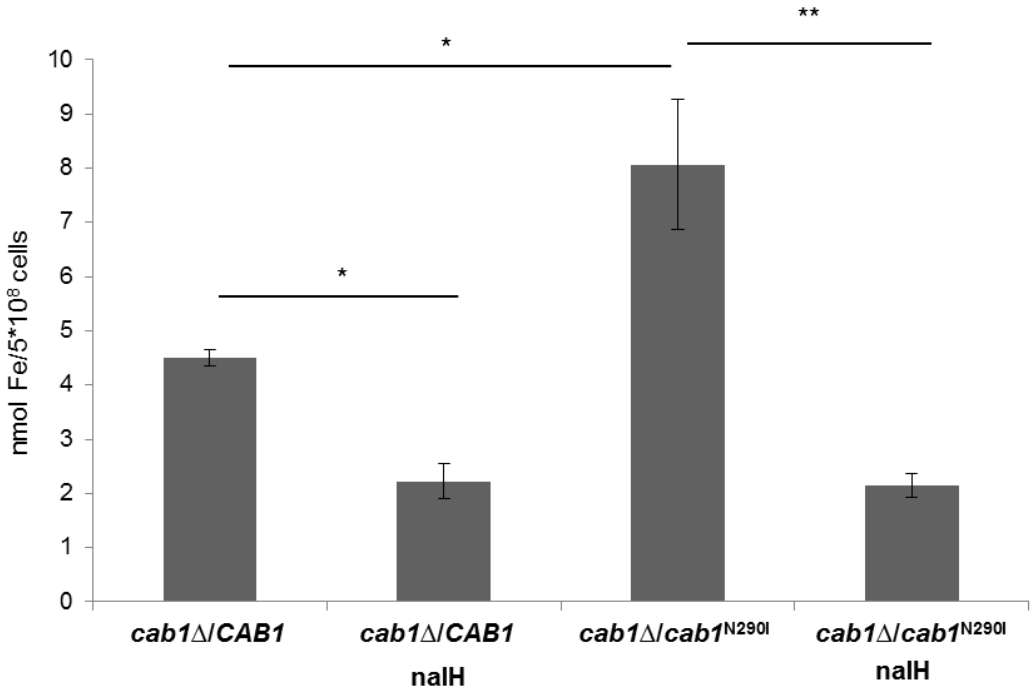

Fig 3.12 Cellular iron levels in *cab1*Δ/pFL39*CAB1* and *cab1*Δ/pFL39*cab1*^{N290I} mutant strain grown with nalH at 28°C in YNB DO-TRP medium plus 2% galactose.

We then evaluated the ability of both drugs to decrease the content of ROS. To this aim we measured the ROS content in cells grown with or without the molecules. The results obtained (Fig 3.13) showed that the 3.5 fold increase of ROS displayed by the mutant strain was significantly reduced in the presence of CQ_{CL} or nalH.

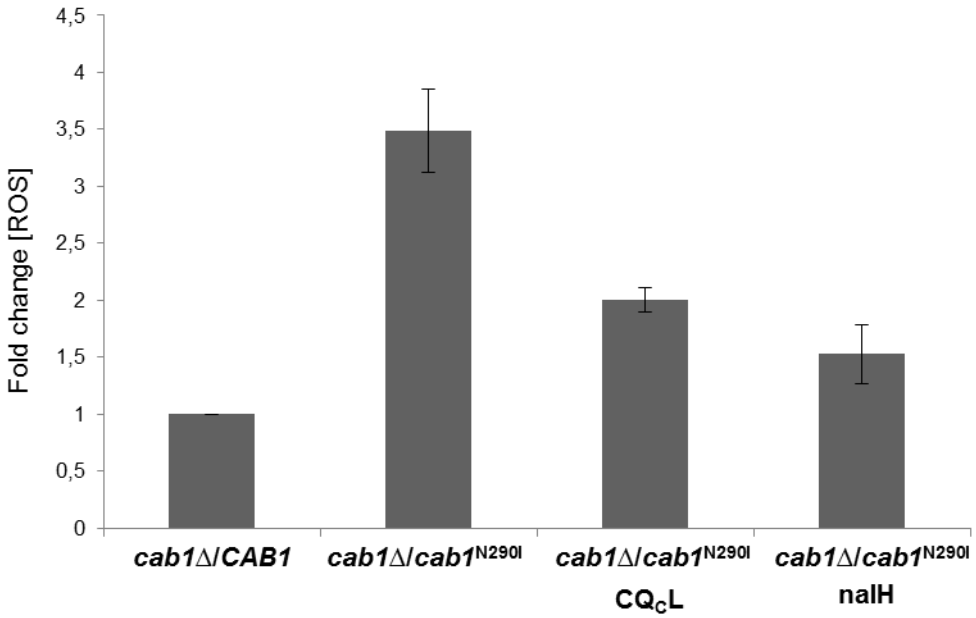

Fig 3.13 Evaluation of ROS content in *cab1*Δ/pFL39*CAB1* and *cab1*Δ/pFL39*cab1*^{N290I} grown in YNB DO-TRP plus 2% galactose with or without CQ_{CL}/nalH. Values are reported as fold change in content over WT

In the same growth conditions the lipid peroxidation was also reduced. In fact, the MDA content of the mutant strain was similar to that of the wild type strain grown under the same conditions (Fig 3.14).

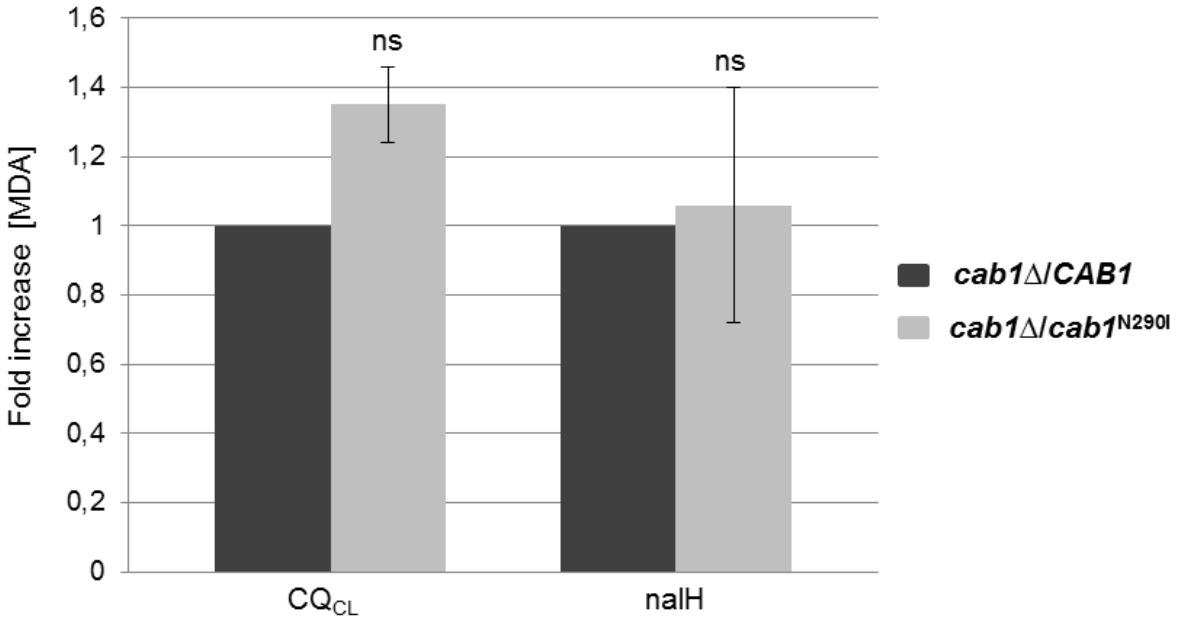

Fig 3.14 MDA content in *cab1*Δ/pFL39*CAB1* and *cab1*Δ/pFL39*cab1*^{N290I} grown in YNB DO-TRP plus 0,6% glucose with CQ_{CL} or nalH. Values are reported as fold change in content over WT

Results

4. Localization studies

4.1 Cellular localization of Cab1p

In silico analysis using the PSORT program (Uberbacher et al., 1991) predicts similar amount of Cab1 protein in the cytosol and mitochondria. Since no commercial antibodies to experimentally investigate the subcellular localization of Cab1p exist, a carboxyl-terminal fusion of HA epitope to Cab1 was constructed. To obtain the Cab1-HA fusion protein we used the "two step overlap extension technique" (described in Materials and Methods). The fusion protein Cab1-HA was then cloned into the pFL38 vector and with the resulting plasmid pFL38*CAB1*HA we transformed the strain *cab1*Δ/pFL39*CAB1*. To obtain the strain containing only the tagged allele, we then counter-selected the pFL39*CAB1* through plasmid shuffling on YNB DO+W, as described in Materials and Methods. The *cab1*Δ lethal phenotype was rescued by the expression of the tagged wild type allele, indicating that the addition of HA did not disrupt the targeting and functioning of the Cab1 protein. From cells expressing the wild type or tagged wild type allele we extracted the mitochondria with intact outer membrane and preserved the cytosolic fraction (PMS, Post Mitochondrial Supernatant) (described in Materials and Methods). Equivalent amounts of mitochondrial pellet (M) and supernatant (PMS) fractions were subjected to SDS-PAGE and Western blotting to identify the indicated protein. The filter was incubated with the following antibodies: α-HA (Roche), α-PORIN (Abcam Mitoscience) and α-PGK1 (Abcam Mitoscience). As shown in Fig. 4.1 the great majority of Cab1-HA co-fractionated with the soluble cytoplasmic protein phosphoglycerate kinase (PGK) while only a small amount remained in the mitochondria with the mitochondrial membrane protein porin, indicating that Cab1 behaves predominantly as a cytoplasmic protein.

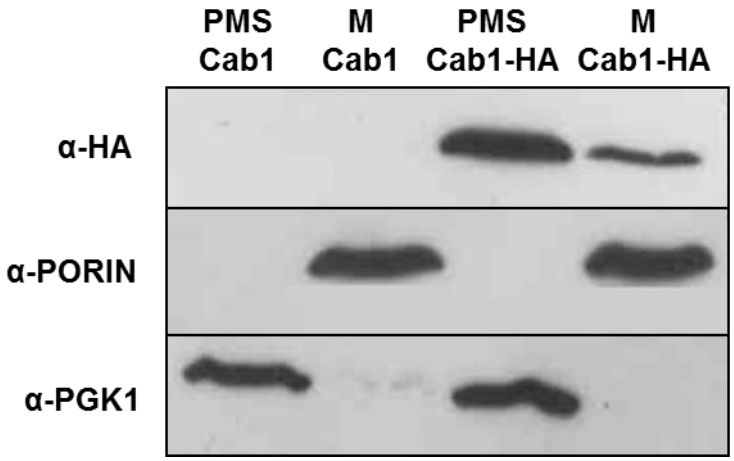

Fig 4.1 Immunoblot analysis of cytosolic fraction (PMS) and intact mitochondria (M), extracted from *cab1*Δ/pFL39*CAB1* and *cab1*Δ/pFL39*CAB1*HA

We further investigated the sub-mitochondrial localization of Cab1p by performing a protease protection assay of intact mitochondria (described in Materials and Methods). For that purpose 200 µg of mitochondrial protein were kept in buffer in the presence or absence of proteinase K (1mg/ml) for 60 minutes on ice. The samples were then subjected to SDS-PAGE and Western blotting. After the treatment the signal concerning Cab1-HA was not detected as shown in Fig 4.2, indicating a vulnerable physicals association of this protein with the outer mitochondrial membrane.

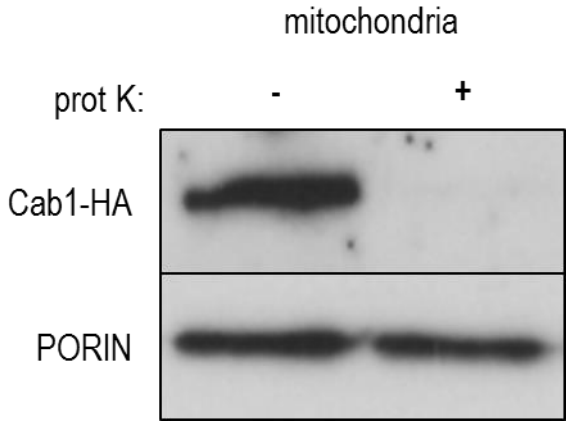

Fig 4.2 Mitochondria were treated for 60 min at 4°C with proteinase K (prot K) (1mg/ml). The filter was incubated with anti-HA and anti-PORIN antibodies.

4.2 Cellular localization of Cab5p

As reported in the introduction, it is known that the human CoA synthase is mitochondrial protein, anchored to the outer mitochondrial membrane by the N-terminal region (Zhyvoloup et al., 2003) or localized within the mitochondrial matrix (Dusi et al., 2014). Contrariwise little is known about the subcellular compartmentalization of the CoA biosynthetic pathway in yeast. Study High-throughput suggests for Cab5 a mitochondrial localization (Reinders et al., 2006), while GFP-fusion analysis identify the protein to “nuclear envelope” level and to endoplasmic reticulum level (Huh et al., 2003). *In silico* analysis using the PSORT and MITOPROT programs (Uberbacher et al., 1991; Claros et al., 1996) predict for Cab5 protein a mitochondrial localization. Moreover human CoA synthase is a mitochondrial enzyme and the human gene is able to complement the *cab5*Δ mutation. To investigate the localization of yeast Cab5p, a carboxyl-terminal fusion of HA epitope to Cab5 was constructed since for Cab5p do not exist commercial antibodies. To construct the Cab5-HA fusion protein we used the “two step overlap extension technique” (described in Materials and Methods). The fusion protein Cab5-HA was then cloned into pFL38 vector

(centromeric, *URA3* marker) obtaining the plasmid pFL38Cab5HA which was then transformed into W303-1b *cab5*Δ/pFL39*CAB5*. To obtain strains containing only the tagged allele, we then counter-selected the pFL39*CAB5* through plasmid shuffling on YNB DO-W, as described in Materials and Methods. The *cab5*Δ lethal phenotype was rescued by the re-expression of the tagged wild type allele, indicating that the addition of HA did not disrupt targeting and function of the Cab5 protein. From cells expressing HA tagged Cab5 (Cab5-HA) the mitochondria with intact outer membrane were extracted and the cytosolic fraction (PMS, Post Mitochondrial Supernatant) was preserved (described in Materials and Methods). Equivalent amounts of mitochondrial pellet (M) and supernatant (PMS) fractions were subjected to SDS-PAGE and Western blotting. The filter was incubated with the following antibodies: α-HA (Roche), α-PORIN (Abcam Mitoscience) and α-PGK1 (Abcam Mitoscience). As shown in Fig. 4.3 the great majority of Cab5-HA co-fractionated with the mitochondrial membrane protein porin, while only a small amount remained in the supernatant with the soluble cytoplasmic protein phosphoglycerate kinase (PGK), indicating that Cab5 behaves as a mitochondrial associated protein.

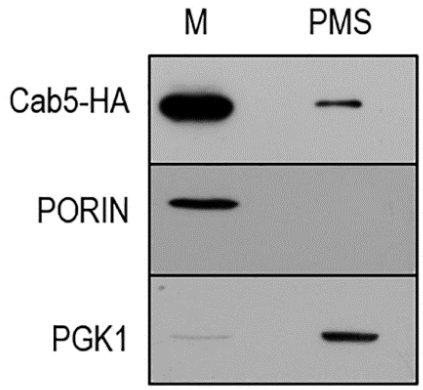

Fig 4.3 Immunoblot analysis of cytosolic fraction (PMS) and intact mitochondria (M), extracted from *cab5*Δ/pFL39*CAB5*HA

We further investigated the sub-mitochondrial localization of Cab5p by performing a protease protection assay of intact mitochondria (described in Materials and Methods). For that purpose 200 μg of mitochondrial protein were kept in buffer in the presence or absence of proteinase K (1mg/ml) for 60 minutes on ice. After the treatment the mitochondria was subject to SDS-PAGE and Western blotting. Cab5-HA exhibited a significant increase in proteinase K sensitivity treatment respect to both porin, which is only partially exposed on the surface, and to the inner membrane protein Core1 (Fig. 4.4A). These data show a physical association of this protein with the outer mitochondrial membrane. In order to investigated whether Cab5p is an intrinsic o

extrinsic protein of outer mitochondrial membrane we determine the resistance of Cab5p to sodium carbonate treatment (Trott and Morano 2004; Fujiki et al., 1982). As depicted in Fig. 4.4B the amount of Cab5 associated with mitochondria was significantly reduced after the treatment while the amount of porin, intrinsic outer membrane protein, was not altered. Taken together these results suggest that Cab5 is an extrinsic outer membrane protein.

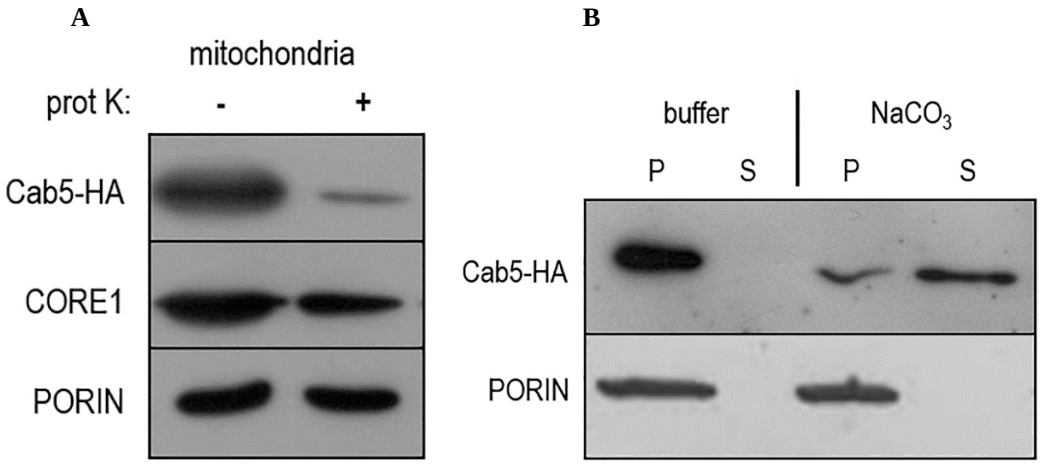

Fig 4.4 (A) Immunoblot analysis on mitochondria treated with proteinase K. The membrane was incubated with the following antibodies: α-HA (Roche), α-PORIN (Abcam Mitoscience) and α-CORE1 (Abcam Mitoscience) (B) Immunoblot analysis on mitochondria treated with Na_2CO_3, pH 11. To the left pellet (P) and soluble fraction (S) of untreated mitochondria, to the right of treated mitochondria

Conclusions and Future Perspectives

PKAN and CoPAN, both subtypes of NBIA (Harting et al., 2006; Leoni et al., 2012;Dusi et al., 2014), are severe and disabling neurodegenerative disorders associated to inborn error of Coenzyme A (CoA) biosynthetic pathway. Mutations in *PANK2* gene, encoding for the mitochondrial isoform of pantothenate kinase account approximately 50% NBIA (Hayflick et al., 2006; Levi and Finazzi, 2014) whereas only few mutations in Coenzyme A synthase encoding gene, *COASY*, have been described so far (Dusi et al., 2015; Evers et al., 2017).

CoA and its derivatives are key molecules involved in several metabolic process: ATP generation via the tricarboxylic acid cycle, fatty acid metabolism, cholesterol and ketone body biosynthesis, and histone and non-histone protein acetylation.

PKAN and CoPAN, as the others forms of NBIA, are characterized by mitochondrial dysfunctions, oxidative stress, altered lipid metabolism and iron accumulation in specific region of the brain but the relationship between CoA deficiency and iron overload is not yet been elucidated.

To investigate the pathogenic mechanism of PKAN and CoPAN diseases and to clarify why iron is accumulated and whether this is a primary event or simply an epiphenomenon, different disease models have been created. The *Drosophila melanogaster fumble* model partially recapitulates the human phenotype, showing locomotor dysfunction and neurodegeneration (Rana et al., 2010). *Pank2* KO mouse model only when subjected to a diet containing high fat level displayed a severe neurological phenotype (Kuo et al., 2005; Brunetti et al., 2014). The *pank2* and *coasy* morphants showed abnormal head development with smaller eyes, perturbation of brain morphology and an altered vasculature structure. *In vitro* studies using PKAN fibroblasts and PKAN hiPSC-derived neuron demonstrated severe functional impairments such as alteration of the oxidative status (increase of ROS and lipid peroxidation) and mitochondrial dysfunctions, including impaired energy production, iron-sulfur cluster (ISC) and heme biosynthesis, with consequent impairment of iron homeostasis (Campanella et al., 2012; Santambrogio et al., 2015; Orellana et al., 2016; Arber et al., 2017). However, none of these models showed iron accumulation, a hallmark sign in the brain of patients.

To investigate the relationship between *PANK2* and *COASY* deficiency and dysregulation of iron homeostasis, a yeast models for PKAN and CoPAN disease were constructed and characterized, taking advantage of the high degree of conservation of the CoA biosynthetic pathway with the only difference that in *Saccharomyces cerevisiae* the last two activities (PPAT and DPCK) reside in two different protein encoded by *CAB4* and *CAB5* gene respectively.

Regarding yeast PKAN model we constructed five pathological variants of PANK2 in the corresponding yeast protein Cab1: Gly26Val, Asn170Ile, Leu179Pro, Asn290Ile and Gly311Arg. These substitutions regarded different domains of the protein: Gly26Val and Gly311Arg are located in the ATP binding site; Leu179Pro and Asn290Ile in the dimerization domain and Asn170Ile is located in the surface of protein with not apparent interactions with other proteins. In the hypothesis that all these substitutions could abolish the protein activity we also constructed a strain carrying the variant Gly351Ser known conferring a temperature sensitive phenotype (Olzhausen et al., 2009). Among the five tested mutant alleles, three totally compromised the activity of Cab1 protein being unable to complement the lethal phenotype associated to *CAB1* deletion. Contrariwise the variants *cab1*^{N170I} and *cab1*^{N290I} were able to complement the *cab1*Δ mutant. First we analyzed the mitochondrial function in the strains *cab1*Δ/pFL39*cab1*^{G351S}, *cab1*Δ/pFL39*cab1*^{N170I} and *cab1*Δ/pFL39*cab1*^{N290I}. Besides a thermosensitive phenotype on glucose the strains *cab1*Δ/*cab1*^{G351S} and *cab1*Δ/*cab1*^{N290I}, showed a severe growth defect on respiratory carbon source both at 37°C and 28°C. On the contrary the mutant strain *cab1*Δ/*cab1*^{N170I} didn't exhibit any evident growth defect. According to their OXPHOS growth phenotype the strains *cab1*Δ/*cab1*^{G351S} and *cab1*Δ/*cab1*^{N290I} showed a respiration rate significantly decreased and the activity of respiratory chain complexes (NCCR, SDH and COX) were reduced, demonstrating a impairment of mitochondrial functions. Moreover the growth of both mutants was severely inhibited in the presence of iron, indirectly suggesting iron accumulation. To better quantify the intracellular iron content we performed the BPS colorimetric assay, demonstrating a two fold increase of iron level. Accordingly the activity of succinate dehydrogenase and aconitase, marker of mitochondrial functionality linked to iron metabolism, were reduced in the mutant strains.

Acetyl-CoA, a CoA derivative, is the primary substrate of mitochondrial and cytosolic fatty acid synthesis. In human and in model organisms has been observed that a deficiency of CoA leads to alterations in lipid metabolism. Accordingly both yeast mutans strains showed a reduction of lipid droplets an index lipid homeostasis perturbation.

We also evaluated the metabolic consequences of CoA deficiency in the yeast model of CoPAN, a yeast strain expressing the Arg499Cys variant in the *COASY* human gene previously constructed.,
Also in this case mitochondrial dysfunctions were revealed; OXPHOS growth was affected and respiration rate significantly decreased. Accordingly, the activity of respiratory chain complexes and steady state levels of MRC subunits were reduced. Also the activities of SDH and aconitase were reduced in the *COASY* mutant. Moreover the growth of the mutant strain is not only strongly inhibited in the presence of iron but that the mutant strain showed iron accumulation; altered lipid metabolism and enhanced oxidative stress were also highlighted.
The reason why this occurs and how the CoA deficit contributes to these phenotypes, in particular to iron accumulation is not clear.
It has been demonstrated that ISC biosynthesis requires GTP, NADH and ATP, other than iron and sulfur (Pandey et al., 2015). One prevailing hypothesis proposes that the impairment of the Krebs cycle due to CoA deficiency might result in a lower production of GTP and NADH, with the consequent partial iron utilization in ISC biosynthesis (Santambrogio et al., 2015). The low Fe-S cluster formation can result in the activation of DMT1 and decrease of Fpn1 with consequent iron accumulation and oxidative stress (Batista-Nascimento et al., 2012). Fpn1 is a ferroportin that mediates the release of iron into the extracellular medium that is captured by transferrin receptor (TfR), enters in the cell by endocytosis and then is translocated across the endosomal membrane through the divalent metal transport 1, *DMT1*.
Even the yeast responds to reduced iron sulfur cluster synthesis increasing cellular iron uptake and changing intracellular iron re-distribution (Lill et al., 2008). In order to test this we analyzed the transcription levels of three gene involved in the iron transport: *FET3*, *FTR1* and *FIT3*. in *cab1*Δ/*cab1*^{N290I} all the three genes were down-regulated both in exponential and stationary growth phase. This suggests that iron accumulation in mutant strain is not due to an increase uptake of the ion. It can be hypothesized that the iron not correctly utilized in the ISC biosynthesis is accumulated and that the cells down-regulate the genes involved in iron uptake in order to counteract its accumulation. Accordingly Arber et al., studying the *PANK2* Knockout cell lines, observed a significant increase in the *FPN* and in mitochondrial ferritin (*FTMT*) expression thus enhancing iron export and iron mitochondrial storage. They assumed that this response could be a further attempt by the cell to sequester excess iron safely and to reduce the potential iron accumulation over time.

The high iron level resulted in an increase in mitochondrial ROS production, which plays a central role in the regulation of ISC enzyme activity and in the lipid membrane composition. The mutant strains *cab1*Δ/*cab1*^{G351S} and *cab1*Δ/*cab1*^{N290I} showed a ROS content by about 3,5-fold higher respect to wild-type strain. These reactive species of oxygen can activate the lipid peroxidation process, with consequent production of downstream substrates such as MDA. In fact both mutant strains showed an increase in MDA content suggesting a membrane damage. The peroxidation of lipids in the mitochondrial inner membrane can result in a limited depolarization (Gall et al., 2012). This could cause the opening of mitochondrial membrane permeability transition pore (Bernardi et al., 1992; Gogvadze et al., 2003) that may facilitate the iron import not utilized in the biosynthetic pathways, thus exacerbating its accumulation.

According to the defect observed in lipid homeostasis, PKAN yeast showed an altered expression of *ACS2* and *HFA1*, key genes involved in the biosynthesis of acetyl-CoA an malonil-CoA respectively both fundamental precursor of lipid biosynthesis. The up-regulation of *ACS2* and *HFA1*, observed in the mutant strain *cab1*Δ/*cab1*^{N290I} might be considered as a cell "emergency response" caused by the lack of Acetyl-CoA.

Moreover since Acetyl-CoA acts as an acetyl group donor for protein acetylation in metabolism, low levels of CoA can cause histone hypoacetylation thus contributing to the neurological phenotype of PKAN (Takahashi et al., 2006; Nakamura et al., 2012; Brunetti et al., 2012).

The impairment of energetic metabolism revealed by the yeast model, and present in the PKAN fibroblasts, could derive from an alteration in the membrane phospholipids caused by a CoA deficiency.

All the results so far obtained indicated that the reduction of CoA level leads to an impairment of the Krebs cycle with lower production of GTP and NADH. A decreased production of these factors leads to defect in mitochondrial ISC biogenesis and in oxidative phosphorylation. These effects together with the alteration of membrane composition and permeability could represent a primary mechanism which triggers abnormal intracellular iron content. Iron overload generates oxidative stress, lipid peroxidation, nucleic acid modification, protein misfolding and aggregation. Finally these events lead to cell death (Fig 1).

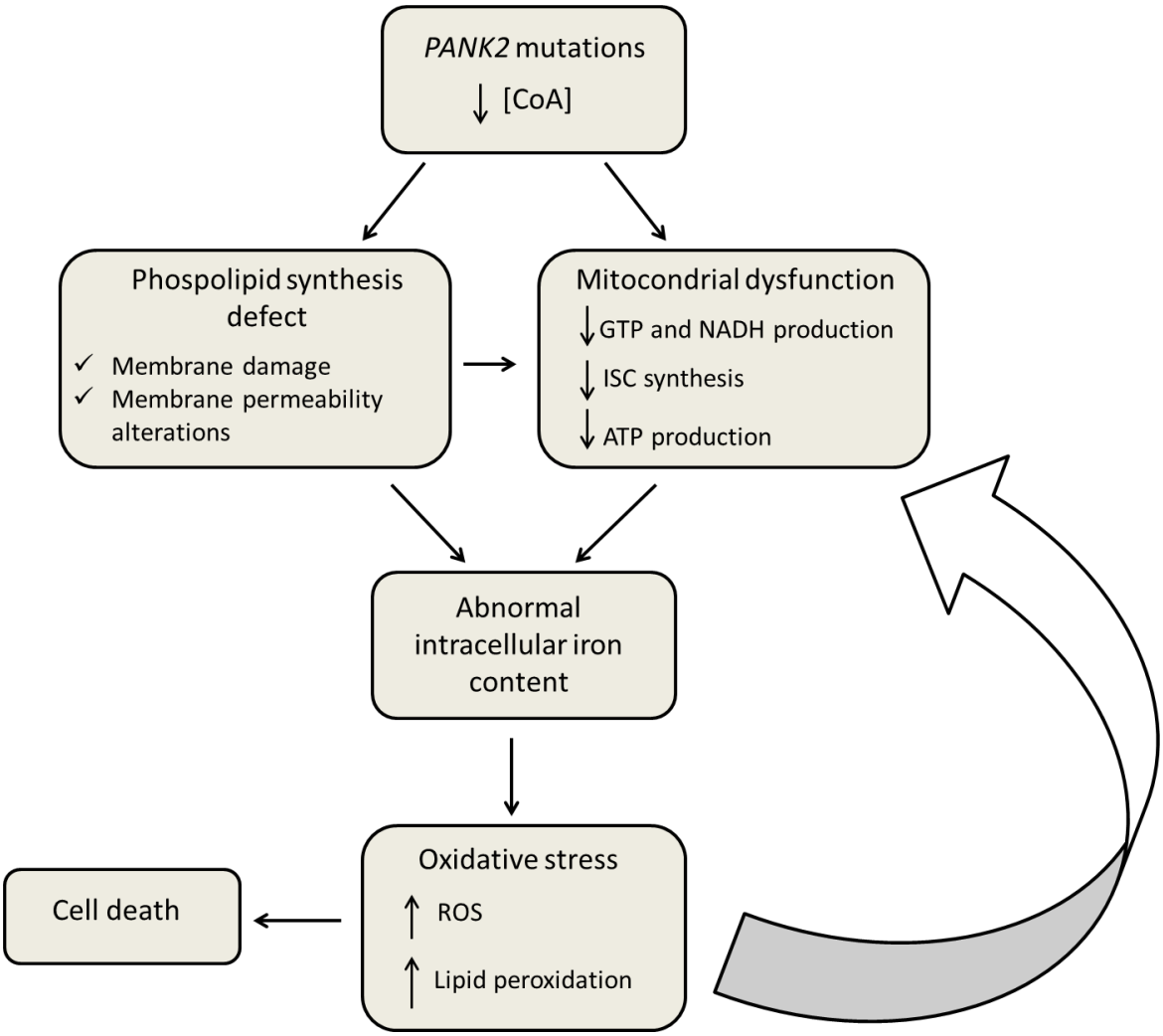

Fig 1 Cause/effect relationship between mitochondrial dysfunction, iron overload, oxidative stress and neurodegeneration

According to Mena et al., these three phenomena (mitochondrial dysfunction, iron accumulation and oxidative damage) generate a feedback loop of increased iron accumulation and oxidative stress.

The PKAN and CoPAN yeast models described in this work recapitulating the majors patient phenotypes and in particular high iron content, could represent a powerful tool for investigate the pathogenic mechanism of these diseases and for searching chemical suppressor i.e. potential therapeutic drug for PKAN and CoPAN.

Starting with PKAN model we tested the 1018 compounds of Selleck-FDA approved chemical library and we found two molecules able to rescue the oxidative growth defect of *cab1*Δ/*cab1*^{N290I} : 5,7 dichloro-8 hydroxyquinoline (CQ_{CL}) and nalidixic acid (nalH). The CQ_{CL} is a heterocycle compound belongs to quinoline family where the precursor is the 8-hydroxyquinoline (8HQ). It is able to bind bivalent ions including iron and its antimicrobial activity is dependent on

the ability to bind metals of bacterial enzymes (Prachayasittikul et al.,2013). Nalidixic acid is a quinolone antibiotic very active against aerobic Gram-negative bacteria. It inhibits a subunit of DNA gyrase and topoisomerase IV and induces the formation of cleavage complexes (Pommier et al., 2010). In addition Nalidixic acid is able to form a complex with various metal cations as iron, copper, zinc, aluminum, calcium and magnesium (Turel 2002).

After the identification of the molecules optimal concentration able to revert the OXPHOS defect, we investigated the ability of both molecules to revert the other phenotypes associated to CoA deficiency. So we demonstrated that the growth in presence of CQ_{CL} or nalH increase the oxygen consumption and the activity of respiratory complexes in *cab1*Δ/*cab1*^{N290I}. Moreover the iron amount is reduced, preventing the over production of harmful ROS and reducing the lipid damage. The results obtained suggest that the mechanism that underlies the rescue ability of both molecules, CQ_{CL} and nalH, could lie on their property to chelate the excess of iron thus reducing oxidative stress. Preliminary results indicated that at least 5,7 dichloro-8 hydroxyquinoline was able to rescue the altered phenotype displayed by CoPAN model.

Although very recently it has been demonstrated the therapeutic effect of exogenous CoA administration in reverting pathological phenotypes in PKAN-derived neurons, in the future the compounds identified could be tested *in vitro* on available hiPS-derived neuronal cells and *in vivo* on zebrafish model and/or on knock out mouse model.

Materials and Methods

1.1 Strains used

All *S. cerevisiae* strains used in this work are listed below:

STRAIN	GENOTYPE	REFERENCES
W303-1B	*Matα, ade2-1, leu2-3, ura3-1, trp1-1, his3-11, can1-100*	Thomas and Rothstein, 1989
W303-1B *cab5*Δ pYEX-BX/*COASY*	W303-1B *cab5::KAN*^{R}	Dusi et al., 2014
W303-1B *cab5*Δ pYEX-BX/*COASY*^{R499C}	W303-1B *cab5::KAN*^{R}	Dusi et al., 2014
W303-1B *cab5*Δ pFL38*CAB5*HA	W303-1B *cab5::KAN*^{R}	This work
W303-1B *cab1*Δ pFL39*CAB1*	W303-1B *cab1::KAN*^{R}	This work
W303-1B *cab1*Δ pFL38*CAB1*	W303-1B *cab1::KAN*^{R}	This work
W303-1B *cab1*Δ pFL38*CAB1*HA	W303-1B *cab1::KAN*^{R}	This work
W303-1B *cab1*Δ pFL39*CAB1*^{G351S}	W303-1B *cab1::KAN*^{R}	This work
W303-1B *cab1*Δ pFL39*CAB1*^{N170I}	W303-1B *cab1::KAN*^{R}	This work
W303-1B *cab1*Δ pFL39*CAB1*^{N290I}	W303-1B *cab1::KAN*^{R}	This work

The bacteria strain used in this work is listed below:

STRAIN	GENOTYPE
DH10B	*F-mcrA Δ(mrr-hsdRMS-mcrBC) φ80d DlacZ ΔM15 ΔlacX74 deoR recA1 endA1 araD139 Δ(ara, leu)7697 galU galKλ-rpsL hupG*

1.2 Media and growth conditions

For yeast the following media were used:

- YP (1% peptone, 0.5% yeast extract)

- YPA (2% peptone, 1% yeast extract, 75mg/ml adenine)

- YNB (YNB ForMedium™ w/o aminoacids w/o NH4SO4 1,9 g/L, NH4SO4 5 g/L). Minimum media was enriched with drop-out powder (Kaiser et al. 1994).

- Mineral medium (40) (Magni et al., 1962): K2PO4 1 g/L, MgSO4 0.5 g/L, (NH4)2SO4 3.5 g/L, 1 mL/L of solutions A (NaCl 100 g/L), B (CaCl2 100 g/L) and C (boric acid 500 mg/L, KI 100 mg/L, FeCl3 200 mg/L, $MnSO_4$ 400 mg/L, $FeSO_4$ 400 mg/L and ammonium molybdate 200 mg/L). Mineral medium was supplemented with mixture of vitamins and amino acids necessary to complement the auxotrophies of different strains. To obtain medium lacking pantothenate (40-Pan), a mixture of vitamins without pantothenate was prepared.

- 5-FOA YNB: YNB ForMedium™ with 1 g/l 5-Fluoroorotic Acid (Melford), 50 mg/l uracile with aminoacids necessary to complement the auxotrophies (Boeke et al., 1984).

If necessary singles amino acids could be excluded from complete drop-out to maintain selective pressure. As solidifying agent agar ForMedium™ 2% was added. Carbon sources were added at final concentration of 2% if not specified differently. The following sources were used: Glucose (D), Ethanol (E), Glycerol (G) and Galactose (Gal). *S. cerevisiae* was cultured at 28˚C, in constant shaking 120 rpm if liquid media was used.

For *E. coli* LB media was used (1% bacto tryptone Difco™, 0.5% yeast extract Difco™, 0.5% NaCl, pH 7.2-7.5). Agar 2% and ampicillin (Sigma-Aldrich®) 100mg/ml were added if needed. For α-complementation selection 80µl of 5-bromo-4-chloro-3-indolyl-b-D-galactopyranoside (Xgal) 2% (dissolved in dimethilformamide) and 40µl isopropyl-beta-D-thiogalactopyranoside (IPTG) 23.8 mg/ml were added. Cultures were incubated at 37˚C in constant shaking if necessary.

1.3 Vectors

PLASMIDS	MARKERS IN *S. cerevisiae*	TYPE	REFERENCES	FIG.
pFL38	*URA3*	Centromeric	Bonneaud et al., 1991	1.1
pFL39	*TRP1*	Centromeric	Bonneaud et al., 1991	1.2
pYEX-BX	*URA3*	Multicopy	Clontech Laboratories	1.3
pSH63	*TRP1*	Centromeric	Güldener at al., 2002	1.4

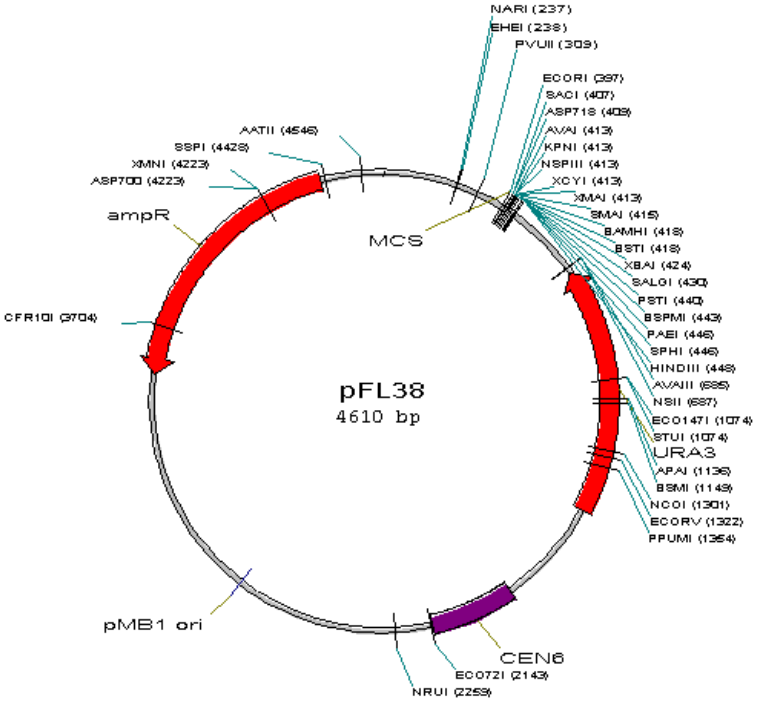

Fig 1.1 pFL38 plasmid

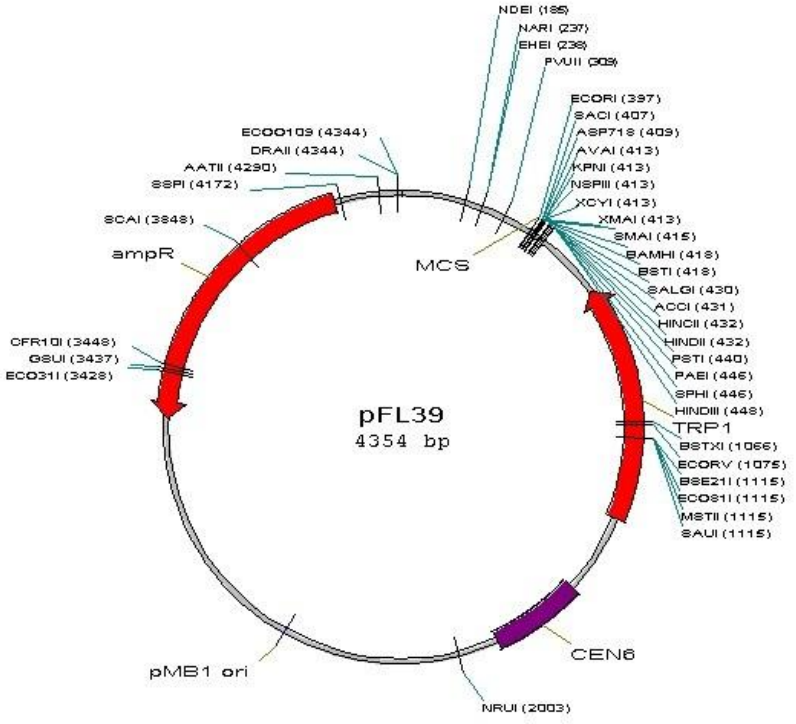

Fig 1.2 pFL39 plasmid

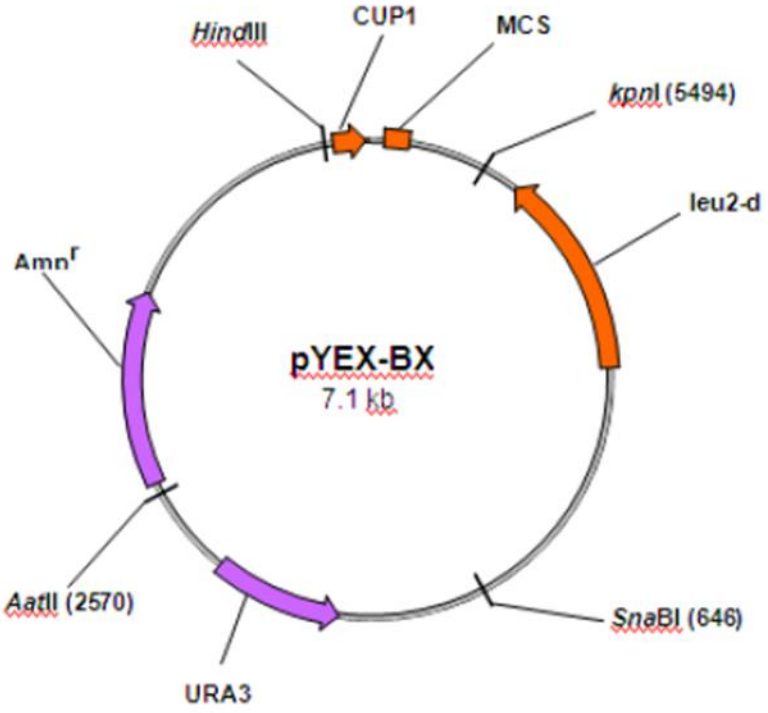

Fig 1.3 pYEX-BX plasmid

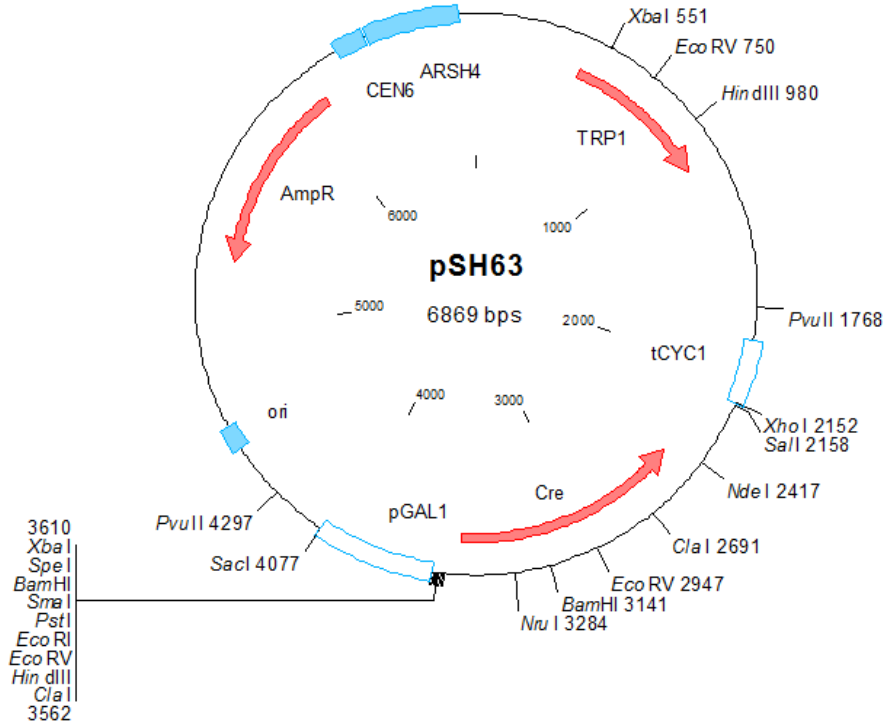

Fig 1.4 pSH63 plasmid

1.4 Polymerase chain reaction

All the reactions were performed following manufacturer indications. For analytical purpose GoTaq® DNA polymerase (©Promega) was used. Preparative reactions for gene cloning and site specific mutagenesis were performed with a high fidelity (HiFi) polymerase. KOD Hot Start HiFi DNA polymerase was used (Novagen®). All the reactions were performed using "Applied Biosystem 2720 Thermal Cycler".

1.4.1 Two step overlap extension technique

The *cab1* mutant alleles were obtained by site-direct mutagenesis using the overlap extension technique (Ho et al., 1989). For each mutation, the first PCR reaction was performed using the external forward primer and the external reverse primer *CAB1*Rv*Bam*HI, each in combination with reverse or forward internal primers for each mutation (see Table 1.5). The final mutagenized product was obtained by using the overlapping PCR fragments as template with *CAB1*Fw*Hind*III and *CAB1*Rv*Bam*HI as external primers. The product was then digested with and cloned in *Hind*III-*Bam*HI digested pFL39 centromeric plasmid.

The same technique was used to added epitope HA (hemagglutinin) to *CAB1* or *CAB5*. The final tagged gene *CAB1*HA and *CAB5*HA digested with *Hind*III-*Bam*HI or *BamH*I-*Kpn*I were cloned in digested *Hind*III-*Bam*HI or *BamH*I-*Kpn*I pFL38 vector.

1.4.2 RT-PCR and qPCR

For RT-qPCR, cells were grown in YNB supplemented with 0,6% glucose or 2% galactose until 0.9-1.2 OD or 6-7 OD. Total RNA was extracted with hot acidic phenol (Ausubel et al., 1994), treated with DNase I (New England Biolabs), retrotranscribed with M-MuLV Reverse Transcriptase (NewEngland Biolabs) with oligo (dT) 20primer (Euroclone) and murine RNase inhibitor (NewEngland Biolabs).

Quantitative PCRs were performed in 20-µl volume using Power Sybr Green mix with ROX (Life Technologies) in a 96-well plate. Triplicates were included for each reaction. The primers used for qPCR, at a final concentration of 120 nM, are listed in Table 1.5. All reactions were performed in the AB 7300 instrument (Life Technologies) at default settings:

- 2' at 50°C
- 10' at 95°C

41 cycles

- 15'' at 95°C

- 1'at 60°C

1 cycle

- 15'' at 95°C

- 15'' at 60°C

For each analyzed gene, the level of expression was calculated using the comparative quantification algorithms -ΔΔCt. In this method the threshold cycles number Cts for the gene of interest in both the test sample (mutant strain) and calibrator sample (wild type strain) are adjusted in relation to a normalizer gene Ct from the same two samples. In particular as normalizer gene *ACT1* was used. To determine the fold difference in expression we used the following expression:

Fold difference = $2^{-\Delta\Delta Ct}$

ΔCt sample – ΔCt calibrator = ΔΔCt

$Ct_{\text{target gene}} - Ct_{\text{norm. gene}}$ = ΔCt sample

$Ct_{\text{target gene}} - Ct_{\text{norm. gene}}$ = ΔCt calibrator

Statistical analysis was performed through an unpaired two-tailed t-test. Only p values of less than 0.05 were considered significant.

1.5 Primers

OLIGONUCLEOTIDE	SEQUENCE 5'-3'	USE
*CAB5*Fw	GGGGGGATCCCCATTGCTTAGAATGGGCGG	*CAB5* cloning
*CAB5*Rv	CCGCGGTACCGAGAACCCATAGAATTCGAC	*CAB5* cloning
*CAB5*HATerFw	TACCCATACGATGTTCCAGATTACGCTGTATAAGGTTGATATCTTATAATTA	*CAB5* tag
*CAB5*HARv	ATCAACCTTATACAGCGTAATCTGGAACATCGTATGGGTACGCTGAAGACT TTTTATTTTG	*CAB5* tag
*CAB1*Fw*Hind*III	CAGGCAAAAAGCTTTACACGTG	*CAB1* cloning and disruption
*CAB1*Rv*Bam*HI	CCCCGGATCCCACAGACATTGAAGC	*CAB1* cloning and disruption

*CAB1*FwKan	GTGCATGCGAAAAGAATCGCAATGCCGCGAATTACTCAAGAGATATCCGT ACGCTGCAGGTCGAC	*CAB1* disruption
*CAB1*RvKan	GCCAAAAAAAAAAGTGAAATCTATCTACGTACTTGTTTTCTTAGTAGATGATC GATGAATTCGAGCTCG	*CAB1* disruption
K2	GAAAGAAGAACCTCAGTGGC	disruption
*CAB1*HATerFw	TACCCATACGATGTTCCAGATTACGTCACGTAGATAGATTTCACTTTTTTT	*CAB1* tag
*CAB1*HARv	AATCTATCTACGTAGCGTAATCTGGAACATCGTATGGGTAACTTGTTTTCTT AGTAGATGA	*CAB1* tag
*CAB1*G351S	Fw: GAAGGCTATTTGGGTGCAATGTCTGCTTTCCTAAGCGCGTCTCG Rv: CGAGACGCGCTTAGGAAAGCAGACATTGCACCCAAATAGCCTTC	*CAB1* mutagenesis
*CAB1*G311R	Fw: TACAGAATATATACTTTGGCAGATCTTATACCAGAGGACATT Rv: AATGTCCTCTGGTATAAGATCTGCCAAAGTATATATTCTGTA	*CAB1* mutagenesis
*CAB1*L179P	Fw: GTAGAGTAGGCGGTTCTTCACCTGGAGGGGAACTCTTTGGGG Rw: CCCCAAAGAGTTCCTCCTCCAGGTGAAGAACCGCCTACTCTAC	*CAB1* mutagenesis
*CAB1*G26V	Fw: CCTTGCTATTGATATCGTTGGTACTCTGGCTAAAGTAGTCTTCTC Rv: GAGAAGACTACTTTAGCCAGAGTACCAACGATATCAATAGCAAGG	*CAB1* mutagenesis
*CAB1*N170I	Fw: CAATATTAAAAGTCACCGAACCAAACATTTTCAGTAGAGTAGGCG Rv: CGCCTACTCTACTGAAAATGTTTGGTTCGGTGACTTTTAATATTG	*CAB1* mutagenesis
*CAB1*N290I	Fw: CTATTCGCCATCTCCAACATTATTGGGCAAATAGCTTATTTGC Rv: GCAAATAAGCTATTTGCCCAATAATGTTGGAGATGGCGAATAG	*CAB1* mutagenesis
*ACT1*q	Fw: GTATGTGTAAAGCCGGTTTTG Rv: CATGATACCTTGGTGTCTTGG	qPCR
*ACS2*q	Fw: CTGCTGTTGTCGGTATTCCA Rv: TGTGTTCTGCATCACCTTCA	qPCR
*HFA1*q	Fw: CGTGGGTGTTATTGCGGTAG Rv: GATACCACACCTGTCCTGCT	qPCR
*FET3*q	Fw: CTACGGTTCAAACACGCACA Rv: GGTTTGGAAAGCGTGACCAT	qPCR
*FTR1*q	Fw: AAGCAGGAGTTGACGGAAGA Rv: TGGTAGTTTGCTCGGGAAGT	qPCR
*FIT3*q	Fw: GCTACATCCTCTAGCACCGC Rv: GCACCCATCAAACCAGTACC	qPCR
M13Fw	AGGGTTTTCCCAGTCACGACGTT	Sequencing
M13RV	GAGCGGATAACAATTTCACACAGG	Sequencing

1.6. Sequencing

Sequencing of all genes was performed with external services (©Eurofins-MWG). The primers used for the sequencing are reported in Table 1.5.

1.7. Nucleid acid manipulation

All the manipulations were carried out with standard techniques (Maniatis et al., 1982). Genomic DNA from *S. cerevisiae* was extracted as previously described (Hoffman and Winston, 1987; Lõoke et al. 2011). Plasmid DNA was extracted from *E. coli* with Wizard® Plus SV Minipreps, Wizard® Plus Minipreps (Promega©) or following standard procedures (Sambrook and Russel, 2001). DNA recovery from agarose gel and purification of PCR products were carried out with GenEluteTM PCR-Clean Up kit (Sigma-Aldrich®) commercial kit. Enzymatic manipulations (restriction, ligation, dephosphorylation) were carried out following manufacturer indications (New England Biolabs® Inc. NEB, Invitrogen™).

1.8. Transformation procedures

1.8.1. *S. cerevisiae* transformation

Yeast transformation was carried out with Lithium Acetate (LiAc) as described by Gietz et al. If a greater efficiency was desired, the long protocol was applied (Gietz and Woods. 2002). For the one gene disruption the cells were regenerated in two ml of YPAD for 2h and then plated on plates added with G418.

1.8.2. *E. coli* transformation

E. coli transformation was achieved with electroporation. Competent cells were prepared as previously described (Dower et al. 1988). Transformation was carried out with 1-3 µl of plasmid DNA or ligation product. 2 mm cuvettes were used, applying respectively a current of 2KV, 25 µF 200 Ω. Alternatively, CaCl2 competent cells were prepared and transformed with standard techniques (Maniatis et al., 1982).

1.9. Analyses in whole cell

1.9.1. Spot assay

Spot assay is a classical phenotypic analysis used to test growth of single strains in different conditions. The principle is a 10-fold serial dilution of a starting culture at $1x10^7$ cells/ml, performed four times to a final $1x10^4$ cells/ml. After an o/n culture at 28 °C in YNBD medium (enriched with drop out powder), the OD 600 was measured for each strain. A first dilution was made to dilute each strain to a concentration of 1 OD ($1x10^7$). Then four 10-fold serial dilutions were made. From these suspensions 5µl were spotted in ordered rows on agar plates and then incubated for several days.

1.9.2. Oxygen consumption

To measure the respiratory activity, strains were pre-grown in YP supplemented with 2% ethanol to counter select *petite* cells. Cells were inoculated at a final concentration of 0.05 OD/ml in YNB supplemented with 0.2% glucose and 2% galactose and grown for approximately 16–18 h. The oxygen consumption rate was measured on whole cells at 30°C using a Clark-type oxygen electrode (Oxygraph System Hansatech Instruments England) with 1 ml of air-saturated respiration buffer (0.1 M phthalate–KOH, pH 5.0), 10 mM glucose. The reaction started by addition of 20 mg of wet-weight cells, as described previously (Goffrini et al., 2009: Panizza et al., 2013). Statistical analysis was performed through an unpaired two-tailed t-test. Only p values of less than 0.05 were considered significant. Oxygen consumption rate was expressed as nmol O_2 for minute for mg of cells (nmolO_2/min mg).

1.9.3. Plasmid shuffling

Haploid strain that contained pFL38*CAB1* plasmid and pFL39 plasmid carrying a mutant allele, and in which the chromosomal copy of the *CAB1* gene has been disrupted, underwent *plasmid shuffling* on 5-FOA medium to counter-select pFL38*CAB1* plasmid. Haploid cells were grown in YNBD+DO-Trp solid medium for 24h in order to counter-select pFL38*CAB1* plasmid. Then the plate was replica-plated on 5-FOA medium and finally on YNBD+DO-Trp. Since 5-FOA is toxic in the presence of the genic product of *URA3* gene, if the mutated allele on pFL39 plasmid was completely functional the pFL38*CAB1* plasmid could be lost without preventing growth of the strain, which would appear to be 5-FOA resistant. On the other hand, if the mutated allele on pFL39 plasmid was completely non-functional the strain would not grow on 5-FOA medium.

Haploid strain that contained pFL39*CAB1* plasmid and pFL38 plasmid carrying a tagged allele, and in which the chromosomal copy of the *CAB1* gene has been disrupted, underwent *plasmid shuffling* on YNB+DO+Trp medium to counter-select pFL39*CAB1* plasmid. Haploid cells were grown in YNBD+DO-Ura liquid medium for 24h. Then 150 cells were plated on YNBD+DO-Ura and finally were replicated on YNBD+DO-Ura-Trp. If the tagged allele on pFL38 plasmid were completely functional the pFL39*CAB1* plasmid could be lost without preventing growth of the strain. On the other hand, if the tagged allele on pFL38 plasmid were completely non-functional the strain would not grow on YNBD+DO-Ura medium.

1.9.4. Aconitase activity

(Brown et al., 1998; Patil et al.,2012)

Cells were pre-grown on YNB medium supplemented with 2% glucose were inoculated in the same medium supplemented with 0.2% glucose and 2% galactose until an OD/ml = 1-2 was reached.

Cell extracts were prepared by resuspending cells in Cell lysis buffer (50 mM Tris Hcl pH8, 50mM KCl, 2mM Sodium Citrate, 10% glycerol, 7mM ß-mercaptoethanol and 1mM PMSF) at concentration of 1gr of cells in 2.5 ml and subjecting them to mechanical breakage with glass beads. Cell debris and unbroken cells were separated by low speed centrifugation (2000 x g for 5 min at 4°C) The obtained supernatant was further centrifuged at 13000 x g for 10 min, and the resulting supernatant was transferred to a new tube. Total protein concentration was determined as described in paragraph 1.11.2.

Aconitase was assayed by the aconitase-isocitrate dehydrogenase coupled assay, in which NADPH formation was monitored at $A_{340.}$ Solutions needed:

- 240µ REACTION MIX (1M Tris HCl pH 8, 10mM $MgCl_{2,}$ 10mM $NADP^{+}$ and 0.32U ICDH)
- 16µl of 50mM Sodium citrate
- 48µl whole-cell extract
- H_2O to 0.8ml

The aconitase activity was recorded on 3 mg/ml whole-cell extract and the specific activity was calculated with ε of 6,22 and the following formula (ΔOD*ε/min mg).). Statistical analysis was performed through an unpaired two-tailed t-test. Only p values of less than 0.05 were considered significant

1.9.5. Measurement of iron content

The iron content was determined by a colorimetric assay, essentially as described before (Tamarit at al., 2006; Almeida et al., 2008). 5X10^8 cells were washed twice with H_2O, resuspended in 0.5 ml of 3% nitric acid and incubated over night at 95°C. After incubation, samples were centrifuged at 12,000 rpm for 5min and the supernatant (400µl) was mixed with 160µl of 38 mg sodium L-ascorbate ml^{-1} (SIGMA), 320 µl of 1.7 mg BPS ml^{-1} (ACROS ORGANICS), and 126 µl of ammonium acetate (SIGMA) (saturated solution diluted 1:3). Non-specific absorbance was measured at 680nm and subtracted from the specific absorbance of the iron-BPS complex (535nm). Iron was quantified by reference to a standard curve using iron sulfate performed as in Tamarit et al, 2006. Iron content was expressed as nmol Fe/ 5*10^8 cells. Statistical analysis was performed through a unpaired two-tailed t-test. p value <0.05 *; <0.01** and < 0,001***.

1.9.6. H_2O_2 sensitivity

To determine the sensitivity to oxygen peroxide, cells growing exponentially were exposed to 0.8, 1 and 2 mM H_2O_2 at 28◦C or 37◦C for 4 h. Cell viability was determined by spotting equal amounts of serial dilutions of cells (10^5, 10^4, 10^3, 10^2, 10^1) onto YP plates (1% yeast extract, 2% peptone ForMedium ™) supplemented with 2% glucose (YPD). Plates were incubated at 28◦C or37◦C for two days. To better quantify H_2O_2 sensitivity cell survival was determined by counting the formation of colonies after the treatment. Statistical analysis was performed through a unpaired two-tailed t-test. Only p values of less than 0.05 were considered significant

1.9.7. Measurement of ROS content

The measure of the ROS amount was performed using dichlorofluorescein diacetate (DCFDA) that Inside the cells can be oxides by ROS to dichlorofluorescein (DCF) , fluorescent molecule, according to the modified version of Marchetti et al., 2006. 1x10^7 cells grown until stationary phase were incubated with DCFDA (20µM) (Sigma-Aldrich®) for 30 minutes at 28°C, washed twice with PBS, and resuspended in lysis buffer (20mM Tris HCl pH 7.5, 150mM NaCl, 1mM EDTA, 1% Triton X-100 and 2.5mM $Na_4P_2O_7$). The samples were mechanical broken with glass beads for 3-4 times for 30 sec and the protein precipitated for 10 min. 100µl of supernatant, whole-cell extract was measurement by the “Tecan SPECTRAR Fluor Plus” system (excitation at 485 nm and emission at 535 nm) indicating indirectly an amount of ROS. The fold change in the ROS content of mutant strains is calculated by dividing its content by the wild-type content value, which yields the fold

change compared with wild type, which now has a value of 1. Statistical analysis was performed through a unpaired two-tailed t-test. Only p values of less than 0.05 were considered significant

1.9.8. Lipid peroxidation: determination of malondialdehyde content (MDA)

(Boominathan et al., 2003; Salehi-Lisar et al., 2015)

Lipid peroxidation was evaluated by measuring malondialdehyde (MDA) content in whole-cell extract. $2x10^9$ cells were washed twice with H_2O, homogenized with 0.1% (W/V) trichloroacetic acid (TCA, Merck, Germany) and broken with glass beads. After the samples were centrifuged at 10,000 rpm for 5min, and the supernatant (150µl) was mixed with 0.8 ml of 20% TCA containing 0.5% of 2-thiobarbituric acid (Merck, Germany) and heated for 30 min in hot water at 95°C. The mixtures were immediately transferred to ice bath and then centrifuged at 10,000 g for 15 min. Finally, the absorbance of supernatants recorded in 532nm and MDA concentration was calculated according to following standard curve prepared by using malondialdehyde (0–250µl).

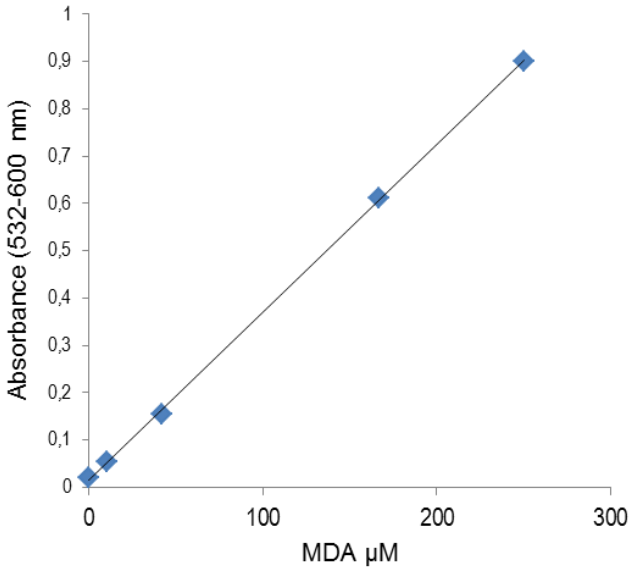

Fig 1.5 Standar curve prepared using MDA (0-250 µM)

The fold change in the MDA content of mutant strain is calculated by dividing its content by the wild-type content value, which yields the fold change compared with wild type, which now has a value of 1. Statistical analysis was performed through a unpaired two-tailed t-test. Only p values of less than 0.05 were considered significant

1.9.9. Lipid droplets content: fluorescence microscopy and fluorimetric analysis

Intracellular lipid droplets were detected using the fluorescent lipophilic dye Nile Red (9-diethylamino-5*H*-benzo[α]phenoxazine-5-one 3 SIGMA-ALDRICH) by fluorescence microscopy and fluorimetric analysis (Greenspan et al., 1985; Kimura et al., 2004; Sitepu et al., 2012). Wild type and *cab5Δ*/COASY^{R499C} strains were grown to mid-log phase in mineral medium (40) containing Yeast Extract (1,5 g/L). To 250µl of the cultures, adjusted to 1OD, 10µl of the stock solution of Nile red [100µg/ml] were added in order to obtain a final concentration of 4 µg/ml of dye. Fluorescence of the stained cells were obtained with a Leica DM2000 microscope using X100 magnification and captured using a Leica DFC310FX digital camera with Leica's Imaging Software (Leica Application Suite-LASAF 3.7.0, Leica Microsystem).

To quantify the fluorescence we used the fluorescence spectrometer Tecan SPECTRA Fluor Plus using the software XFLUOR4 V4.51 (excitation at 535 nm and emission at 595 nm). Aliquots of 100 µl of cells stained with Nile red were transferred into 96-well microplates in 4 replicates. For each strain a negative control was performed in which the dye was omitted in order to exclude a possible auto fluorescence of samples. The evaluation of the fluorescence was repeated at 5-minute intervals in a time interval of 20 minutes. Statistical analysis was performed through a unpaired two-tailed t-test. Only p values of less than 0.05 were considered significant

1.10. Mutational rate analysis: *petite* frequency determination

mtDNA stability was evaluated by the frequency of spontaneous cytoplasmic *petite*. They grow as small colonies on medium supplemented with respiratory carbon sources such as ethanol and glycerol. The protocol is the following:

1. The pre-existing petite were counter-selected on YNB+DO-Trp medium supplemented with 2% ethanol.
2. Replicate the YNB+DO-Trp 2% ethanol plates on selectable medium supplemented with 2% glucose. The strains were grown for 24h at 28°C.
3. Replicate on a new plate of the same medium and incubate again for 24h.
4. Resuspend a part of cells in H_2O and evaluate the cellular concentration.
5. Plate about 250 cells on YNB+DO-Trp medium supplemented with 0.3% glucose and 2% ethanol. Incubate at 28°C for 5-6 days and count the cells.

0.4% glucose is added in order to allow the growth of petite mutants which are respiratory deficient and are unable to use ethanol like the "wild-type" cells. When glucose is exhausted the

wild-type cells uses ethanol to grow, while the petite mutants arrest their growth. Indeed the petite mutants will form small colonies unlike the big colonies formed by wild-type cells.

1.11. Analysis in mitochondria

1.11.1 Preparation of yeast mitochondria with intact outer membrane

(Glick et al., 1995)

Cells were pre-grown on YNB medium supplemented with 2% glucose were inoculated in the same medium supplemented with 0.6% glucose until an OD/ml = 4-5 was reached.

The following protocol was used:

1. Harvest cells at 2000-3500 rpm for 7 minutes and wash once with sorbitol 1.2M

2. Resuspend washed cells in digestion buffer at concentration of 1gr of cells in 3ml

Digestion Buffer: 30ml 2M sorbitol

3ml 1M phosphate buffer, pH 7.5

0.1ml 0.5M EDTA pH 8

0.5ml ß-mercaptoethanol

50mg of zymolyase 20000

16ml of water (Vf=50ml)

Incubate at 30˚C or 37˚C depending on the used growth conditions until most of the cells have been converted to spheroplasts.

3. Add cold Buffer A and immediately centrifuge 4000rpm for 10 minutes. Wash two additional times with Buffer A

Buffer A: 1.2M deionized sorbitol (BioRad® AG501-X8 resin)

20mM KPO4 pH 7.5

4. Suspend washed spheroplasts in 0.6M sorbitol, 20mM KMES pH 6, 0.5mM PMSF at concentration of 1gr/3ml. Homogenize with and glass/Teflon pestle and overhead stirrer (Wheaton Science Products)

5. Centrifuge 3000rpm for 5 minutes to pellet debries. Collect the supernatant and centrifuge 12000rpm for 10 minutes to sediment mitochondria. The supernatant is the post mitochondrial fraction (PMS) and represent the cytosolic component

6. Suspend mitochondria briefly with plastic sticks in 0.6M sorbitol, 20mM KMES pH 6 (1ml/g of starting cells wet weight) in eppendorf tubes. Centrifuge at 3000rpm for 5 minutes to pellet broken mitochondria

7. Collect supernatant and centrifuge at 12000rpm for 10 minutes. Suspend mitochondrial pellet in 0.6M sorbitol, 20mM KMES (100 µl/g of starting cells wet weight) and dilute with 20ml of 0.6M sorbitol, 20mM HEPES pH 7.4 (1ml/g of starting cells wet weight). Centrifuge 12000rpm for 10 minutes.

8. Suspend mitochondrial pellet in 0.6M sorbitol, 20mM HEPES accordingly to the pellet dimension. Mitochondria can be stored at -80˚C.

1.11.2. Quantification of proteins with Bradford method

Protein concentration was determined with Bradford method (Bradford, 1976). The "BioRad Protein Assay" commercial kit was utilized according to the manufacturer's instructions.

1.11.3. Mitochondrial Protein Localization and membrane association

(Glick et al., 1995; Diekert et al., 2001; Trott and Morano et al., 2004)

200µg of mitochondria with intact outer membrane were kept in 20mM HEPES pH 7.4, 0,6M sorbitol in the presence or absence of proteinase K (1mg/ml) for 60 minutes on ice. 0,1M PMSF (phenylmethylsulfonyl fluoride) was added to stop the reaction. The protein pellets were washed once with 20mM HEPES pH 7.4 plus 0,6M sorbitol, and suspended in SDS-PAGE sample buffer.

A modified version of the membrane association experiments of Trott and Morano was utilized to determine the resistance of Cab5p to sodium carbonate (pH 11.5) treatment. Equal amounts (150 µg) of the mitochondrial fraction was resuspended in TEGN (20 mM Tris-HCl pH 7.9, 0.5mM EDTA, 10% glycerol, 50mM NaCl) or TEGN and with 0.1 M $NaCO_3$ for 30 min on ice. The samples were subsequently centrifuged at 17,000 x g at 4°C to obtain soluble and membrane fractions.

1.11.4. Protein separation with SDS-page

Protein separation with SDS-page was performed with classical Laemmli system (Laemmli 1970). Separating gels were prepared at 12% polyacrylamide, stacking gels at 6%.

SOLUTION	Separating gel 12% For two gels	Stacking gel 6% For two gels
Tris HCL 1M pH 8.8	1.876 ml	-
Tris HCL 1M pH 6.8	-	0.751 ml
Polyacrylamide-bis (37.5-1)	4.5 ml	900 µl
SDS 20%	150 µl	60 µl
APS 10%	50 µl	30 µl
TEMED	12.5 µl	9 µl
H_2O	8.4 ml	4.26 ml

Running Buffer 5X for 1 liter: 15 g Tris-Base, 72 g glycine, H_2O to final volume. Diluite to 1X and add 0.5% SDS 20%. Running was performed for 1h 30'-2h at 100-120 Volts.

1.11.5. Western Blotting and Ig-detection

Separated proteins were transferred to nitrocellulose membranes by electro-blot for 1hr 40' at 2.5-3mA/cm2 in PerfectBlue™ Semi-Dry ElectroBlotter (PeqLab). Transfer buffer (200mM glycine, 25 mM Tris, 20% methanol) was used.

After semi-dry blotting membranes were blocked 1hr at RT with 5% non-fat dry milk prepared in washing buffer (TBS 1%, tween 0.1%) and then incubated o/n with appropriate primary antibody (mono or polyclonal, 5% non-fat dry milk prepared in washing buffer) at 4°C.

Blocked membranes were washed 3 times 10 min with washing buffer prior incubation with suitable secondary antibodies (Anti-mouse, anti-Rabbit and Anti-Rat), conjugated with horseradish peroxidase (1:5000 in 5% milk).

Primary antibodies	Secondary antibodies
α-HA 1:1000 (Roche)	α-rat 1:2500 (Millipore)
α-porin 1:5000 (Abcam Mitoscience)	α-mouse 1:7500 (Millipore)
α-PGK1 1:10000 (Abcam Mitoscience)	α-mouse 1:5000 (Millipore)
α-CoxII 1:5000 (Abcam Mitoscience)	α-mouse 1:5000 (Millipore)
α-CoxIV 1:8000 (Abcam Mitoscience)	α-mouse 1:5000 (Millipore)

α-Core1 1:500 (a kind gift from Prof. A. Barrientos)	α-rabbit 1:5000 (Millipore)
α-Rip1 1:500 (a kind gift from Prof. A. Tzagoloff)	α-rabbit 1:5000 (Millipore)

After 2hr incubation membranes were washed as above and developed with ClarityTM Western ECL Substrate (BIO-RAD) commercial kit.

1.11.6. Preparation of a mitochondrial enriched fraction

(Soto et al., 2009)

Cells were pre-grown on YNB medium supplemented with 2% glucose were inoculated in the same medium supplemented with 0.2% glucose and 2% galactose until an OD/ml = 1.5-2 was reached. Galactose was chosen as carbon source since it does not inhibit mitochondrial function and minimizes the presence of petite cells (galactose does not allow the growth on YNB medium of petite cells, whose frequency was lower than 3%).

The following protocol was used:

1. Harvest 20-40 ml of cells at about 2 OD
2. Spin at 4000-5000 rpm for 5 min
3. Resuspend pellet in 25 ml of H20 and spin at 4000-5000 rpm for 3 min
4. Resuspend pellet in 1 ml of H20 and transfer cells to eppendorf tubes. Centrifuge at 7000 rpm for 30 sec and get rid of the supernatant.
5. Resuspend pellet in 400 µl of sorbitol 0.6M and DTT 5mM and store at RT for 10 min
6. Centrifuge at 7000 rpm for 30 sec and get rid of the supernatant
7. Resuspend pellet in 400 µl of sorbitol 1.2M and Tris-HCl 10mM pH 7.5 and zymolyase 5mg/ml
8. Incubate at RT for 10-40 min until 80-90% of the cells have been converted to spheroplasts
9. Work on ice. Centrifuge at 5400 g for 8 min at 4°C and get rid of the supernatant
10. Wash pellet twice with 1 ml of STE solution (sorbitol 0.6M, Tris-HCl 20mM pH 7.5, EDTA 1mM). Centrifuge at 5400 g for 5 min at 4°C.
11. Suspend pellet in 100-200 µl STE solution accordingly to the pellet
12. Freeze at -80°C and defrost at RT three times (10 min freeze + 10 min defrost)
13. Determine protein concentration as described in paragraph 1.11.2

1.11.7. Succinate Dehydrogenase (SQDR) activity

This assay measures the rate of reduction of an artificial electron acceptor as dichlorophenolindophenol (DCPIP) by complex II as modified by Kim and Beattie, 1973. Mitochondria were prepared as described in section 1.11.6.

Solutions needed:

- 10 mM K-phosphate pH 7.8 + EDTA 2mM
- 80mM KCN
- 10mM succinate pH 7.4
- 20mM DCPIP
- 100mM NaN3
- 50mM ATP
- 1% Na-DOC
- 20mM dUQ2

The SDH activity was recorded at 600nm on 4 mg/ml mitochondrial aliquots. Specific activity: SQDR activity was calculated with ε of 22 and the following formula (ΔOD*ε/min mg).

1.11.8. Cytochrome c oxidase (COX) activity

This assay measures the rate of cytochrome c oxidation by complex IV in yeast as described by Wharton and Tzagaloff, 1967. Mitochondria were prepared as described in section 1.11.6.

Solutions needed:

- 20mM K-phosphate pH 7.5
- 1% cytochrome c in 20mM K-phosphate pH 7.5
- 1% Na-DOC
- KFeCN3

COX activity was recorded at 550 nm on 2 mg/ml mitochondrial aliquots. Specific Activity: COX activity was calculated with ε of 18.5 and the following formula [2.3log (A1/A2)/ (ε*min*mg)]*ΔOD.

1.11.9. NADH Cytochrome c Reductase (NCCR) activity

This assay measures the combined activity of NADH dehydrogenase and complex III in yeast. Electron flux is from NADH-DH to complex III *via* ubiquinol to the final acceptor cytochrome c. Mitochondria were prepared as described in section 1.11.6.

Solution needed:

- 10mM K-phosphate pH 7.5
- 80mM KCN
- 1% cytochrome c (bovine or horse heart, in K-phosphate pH 7.5 buffer)
- 0.1M NADH in K-phosphate pH 7.5
- 1% Na-DOC

NCCR activity is registered at 550nm on 2mg/ml mitochondrial aliquots. Specific activity is calculated with cytochrome c ε of 18.5 and the following formula (ΔOD*ε/min mg).

For all these respiratory complex activity statistical analysis was performed through a unpaired two-tailed t-test. Only p values of less than 0.05 were considered significant

1.12. High throughput screening: Drug drop test

(Couplan et al., 2011)

Cells were inoculated in YP medium + 2% ethanol and incubated at 28°C in constant shaking. 12x12 plates were filled with 90 ml of YP solid medium supplemented with 2% ethanol and 0.5X streptomycin. After 2 days of growth $4x10^5$ (*cab1l*^{G351S}) cells are seeded onto the plates. After the seed, filters of 6 mm of diameter were put on the agar surface and spotted with the compound to test varying the quantity both of the filters and the molecule depending on primary or secondary screening. As positive control a central spot by of *cab1*Δ/pFL39*CAB1* was used while DMSO was used as negative control. Plates were incubated at 37°C for 7 days and the growth of the mutant strain was monitored. For the screening on the mutant strain *cab1l*^{N290I} we used the screening conditions previously described for *cab1l*^{G351S} (number of cells, temperature and carbon sources).

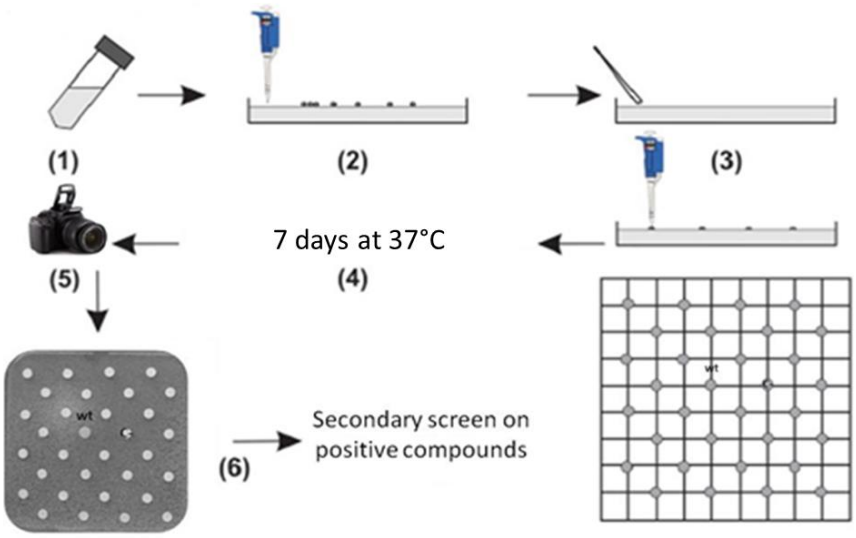

Fig 1.6 Schematic representation of Drug drop test. From Couplan et al., 2011.

References

Afshar, K., Gönczy, P., DiNardo, S., Wasserman, S.A. **(2001)** *fumble* Encodes a Pantothenate Kinase Homolog Required for Proper Mitosis and Meiosis in *Drosophila melanogaster*. **Genetics** 157: 1267–1276

Alfonso-Pecchio, A., Garci, M., Leonardi, R., and Jackowski, S. **(2012**). Compartmentalization of mammalian pantothenate kinases**. PLoS. One**.

Almeida,T., Marques, M., Mojzita, D., Amorim, M.A., Silva, R.D., Almeida, B., Rodrigues, P., Ludovico, P., Hohmann, S., Moradas-Ferreira, P., Côrte-Real, M., Costa, V. **(2008).** Isc1p plays a key role in hydrogen peroxide resistance and chronological lifespan through modulation of iron levels and apoptosis. **Mol Biol Cell** 19(3):865-76

Amamoto, R., Arlotta, P., **(2014)**. Development-inspired reprogramming of the mammalian central nervous system. **Science** 343: 1239882.

Aoun, M., A., Tiranti, V. **(2015)** Mitochondria: A crossroads for lipi metabolism defect in neurodegeneration with brain iron accumulation diseases. **The Internationla Journal of Biochemstry & Cell Biology** 63:25-31

Arber ,C., Angelova, P.R., Wiethoff, S., Tsuchiya, Y., Mazzacuva, F., Preza, E., Bhatia, K.P., Mills, K., Gout, I., Abramov, A.Y., Hardy, J., Duce, J.A., Houlden, H., Wray, S. **(2017)** iPSC-derived neuronal models of PANK2-associated neurodegeneration reveal mitochondrial dysfunction contributing to early disease.**PLoS One**. ;12(9):e0184104.

Arber, C.E., Li, A.,Houlden, H., Wray, S. **(2016)** Review: Insights into molecular mechanisms of disease in neurodegeneration with brain iron accumulation: unifying theories. **Neuropathol Appl Neurobiol.** 42(3):220-41

Armstrong, J.W. (1999). A review of high-throughput screening approaches for drug discovery. **Thousand Oaks,** CA: HTS Consulting Ltd*.:* 19-33.

Ausubel, F.M., Brent, R., Kingston, R.E., Moore, D.D., Seidman, J.G., Smith, J.A., Struhl, K. **(1994**). Current Protocols in Molecular Biology. **Wiley, New York.**

Ayala, A., Muñoz, M.F., Argüelles, S. **(2014)** Lipid peroxidation: production, metabolism, and signaling mechanisms of malondialdehyde and 4-hydroxy-2-nonenal. **Oxid Med Cell Longev**. 2014:360438.

Baddiley, J., Thain, E.M., Novelli, G.D., and Lipmann, F. **(1953)** Structure of coenzyme A. **Nature** 171, 76

Barberis, A., Gunde, T., Berset, C., Audetat, S., Luthi, U. **(2005).** Yeast as a screening tool. **Drug Discovery Today: Technologies** 2: 2187-92.

Baruffini, E., Ferrero, I., Foury, F. **(2010)** In vivo analysis of mtDNA replication defects in yeast. **Methods**.51(4): 426-36

Bassett, D..E.. Jr, Boguski, M.S., Hieter, P. **(1996)** Yeast genes and human disease**. Nature** 379: 589-90.

Batista-Nascimento, L., Pimentel, C., Menezes, R.A., Rodrigues-Pousada, C. **(2012)** Iron and Neurodegeneration: From Cellular Homeostasis to Disease. **Oxidative Medicine and Cellular Longevity** 2012:128647

Bernardi, P., Vassanelli, S., Veronese, P., Colonna, R., Szabo, I., Zoratti,M. **(1992)** Modulation of the mitochondrial permeability transition pore. Effect of protons and divalent cations**. J. Biol. Chem.** 267: 2934–2939.

Bettencourt, C., Forabosco, P., Wiethoff, S., Heidari, M., Johnstone, D.M., Botía, J.A., Collingwood, J.F., Hardy, J.; et al., **(2015)** Gene co-expression networks shed light into diseases of brain iron accumulation. **Neurobiol Dis.** 87:59-68

Bleackley, M.R., MacGillivray, R.T.A. **(2011)** Transition metal homeostasis: from yeast to human disease. **Biometals** 24(5): 785-809

Boeke, J.D., LaCroute, F., Fink, G.R. **(1984).** A positive selection for mutants lacking orotidine-5'-phosphate decarboxylase activity in yeast: 5-fluoro-orotic acid resistance. **Mol. Gen. Genet***.* 197: 345-6.

Bonaccorsi di Patti, M.C., Miele,R., Eugenia Schininà, M., Barra, D. **(2005)** The yeast multicopper oxidase Fet3p and the iron permease Ftr1p physically interact. **Biochem Biophys Res Commun** 333(2):432–437

Bonneaud, N., Ozier-Kalogeropoulos ,O., Li, G.Y., Labouesse, M., Minvielle-Sebastia, L., Lacroute, F. **(1991).** A family of low and high copy replicative, integrative and single-stranded *S. cerevisiae/E. coli* shuttle ectors. **Yeast**, 7: 609-15.

Boominathan, R., Doran, P.M. **(2003)** Cadmium tolerance and antioxidative defenses in hairy roots of the cadmium hyperaccumulator, Thlaspi caerulescens. **Biotechnol Bioeng**.83(2):158-67.

Bosveld, F., Rana, A., Lemstra, W., Kampinga, H.H., Sibon, O.C. **(2008)** Drosophila phosphopantothenoylcysteine synthetase is required for tissue morphogenesis during oogenesis. **BMC Res Notes** 29 (1):75.

Bozaquel-Morais, B.L., Madeira, J.B., Maya-Monteiro, C.M., Masuda, C.A. and Montero-Lomeli, M. **(2010)** A new fluorescence-based method identifies protein phosphatases regulating lipid droplet metabolism. **PLoS One 5**, e13692.

Bradford M.M. **(1976)**. A rapid and sensitive method for the quantitation of microgram quantities of proteins utilizing the principle of protein dye binding. **Anal. Biochem** 72: 248–254.

Brown, N.M., Anderson, S.A., Steffen, D.W., Carpenter, T.B., Kennedy, M.C., Walden, W.E., Eisenstein, R.S.**(1998)** Novel role of phosphorylation in Fe-S cluster stability revealed by phosphomimetic mutations at Ser-138 of iron regulatory protein 1. **Proc Natl Acad Sci U S A** 95(26):15235-40.

Brunetti, D., Dusi, S., Giordano, C., Lamperti, C., Morbin, M., Fugnanesi, V., Marchet, S., Fagiolari, G., Sibon, O., Moggio, M., d'Amati, G., Tiranti, V. **(2014)** Pantethine treatment is effective in recovering the disease phenotype induced by ketogenic diet in a pantothenate kinase-associated neurodegeneration mouse model**. Brain A Journal of Neurology**

Brunetti, D., Dusi, S., Morbin, M., Uggetti, A., Moda, F., D'Amato, I., Giordano, C., d'Amati, G., Cozzi, A., Levi, S., Hayflick, S., And Tiranti, V. **(2012).** Pantothenate kinase-associated neurodegeneration: altered mitochondria membrane potential and defective respiration in Pank2 knock-out mouse model. **Human Molecular Genetics** 21(24): 5294-5305.

Bulteau AL, O'Neill, H.A., Kennedy, M.C., Ikeda-Saito, M., Isaya, G., Szweda, L.I. **(2004)** Frataxin acts as an iron chaperone protein to modulate mitochondrial aconitase activity. **Science** 305(5681): 242–245

Caiazzo, M., Dell'Anno, M.T., Dvoretskova, E., Lazarevic, D., Taverna, S., Leo, D., Sotnikova, T.D., et al., **(2011)**. Direct generation of functional dopaminergic neurons from mouse and human fibroblasts. **Nature** 476: 224–227

Campanella, A., Privitera, D., Guaraldo, M., Rovelli, E., Barzaghi, C., Garavaglia, B., Santambrogio, P., Cozzi, A., Levi, S. **(2012)** Skin fibroblasts from pantothenate kinase-associated neurodegeneration patients show altered cellular oxidative status and have defective iron-handling properties. **Human Molecular Genetics**

Campuzano, V., Montermini, L., Moltò MD, Pianese, L., Cossée, M., Cavalcanti, F.,et al., **(1996)**. Friedreich's ataxia: autosomal recessive disease caused by an intronic GAA triplet repeat expansion. **Science**. 271(5254): 1423-7

Carnero, A. **(2006).** High Throughput Screening in drug discovery. **Clinical and Translational Oncology** 8: 482-90.

Caroline, C., Philpott **(2006)** Iron uptake in fungi: A system for every source. **Biochimica et Biophysica Acta (BBA) Molecular Cell Research** 1763(7): 636-645

Chen, X.Z., Peng, J.B. Cohen, A.,Nelson, H.,Nelson, N., Hediger, M.A. **(1999)** Yeast SMF1 mediates H(+)-coupled iron uptake with concomitant uncoupled cation currents. **J Biol Chem** 274(49): 35089–35094

Chen, Y., Siewers, V., Nielsen, J. **(2012)** Profiling of Cytosolic and Peroxisomal Acetyl-CoA Metabolism in Saccharomyces cerevisiae. **Plos. One**. 7(8) e42475

Claros, M.G., and Vincens, P. **(1996).** Computational method to predict mitochondrially imported proteins and their targeting sequences. **Eur J Biochem** 241(3): 779–786.

Colombelli, C., Aoun, M., Tiranti V. **(2014)**. Defective lipid metabolism in neurodegeneration with brain iron accumulation (NBIA) syndromes: not only a matter of iron. **J Inherit Metab Dis**. 38(1):123-36.

Couplan, E., Aiyar, R.S., Kucharczyk, R., Kabala, A., Ezkurdia, N., Gagneur, J., St. Onge, R.P., Sali, B., Soubigou, F., Le Cann, M., Steinmetz, L.M., di Rago, J-P., Blondel, M. **(2011).** A yeast-based assay identifies drugs active against human mitochondrial disorders. **Proceedings of the National Academy of Sciences of the United States of America** 108: 11989-94.

Daum ,G., Lees, N.D., Bard, M., Dickson, R. **(1998)** Biochemistry, cell biology and molecular biology of lipids of Saccharomyces cerevisiae. **Yeast**.14(16): 1471-510.

Daum, G., Tuller, G., Nemec, T., Hrastnik, C., Balliano, G., Cattel, L., Milla, P., Rocco, F., Conzelmann, A., Vionnet, C., Kelly, D.E., Kelly, S., Schweizer, E., Schüller, H.J., Hojad, U., Greiner, E., Finger, K. **(1999)** Systematic analysis of yeast strains with possible defects in lipid metabolism **Yeast** 15(7): 601-14.

De Virgilio, C., Burckert, N., Barth, G., Neuhaus, J.M., Boller, T., et al. **(1992)** Cloning and disruption of a gene required for growth on acetate but not on ethanol: the acetyl-coenzyme A synthetase gene of *Saccharomyces cerevisiae*. **Yeast** 8: 1043–1051

Diekert, K., De Kroon, A.I., Kispal, G, Lill, R. **(2001)**. Isolation and subfractionation of mitochondria from the yeast Saccharomyces cerevisiae. **Methods Cell Biol** 65: 37-5

Dower, W. J., Miller, J. F., Ragsdale, C. W. **(1988).** High efficiency transformation of *E. coli* by high voltage electroporation. **Nucleic Acids Res** 16: 6127-45

Dusi, S., Valletta, L., Haack, T.B., Tsuchiya, Y., Venco, P., Pasqualato, S., Goffrini, P., Tigano, M., Demchenko, N., Wieland, T., Schwarzmayr, T., Strom, T.M., Invernizzi, F., Garavaglia, B., Gregory, A., Sanford, L., Hamada, J., Bettencourt, C., Houlden, H., Chiapparini, L., Zorzi, G., Kurian, M.A., Nardocci, N., Prokisch, H., Hayflick, S., Gout, I., Tiranti, V. **(2014)** Exome sequence reveals mutations in CoA synthase as a cause of neurodegeneration with brain iron accumulation. **American Journal Human Genetics** 94(1):11-22

Esterbauer, H., Schaur, R.J., Zollner, H. **(1991)** Chemistry and biochemistry of 4-hydroxynonenal, malonaldehyde and related aldehydes. **Free Radic Biol Med.** 11(1):81-128. R

Evers, C., Seitz, A., Assmann, B., Opladen, T., Karch, S., Hinderhofer, K., Granzow, M., Paramasivam, N., Eils, R., Diessl, N., Bartram, C.R., Moog, U**.(2017)** Diagnosis of CoPAN by whole exome sequencing: Waking up a sleeping tiger's eye **Am J Med Genet A**.

Foury, F,and Cazzalini, O **(1997)**. Deletion of the yeast homologue of the human gene associated with Friedreich's ataxia elicits iron accumulation in mitochondria. **FEBS Lett** 411(2-3): 373-7

Fujiki, Y., Hubbard, A.L., Fowler, S., Lazarow, P.B. **(1982)** Isolation of intracellular membranes by means of sodium carbonate treatment: application to endoplasmic reticulum. **J Cell Biol.**93(1):97-102.

Gall, J., JJr, Skrha, Buchal, R., Sedlackova, E., Verebova, K., Platenik, J. **(2012).** Induction of the mitochondrial permeability transition (MPT) by micromolar iron: liberation of calcium is more important than NAD(P)H oxidation. **Biochim. Biophys. Acta** 1817: 1537–1549.

Galy, B., Ferring, D., Benesova, M., Benes, V., Hentze, M.W. **(2004)** Targeted mutagenesis of the murine IRP1 and IRP2 genes reveals context-dependent RNA processing differences in vivo. **RNA**.10(7): 1019-25.

Garber Morales, J., Holmes-Hampton, G. P., Miao, R., Guo, Y., Münck, E., Lindahl, P. A. **(2010)** Biophysical characterization of iron in mitochondria isolated from respiring and fermenting yeast. **Biochemistry** 49: 5436-5444

Geerlof, A., Lewendon, A., Shaw, W.V. **(1999)** Purification and Characterization of Phosphopantetheine Adenylyltransferase from Escherichia coli. **The Journal of Biological Chemistry** 274(38) 27105–27111

Georgatsou, E., and Alexandraki, D. **(1994)** Two distinctly regulated genes are required for ferric reduction, the first step of iron uptake in *Saccharomyces cerevisiae*. **Molecular and Cellular Biology** 14(5): 3065–3073

Gietz, R.D. and Wood, R.A. **(2002)** Transformation of yeast by the LiAc/SS carrier DNA/peg method. **Methods Enzymol.** 350: 87-96.

Glick, B.S., and Pon, L.A. **(1995)**. Isolation of highly purified mitochondria from Saccharomyces cerevisiae. **Methods Enzymol** 260: 213–223.

Goffeau, A., Barrell, B.G., Bussey, H., Davis, R.W., Dujon, B., Feldmann, H., Galibert, F., Hoheisel, J.D., Jacq, C., Johnston, M., Louis, E.J., Mewes, H.W., Murakami, Y., Philippsen, P., Tettelin, H., Oliver, S.G. **(1996)** Life with 6000 genes. **Science** 274(5287): 546, 563-7

Goffrini, P., Ercolino, T., Panizza, E., Giachè, V., Cavone, L., Chiarugi, A., Dima, V., Ferrero, I., Mannelli, M. **(2009)** Functional study in a yeast model of a novel succinate dehydrogenase subunit B gene germline missense mutation (C191Y) diagnosed in a patient affected by a glomus tumor. **Hum. Mol. Genet***.* 18: 1860-68.

Gogvadze, V., Walter, P.B., Ames, B.N. **(2003).** The role of $Fe2^{+}$ induced lipid peroxidation in the initiation of the mitochondrial permeability transition. **Arch. Biochem. Biophys**. 414: 255–260.

Greenspan, P., Mayer, E.P., Fowler, S.D. **(1985)**. Nile red: a selective fluorescent stain for intracellular lipid droplets. **J Cell Biol** 100(3): 965-73

Gregory, A., and Hayflick, S.J. **(2005)**. Neurodegeneration with brain iron accumulation. **Folia Neuropatho** 43(4): 286-96.

Gregory, A., Polster, B.J., Hayflick, S.J. **(2009)** Clinical and genetic delineation of neurodegeneration with brain iron accumulation. **J Med Genet.** 46(2):73-80

Gutteridge, J.M. and Halliwell, B. **(2000)** Free radicals and antioxidants in the year 2000. A historical look to the future. **Ann. N. Y. Acad. Sci** 899: 136-147

Halliwell, B. **(1992)** Reactive oxygen species and the central nervous system. **Journal of Neurochemistry** 59(5): 1609–1623

Halliwell, B. **(1996)** Free radicals, proteins and DNA: oxidative damage versus redox regulation. **Biochemical Society Transactions** 24(4): 1023–1027

Hancock, L.C., Behta, R.P., Lopes, J.M. **(2006)** Genomic analysis of the Opiphenotype. **Genetics** 173: 621–634.

Harris, Z.L., Durley, A.P., Man, T.K., Gitlin, J.D. **(1999)** Targeted gene disruption reveals an essential role for ceruloplasmin in cellular iron efflux. **Proceedings of the National Academy of Sciences of the United States of America** 96(19): 10812–10817

Harting, M.B., Hörtnagel, K., Garavaglia, B., Zorzi, G., Kmiec, T., Klopstock, T, Rostasy, K., Svetel, M., Kostic, V.S., Schuelke, M., Botz, E., Weindl, A., Novakovic, I., Nardocci, N., Prokisch, H., Meitinger, T. **(2006)**. Genotypic and phenotypic spectrum of *PANK2* mutations in patients with neurodegeneration with brain iron accumulation. **Annals Of Neurology** 59(2): 248-256.

Hassett, R., Dix, D.R. et al **(2000)** The Fe(II) permease Fet4p functions as a low affinity copper transporter and supports normal copper trafficking in *Saccharomyces cerevisiae.* **Biochem J** 351(2): 477–484

Hayflick, S.J., Westaway, S.K., Levinson, B., Zhou, B., Johnson, M.A., Ching, K.H.L., Gitschier, J. **(2003)** Genetic, Clinical, and Radiographic Delineation of Hallervorden–Spatz Syndrome. **The new england journal of medicine** 2003;348:33-40

Hayflick, SJ. **(2006)** Neurodegeneration with brain iron accumulation: from genes to pathogenesis. **Semin Pediatr Neurol**.3(3):182-5.

Ho, S.N., Hunt, H.D., Horton, R.M., Pullen, J.K., Pease, L.R. **(1989).** Site-directed mutagenesis by overlap extension using the polymerase chain reaction. **Gene**, 77: 51-9.

Hoffman, C. S. and Winston, F. **(1987)** A ten-minute DNA preparation from yeast efficiently releases autonomous plasmids for transformation of Escherichia coli. **Gene** 57: 267-72.

Hong, B.S., Senisterra, G., Rabeh, W.M., Vedadi, M., Leonardi, R., Zhang, Y.M., Rock, C.O., Jackowski, S., Park, H.W. **(2007)** Crystal structures of human pantothenate kinases. Insights into allosteric regulation and mutations linked to a neurodegeneration disorder. **J Biol Chem.** 282(38):27984-93

Hörtnage,l K., Prokisch, H., Meitinger, T., **(2003)** An isoform of hPANK2, deficient in pantothenate kinase-associated neurodegeneration, localizes to mitochondria**. Hum Mol Genet.** 12(3):321-7.

Hughes, T.R. **(2002)** Yeast and drug discovery. **Funct. Integr. Genomics** 2: 199-211.

Huh, W., Falvo, J.V., Gerke, L.C., Carroll, A.S., Russell, W., Howson, Jonathan, S., Weissman, Erin, K. O'Shea **(2003)** Global analysis of protein localization in budding yeast. **Nature** 425, 686-691

Johnson, M.A., Kuo, Y.M., Westaway, S.K., Parker, S.M., Ching, K.H., Gitschier, J., and Hayflick, S.J. **(2004)** Mitochondrial localization of human PANK2 and hypotheses of secondary iron accumulation in pantothenate kinase-associated neurodegeneration. **Ann. N. Y. Acad. Sci**. 1012, 282–298.

Kaiser, C., Michaelis, S. and Mitchell, A**. (1994)** Methods in Yeast Genetics: a Laboratory Course Manual. **Cold Spring Harbor Laboratory Press** Cold Spring Harbor, NY.

Kaplan, J., McVey Ward, D., Crisp, R.J., Philpott, C.C. **(2006)** Iron dependent metabolic remodeling in S. cerevisiae. **Biochim. Biophys. Acta** 1763: 646-651

Khatri, D., Zizioli, D., Tiso, N., Facchinello, N., Vezzoli, S., Gianoncelli, A., Memo, M., Monti, E., Borsani, G., Finazzi, D. **(2016)** Down-regulation of coasy, the gene associated with NBIA-VI, reduces Bmp signaling, perturb dorso-ventral patterning and alters neuronal development in zebrafish. **Sci Rep**. 28(6): 37660

Khurana,V., Lindquist, S. **(2010)** Modelling neurodegeneration in Saccharomyces cerevisiae: why cook with baker's yeast? **Nat Rev Neurosci** 11(6): 436-49.

Kim, I.C, and Beattie, D.S. **(1973)** Formation of the yeast mitochondrial membrane. 1. Effects of inhibitors of protein synthesis on the kinetics of enzyme appearance during glucose derepression. **Eur. J. Biochem**. 36: 509-18.

Kimura, K., Yamaola, M., Kamisaka, Y. **(2004)**. Rapid estimation of lipids in oleaginous fungi and yeasts using Nile red fluorescence. **J Microbiol Methods** 56(3): 331-338

Klein, H.P., Jahnke, L, **(1979)** Effects of aeration on formation and localization of the acetyl coenzyme A synthetase of *Saccharomyces cerevisiae*. **J Bacteriol** 137: 179–184.

Kosman, D.J. **(2003)** Molecular mechanisms of iron uptake in fungi. **Mol Microbiol** 47(5): 1185–1197

Kotzbauer, P.T., Truax, A.C., Trojanowski, J.Q., Lee, V.M.Y. **(2005)** Altered Neuronal Mitochondrial Coenzyme A Synthesis in Neurodegeneration with Brain Iron Accumulation Caused by Abnormal Processing, Stability, and Catalytic Activity of Mutant Pantothenate Kinase 2. **The Journal of Neuroscience**

Kruer, M.C., Hiken, M., Gregory, A.,Malandrini, A., Clark, D., Hogarth, P., Grafe, M., Hayflick, S.J.,Woltjer, R.L., **(2011).** Novel histopathologic findings in molecularly-confirmed pantothenate. **Brain**. 134, 947-58.

Kumar, A., Agarwal, S., Heyman, J.A., Matson, S., Heidtman, M., et al. **(2002)** Subcellular localization of the yeast proteome. **Genes Dev** 16: 707–719.

Kuo, Y.M., Duncan, J.L., Westaway, S.K., Yang, H., Nune, G., Xu, E.Y., Hayflick, S.J., Gitschier, J. **(2005)** Deficiency of pantothenate kinase 2 (Pank2) in mice leads to retinal degeneration and azoospermia. **Human Molecular Genetics**

Kuo, Y.M., Hayflick, S. J., Gitschier, J. **(2007)** Deprivation of pantothenic acid elicits a movement disorder and azoospermia in a mouse model of pantothenate kinase-associated neurodegeneration. **Journal of Inherited Metabolic Disease**.30(3): 310-317

Kupke, T. **(2002)** Molecular Characterization of the 4'-Phosphopantothenoylcysteine Synthetase Domain of Bacterial Dfp Flavoproteins. **The Juornal of Biological Chemistry** 277 (39) 36137–36145

Kwork, E.Y., Severance, S., Kosman, D.J.**(2006)** Evidence for iron channeling in the Fet3p-Ftr1p high-affinity iron uptake complex in the yeast plasma membrane. **Biochemistry** 45(20): 6317–6327

Laemmli, U.K. **(1970).** Cleavage of structural proteins during the assembly of the head of bacteriophage T4. **Nature** 227: 680-5.

Leonardi, R., Zhang, Y.M., Lykidis, A., Rock, C.O., Jackowski, S.**(2007)** Localization and regulation of mouse pantothenate kinase 2.**FEBS Lett.**581(24):4639-44.

Leonardi, R., Zhang, Y.M., Rock, C.O., Jackowski, S. **(2005)** Coenzyme A: Back in action. **Progress in Lipid Research** 44(2-3): 125-53

Leoni, V., Strittmatter, L., Zorzi, G., Zibordi, F., Dusi, S., Garavaglia, B., Venco, P., Caccia, C., Souza, A.L., Deik, A., Clish, C.B., Rimoldi, M., Ciusani, E., Bertini, E., Nardocci, N., Mootha, V.K., Tiranti, V. **(2012)** Metabolic

consequences of mitochondrial coenzyme A deficiency in patients with PANK2 mutations. Molecular Genetics and Metabolism **Mol Genet Metab**.105(3):463-71

Levi, S., and Finazzi, D**.(2014)** Neurodegeneration with brain iron accumulation: update on pathogenic mechanisms. **Front Pharmacol**. 7(5).:99

Li, L., Bagley, D., Ward, D.M., and Kaplan, J. **(2008)** Yap5 is an ironresponsive transcriptional activator that regulates vacuolar iron storage in yeast. **Molecular and Cellular Biology** 28(4): 1326–1337

Li, L., Chen, O.S., McVey Ward, D., Kaplan, J. **(2001)** CCC1 is a transporter that mediates vacuolar iron storage in yeast. **J Biol Chem** 276(31): 29515–29519

Lill, R., and Muhlenhoff, U. **(2008)** Maturation of Iron-Sulfur Proteins in Eukaryotes: Mechanisms, Connected Processes, and Diseases. **Annu. Rev. Biochem.** 77:669-700

Lodi, R., Cooper, J.M.,Bradley, J.L., Manners, D., Styles, P.,Taylor, D.J.,Schapira, A.H. **(1999)** Deficit of in vivo mitochondrial ATP production in patients with Friedreich ataxia **Proc Natl Acad Sci U S A.** 96(20):11492-5.

Lõoke, M., Kristjuhan, K., Kristjuhan, A. **(2011)** Extraction of genomic DNA from yeasts for PCR-based applications. **Biotechniques** 50: 325-8.

Magni, G.E. and Von Borstel, R.C. **(1962)**. Different rates of spontaneous mutation during mitosis and meiosis in yeast. **Genetics** 47(8): 1097-1108.

Maniatis,T., Fritsch, E., Sambrook, J**.(1982).** Molecular cloning. A laboratory manual. **Cold Spring Harbor Laboratory Press** Cold Spring Harbor, NY.

Marchetti, M.A., Weinberger, M., Murakami, Y., Burhans, W.C., Huberman, J.A. **(2006)** Production of reactive oxygen species in response to replication stress and inappropriate mitosis in fission yeast. **J Cell Sci**. 119(1):124-31.

Martinez, D.L., Tsuchiya, Y., Gout, I. **(2014)** Coenzyme A biosynthetic machinery in mammalian cells. **Biochem Soc Trans**. 42(4):1112-7

Matlack, K.E., Tardiff, D.F., Narayan, P., Hamamichi, S., Caldwell, K.A., Caldwell, G.A., Lindquist, S. **(2014)** Clioquinol promotes the degradation of metal-dependent amyloid-β (Aβ) oligomers to restore endocytosis and ameliorate Aβ toxicity. **Proc Natl Acad Sci U S A**. 111(11):4013-8

Mena, N. P., Urrutia, P. J., Lourido, F., Carrasco, C. M., Nunez, M. T**. (2015)** Mitochondrial iron homeostasis and its dysfunctions in neurodegenerative disorders. **Mitochondrion** 21: 92-105

Mishra, P.K., Park, P.K., Drueckhammer, D.G. **(2001)** Identification of yacE (coaE) as the Structural Gene for Dephosphocoenzyme A Kinase in Escherichia coli K-12. **Journal of Bacteriology** 183(9) 2774–2778

Moreno-Cermeño, A., Obis, E., Bellì, G., Cabiscol, E., Ros, J., Tamarit, J. **(2010)** Frataxin depletion in yeast triggers up-regulation of iron transport systems before affecting iron-sulfur enzyme activities. **J Biol. Chem** 285(53): 41653-64

Mühlenhoff, U., Richhardt, N., Ristow, M., Kispal, G. Lill, R. **(2002).** The yeast frataxin homolog Yfh1p plays a specific role in the maturation of cellular Fe/S proteins. **Hum Mol Genet** 11(17): 2025–2036

Muhlenhoff, U., Stadler, J.A., Richhardt, N., Seubert, A., Eickhorst, T., Schweyen, R.J., et al., **(2003)** A specific role of the yeast mitochondrial carriers MRS3/4p in mitochondrial iron acquisition under iron-limiting conditions. **J Biol Chem** 278(42): 40612–40620

Nakamura, T., Pluskal, T., Nakaseko, Y., and Yanagida, M. **(2012)**. Impaired coenzyme A synthesis in fission yeast causes defective mitosis, quiescence-exit failure, histone hypoacetylation and fragile DNA. **Open Biol** 2(9): 120117

Neilands, J.B. **(1995)** Siderophores: structure and function of microbial iron transport compounds. **J Biol Chem** 270(45): 26723–26726

Nelson, D.L. and Cox, M.M. **(2010)** "I principi di biochimica di Lehninger" Zanichelli editore; quinta edizione

Nevitt, T., **(2011)** War-Fe-Re: iron at the core of fungal virulence and host immunity. **BioMetals**, 24(3): 547–558

Olzhausen ,J., Schübbe, S., Schüller, H.J. **(2009)** Genetic analysis of coenzyme A biosynthesis in the yeast *Saccharomyces cerevisiae*: identification of a conditional mutation in the pantothenate kinase gene *CAB1*. **Curr Genet** 55(2):163-73

Olzhausen, J., Moritz, T., Neetz, T., Schüller, H..J. **(2013)** Molecular characterization of the heteromeric coenzyme A-synthesizing protein complex (CoA-SPC) in the yeast Saccharomyces cerevisiae. **FEMS Yeast Research** 13(6):565-73

Orellana, D.I., Santambrogio, P., Rubio, A., Yekhlef, L., Cancellieri, C., Dusi, S., Giannelli, S.G., Venco, P., Mazzara, P.G., Cozzi, A., Ferrari, M., Garavaglia, B., Taverna, S., Tiranti, V., Broccoli, V., Levi, S. **(2016)** Coenzyme A corrects pathological defects in human neurons of PANK2-associated neurodegeneration. **EMBO Mol Med**. 8(10): 1197-1211

Pandey, A., Pain, J., Ghosh, A.K., Dancis, A., Pain, D. **(2015)** Fe–S cluster biogenesis in isolated mammalian mitochondria: coordinated use of persulfide sulfur and iron and requirements for GTP, NADH, and ATP. **J. Biol. Chem**. 290(1): 640–657.

Panizza, E., Ercolino, T., Mori, L., Rapizzi, E., Castellano, M., Opocher, G., Ferrero, I., Neumann, H.P., Mannelli, M., Goffrini, P. **(2013).** Yeast model for evaluating the pathogenic significance of SDHB, SDHC and SDHD mutations in PHEO-PGL syndrome. **Hum. Mol. Genet.** 22: 804-15.

Patil, V.A., Fox, J.L., Gohil, V.M., Winge, D.R., Greenberg, M.L. **(2012)** Loss of cardiolipin leads to perturbation of mitochondrial and cellular iron homeostasis. J **Biol Chem**. 288(3):1696-705.

Perry, T.L., Norman, M.G., Yong, V.W., Whiting, S., Crichton, J.U., Hansen, S. and Kish S.J. **(1985)** Hallervorden-Spatz disease: cysteine accumulation and cysteine dioxygenase deficiency in the globus pallidus. **Ann. Neurol.** 18, 482–489

Petersen Shay, K., Moreau, R.F., Smith, E.J., Smith, A.R., Hagen, T.M. (**2008)** Alpha-lipoic acid as a dietary supplement: Molecular mechanisms and therapeutic potential. **Biochim Biophys Acta**. 1790(10): 1149–1160.

Philpott CC, Protchenko O., Kim, Y.W., Boretsky, Y., Shakoury-Elizeh, M. **(2002)** The response to iron deprivation in *Saccharomyces cerevisiae*: expression of siderophore-based systems of iron uptake. **Biochem Soc Trans** 30(4): 698–702

Philpott, C.C. and Protchenko, O., **(2008)** Response to iron deprivation in *Saccharomyces cerevisiae*. **Eukaryotic Cell** 7(1): 20–27, 2008

Pitayu, L., Baruffini, E., Rodier, C., Rötig, A., Lodi, T., Delahodde, A. **(2016)** Combined use of Saccharomyces cerevisiae, Caenorhabditis elegans and patient fibroblasts leads to the identification of clofilium tosylate as a potential therapeutic chemical against POLG-related diseases. **Hum Mol Genet**. 25(4): 715-27.

Pommier, Y., Leo, E., Zhang, H., Marchand, C. **(2010)** DNA topoisomerases and their poisoning by anticancer and antibacterial drugs. **Chem Biol.** 17(5):421-33

Prachayasittikul, V., Prachayasittikul, S., Ruchirawat, S., Prachayasittikul, V. **(2013)** 8-Hydroxyquinolines: a review of their metal chelating properties and medicinal applications. **Drug Des Devel Ther**. 7:1157-78

Pronk, J.T., Steensma, H.Y., vanDijken ,J.P. **(1996)** Pyruvate metabolism in *Saccharomyces cerevisiae*. **Yeast** 12: 1607–1633.

Proszynski,T.J., Klemm, R.W., Gravert, M., Hsu, P.P., Gloor, Y., Wagner, J., Kozak, K., Grabner, H., Walzer, K., Bagnat, M., Simons, K., Walch-Solimena, C. **(2005)** A genome-wide visual screen reveals a role for sphingolipids and ergosterol in cell surface delivery in yeast. **Proc Natl Acad Sci U S A**. (50): 17981-6.

Protchenko, O., Ferea, T., Rashford, J., Tiedeman, J., Brown, P.O., Botstein, D., Philpott, C.C. **(2001)** Three cell wall mannoproteins facilitate the uptake of iron in Saccharomyces cerevisiae. **J Biol Chem.** 276(52):49244-50.

Puig, S., Askeland, E., Thiele, D.J. **(2005)** Coordinated remodeling of cellular metabolism during iron deficiency through targeted mRNA degradation. **Cell** 120(1): 99–110,

Rana, A., Seinen, E., Siudeja, K., Muntendam, R., Srinivasan, B., van der Want, J.J., Hayflick,S., Reijngoud, D.J., Kayser, O., Sibon, O.C **(2010)** Pantethine rescues a Drosophila model for pantothenate kinaseassociated neurodegeneration. **Proc. Natl. Acad. Sci. U. S. A**. 107(15): 6988–6993.

Reinders, J., Zahedim,R,P, Pfanner, N., Meisinger, C., Sickmann, A. **(2006).** Toward the complete yeast mitochondrial proteome: multidimensional separation techniques for mitochondrial proteomics. **J Proteome Res** 5:1543-5

Resnick, M.A., And Cox, B.S. **(2000)** Yeast as an honorary mammal. **Mutat Res Jun** 45 (1-2): 1-11

Rinaldi,T., Dallabona, C., Ferrero, I., Frontali, L., Bolotin-Fukuhara, M. **(2010)** Mitochondrial diseases and role of the yeast models **FEMS Yeast Res** 10(8): 1006-22

Romney, S. J., Thacker, C., and Leibold, E.A. **(2008)** An Iron Enhancer Element in the FTN-1 gene directs iron-dependent expression in Caenorhabditis elegans intestine. **Journal of Biological Chemistry** 283(2): 716–72

Rothstein, R.J. **(1983)** One step gene disruption in yeast. **Methods in Enzymology** 101: 202-11.

Rouault T.A. **(2013)** Iron metabolism in the CNS: implications for neurodegenerative diseases. **Nature** 14(8):551-64

Rouault, T.A. **(2006)** The role of iron regulatory proteins in mammalian iron homeostasis and disease. **Nat Chem Biol.** 2(8): 406-14.

Salehi-Lisar, S. Y., and Deljoo, S. **(2015)** The physiological effect of fluorene on *Triticum aestivum*, *Medicago sativa*, and *Helianthus annus.* **Cogent Food & Agriculture**. 1:1020189

Sambrook, J. and Russel, D. W. **(2001).** Molecular Cloning: a Laboratory Manual. **Cold Spring Harbor Laboratory Press**, Cold Spring Harbor, NY

Santambrogio, P., Dusi, S., Guaraldo, M., Rotundo, L. I., Broccoli, V., Garavaglia, B., Tiranti, V., Levi, S. **(2015)** Mitochondrial iron and energetic dysfunction distinguish fibroblasts and induced neurons from pantothenate kinase-associated neurodegeneration patients. **Neurobiol Dis.** 81: 144-53.

Schilke, B., Voisine, C., Beinert, H., Craig, E **(1999).** Evidence for a conserved system for iron metabolism in the mitochondria of *Saccharomyces cerevisiae*. **Proc Natl Acad Sci U.S.A.** 96(18): 10206–10211.

Schonauer, M.S., Kastaniotis, A.J., Kursu, V.A.S., Hiltunen, J.K., Dieckmann, C.L. **(2009)** Lipoic Acid Synthesis and Attachment in Yeast Mitochondria. **The Journal of Biological Chemistry** 284(35): 23234–23242

Shakoury-Elizeh M, Tiedeman J., Rashford, J., Ferea, T., Demeter, J., Garcia, E., et al., **(2004)** Transcriptional remodeling in response to iron deprivation in *Saccharomyces cerevisiae*. **Mol Biol Cell** 15(3): 1233–1243

Singh,P. **(2017).** Budding Yeast: An Ideal Backdrop for In vivo Lipid Biochemistry. **Front Cell Dev Biol**.10(4):156

Sitepu, I.R., Ignatia, L., Franz, A.K., Wong, D.M., Faulina, S.A., Tsui, M., Kanti, A., Boundy-Mills, K. **(2012)**. An improved high-throughput Nile red fluorescence assay for estimating intracellular lipids in a variety of yeast species. **J Microbiol Methods** 91(2): 321–328.

Smith, A.M., Ron Ammar, R., Corey Nislow, C., Giaever, G. **(2010).** A survey of yeast genomic assays for drug and target discovery. **Pharmacology & Therapeutics** 127: 156-64.

Song, W.,and Jackowski., S. **(1992)** Cloning, Sequencing, and Expression of the Pantothenate Kinase (coaA) Gene of Escherichia coli. **Journal of Bacteriology**, 174 (20) 6411-6417

Soto, I.C., Fontanesi, F., Valledor, M., Horn, D., Singh, R., Barrientos, A. **(2009)** Synthesis of cytochrome c oxidase subunit 1 is translationally downregulated in the absence of functional F1F0-ATP synthase. **Biochim. Biophys. Acta.** 1793: 1776-86.

Stearman, R., Yuan, D.S., Yamaguchi-Iwai, Y., Klausner, R.D., Dancis, A. **(1996)** A permease-oxidase complex involved in high-affinity iron uptake in yeast. **Science**.271(5255):1552-7.

Stehling, O., Mascarenhas, J., Vashisht, A.A., Sheftel, A.D., Niggemeyer, B., Rosser, R., Pierik, A.J., Wohlschlegel, J.A., Lill, R. **(2013)** Human CIA2A-FAM96A and CIA2B-FAM96B integrate iron homeostasis and maturation of different subsets of cytosolic-nuclear iron–sulfur proteins. **Cell Metab**. 18: 187–198.

Stolz, J., Sauer, N. **(1999**) The fenpropimorph resistance gene *FEN2* from *Saccharomyces cerevisiae* encodes a plasma membrane H+-pantothenate symporter. **J Biol Chem**. 274(26):18747-52.

Strauss, E. **(2010)** Coenzye A biosynthesis and enzymology. **Comprehensive Natural Products II** 351-410

Strauss, E., Kinsland, C., Ge, Y., McLafferty, F.W., Begley, T.P. **(2001)** The Identification and Characterization of Phosphopantothenoylcysteine Synthetase from E. coli Completes the Identification of Coenzyme A Biosynthetic Enzymes in Bacteria. **Journal of Biological Chemistry**

Subramanian, C., Yun, M.K., Yao, J., Sharma, L.K., Lee, R.E., White, S.W., Jackowski, S., Rock, C.O.J. **(2016)** Allosteric Regulation of Mammalian Pantothenate Kinase. **Biol Chem**. 291(42): 22302-22314

Takahashi, H., McCaffery, J.M., Irizarry, R.A., Boeke, J.D**. (2006)** Nucleocytosolic acetyl-coenzyme A synthetase is required for histone acetylation and global transcription. **Mol Cell** 23: 207–217.

Tamarit, J., Irazusta, V., Moreno-Cermeño, A., Ros ,J. **(2006)**. Colorimetric assay for the quantitation of iron in yeast. **Anal Biochem** 351(1):149-51

Tanzer, J.M., Slee, A.M., Kamay, B., Scheer, E. **(1978)** Activity of three 8-hydroxyquinoline derivatives against in vitro dental plaque. **Antimicrob Agents Chemother**. 13(6):1044-5.

Tardiff, D.F., and Lindquist, S. **(2013)** Phenotypic screens for compounds that target the cellular pathologies underlying Parkinson's disease. **Drug Discovery Today: Technologies** 10: 121-8.

Tenreiro, S., and Outeiro, T.F. **(2010)** Simple is good: yeastmodels of neurodegeneration. **FEMS Yeast Res** 10(8):970-9

Theil, E.C., Eisenstein, R.S**.(2000)** Combinatorial mRNA regulation: iron regulatory proteins and iso-iron-responsive elements (Iso-IREs). **J Biol Chem.** 275(52): 40659-62

Thomas, B. J. and Rothstein, R.**(1989)** Elevated recombination rates in transcriptionally active DNA. **Cell** 56: 619-30.

Torti, F.M., Torti, S.V. **(2002)** Regulation of ferritin genes and protein. **Blood** 99(10): 3505–3516

Trott, A., and Morano, K.A. **(2004).** SYM1 is the stress-induced Saccharomyces cerevisiae ortholog of the mammalian kidney disease gene Mpv17 and is required for ethanol metabolism and tolerance during heat shock. **Eukaryot Cell** 3(3):620-31

Turel, I **(2002),** The interactions of metal ions with quinolone antibacterial agents. **Coordination Chemistry Reviews** 232(1-2): 27-47

Uberbacher, E.C., and Mural, R.J. **(1991)**. Locating protein-coding regions in human DNA sequences by a multiple sensor-neural network approach. **Proc Natl Acad Sci USA** 88 (24):

Urbanowski, J.L., and Piper, R.C**.(1999)** The iron transporter Fth1p forms a complex with the Fet5 iron oxidase and resides on the vacuolar membrane. **J Biol Chem** 274(53):38061–38070

Van den Berg, M.A., Steensmam H.Y. **(1995)** ACS2, a *Saccharomyces cerevisiae* gene encoding acetyl-coenzyme A synthetase, essential for growth on glucose. **Eur J Biochem** 231: 704–713.

Van Roermund, C.W., Hettema, E.H., van den Berg, M., Tabak, H.F., Wanders, R.J. **(1999)** Molecular characterization of carnitine-dependent transport of acetyl-CoA from peroxisomes to mitochondria in *Saccharomyces cerevisiae* and identification of a plasma membrane carnitine transporter, Agp2p. **EMBO J** 18: 5843–5852.

Van Roermund, C.W.T., Elgersma, Y., Singh, N., Wanders, R.J.A., Tabak, H.F. **(1995)** The membrane of peroxisomes in *Saccharomyces cerevisiae* is impermeable to NAD(H) and acetyl-CoA under *in vivo* conditions**. EMBO J** 14: 3480–3486.

Venter, J.C. Adams, M.D., Myers, E.W., Li, P.W., Mural, R.J., Sutton, G.G. et al., **(2001)** The sequence of the Human genome. **Science**. 291: 1304-1351

Villa-Garcia, M., Choi, M., Hinz, F., Gaspar, M., Jesch, S. and Henry, S. **(2011)** Genome-wide screen for inositol auxotrophy in Saccharomyces cerevisiae implicates lipid metabolism in stress response signalingMol. **Genet. Genomics** 285: 125–149.

Wach, A., Brachat, A., Pohlmann, R. Philippsen, P. **(1994).** New heterologous modules for classical or PCR-based gene disruptions in *Saccharomyces cerevisiae*. **Yeast** 10; 1793–1808.

Waters, B.M., Eide, D.J. **(2002)** Combinatorial control of yeast FET4 gene expression by iron, zinc, and oxygen. **J Biol Chem** 277(37): 33749–33757

Wharton, D.C. and Tzagoloff, A. **(1967).** Cytochrome oxidase from beef heart mitochondria. **Methods Enzymol.** 10: 245-50.

Wilczynska, A., Aigueperse, C., Kress, M., Dautry, F., Weil, D. **(2005)** The translational regulatori CPEB1 provides a link between dcp1 bodies and stress granules. **Journal of Cell Science** 118(5): 981-992

Wu, Z., Li, C., Lv, S., Zhou, B **(2009)** Pantothenate kinase-associated neurodegeneration: insights from a Drosophila model. **Hum Mol Genet**.18(19): 3659-72.

Zhou, B., Westaway, S.K., Levinson, B., Johnson, M.A., Gitschier, J., and Hayflick, S.J. **(2001)**. A novel pantothenate kinase gene (PANK2) is defective in Hallervorden-Spatz syndrome. **Nat. Genet**. 28 345–349

Zhyvoloup, A., Nemazanyy, I., Panasyuk, G., Valovka, T., Fenton, T., Rebholz, H., Wang,, M.L., Foxon, R., Lyzogubov ,V., Usenko ,V., Kyyamova, R., Gorbenko, O., Matsuka, G., Filonenko, V., and Gout, I.T. **(2003)** Subcellular localization and regulation of coenzyme A synthase. **J Biol Chem** 278(50): 50316–50321.

Zizioli, D., Tiso, N., Guglielmini, A., Saraceno, C., Busolin, G., Giuliani, R., Khatri, D., Monti, E., Borsani, G., Argenton, F., Finazzi, D. **(2015)** Knock-out of pantothenate kinase 2 severly affects the development of the nervous and vascular system in zebrafish, providing new insights into PKAN disease. **Neurobiology of disease** 85: 35-48

Acknowledgements

I would like to thank my supervisor Prof.ssa Paola Goffrini for transmitting to me the love for research and science as well as her scientific support and her cordiality throughout these years.

I would also like to thank the Professors of the “Yeast Group”: Claudia Donnini, Tiziana Lodi and Enrico Baruffini. Many thanks to our collaborators Sabrina Dusi and Valeria Tiranti. Last but not least I would like to thank my past and present colleagues Cristina Dallabona, Micol Gilberti, Cecilia Nolli, Elisa Petennati, Laura Soliani, Jade Quartararo and Alberto Ferrari for their scientific and moral support and for the moments of fun shared throughout these years.

Published paper

Ceccatelli Berti C, Dallabona C, Lazzaretti M, Dusi S, Tosi E, Tiranti V, Goffrini P. **Modeling human Coenzyme A synthase mutation in yeast reveals altered mitochondrial function, lipid content and iron metabolism**. Microbial Cell 2015, Vol. 2, No. 4, pp. 126 - 135.

During my PhD, I also assessed the pathogenic role of two mutations in *SDH4* and *ISU1* genes using yeast as model system. *SDH4* encodes for a subunit of succinate dehydrogenase or respiratory complex II, while *ISU1* encodes for the protein scaffold involved in Fe-S cluster synthesis. The results obtained are reported in the following published paper:

Alston CL, **Ceccatelli Berti C,** Blakely EL, Olahova M, He L, McMahon CJ, Olpin SE, Hargreaves IP, Nolli C, McFarland R, Goffrini P, O'Sullivan MJ, Taylor RW. **A recessive homozygous p.Asp92Gly SDHD mutation causes prenatal cardiomyopathy and severe mitochondrial complex II deficiency**. Human Genetics 2015, Vol. 134, No. 8, pp. 869 – 879

Legati A, Reyes A, **Ceccatelli Berti C**, Stheling O, Marchet S, Lamperti C, Ferrari A, Robinson AJ, Mühlenhoff U, Lill R, Zeviani M, Goffrini P, Ghezzi D. **A novel de novo dominant mutation in ISCU associated with mitochondrial myopathy**. Journal of Medical Genetics 2017, Vol. 54, No 12, pp. 815-824. doi: 10.1136/jmedgenet-2017-104822

microbial cell

Research Article

www.microbialcell.com

Modeling human Coenzyme A synthase mutation in yeast reveals altered mitochondrial function, lipid content and iron metabolism

Camilla Ceccatelli Berti[1], Cristina Dallabona[1], Mirca Lazzaretti[1], Sabrina Dusi[2], Elena Tosi[1], Valeria Tiranti[2], Paola Goffrini[1,*]

[1] Department of Life Sciences, University of Parma, Parma, Italy.

[2] Unit of Molecular Neurogenetics – Pierfranco and Luisa Mariani Center for the study of Mitochondrial Disorders in Children, IRCCS Foundation Neurological Institute "C. Besta", Milan, Italy.

* Corresponding Author: Paola Goffrini, Department of Life Sciences, University of Parma, Parco Area delle Scienze 11/A; 43123 Parma, Italy; Tel: +39 0521905107; Fax: +39 0521905604; E-mail: paola.goffrini@unipr.it

ABSTRACT **Mutations in nuclear genes associated with defective coenzyme A biosynthesis have been identified as responsible for some forms of neurodegeneration with brain iron accumulation (NBIA), namely PKAN and CoPAN. PKAN are defined by mutations in *PANK2*, encoding the pantothenate kinase 2 enzyme, that account for about 50% of cases of NBIA, whereas mutations in CoA synthase *COASY* have been recently reported as the second inborn error of CoA synthesis leading to CoPAN. As reported previously, yeast cells expressing the pathogenic mutation exhibited a temperature-sensitive growth defect in the absence of pantothenate and a reduced CoA content. Additional characterization revealed decreased oxygen consumption, reduced activities of mitochondrial respiratory complexes, higher iron content, increased sensitivity to oxidative stress and reduced amount of lipid droplets, thus partially recapitulating the phenotypes found in patients and establishing yeast as a potential model to clarify the pathogenesis underlying PKAN and CoPAN diseases.**

doi: *10.15698/mic2015.04.196*
Received *originally: 05.12.2014;*
in revised form: 16.03.2015,
Accepted *22.03.2015,*
Published *06.04.2015.*

Keywords*: Saccharomyces cerevisiae, yeast model, Coenzyme A, NBIA, COASY, mitochondria, iron accumulation, lipid content.*

Abbreviations:
COASY - Coenzyme A synthase,
CoPAN - COASY protein-associated neurodegeneration,
COX - cytochrome c oxidase,
NCCR - NADH-cytochrome c oxidoreductase,
NBIA - neurodegeneration with brain iron accumulation,
PKAN - pantothenate kinase associated neurodegeneration.

INTRODUCTION

In all living cells Coenzyme A (CoA) is the major carrier of acetyl and acyl groups playing a central role in basic cellular functions such as lipids metabolism, Krebs cycle and aminoacid biosynthesis. CoA biosynthesis proceeds through a highly conserved pathway, involving five enzymatic steps: pantothenic acid (vitamin B5) phosphorylation, cysteine conjugation, decarboxylation, conjugation to an adenosyl group and phosphorylation.

Whereas in mammals the last two steps are catalyzed by Coenzyme A synthase (COASY), a mitochondrial bifunctional enzyme possessing both 4'-phospho-pantetheine adenylyltransferase (PPAT) and dephospho-CoA kinase (DPCK) activities [1, 2], in other organisms, such as yeast, PPAT and DPCK activities reside in two different enzymes, Cab4 and Cab5, the products of the essential genes *CAB4* and *CAB5* [3] whose compartmentalization is not well understood.

Recently, it has been reported that dysfunctions of CoA biosynthetic pathway may play a role in the pathogenesis of neurodegeneration with brain iron accumulation (NBIA), a wide spectrum of clinically and genetically heterogeneous diseases characterized by progressive neurodegeneration and high iron content in specific brain region [4, 5, 6].

This concept is supported by the fact that mutations in *PANK2,* encoding the first enzyme in the CoA synthesis, approximately account for 50% of NBIA cases, classified as PKAN (Pantothenate Kinase Associated Neurodegeneration) [7, 8]. Moreover *COASY* gene has been identified as a novel NBIA-associated gene and these NBIA cases have been termed CoPAN (COASY Protein-Associated Neurodegeneration)[9].

Neurodegenerative diseases are often characterized by mitochondrial dysfunctions, altered lipid metabolism and iron accumulation [10, 11, 12] and several evidences linking PKAN and CoPAN to these metabolic alterations have been reported [8, 13, 14, 15, 16].

The development of cellular and animal models is crucial for advancing our understanding of the pathophysiology of these diseases. In the last decade, the yeast *Saccharomyces cerevisiae* has been used as *in vivo* model system to gain insights into the molecular basis of mitochondrial pathologies and neurodegenerative disorders [17, 18]. Despite their simplicity, yeast cells possess most of the basic cellular machinery including pathways required for energy metabolism and protein homeostasis. Moreover, many of the genes and biological systems that function in yeast iron homeostasis are conserved throughout eukaryotes [19].

To investigate if defective CoA metabolism could underlie a more general disequilibrium of lipid metabolism and mitochondrial dysfunctions and its relationship with brain iron accumulation, we have performed phenotypic and biochemical investigation in a recently developed yeast model expressing the pathogenic missense mutation *COASY*^{R499C} found in NBIA patients [9].

The results obtained in this study showed that yeast mutant defective in CoA biosynthesis recapitulates the most important phenotypes found in patients and validated this system to model CoPAN in order to help elucidating important cellular and biochemical aspects of mitochondrial, lipid and iron homeostasis underpinning this disease.

RESULTS

Cellular localization of yeast Cab5 protein

Proteomics studies [20] and *in silico* analysis using the PSORT and MITOPROT programs [21, 22], which allows the prediction of protein localization, suggest for Cab5 a mitochondrial localization. Moreover human CoA synthase is a mitochondrial enzyme and the human gene is able to complement the *cab5*Δ mutation. To confirm experimentally the mitochondrial localization of Cab5p, a carboxyl-terminal fusion of HA epitope to Cab5 was constructed. The *cab5*Δ lethal phenotype was rescued by the re-expression of the tagged wild type allele, indicating that the addition of HA did not disrupt targeting and function of the Cab5 protein. Equivalent amounts of mitochondrial pellet (M) and supernatant (PMS) fractions from cells expressing HA tagged Cab5 (Cab5-HA) were subjected to SDS-PAGE and Western blotting to identify the indicated protein. The great majority of Cab5-HA co-fractionated with the mitochondrial membrane protein porin, while only a small amount remained in the supernatant with the soluble cytoplasmic protein phosphoglycerate kinase (PGK), indicating that Cab5 behaves as a mitochondrial associated protein (Fig. 1A). We further investigated the mitochondrial localization of Cab5p by performing a protease protection assay of intact mitochondria. Cab5-HA exhibited a significant increase in proteinase K sensitivity treatment in respect to both porin, which is only partially exposed on the surface, and to the inner membrane protein Core1 (Fig. 1B). The mitochondria were then treated with 0.1 M Na_2CO_3, pH 11, and supernatant and pellet fractions were generated by centrifugation. As depicted in Fig. 1C the amount of Cab5 associated with mitochondria was significantly reduced but the amount of porin was not altered. Taken together these results suggest that Cab5 is an extrinsic outer membrane protein.

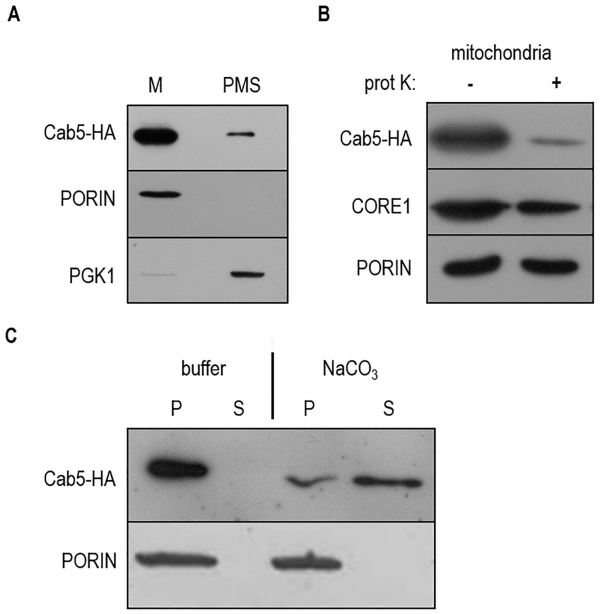

FIGURE 1: Localization of Cab5p. (A) Equal amounts (20 mg) of the mitochondrial fraction (M) and post mitochondrial fraction (PMS) were resolved by SDS-PAGE and analyzed by immunoblotting with HA, PGK1 (cytosolic marker), PORIN (mitochondrial outer membrane marker) antibodies. **(B)** Mitochondria were treated for 60 min at 4°C with proteinase K (prot K) (1 mg/ml). The filter was incubated with anti-HA, anti-CORE1, and anti-PORIN antibodies. Core1 was used as an inner membrane protein control. **(C)** 150 µg of mitochondrial proteins were treated with TEGN buffer or TEGN and 0.1M $NaCO_3$. The insoluble pellet (P) and supernatant (S) fractions were resolved by SDS-PAGE and analyzed by immunoblotting with HA and PORIN antibodies.

Characterization of mitochondrial functions

We have previously demonstrated by HPLC analysis that in the strain expressing the human *COASY*^{R499C} or the yeast *cab5*^{R146C} mutant versions the level of CoA in mitochondria was reduced by 40% compared to wild-type [9]. Given that defective CoA biosynthesis could lead to a variety of metabolic defects we looked for evidence of mitochondrial dysfunction.

In order to reveal a possible respiratory growth defect, serial dilutions of the strains were spotted on mineral medium without pantothenate supplemented with either ethanol or glycerol, at 28°C. As shown in Fig. 2A the OXPHOS growth of the *cab5*Δ/*COASY*^{R499C} mutant was partially affected compared to *COASY* wild type expressing strain. To confirm the growth delay we determined the cell

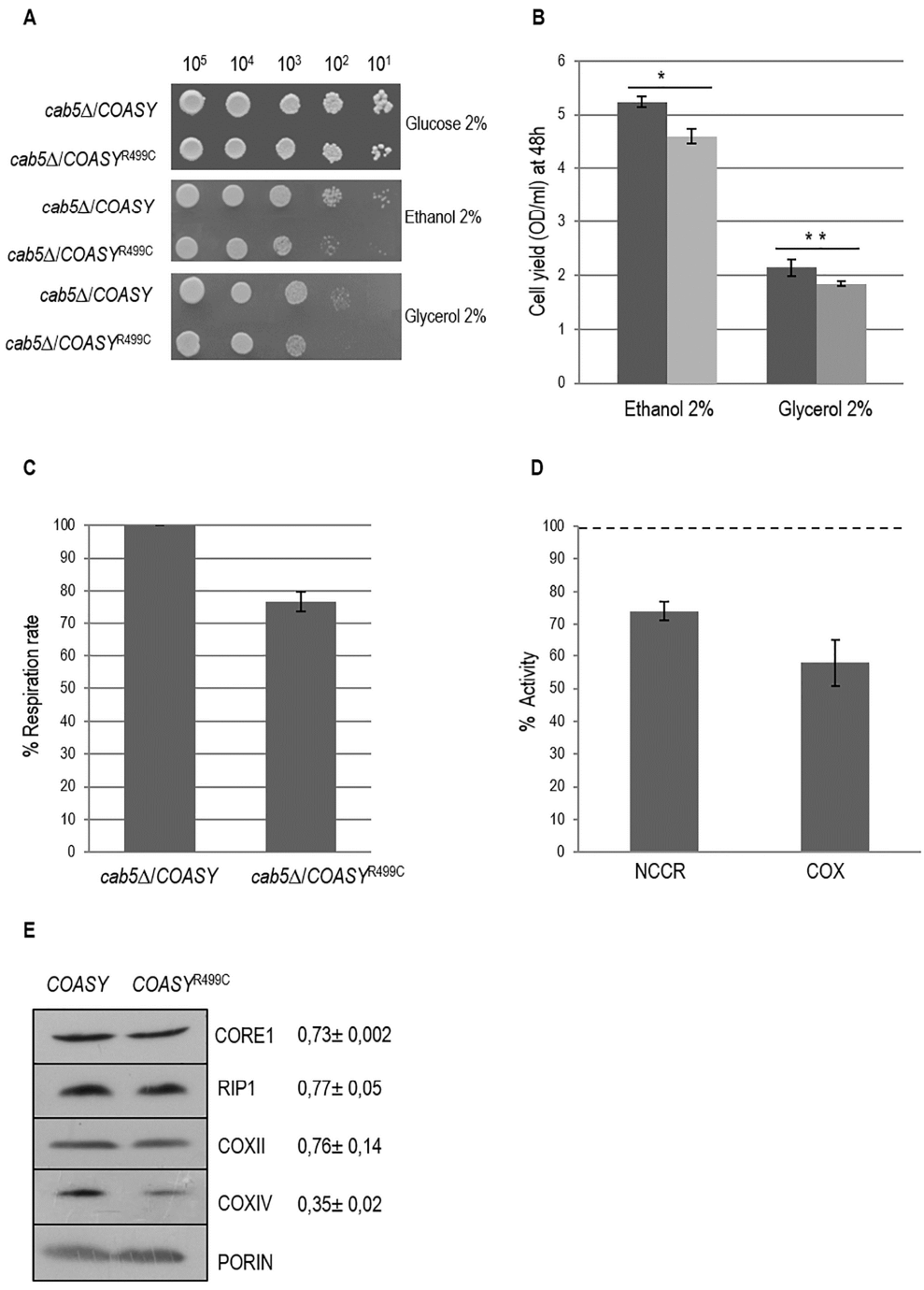

FIGURE 2: Characterization of mitochondrial functions. (A) Oxidative growth phenotype. The strain W303-1B *cab5*Δ was transformed with a pYEX-BX plasmid carrying the wild-type *COASY* or the mutant allele *COASY*^{R499C}. Equal amounts of serial dilutions of cells from exponentially grown cultures (10^5, 10^4, 10^3, 10^2, 10^1) were spotted onto mineral medium (40) plus 2% glucose, 2% ethanol or 2% glycerol without pantothenate. The growth was scored after 5 days of incubation at 28°C. **(B)** Cell yield. Cell yield was calculated by growing cells on liquid medium containing ethanol or glycerol and measuring the optical density at 600 nm after 48h of growth (*COASY* black columns and *COASY*^{R499C} grey columns). Values are mean of three independent experiments. * P < 0.05; **P < 0.01 (unpaired two-tailed t-test). **(C)** Oxygen consumption rates. Respiration was measured in cells grown in mineral medium (40) plus 0.2% glucose and 2% galactose without pantothenate at 28°C. The values observed for the *COASY* mutant strain are reported as percentage of the respiration obtained in cells expressing the wild-type *COASY* gene. **(D)** NADH-cytochrome *c* oxidoreductase (NCCR) and cytochrome *c* oxidase (COX) activities were measured in mitochondria extracted from cells grown exponentially at 28°C in mineral medium (40) plus 0.2% glucose and 2% galactose without pantothenate. The values of the *COASY* mutant are expressed as percentage of the activities obtained in the wild type strain. **(E)** Steady state level of cIII and cIV subunits in cells carrying the wild-type *COASY* and the mutant allele. The filter was incubated with specific antibodies against Core1, Rip1, CoxII, CoxIV and Porin. The signals were normalized according to the control signal (porin) and taken as 1.00 the signal of the *cab5*Δ/*COASY* (wild-type) strain.

yield for each yeast strain grown on ethanol or glycerol. We observed that the OXPHOS growth of the mutant strain was 20% lower as compared to wild type (Fig. 2B).

To further analyze the respiratory deficiency, oxygen consumption and activity of respiratory complexes were measured. Accordingly to the OXPHOS growth phenotype the oxygen consumption rate of the *cab5*Δ/*COASY*^{R499C} was 25% less than that of *cab5*Δ/*COASY* (Fig. 2C). Likewise, the NADH-cytochrome *c* oxidoreductase (NCCR) and cytochrome *c* oxidase (COX) activities were reduced in the mutant strain respectively to 26% and 42% as compared to wild type (Fig. 2D). Accordingly, the steady state levels of complex III and IV subunits are decreased (Fig. 2E). Altogether these results indicate a mitochondrial dysfunction associated to the reduced CoA level.

Mutation in CoA synthase determines an increase of iron content and increased sensitivity to oxidative stress

NBIA disorders, PKAN and CoPAN included, are characterized by iron deposition in the brain but the mechanisms leading to iron overload and its pathophysiological role remain unclear. Since in yeast excessive iron accumulation in the mitochondria led to an increased sensitivity to this ion [23, 24], we first evaluated the inhibition of cellular growth in the *COASY*^{R499C} mutant strain by the addition of $FeSO_4$ to the medium.

As depicted in Fig. 3A, the mutant strain showed a clear growth defect when compared to wild type strain, indirectly indicating a higher iron content.

We then performed a quantitative determination of cellular iron level by a colorimetric assay that relies on the formation of colored iron complexes with BPS after nitric acid digestion of yeast cells and gives results comparable

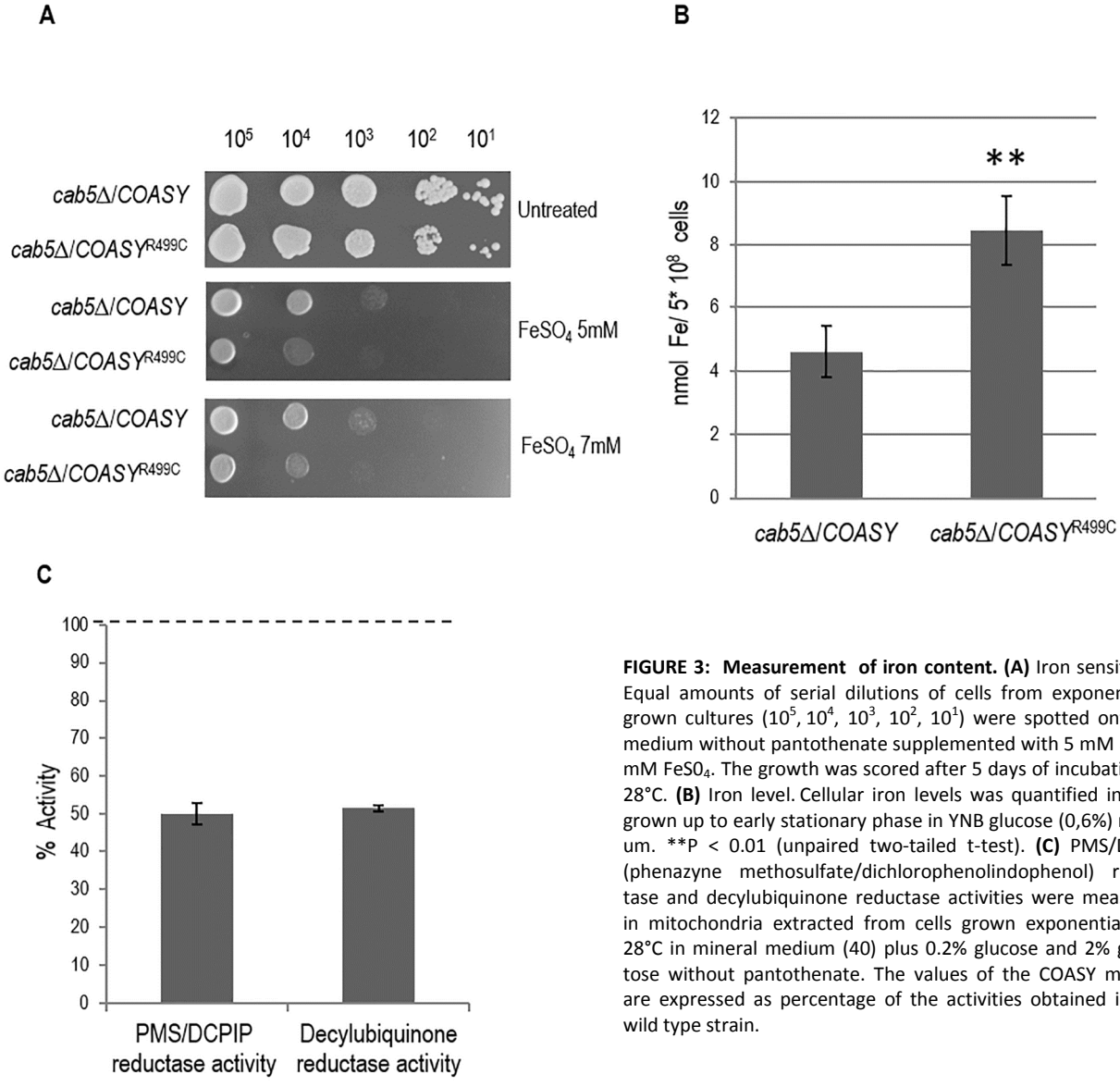

FIGURE 3: Measurement of iron content. (A) Iron sensitivity. Equal amounts of serial dilutions of cells from exponentially grown cultures (10^5, 10^4, 10^3, 10^2, 10^1) were spotted onto 40 medium without pantothenate supplemented with 5 mM and 7 mM $FeSO_4$. The growth was scored after 5 days of incubation at 28°C. **(B)** Iron level. Cellular iron levels was quantified in cells grown up to early stationary phase in YNB glucose (0,6%) medium. **P < 0.01 (unpaired two-tailed t-test). **(C)** PMS/DCPIP (phenazyne methosulfate/dichlorophenolindophenol) reductase and decylubiquinone reductase activities were measured in mitochondria extracted from cells grown exponentially at 28°C in mineral medium (40) plus 0.2% glucose and 2% galactose without pantothenate. The values of the COASY mutant are expressed as percentage of the activities obtained in the wild type strain.

with those with ICP-mass spectrometry [25, 26]. The results obtained showed a two-fold increase in iron content in the *COASY*^{R499C} mutant respect to the parental strain (Fig. 3B).

We then investigated whether the biosynthesis of the Fe-S cluster, a marker of mitochondrial functionality linked to iron metabolism, was affected by COASY deficiency. We determined the activity of succinate dehydrogenase (SDH), a mitochondrial Fe-S cluster enzyme. As shown in Fig. 3C, SDH activity was decreased by about 50%, in the mutant as compared to wild-type strain.

It is known that an excess of iron causes an altered oxidative status [24, 27, 28], another key feature of disease associated to CoA deficiency [14, 29, 30], which may be reflected in hypersensitivity to oxidative stress-induced cell death. To test this hypothesis *COASY*^{R499C} mutant and control strain were exposed to H_2O_2 and cell viability was determined by both spot assay analysis (Fig. 4A) and by counting the formation of colonies (Fig 4B). At the highest H_2O_2 concentration tested (2 mM) wild type cells showed a viability of 10%, while mutant cells showed a viability of 2% (Fig. 4B) demonstrating that a COASY defect leads to oxidative stress susceptibility.

Evaluation of lipid droplets content

Acetyl-CoA is necessary for the production of neutral lipids, which serve as power reserve for the cell and are stored in lipid droplets. Since CoA is involved in the biosynthesis of fatty acids and having demonstrated that the mutant *cab5*Δ/*COASY*^{R499C} shows a 40% reduction of coenzyme A, the content of intracellular lipid droplets in the mutant compared to the wild type was evaluated by fluorescence microscopy and fluorimetric analysis after incubation of the cells with the fluorescent lipophilic dye Nile Red [31]. As shown in Fig. 5A the content of lipid droplets is decreased in the mutant expressing the *COASY*^{R499C}. In order to better quantify this reduction, the fluorescence of cells stained with Nile Red was measured using a fluorescence spectrometer. The measures, performed in triplicate, highlighted a reduction of lipid droplets of 25% in mutant strain compared to wild-type (Fig. 5B).

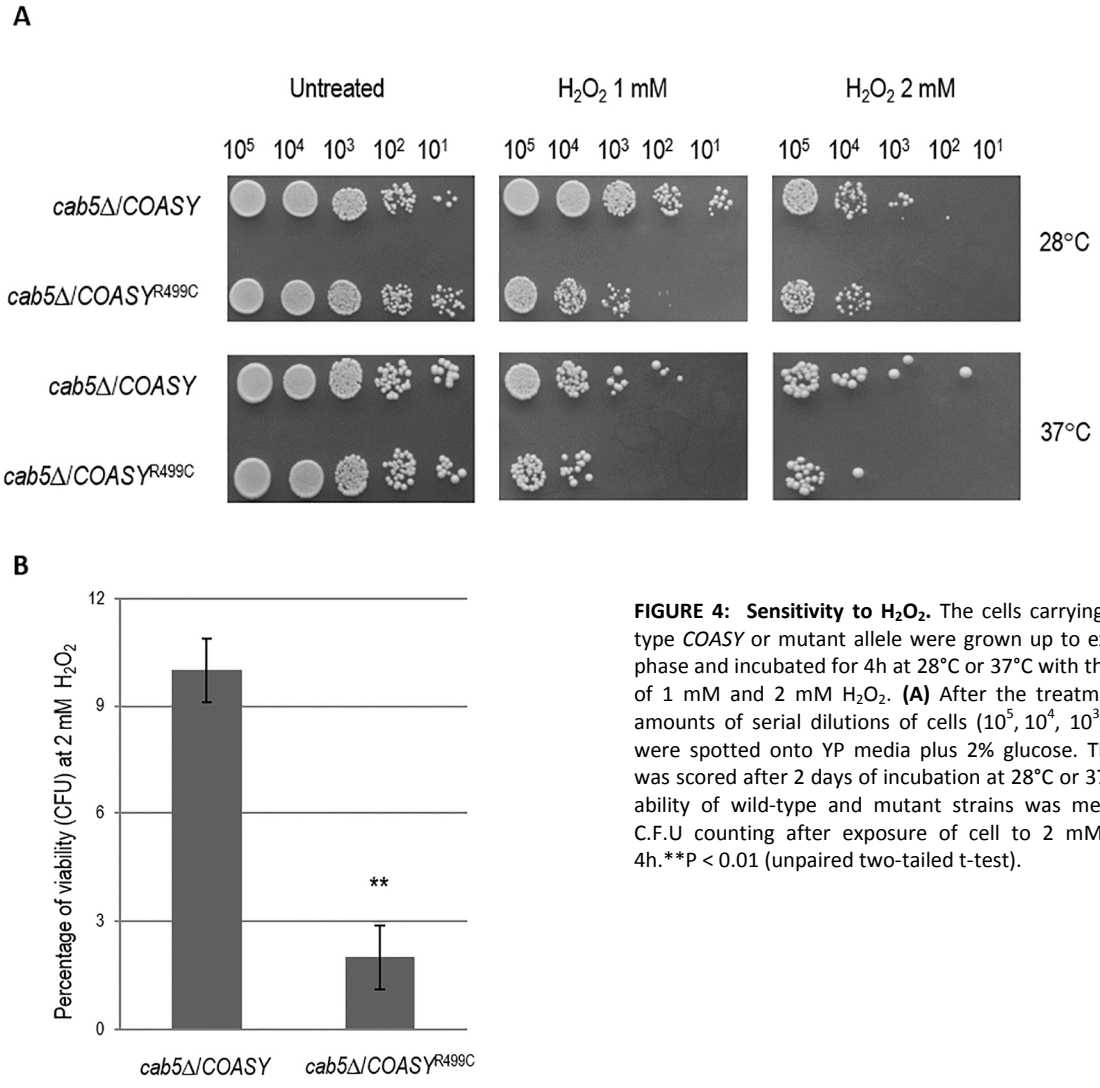

FIGURE 4: Sensitivity to H_2O_2. The cells carrying the wild-type *COASY* or mutant allele were grown up to exponential phase and incubated for 4h at 28°C or 37°C with the addition of 1 mM and 2 mM H_2O_2. **(A)** After the treatment, equal amounts of serial dilutions of cells (10^5, 10^4, 10^3, 10^2, 10^1) were spotted onto YP media plus 2% glucose. The growth was scored after 2 days of incubation at 28°C or 37°C. **(B)** Viability of wild-type and mutant strains was measured by C.F.U counting after exposure of cell to 2 mM H_2O_2 for 4h.**P < 0.01 (unpaired two-tailed t-test).

DISCUSSION

In all living organisms Coenzyme A (CoA) is an essential cofactor in cellular metabolism. CoA biosynthesis follows a highly conserved pathway, involving five enzymatic steps, which utilize pantothenate (vitamin B5), ATP, and cysteine. Mutations in nuclear genes directly involved in CoA biosynthetic pathway have been identified as responsible for some forms of NBIA, namely PKAN and CoPAN. PKAN is caused by mutations in PANK2, encoding the pantothenate kinase 2 enzyme, that account for about 50% of NBIA cases, whereas mutations in CoA synthase COASY have been recently reported as the second inborn error of CoA synthesis leading to CoPAN [9]. In PKAN and CoPAN brain iron accumulation is dramatic but its link with defective CoA synthesis is unknown.

Moreover, many neurodegenerative diseases, PKAN and CoPAN included, are characterized by mitochondrial dysfunctions, oxidative stress, altered lipid metabolism but again the complex relationships linking these factors in the context of disease conditions remain to be elucidated.

Previous attempts to understand the mechanism of PKAN using animal models have met with limited success. A mouse model of PKAN exhibits azoospermia but lacks any neurological phenotype [32]. A *Drosophila* model of PKAN does have a brain phenotype, but this involves the formation of vacuoles, not iron accumulation [33]. The identification and generation of other cellular model may allow a deeper characterization of *COASY* and *PANK2* disease gene products, and the investigation of their pathophysiology *in vivo*. With this aim we developed and characterized a yeast model for CoPAN disease.

Although in yeast, differently from mammalian cells, the last two steps of CoA biosynthesis are catalyzed by two separate enzymes, namely the products of the essential genes *CAB4* and *CAB5*, we have demonstrated that the lethality associated to deletion in *CAB5* could be complemented by human *COASY*. This allowed us to study the human Arg499Cys substitution in yeast and to support the pathogenic role of this mutation associated to a reduced level of CoA [9].

The evaluation of the metabolic consequences of coenzyme A deficiency in yeast revealed mitochondrial dysfunctions; OXPHOS growth was affected and respiration rate significantly decreased. Accordingly, the activity of respiratory chain complexes and steady state levels of mitochondrial respiratory chain subunits were reduced. We also demonstrated that the growth of the mutant strain is not only strongly inhibited in the presence of iron but that the mutant strain showed iron accumulation. This result is consistent with the patient phenotype, with iron overload being a typical sign of PKAN and CoPAN. We have also found that *cab5*Δ/*COASY*^{R499C} mutant was more sensitive to the ROS-inducing agent H_2O_2 indicating an increased oxidative stress that may contribute to the pathogenesis of these diseases. Accordingly, the activity of SDH, a marker of mitochondrial functionality linked to iron metabolism, was reduced in the *COASY* mutant.

Since Acetyl-CoA, one of the most important derivatives of CoA, is also required for the synthesis of fatty acids, we investigated the impact of reduced CoA level by meas-

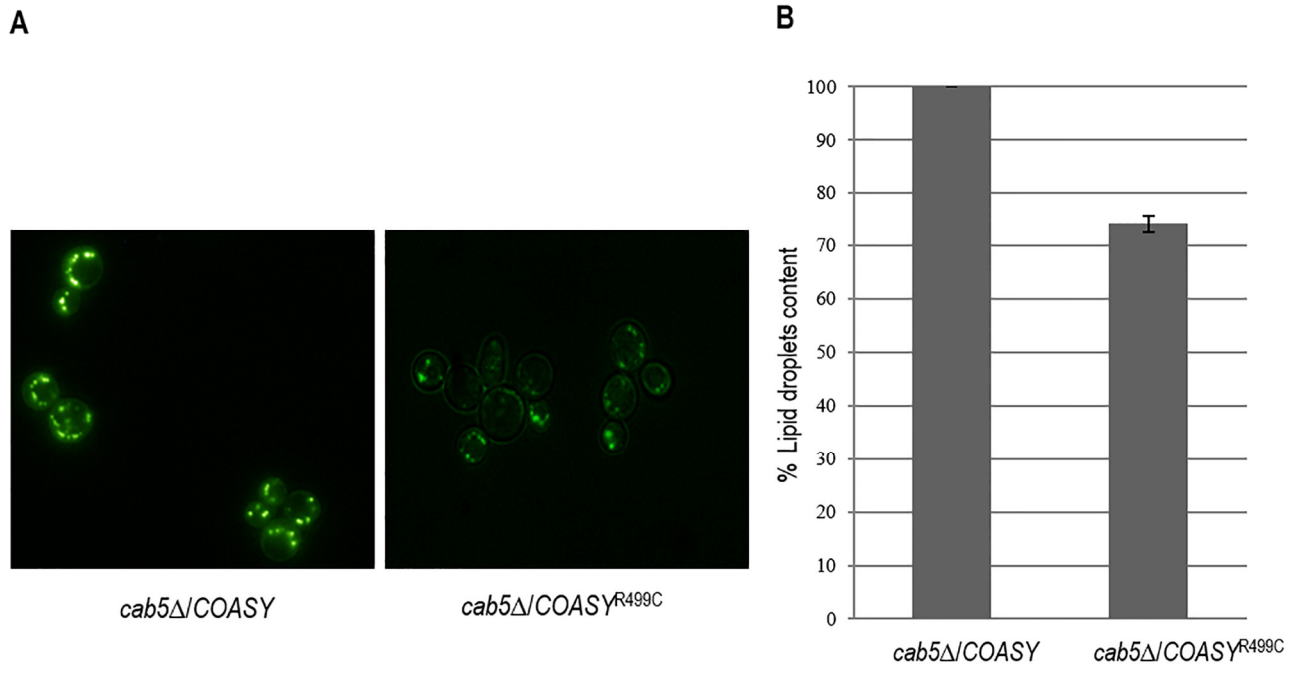

FIGURE 5: Evaluation of lipid droplets content. The intracellular lipid droplets content has been detected by fluorescence microscopy **(A)** and fluorimetric analysis **(B)** after incubation of wild type and mutant cells with the fluorescent lipophilic dye Nile Red (4 μg/ml). The values corresponding to mutant *COASY* are expressed as percentage of the content obtained in the wild type strain.

uring the lipid droplets content in mutant cells by fluorimetric analysis of Nile Red stained cells. Interestingly enough, lipid droplets content was 25% lower in mutant strain as compared to wild-type. The same altered lipid metabolism was also observed in mutant strain for phosphopantothenoylcysteine synthetase (PPCS), another essential enzyme in CoA biosynthetic pathway [34]. These results are in agreement with the hypothesis that low CoA perturbs lipid homeostasis; lipid deregulation was also observed in *Drosophila* CoA mutants and from global metabolic profiling studies in patient-derived fibroblasts [8, 35]. The transcriptional analysis of key genes involved in lipid metabolism would help in elucidating the role of lipid metabolism in the pathology.

Altogether these results established yeast as an appropriate model to study the molecular mechanisms involved in CoA metabolism, and to understand the connection between iron management, mitochondrial function and lipid metabolism in neurodegeneration.

Several pathological phenotypes have been identified in the mutant *COASY* yeast strain thus representing ideal readouts for high throughput screening of chemical libraries as described by Couplan *et al.* [36]. This could allow the identification of new molecules, the first step to set up future therapeutic experimental approaches.

MATERIALS AND METHODS

Yeast strains, media and vectors

Yeast strains used in this study were W303-1B *cab5*Δ (MATα; *cab5*::*KanMx4 ade2-1 leu2-3,112 ura3-1 his3-22,15 trp1-1 can1-100*) carrying pYEX-BX-COASY or pYEX-BX COASY^{R499C} plasmid [9]. For localization studies we used the strain BY4741 (MAT*a*; *his3*Δ*1 leu2*Δ*0 met15*Δ*0 ura3*Δ*0*) transformed with pFL38-Cab5-HA plasmid.

Cells were cultured in mineral medium (40) supplemented with appropriate amino acids and bases for auxotrophy as previously described [37]. To obtain medium lacking pantothenate (40-Pan) a mixture of vitamins without pantothenate was prepared. Yeast cells were transformed by the standard lithium acetate method [38] and cultured in YNB synthetic defined media (For-MediumTM, UK) supplemented with 1 g/l of drop-out powder [39] containing all amino acids and bases, except those required for plasmid selection. Various carbon sources (Carlo Erba Reagents, Italy) were added at the indicated concentration. Media were solidified with 20 g/l agar (For-Medium™). Strains were incubated at 28 or 37°C as indicated.

Plasmid pFL38-Cab5-HA was obtained by PCR overlap technique [40]. In the first set of PCR reactions, the *CAB5* region was obtained using the forward primer CAB5Fw-GGGGGGATCCCCATTGCTTAGAATGGGCGG and the following reverse tag primer CAB5HARv ATCAACCTTATAC**AGCGTAATCTGGAACATCGTATGGGTACGCTGA**AGACTTTTTATTTTG where hemagglutinin (HA) tag sequence is indicated in bold. The second *CAB5* region was obtained using the forward tag primers CAB5HATERFw complementary to CAB5HARv , and the reverse primer CAB5Rv-CCGCGGTACCGAGAACCCATAGAATTCGAC. The final product was obtained using the overlapping PCR fragments as template with CAB5Fw and CAB5Rv as external primers. The product was then digested with *BamH*I and *Kpn*I and cloned in *BamH*I/*Kpn*I digested pFL38 centromeric plasmid [41].

Respiration measurement, biochemical assays and immunoblot analysis of respiratory chain subunits.

Respiratory activity measurement was performed on whole cells at 30°C using a Clark-type oxygen electrode (Oxygraph System, Hansatech Instruments, England) with 1 ml of air-saturated respiration buffer (0.1 M phthalate–KOH, pH 5.0). The reaction started by addition of 20 mg of wet-weight cells [42].

Complex II (SDH), NADH-cytochrome *c* oxidoreductase (NCCR) and complex IV specific activities were measured spectrophotometrically as previously described [42, 43, 44, 45] on a mitochondrial enriched fraction prepared according to Soto *et al*. [46]. Protein concentration was determined by the method of Bradford using the BioRad protein assay following manufacturer's instructions [47]. For SDS-PAGE, 20 µg of mitochondrial proteins were separated on 12% polyacrylamide gels and electroblotted onto a nitrocellulose membrane. The subunits of mitochondrial respiratory complexes were immunovisualized by specific antibodies. The sources of primary antibodies are indicated: anti-Core1 (a kind gift from Prof. Antoni Barrientos), anti-Rip1 (a kind gift from Prof. Alexander Tzagoloff), anti CoxIIp (Abcam Mitoscience), anti-CoxIV (Abcam Mitoscience) and anti-Porin (Abcam Mitoscience). Quantification of protein bands was performed using Multi Analyst software. The signals were normalized according to the control signal (α-Porin) and the signal of the *cab5*Δ/COASY (wild-type) strain was set as 1.00.

Intact mitochondria isolation, subcellular localization experiments and membrane association

Intact mitochondria were isolated from BY4741 strain transformed with a plasmid expressing Cab5-HA under the native *CAB5* promoter after cell wall removal by Zymoliase20T digestion (Nacalai Tesque) and cell disruption with a glass-teflon potter homogenizer [48]. Whole cell extract was centrifuged at 12,000 g for 30 min to yield the mitochondrial pellet (M) and post-mitochondria supernatant (PMS). These fractions were analyzed by immunoblotting with the indicated antibodies (Porin: mitochondrial marker; PGK cytoplasmic marker (Abcam Mitoscience)). The Cab5 protein was immunovisualized using an anti-HA (Roche) specific antibody. Proteinase K protection assay for sub-mitochondrial localization study was performed as previously described [48, 49]. Briefly, 200 µg of mitochondrial proteins were kept in 20 mM HEPES pH 7.4, 0,6 M sorbitol in the presence or absence of proteinase K (1 mg/ml) for 60 minutes on ice. 0,1 M PMSF (phenylmethylsulfonyl fluoride) was added to stop the reaction. The protein pellets were washed once with 20 mM HEPES pH 7.4 plus 0,6 M sorbitol, and suspended in SDS-PAGE sample buffer.

A modified version of the membrane association experiments of Trott and Morano [50] was utilized to determine the resistance of Cab5p to sodium carbonate (pH 11.5) treatment. Equal amounts (150 µg) of the mitochondrial fraction was resuspended in TEGN (20 mM Tris-HCl [pH 7.9], 0.5 mM EDTA, 10% glycerol, 50 mM NaCl) or TEGN and with 0.1 M $NaCO_3$ for 30 min on ice. The samples were subsequently centrifuged at 17,000 g at 4°C to obtain soluble and membrane fractions. The fractions obtained in all type of extraction were separated by

SDS-PAGE and probed with anti-HA and anti-PORIN antibodies.

Measurement of iron content

The iron content was determined by a colorimetric assay, essentially as described before [25, 51]. 5x10^8 cells were washed twice with H_2O, resuspended in 0.5 ml of 3% nitric acid and incubated over night at 95°C. After incubation, samples were centrifuged at 12,000 rpm for 5 min and the supernatant (400 µl) was mixed with 160 µl of 38 mg sodium L-ascorbate ml^{-1} (SIGMA), 320 µl of 1.7 mg BPS ml^{-1} (ACROS ORGANICS), and 126 µl of ammonium acetate (SIGMA) (saturated solution diluted 1:3). Non-specific absorbance was measured at 680 nm and subtracted from the specific absorbance of the iron-BPS complex (535 nm). Iron was quantified by reference to a standard curve using iron sulfate performed as in Tamarit *et al*. [25].

H_2O_2 sensitivity

To determine the sensitivity to oxygen peroxide, cells growing exponentially were exposed to 1 and 2 mM H_2O_2 at 28°C or 37°C for 4 h. Cell viability was determined by spotting equal amounts of serial dilutions of cells (10^5, 10^4, 10^3, 10^2, 10^1) onto YP plates (1% yeast extract, 2% peptone ForMedium™) supplemented with 2% glucose (YPD). Plates were incubated at 28°C or 37°C for two days. To better quantify H_2O_2 sensitivity cell survival was determined by counting the formation of colonies after the treatment.

Lipid droplets content: fluorescence microscopy and fluorimetric analysis

Intracellular lipid droplets were detected using the fluorescent lipophilic dye Nile Red (9-diethylamino-5*H*-benzo[α]phenoxazine-5-one 3 SIGMA-ALDRICH) by fluorescence microscopy and fluorimetric analysis [31, 52, 53]. Wild type and *cab5*Δ/*COASY*^{R499C} strains were grown to mid-log phase in mineral medium (40) containing Yeast Extract (1,5 g/L). To 250 µl of the cultures, adjusted to 1 OD, 10 µl of the stock solution of Nile red [100 µg/ml] were added in order to obtain a final concentration of 4 µg/ml of dye. Fluorescence of the stained cells were obtained with a Leica DM2000 microscope using x 100 magnification and captured using a Leica DFC310FX digital camera with Leica's Imaging Software (Leica Application Suite-LASAF 3.7.0, Leica Microsystem).

To quantify the fluorescence we used the fluorescence spectrometer Tecan SPECTRA Fluor Plus using the software XFLUOR4 V4.51 (excitation at 535 nm and emission at 595 nm). Aliquots of 100 µl of cells stained with Nile red were transferred into 96-well microplates in 4 replicates. For each strain a negative control was performed in which the dye was omitted in order to exclude a possible auto fluorescence of samples. The evaluation of the fluorescence was repeated at 5-minute intervals in a time interval of 20 minutes [53].

ACKNOWLEDGMENTS

The financial support of Telethon GGP11011, Telethon GGP11088 and Fondazione CARIPLO 2011/0526 are gratefully acknowledged. This work was supported by TIRCON project of the European Commission's seventh Framework Programme (FP7/2007-2013, HEALTH-F2-2011, grant agreement no. 277984). We wish to thank Antonietta Cirasolo (University of Parma) for the skillful technical assistance.

CONFLICT OF INTEREST

The authors declare no conflict of interest.

COPYRIGHT

Please cite this article as: Camilla Ceccatelli Berti, Cristina Dallabona, Mirca Lazzaretti, Sabrina Dusi, Elena Tosi, Valeria Tiranti, Paola Goffrini (2015). Modeling human Coenzyme A synthase mutation in yeast reveals altered mitochondrial function, lipid content and iron metabolism. **Microbial Cell** 2(4): 126-135. doi: 10.15698/mic2015.04.196

REFERENCES

1. Zhivoloup A, Nemazanyy I, Babich A, Panasyuk G, Pobigailo N, Vudmaska M, Naidenov V, Kukharenko O, Palchevskii S, Savinska L, Ovcharenko G, Vardier F, Valovka T, Fenton T, Rebholz H, Wang M, Sheperd P, Matsuka G, Filonenko V, and Gout IT **(2002)**. Molecular cloning of CoA Synthase. The missing link in CoA biosynthesis. **The Journal Of Biological Chemistry** 277(25): 22107-22110.

2. Zhyvoloup A, Nemazanyy I, Panasyuk G, Valovka T, Fenton T, Rebholz H, Wang, ML, Foxon R, Lyzogubov V, Usenko V, Kyyamova R, Gorbenko O, Matsuka G, Filonenko V, and Gout IT **(2003).** Subcellular localization and regulation of coenzyme A synthase**. J Biol Chem** 278(50): 50316–50321.

3. Olzhausen J, Schübbe S, and Schüller H **(2009)**. Genetic analysis of coenzyme A biosynthesis in the yeast *Saccharomyces cerevisiae*: identification of a conditional mutation in the pantothenate kinase gene *CAB1*. **Current Genetics** 55(2): 163-173.

4. Gregory A and Hayflick SJ **(2005)**. Neurodegeneration with brain iron accumulation. **Folia Neuropatho** 43(4): 286-96.

5. Brunetti D, Dusi S, Morbin M, Uggetti A, Moda F, D'Amato I, Giordano C, d'Amati G, Cozzi A, Levi S, Hayflick S, And Tiranti V **(2012).** Pantothenate kinase-associated neurodegeneration: altered mitochondria membrane potential and defective respiration in Pank2 knock-out mouse model. **Human Molecular Genetics** 21(24): 5294-5305.

6. Hayflick SJ **(2014)**. Defective pantothenate metabolism and neurodegeneration. **Biochem Soc Tran**s 42(4): 1063-8.

7. Hartig MB, Hörtnagel K, Garavaglia B, Zorzi G, Kmiec T, Klopstock T, Rostasy K, Svetel M, Kostic VS, Schuelke M, Botz E, Weindl A, Novakovic I, Nardocci N, Prokisch H, and Meitinger T **(2006)**. Genotypic and phenotypic spectrum of *PANK2* mutations in patients with neurodegeneration with brain iron accumulation. **Annals Of Neurology** 59(2): 248-256.

8. Leoni V, Strittmatter L, Zorzi G, Zibordi F, Dusi S, Garavaglia B, Venco P, Caccia C, Souza AL, Deik A, Clish CB, Rimoldi M, Ciusani E, Bertini E, Nardocci N, Mooth VK, and Tiranti V **(2012)**. Metabolic consequences of mitochondrial coenzyme A deficiency in patients eith PANK2 mutations. **Molecular Genetics And Metabolism** 105(3): 463–47.

9. Dusi, S, Valletta L, Haach TB, Tsuchiya Y, Venco P, Pasqualato S, Goffrini P, Tigano M, Demchenko N, Weiland T, Schwarzmayr T, Strom TM, Invernizzi F, Garavaglia B, Gregory A, Sanford L, Hamada J, Fontanesi, Bettencourt C, Houldel H, Chiapparini L, Zorzi G, Kurian MA, Nardocci N, Prokisch H, Hayflick S, Gout I, and Tiranti V **(2014)**. Exome sequencing reveals mutation in CoA synthase as a cause of neurodegeneration with brain iron accumulation. **Am J Hum Genet** 94(1): 11-22.

10. Campbell GR, Worrall JT, and Mahad DJ **(2014).** The central role of mitochondria in axonal degeneration in multiple sclerosis. **Mult Scler** 20(14): 1806-1813.

11. Palomo GM and Manfredi G **(2014).** Exploring new pathways of neurodegeneration in ALS: The role of mitochondria quality control. **Brain Res**, doi: 10.1016/j.brainres.2014.09.065.

12. Urrutia PJ, Mena NP, and Núñez MT **(2014).** The interplay between iron accumulation, mitochondrial dysfunction, and inflammation during the execution step of neurodegenerative disorders. **Front Pharmacol** 5:38.

13. Kotzbauer PT, Truax AC, Trojanowski JQ, and Lee VM **(2005)**. Altered neuronal mitochondrial coenzyme A synthesis in neurodegeneration with brain iron accumulation caused by abnormal processing, stability, and catalytic activity of mutant pantothenate kinase 2. **J Neurosci** 25(3): 689-98.

14. Campanella A, Privitera D, Guaraldo M, Rovelli E, Barzaghi C, Garavaglia B, Santambrogio P, Cozzi A, and Levi S **(2012)**. Skin fibroblasts from pantothenate kinase-associated neurodegeneration patients show altered cellular oxidative status and have defective iron-handling properties. **Hum Mol Genet** 21(18): 4049-4059.

15. Colombelli C, Aoun M, and Tiranti V **(2014)**. Defective lipid metabolism in neurodegeneration with brain iron accumulation (NBIA) syndromes: not only a matter of iron. **J Inherit Metab Dis** 38(1): 123-136.

16. Levi S and Finazzi D **(2014)**. Neurodegeneration with brain iron accumulation: update on pathogenic mechanisms. **Front Pharmacol** 5:99.

17. Rinaldi T, Dallabona C, Ferrero I, Frontali L, and Bolotin-Fukuhara M **(2010)**. Mitochondrial diseases and the role of the yeast models. **FEMS Yeast Res** 10(8): 1006-22.

18. Tenreiro S, Munder MC, Alberti S, and Outeiro TF **(2013)**. Harnessing the power of yeast to unravel the molecular basis of neurodegeneration. **J Neurochem** 127(4): 438-52.

19. Bleackley MR and MacGillivray RT **(2011)**. Transition metal homeostasis: from yeast to human disease. **BioMetals** 24(5): 785–809.

20. Reinders J, Zahedi RP, Pfanner N, Meisinger C and Sickmann A **(2006).** Toward the complete yeast mitochondrial proteome: multidimensional separation techniques for mitochondrial proteomics. **J Proteome Res** 5:1543-5.

21. Uberbacher EC, and Mural RJ **(1991)**. Locating protein-coding regions in human DNA sequences by a multiple sensor-neural network approach. **Proc Natl Acad Sci USA** 88 (24): 11261–11265.

22. Claros MG, and Vincens P **(1996).** Computational method to predict mitochondrially imported proteins and their targeting sequences. **Eur J Biochem** 241(3): 779–786.

23. Foury F, and Cazzalini O **(1997)**. Deletion of the yeast homologue of the human gene associated with Friedreich's ataxia elicits iron accumulation in mitochondria. **FEBS Lett** 411(2-3): 373-7.

24. Patil Vinay A, Fox Jennifer L, Vishal M, Gohil Dennis R Winge, and Miriam L Greenberg **(2013)**. Loss of Cardiolipin Leads to Perturbation of Mitochondrial and Cellular Iron Homeostasis. **J Biol Chem** 288: 1696-1705.

25. Tamarit J, Irazusta V, Moreno-Cermeño A, Ros J **(2006)**. Colorimetric assay for the quantitation of iron in yeast. **Anal Biochem** 351(1):149-51.

26. Molik S, Lill R, Mühlenhoff U **(2007).** Methods for studying iron metabolism in yeast mitochondria. **Methods Cell Biol** 80:261-80

27. Schilke B, Voisine C, Beinert H and Craig E **(1999).** Evidence for a conserved system for iron metabolism in the mitochondria of *Saccharomyces cerevisiae*. **Proc Natl Acad Sci U.S.A.** 96(18): 10206–10211.

28. Mühlenhoff U, Richhardt N, Ristow M, Kispal G and Lill R **(2002).** The yeast frataxin homolog Yfh1p plays a specific role in the maturation of cellular Fe/S proteins. **Hum Mol Genet** 11(17): 2025–2036.

29. Wu M, Liu H, Chen W, Fujimoto Y, Liu J **(2009).** Hepatic expression of long-chain acyl-CoA synthetase 3 is upregulated in hyperlipidemic hamsters. **Lipids** 44(11):989-98.

30. Rana A, Seinen E, Siudeja K, Muntendam R, Srinivasan B, Van der Want JJ, Hayflick S, Reijngoud DJ, Kayser O, Sibon OC **(2010).** Pantethine rescues a Drosophila model for pantothenate kinase-associated neurodegeneration. **Proc Natl Acad Sci U S A** 107(15):6988-93.

31. Greenspan P, Mayer EP, and Fowler SD **(1985)**. Nile red: a selective fluorescent stain for intracellular lipid droplets. **J Cell Biol** 100(3): 965-73.

32. Kuo YM, Duncan JL, Westaway SK, Yang H, Nune G, Xu EY, Hayflick SJ and Gitschier J **(2005).** Deficiency of pantothenate kinase 2 (Pank2) in mice leads to retinal degeneration and azoospermia. **Hum Mol Genet** 14(1): 49–57.

33. Yang Y, Wu Z, Kuo YM and Zhou B **(2005).** Dietary rescue of fumblea Drosophila model for pantothenate-kinase-associated neurodegeneration. **J Inherit Metab Dis** 28(6):1055-1064.

34. Nakamura T, Pluskal T, Nakaseko Y, and Yanagida M **(2012)**. Impaired coenzyme A synthesis in fission yeast causes defective mitosis, quiescence-exit failure, histone hypoacetylation and fragile DNA. **Open Biol** 2(9): 120117.

35. Bosveld F, Rana A, van der Wouden PE, Lemstra W, Ritsema M, Kampinga HH, and Sibon OC **(2008).** De novo CoA biosynthesis is required to maintain DNA integrity during development of the Drosophila nervous system. **Hum Mol Genet** 17(13): 2058-69.

36. Couplan E, Aiyar RS, Kucharczyk R, Kabala A, Ezkurdia N, Gagneur J, St Onge RP, Salin B, Soubigou F, Le Cann M, Steinmetz LM, di Rago JP, and Blondel M **(2011**). A yeast-based assay identifies drugs active against human mitochondrial disorders. **Proc Natl Acad Sci U S A** 108(29):11989-94.

37. Magni GE and Von Borstel RC **(1962)**. Different rates of spontaneous mutation during mitosis and meiosis in yeast. **Genetics** 47(8): 1097-1108.

38. Schiestl RH and Gietz RD **(1989)**. High efficiency transformation of intact yeast cells using single stranded nucleic acids as a carrier. **Curr Genet** 16(5-6): 339-4.

39. Kaiser C, Michaelis S, and Mitchell A **(1994)**. Methods in Yeast Genetics. **Cold Spring Harbor Laboratory Press**.

40. Ho SN, Hunt HD, Horton RM, Pullen JK, Pease LR **(1989)**. Site-directed mutagenesis by overlap extension using the polymerase chain reaction. **Gene** 77(1): 51–59.

41. Bonneaud N, Ozier-Kalogeropoulos O, Li GY, Labouesse M, Minvielle-Sebastia L, and Lacroute F **(1991)**. A family of low and high copy replicative, integrative and single-stranded S. cerevisiae/E. coli shuttle vectors. **Yeast** 7(6): 609–615.

42. Goffrini P, Ercolino T, Panizza E, Giache' V, Cavone L, Chiarugi A, Dima V, Ferrero I, and Mannelli M **(2009)**. Functional study in a yeast model of a novel succinate-dehydrogenase subunit B gene germline missense mutation (C191Y) diagnosed in a patient affected by a glomus tumor. **Hum Mol Genet** 18(10): 1860–1868.

43. Fontanesi F, Soto IC, and Barrientos A **(2008)**. Cytochrome c oxidase biogenesis: new levels of regulation. **IUBMB Life** 60(9): 557-68.

44. Barrientos A, , and Díaz F **(2009)**. Evaluation of the mitochondrial respiratory chain and oxidative phosphorylation system using polarography and spectrophotometric enzyme assays. **Curr Protoc Hum Genet** chapter 19:Unit19.3.

45. Jarreta D, Orús J, Barrientos A, Miró O, Roig E, Heras M, Moraes CT, Cardellach F, and Casademont J **(2000)**. Mitochondrial function in heart muscle from patients with idiopathic dilated cardiomyopathy. **Cardiovasc Res** 45(4): 860-865.

46. Soto IC, Fontanesi F, Valledor M, Horn D, Singh R, Barrientos A **(2009)**. Synthesis of cytochrome c oxidase subunit 1 is translationally downregulated in the absence of functional F1F0-ATP synthase. **Biochim Biophys Acta** 1793(11):1776-86.

47. Bradford MM **(1976)**. A rapid and sensitive method for the quantitation of microgram quantities of proteins utilizing the principle of protein dye binding. **Anal. Biochem** 72: 248–254.

48. Glick BS, and Pon LA **(1995)**. Isolation of highly purified mitochondria from Saccharomyces cerevisiae. **Methods Enzymol** 260: 213–223.

49. Diekert K, De Kroon AI, Kispal G, Lill R **(2001)**. Isolation and subfractionation of mitochondria from the yeast Saccharomyces cerevisiae. **Methods Cell Biol** 65: 37-5.

50. Trott A and Morano KA **(2004).** SYM1 is the stress-induced Saccharomyces cerevisiae ortholog of the mammalian kidney disease gene Mpv17 and is required for ethanol metabolism and tolerance during heat shock. **Eukaryot Cell** 3(3):620-31.

51. Almeida T, Marques M, Mojzita D, Amorim MA, Silva RD, Almeida B, Rodrigues P, Ludovico P, Hohmann S, Moradas-Ferreira P, Côrte-Real M, and Costa V **(2008).** Isc1p plays a key role in hydrogen peroxide resistance and chronological lifespan through modulation of iron levels and apoptosis. **Mol Biol Cell** 19(3):865-76.

52. Kimura K, Yamaola M, and Kamisaka Y **(2004)**. Rapid estimation of lipids in oleaginous fungi and yeasts using Nile red fluorescence. **J Microbiol Methods** 56(3): 331-338.

53. Sitepu IR, Ignatia L, Franz AK, Wong DM, Faulina SA, Tsui M, Kanti A, and Boundy-Mills K **(2012)**. An improved high-throughput Nile red fluorescence assay for estimating intracellular lipids in a variety of yeast species. **J Microbiol Methods** 91(2): 321–328.

Hum Genet (2015) 134:869–879
DOI 10.1007/s00439-015-1568-z

ORIGINAL INVESTIGATION

A recessive homozygous p.Asp92Gly *SDHD* mutation causes prenatal cardiomyopathy and a severe mitochondrial complex II deficiency

Charlotte L. Alston[1] · Camilla Ceccatelli Berti[2] · Emma L. Blakely[1] · Monika Oláhová[1] · Langping He[1] · Colin J. McMahon[3] · Simon E. Olpin[4] · Iain P. Hargreaves[5] · Cecilia Nolli[2] · Robert McFarland[1] · Paola Goffrini[2] · Maureen J. O'Sullivan[6] · Robert W. Taylor[1]

Received: 20 February 2015 / Accepted: 16 May 2015 / Published online: 26 May 2015

Abstract Succinate dehydrogenase (SDH) is a crucial metabolic enzyme complex that is involved in ATP production, playing roles in both the tricarboxylic cycle and the mitochondrial respiratory chain (complex II). Isolated complex II deficiency is one of the rarest oxidative phosphorylation disorders with mutations described in three structural subunits and one of the assembly factors; just one case is attributed to recessively inherited *SDHD* mutations. We report the pathological, biochemical, histochemical and molecular genetic investigations of a male neonate who had left ventricular hypertrophy detected on antenatal scan and died on day one of life. Subsequent postmortem examination confirmed hypertrophic cardiomyopathy with left ventricular non-compaction. Biochemical analysis of his skeletal muscle biopsy revealed evidence of a severe isolated complex II deficiency and candidate gene sequencing revealed a novel homozygous c.275A>G, p.(Asp92Gly) *SDHD* mutation which was shown to be recessively inherited through segregation studies. The affected amino acid has been reported as a Dutch founder mutation p.(Asp92Tyr) in families with hereditary head and neck paraganglioma. By introducing both mutations into *Saccharomyces cerevisiae,* we were able to confirm that the p.(Asp92Gly) mutation causes a more severe oxidative growth phenotype than the p.(Asp92Tyr) mutant, and provides functional evidence to support the pathogenicity of the patient's *SDHD* mutation. This is only the second case of mitochondrial complex II deficiency due to inherited *SDHD* mutations and highlights the importance of sequencing all *SDH* genes in patients with biochemical and histochemical evidence of isolated mitochondrial complex II deficiency.

✉ Robert W. Taylor
robert.taylor@ncl.ac.uk

1 Wellcome Trust Centre for Mitochondrial Research, Institute of Neuroscience, The Medical School, Newcastle University, Newcastle upon Tyne NE2 4HH, UK

2 Department of Life Sciences, University of Parma, Parma, Italy

3 Children's Heart Centre, Our Lady's Children's Hospital, Crumlin, Dublin, Ireland

4 Department of Clinical Chemistry, Sheffield Children's Hospital, Sheffield, UK

5 Neurometabolic Unit, National Hospital for Neurology and Neurosurgery, London, UK

6 Department of Pathology, Our Lady's Children's Hospital, Crumlin, Dublin, Ireland

Introduction

Mitochondrial respiratory chain disease arises from defective oxidative phosphorylation (OXPHOS) and represents a common cause of metabolic disease with an estimated prevalence of 1:4300 (Gorman et al. 2015; Skladal et al. 2003). Under aerobic conditions, metabolised glucose, fatty acids and ketones are the OXPHOS substrates, shuttling electrons along the respiratory chain whilst concomitantly creating a proton gradient by actively transporting protons across the mitochondrial membrane. The resultant proton gradient is exploited by ATP synthase to drive ATP production. Under anaerobic conditions, for example where atmospheric oxygen is scarce or during periods of exertion, ATP synthesis is produced primarily during glycolysis (Horscroft and Murray 2014).

The mitoproteome consists of an estimated 1400 proteins (Pagliarini et al. 2008), including the 13 polypeptides and 24 non-coding tRNA and rRNA genes encoded by the

mitochondria's own genetic material (mtDNA) that are exclusively maternally transmitted. The remaining genes of the mitoproteome are located on either the autosomes or sex chromosomes and as such are transmitted from parent to child in a Mendelian fashion. Defects in a number of mtDNA and nuclear-encoded genes have been linked to human disease, often associated with a vast genetic and clinical heterogeneity and further compounded by few genotype–phenotype correlations which help guide molecular genetic investigations.

Succinate dehydrogenase is a crucial metabolic enzyme complex that is involved in both the Krebs cycle and the mitochondrial respiratory chain. It is composed of two catalytic subunits (the flavoprotein SDHA, and Fe–S-containing SDHB) anchored to the inner mitochondrial membrane by the SDHC and SDHD subunits. All four subunits and the two known assembly factors are encoded by autosomal genes (*SDHA*, *SDHB*, *SDHC*, *SDHD*, *SDHAF1* and *SDHAF2*, hereafter referred to as *SDHx*). Congenital recessive defects involving *SDHx* genes are associated with diverse clinical presentations, including leukodystrophy and cardiomyopathy (Alston et al. 2012).

A recent review describes *SDHA* mutations as the most common cause of isolated complex II deficiency, with 16 unique mutations reported in 30 patients (Ma et al. 2014; Renkema et al. 2014); the next most common cause are mutations in *SDHAF1*, 4 mutations have been reported in 13 patients (Ghezzi et al. 2009; Ohlenbusch et al. 2012). Just one mitochondrial disease patient is reported to harbour either *SDHB* (Alston et al. 2012) or *SDHD* (Jackson et al. 2014) mutations and metabolic presentations have yet to be reported in association with *SDHC* or *SDHAF2*.

In addition to their role in primary respiratory chain disease, SDHx mutations can act as drivers of neoplastic transformation following loss of heterozygosity (LOH). One of the most common causes of head and neck paraganglioma (HNPGL) is LOH at the SDHD locus. These mutations are inherited in a dominant manner with a parent of origin effect; typically only paternally inherited SDHD mutations are associated with HNPGL development (Hensen et al. 2011).

Here, we report a neonate who presented prenatally with cardiomyopathy due to a novel homozygous *SDHD* mutation. This is the second report of recessive *SDHD* mutations resulting in a primary mitochondrial disease presentation and serves to characterise the biochemical, histochemical and functional consequences of our patient's molecular genetic defect. Moreover, the affected amino acid, p.Asp92, has been reported as a Dutch founder mutation in families with hereditary PGL, albeit the substituted residue differs. We have used the yeast, *Saccharomyces cerevisiae,* which has proven to be a useful model system to study the effects of SDHx gene mutations (Goffrini et al. 2009; Panizza et al. 2013), to provide functional evidence supporting the pathogenicity of the *SDHD* mutation identified in our patient and, to a lesser extent, that of the PGL-associated p.Asp92Tyr mutation.

Patient and methods

The patient is the third child born to unrelated Irish parents. Foetal heart abnormalities were identified on an anomaly scan at 31-weeks gestation, which prompted foetal echocardiography. A normally situated heart with normal systemic and pulmonary venous drainage was reported. Right to left shunting was noted at the patent foramen ovale and ductus arteriosus, consistent with gestational age. The left ventricle and left atrium were severely dilated with moderate–severe mitral regurgitation. There was severe left ventricular systolic dysfunction, but no evidence of pericardial effusion or ascites. Rhythm was normal sinus with a foetal heart rate between 100 and 120 beats per minute and subsequent weekly foetal echocardiogram showed no further progression of cardiac dysfunction or development of hydrops. Cardiac MRI at 32-weeks gestation showed marked left ventricular hypertrophy and dilation. A clinical diagnosis of dilated cardiomyopathy was considered and the parents were counselled that the prognosis for postpartum survival was poor. The proband was born by elective caesarean section at 37 + 6 weeks gestation with a birth weight of 2620 g (9th–25th centile) and occipital circumference of 34.5 cm (50th–75th centile). He had no dysmorphic features. He was transferred to neonatal intensive care on 100 % oxygen to maintain his saturations in the low 90 s. An additional heart sound and loud murmur were noted, along with hepatomegaly (4 cm below costal margin) but without splenomegaly. By 12 h of age, his condition had deteriorated significantly; echocardiogram showed dilation of the inferior vena cava, hepatic veins, right atrium and interatrial septal bowing. He had moderate tricuspid regurgitation and very poor biventricular function with non-compaction hypertrophy. The proband died the following evening following withdrawal of life support with parental consent. At postmortem examination, the heart weighed 43 g (normal = 13.9 ± 5.8 g). The right atrium was particularly enlarged. The endocardium of the right atrium but particularly also the right ventricle showed fibroelastosis. The right ventricle was remarkably diminutive and underdeveloped. The right atrium had a 7-mm-diameter patent foramen ovale. There was obvious non-compaction of the hypertrophic left ventricular myocardium (Fig. 1). Cardiac muscle, skeletal muscle and a skin biopsy were referred for laboratory investigations. Informed consent was obtained from the parents for the clinical and laboratory investigations and publication of the results.

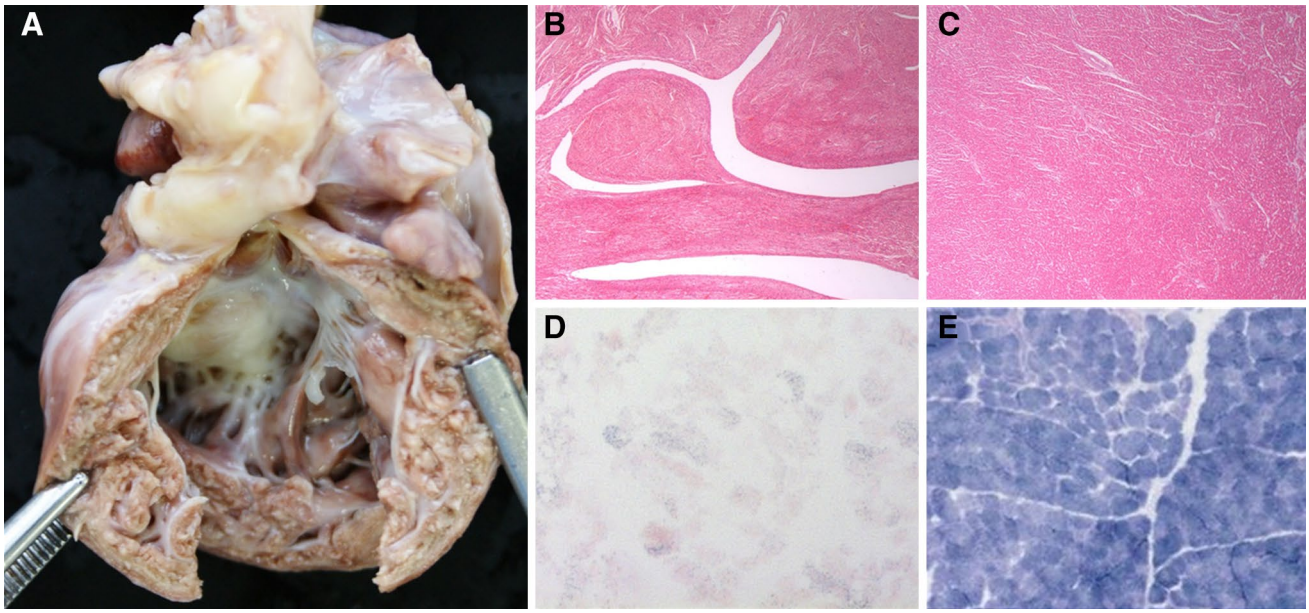

Fig. 1 Macroscopic and microscopic analysis of patient cardiac and skeletal muscle. **a** Macroscopic examination of patient heart revealed obvious non-compaction of the hypertrophic left ventricle. **b** Microscopic assessment of left ventricle confirms non-compaction compared to neonatal control tissue (**c**). Histochemical assessment of patient muscle biopsy shows a marked decrease in the activity of succinate dehydrogenase activity (**d**) compared with a control muscle (**e**)

Histochemical and biochemical assessment of metabolic function

Histological and histochemical assay of 10 μm serial sections of patient muscle biopsy was performed according to standard protocols. The measurement of respiratory chain enzyme activities was determined spectrophotometrically as described previously (Kirby et al. 2007). Fibroblast culture and measurement of β-oxidation flux in cultured fibroblasts using [9, 10-^{3}H] myristate, [9, 10-^{3}H]palmitate and [9, 10-^{3}H]oleate was performed as described elsewhere (Manning et al. 1990; Olpin et al. 1992, 1997).

Cytogenetic and molecular genetic investigations

Karyotyping of cultured fibroblasts and DNA extraction from patient muscle were performed according to standard protocols. Primers were designed to amplify each coding exon, plus intron–exon boundaries, of the *SDHA*, *SDHB*, *SDHC*, *SDHD*, *SDHAF1* and *SDHAF2* genes. PCR amplicons were Sanger sequenced using BigDye3.1 chemistry (Applied Biosystems) and capillary electrophoresed on an ABI3130xl bioanalyser (Applied Biosystems) using standard methodologies. Resultant sequencing chromatograms were compared to the Genbank reference sequences: *SDHA* (NM_004168.2), *SDHB* (NM_003000.2), *SDHC* (NM_003001.3), *SDHD* (NM_003002.3), *SDHAF1* (NM_001042631.2) and *SDHAF2* (NM_017841.2). All gene variants were annotated using dbSNP build 138 whilst ESP6500 and 10 k genome project data allowed determination of allele frequencies. Parental DNA samples were screened to investigate allele transmission.

In silico pathogenicity prediction tools and structural modelling

The effect of the p.(Asp92Gly) substitution on SDHD function was predicted using the in silico tools SIFT (Ng and Henikoff 2003), Align GVGD (Tavtigian et al. 2006) and Polyphen (Adzhubei et al. 2010), all running recommended parameters. To determine whether the tertiary structure of the protein was affected by the mutation, the wild-type (NP_002993) and mutant SDHD protein sequences were input to PSIPRED (Jones 1999) and I-TASSER (Yang et al. 2014); I-TASSER output was visualised using UCSF Chimera (Pettersen et al. 2004).

Blue native polyacrylamide gel electrophoresis (BN-PAGE)

Mitochondria-enriched pellets were obtained from 15 mg skeletal muscle as previously described (Nijtmans et al. 2002) and solubilised in 1× sample buffer (Invitrogen,

BN20032), 2 % dodecyl-β-d-maltoside (Sigma) and 5 % glycerol. Mitochondria were pelleted for 15 min at 100,000 g. Protein concentrations were determined by Pierce™ BCA Protein Assay Kit according to manufacturer's protocol (ThermoScientific). Protein samples (25 µg) were separated on NativePAGE™ Novex® 4–16 % Bis–Tris Protein Gels (Sigma) then transferred onto a PVDF membrane. Immunodetection of assembled respiratory chain complexes was performed using primary monoclonal antibodies (mitosciences) raised against complex-specific proteins: Complex I (NDUFB8, Abcam, ab110242), Complex II (SDHA, MitoSciences, MS204), Complex III (CORE2 Abcam, ab14745), Complex IV (COX1 Abcam, ab14705) and Complex V (ATP5A Abcam, ab14748). Following HRP-conjugated secondary antibody application (Dako), detection was undertaken using the ECL® plus chemiluminescence reagent (GE Healthcare Life Sciences, Buckinghamshire, UK) and a ChemiDoc MP imager (Bio-Rad Laboratories).

Western blot

Mitochondria-enriched pellets prepared as above were lysed on ice in 50 mM Tris pH 7.5, 130 mM NaCl, 2 mM $MgCl_2$, 1 mM PMSF and 1 % NP-40. Protein concentration was calculated using the Bradford method (Bradford 1976). 13 µg of enriched mitochondrial proteins was loaded on a 12 % sodium dodecyl sulphate polyacrylamide gel with 1× dissociation buffer, electrophoretically separated and subsequently transferred onto a PVDF membrane. Immunodetection was performed using primary antibodies raised against complex II SDHA (MitoSciences, MS204) and SDHD (Merck Millipore, ABT110) and a mitochondrial marker protein, Porin (Abcam, ab14734). Following secondary antibody application (Dako), detection was undertaken using the ECL® plus chemiluminescence reagent (GE Healthcare Life Sciences, Buckinghamshire, UK) and ChemiDoc MP imager (Bio-Rad Laboratories).

Yeast strains and media

Yeast strains used in this study were BY4741 (*MATa*; *his3Δ1 leu2Δ0 met15Δ0 ura3Δ0*) and its isogenic sdh4:kanMX4. Cells were cultured in yeast nitrogen base (YNB) medium: 0.67 % yeast nitrogen base without amino acids (ForMediumTM), supplemented with 1 g/l of drop-out powder (Kaiser et al. 1994) containing all amino acids and bases, except those required for plasmid maintenance. Various carbon sources (Carlo Erba Reagents) were added at the indicated concentration. For the respiration and mitochondria extraction, cells were grown to late-log phase in the YNB medium supplemented with 0.6 % glucose. Media were solidified with 20 g/l agar (ForMediumTM) and strains were incubated at 28 or 37 °C.

Construction of yeast mutant alleles

The *sdh4*Asp98Gly and *sdh4*Asp98Tyr mutant alleles were obtained by site-directed mutagenesis using the overlap extension technique (Ho et al. 1989). In the first set of PCR reactions, the *SDH4* region was obtained using the forward primer ESDH4F and the following reverse mutagenic primer sdh4R98G 5′-CATGACAG AAAAGAAAGA**ACC**AGCTGCAGTGGATAACGG AC-3′ and sdh4R98Y 5′-CATGACAGAAAAGAAAG A**GTA**AGCTGCAGTGGATAACGGAC-3′ where base changes are indicated in bold. The second *SDH4* region was obtained using the forward mutagenic primer sdh4F98G and sdh4F98Y, complementary to sdh4R98G and sdh4R98Y, and the reverse primer XSDH4R. The final mutagenized products were obtained using the overlapping PCR fragments as template with ESDH4F and XSDH4R as external primers. The products were then digested with *Eco*RI and *Xba*I and cloned in *Eco*RI–*Xba*I-digested pFL38 centromeric plasmid (Bonneaud et al. 1991). The mutagenized inserts were verified by sequencing and the pFL38 plasmid-borne *SDH4* and *SDH4* mutant alleles were transformed in the BY4741 using the lithium-acetate method (Gietz and Schiestl 2007).

Isolation of mitochondria, enzyme assay and respiration

Oxygen uptake was measured at 28 °C using a Clark-type oxygen electrode in a 1-ml stirred chamber containing 1 ml of air-saturated respiration buffer (0.1 M phthalate–KOH, pH 5.0) and 10 mM glucose (Oxygraph System, Hansatech Instruments, England). The reaction was initiated with the addition of 20 mg of wet weight of cells, as previously described (Goffrini et al. 2009). Preparation of mitochondria and succinate dehydrogenase DCPIP assay was conducted as described (Goffrini et al. 2009). The succinate:decylubiquinone DCPIP reductase assay was conducted as previously described (Jarreta et al. 2000; Oyedotun and Lemire 2001). Protein concentration was determined by the Bradford method using the Bio-Rad protein assay following the manufacturer's instructions (Bradford 1976).

Results

Pathological, histochemical and biochemical analysis

Histopathological examination of the patient's heart revealed non-compaction of the left ventricular myocardium (Fig. 1a, b). Histological investigations reported normal skeletal muscle morphology whilst histochemical analysis of fresh-frozen muscle biopsy sections revealed a global reduction of succinate dehydrogenase (complex II) activity compared to aged-matched control samples (Fig. 1d, e). Spectrophotometric analysis of respiratory chain function in patient muscle homogenate revealed a marked defect in complex II activity (patient 0.042 nmols/min/unit citrate synthase activity; controls 0.145 ± 0.047 nmols/min/unit citrate synthase activity ($n = 25$) representing ~30 % residual enzyme activity; the activities of complex I, complex III and complex IV were all normal (not shown). Fatty acid oxidation flux studies on cultured fibroblasts gave normal results which excluded virtually all primary defects of long- and medium-chain fatty acid oxidation as the cause of the underlying cardiac pathology. There was no evidence of an underlying aminoacidopathy and serum urea and electrolytes were within normal limits. Investigations of glucose and lactate levels were not performed. The monolysocardiolipin/cardiolipin (ML/CL) ratio on a postmortem sample was 0.03 and the neutrophil count was within normal limits.

Cytogenetic and molecular genetic investigations

Karyotyping reported a normal 46 XY profile, consistent with no large genomic rearrangements. Following identification of an isolated complex II deficiency, Sanger sequencing of all six *SDHx* genes was undertaken and a novel homozygous c.275A>G, p.(Asp92Gly) variant was identified in *SDHD* (ClinVar Reference ID: SCV000196921). Results from parental carrier testing were consistent with an autosomal recessive inheritance pattern, with each parent harbouring a heterozygous c.275A>G, p.(Asp92Gly) *SDHD* variant (Fig. 2a). The p.Asp92 *SDHD* residue is highly conserved (Fig. 2d) and the c.275A>G variant is not reported on either the ESP6500 or 1KGP suggesting that it is rare in the general population. Whilst the c.275A>G, p.(Asp92Gly) *SDHD* variant has not been previously reported, another mutation affecting the same residue—c.274G>T, p.(Asp92Tyr)—has been reported in association with familial PGL and PCC (Hensen et al. 2011). In silico predictions were strongly supportive of a deleterious effect; 100 % sensitivity and 100 % specificity were reported by SIFT and polyphen for both the p.(Asp92Gly) and p.(Asp92Tyr) variants. Both variants were assigned an aGVGD class of C65 (highly likely to be detrimental to protein function)—the p.(Asp92Gly) variant was reported to have a grantham difference (GD) value of 93.77, whilst the GD for the p.(Asp92Tyr) variant was 159.94 (GD > 70 is associated with C55/C65 variant classes). SDHD tertiary structure was not predicted to be markedly impacted by the patient's p.(Asp92Gly) substitution; no gross conformational change was reported by I-TASSER (Fig. 2b), whilst PSIPRED predicted only a mild alteration to the helix structure (Fig. 2c).

Functional effect of the c.275A>G, p.(Asp92Gly) SDHD mutation on protein expression and complex assembly

Having identified an excellent candidate mutation, assessment of respiratory chain complex assembly by one-dimensional BN-PAGE revealed a marked decrease in fully assembled Complex II, whilst levels of fully assembled complexes I, III, IV and V were comparable to controls (Fig. 3a). Western blot of mitochondrial proteins in patient muscle was performed which confirmed a significant reduction of the SDHD and SDHA proteins compared to both equally loaded control muscle samples and Porin, a mitochondrial marker protein (Fig. 3b).

Functional studies in a yeast model

To further assess the pathogenicity of the patient's novel p.(Asp92Gly) *SDHD* variant, we performed complementation studies using a strain of *S. cerevisiae* lacking the *SDH4* gene hereafter referred to as Δ*sdh4*. The *SDH4* gene is the yeast orthologue of human *SDHD* and although the human and yeast protein have a low degree of conservation (16 % identity and 36 % similarity) the p.Asp92 residue is conserved between the two species, corresponding to p.Asp98 in yeast (Fig. 2d). We then introduced the change equivalent to the human p.(Asp92Gly) variant into the yeast *SDH4* wild-type gene cloned in a centromeric vector thus obtaining the $sdh4^{D98G}$ mutant allele. Since another mutation involving the same residue, p.(Asp92Tyr), has been reported as a cause of paraganglioma, a second mutant allele, $sdh4^{D98Y}$, was also constructed to compare the phenotype between the two different amino acid substitutions. The *SDH4*, $sdh4^{D98G}$ and $sdh4^{D98Y}$ constructs and the empty plasmid pFL38 were then transformed into the Δ*sdh4* strain. To test the possible effects on mitochondrial function, we first evaluated the oxidative growth by spot assay analysis on mineral medium supplemented with either glucose or ethanol, at 28 and 37 °C.

A clear growth defect was observed for the $\Delta sdh4/sdh4^{D98G}$ strain in ethanol-containing plates incubated both at 28 and 37 °C (Fig. 4a), with growth similar to that of the *sdh4* null mutant. Contrariwise, the $\Delta sdh4/sdh4^{D98Y}$

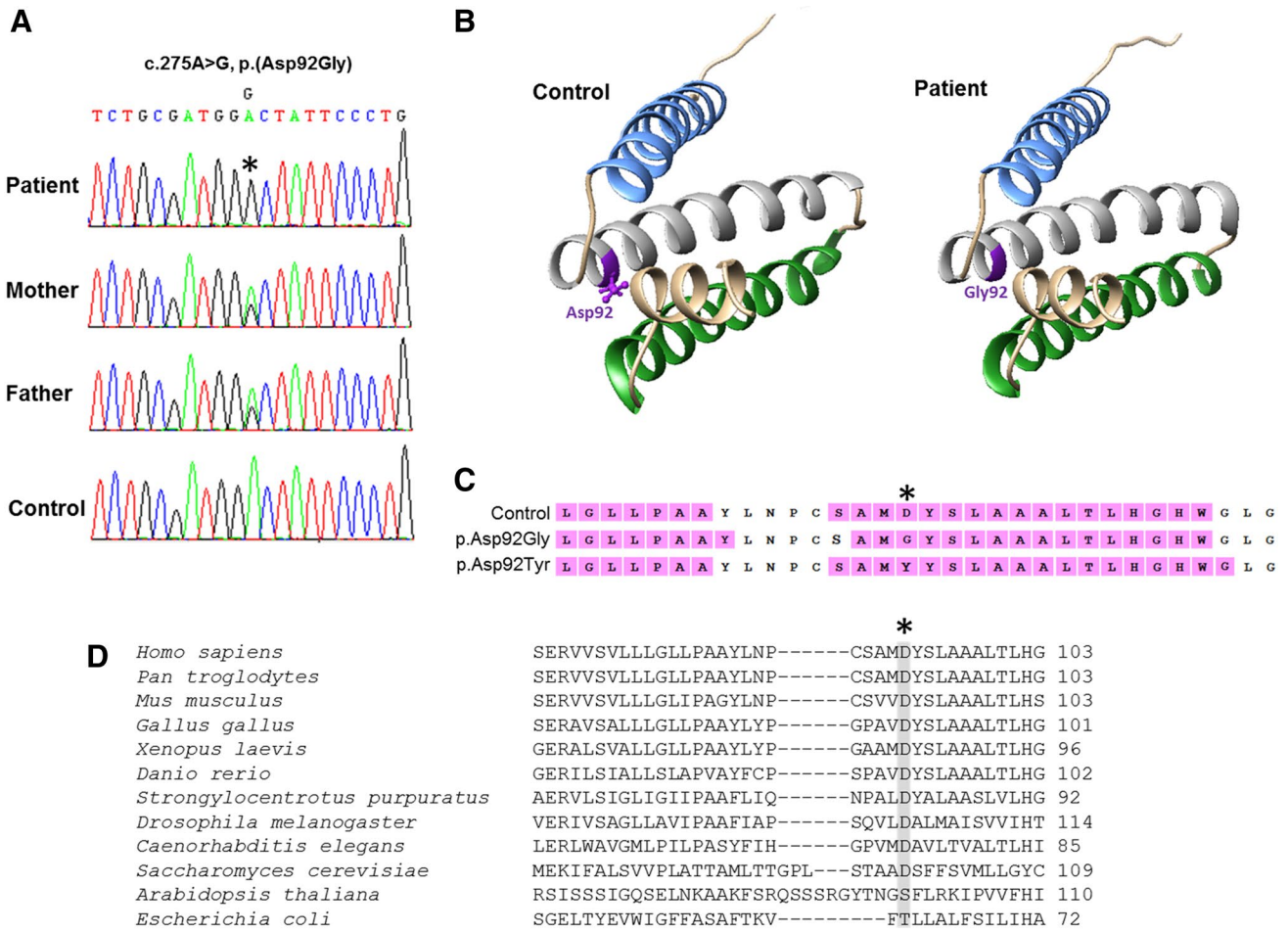

Fig. 2 Molecular genetic and in silico investigations. **a** Identification of a pathogenic *SDHD* mutation. A homozygous c.275A>G, p.(Asp92Gly) *SDHD* mutation was identified in the proband, with parental DNA screening supporting recessive inheritance. The mutation affects a highly conserved p.Asp92 residue in the *SDHD*-encoded subunit of succinate dehydrogenase (SDH). **b** Structural modelling. I-TASSER prediction of control and patient SDHD tertiary structure shows the p.Asp92 residue located within a transmembrane helix domain and the p.Asp92Gly substitution is predicted to have little impact on SDHD tertiary structure. **c** PSIPRED output predicts minor alterations to two of the SDHD helices from the patient p.(Asp92Gly) and HNPGL p.(Asp92Tyr) substitutions compared to control sequence. Predicted helix residues shown in *pink*; unshaded residues are located in coil domains. **d** Multiple sequence alignment of this region of the SDHD subunit was performed using ClustalW and confirms that the p.(Asp92Gly) mutation affects an evolutionary conserved residue (*shaded*). Alignments were manually corrected on the basis of the pairwise alignment obtained with PSI-BLAST

strain did not exhibit an OXPHOS-deficient phenotype at either temperature tested (Fig. 4b) or in either oxidative carbon source analysed (not shown). To further investigate the OXPHOS defect, oxygen consumption and SDH activity were measured. The oxygen consumption rate of the Δ*sdh4*/*sdh4*^{D98G} mutant was 55 % less than that of the parental strain Δsdh4/SDH4 (Fig. 5a), likewise, succinate dehydrogenase enzyme activities (PMS/DCPIP reductase and decylubiquinone reductase) were both severely reduced, with levels similar to those of the null mutant (Fig. 5b). Consistent with the results obtained from growth experiments the oxygen consumption rate of the Δ*sdh4*/*sdh4*^{D98Y} mutant was not impaired (Fig. 5a) but both SDH activities (PMS/DCPIP reductase and decylubiquinone reductase) were partially reduced (80 and 75 % residual activity) in Δ*sdh4*/*sdh4*^{D98Y} mitochondria (Fig. 5b). Together, these data support the pathogenicity of our patient's novel p.(Asp92Gly) *SDHD* variant.

Discussion

Mitochondrial complex II deficiency is one of the rarest disorders of the OXPHOS system, accounting for between 2 and 8 % of mitochondrial disease cases (Ghezzi et al. 2009; Parfait et al. 2000) with only ~45 cases reported in

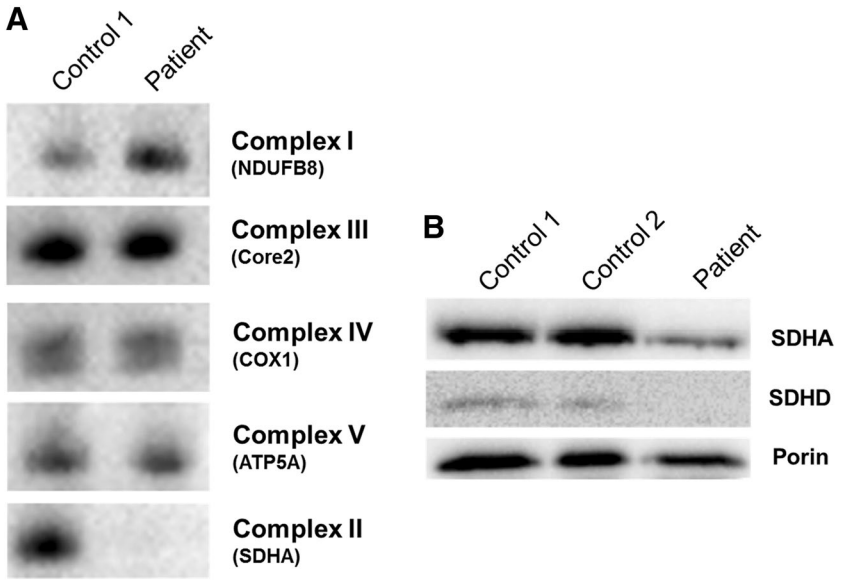

Fig. 3 Investigation of OXPHOS complex activities and protein expression in patient and controls. **a** BN-PAGE analysis of mitochondria isolated from patient and control muscle homogenates revealed a reduction of assembled complex II in patient muscle with normal assembly of all other OXPHOS complexes. **b** SDS-PAGE analysis of patient and control proteins probed with antibodies against Porin (a loading control) and the SDHA and SDHD subunits of succinate dehydrogenase revealed a stark reduction in SDH steady-state protein levels in patient muscle, consistent with subunit degradation thereby supporting the pathogenicity of the p.(Asp92Gly) variant

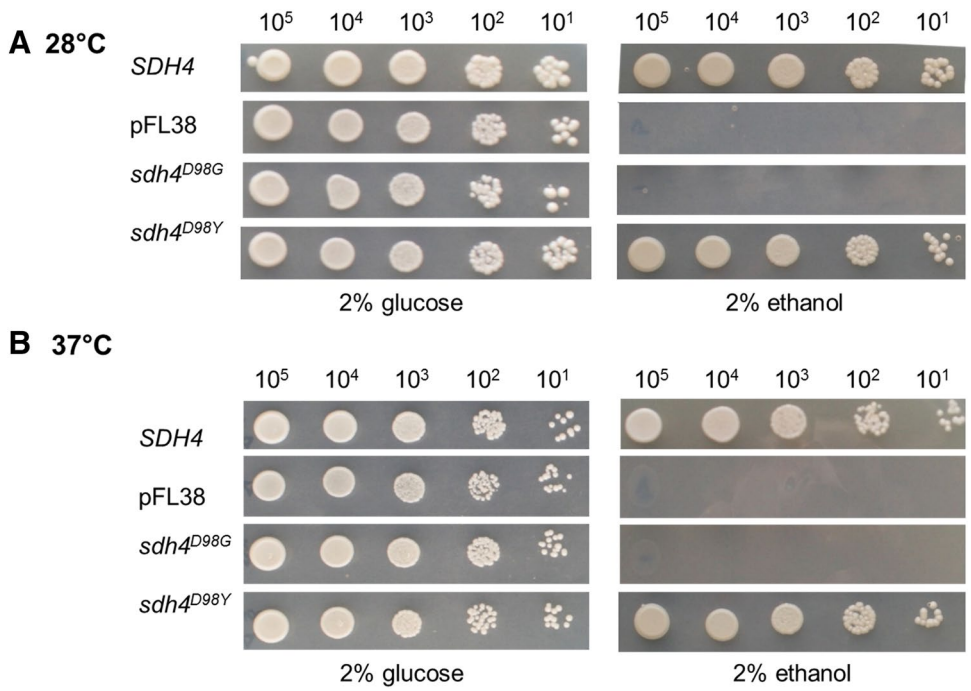

Fig. 4 Oxidative growth phenotype in yeast. The strain BY4741 Δ*sdh4* was transformed with a pFL38 plasmid carrying either the wild-type *SDH4*, the empty vector or the mutant alleles $sdh4^{D98G}$ and $sdh4^{D98Y}$. Equal amounts of serially diluted cells from exponentially grown cultures (10^5, 10^4, 10^3, 10^2, 10^1) were spotted onto yeast nitrogen base (YNB) plates supplemented with either 2 % glucose or 2 % ethanol. The growth was scored after 3-day incubation at 28 °C (**a**) and 37 °C (**b**)

the literature. We report a newborn boy presenting with left ventricular hypertrophy on foetal ultrasound at 32-weeks gestation who rapidly deteriorated after delivery due to cardiopulmonary insufficiency, dying on day one of life. Postmortem examination confirmed a non-compacted hypertrophic left ventricle but assessment of monolysocardiolipin and cardiolipin levels excluded a diagnosis of Barth syndrome. Biochemical analysis of his muscle biopsy revealed evidence of a marked isolated complex II deficiency. Sequencing the genes involved in succinate dehydrogenase structure and assembly was undertaken and revealed a novel homozygous c.275A>G, p.(Asp92Gly) *SDHD* mutation which was shown to be recessively inherited through segregation studies.

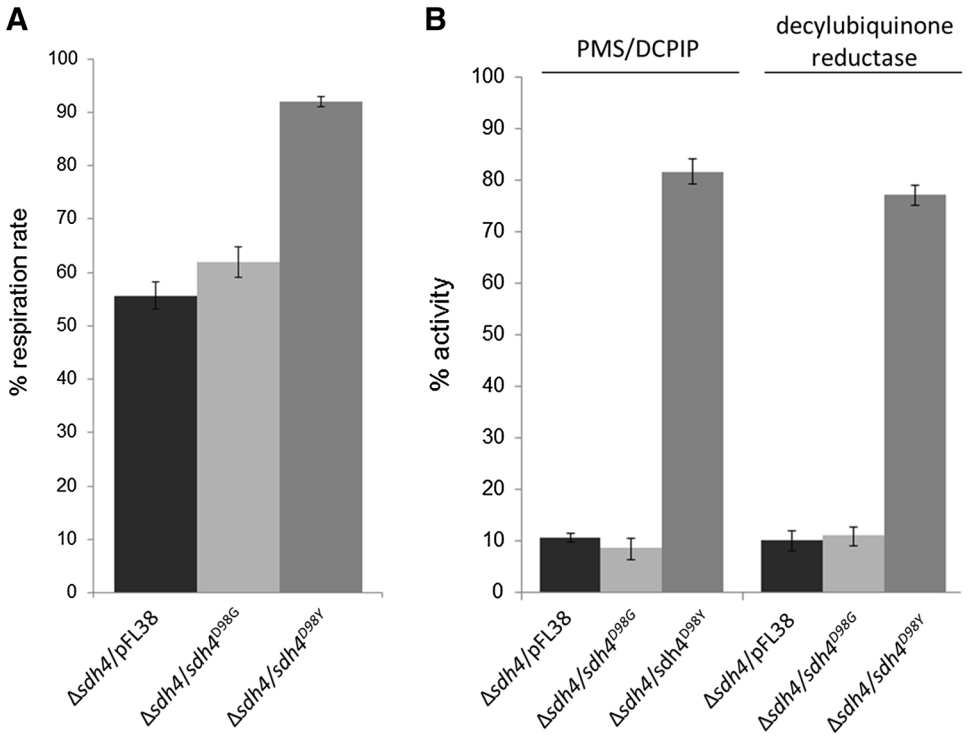

Fig. 5 **a** Oxygen consumption rates. Respiration was measured in cells grown in YNB supplemented with 0.6 % glucose at 28 °C. The values observed for the *sdh4* mutant cells are reported as a percentage of the wild-type *SDH4* cell respiratory rate, 40.46 ± 1.54 nmol min^{-1} mg^{-1}. **b** Complex II activity. PMS/DCPIP reductase and decylubiquinone reductase activities were measured in mitochondria extracted from cells grown exponentially at 28 °C in YNB supplemented with 0.6 % glucose. The values of the *sdh4* mutants are expressed as percentage of the activities obtained in the wild-type strain

Patients with an isolated complex II deficiency harbour either compound heterozygous or homozygous mutations in an SDH structural or assembly factor gene. The resultant loss of OXPHOS-driven ATP synthesis is associated with clinical presentations including Leigh syndrome, cardiomyopathy and leukodystrophy, that often present during infancy, though adult cases are reported (Taylor et al. 1996; Birch-Machin et al. 2000). Complex II deficiency is very rare, perhaps reflecting an incompatibility with life for many cases and our patient's clinical history with prenatal cardiomyopathy and rapid deterioration postpartum supports this hypothesis. Although the published cohort of patients with complex II deficiency is small, mutations which affect the ability of complex II to bind to the mitochondrial membrane are evolving to be the most deleterious.

The only other *SDHD*-deficient patient reported in the literature harboured compound heterozygous variants, one missense and one that extended the protein by three amino acids (Jackson et al. 2014). The clinical presentation of this individual differed from that of our patient who presented in utero with a cardiomyopathy that was incompatible with life. The previously described case was delivered at term after a normal pregnancy and presented at age 3 months with developmental regression following a viral infection with progressive neurological deterioration (epileptic seizures, ataxia, dystonia and continuous intractable myoclonic movements) and died at the age of 10 years. The patient described by Jackson et al. also had comparably low levels of SDHD protein on Western blot with greatly reduced levels of fully assembled complex II; a residual level of complex activity is therefore unlikely to account for the difference in presentation. We hypothesised that the p.(Asp92Gly) variant might have caused a conformational change given the location of the conserved acidic p.Asp92 residue at the N-terminus of one of the protein's helical domains. With this in mind, we modelled the predicted impact of the patient's p.(Asp92Gly) *SDHD* mutation on tertiary structure using in silico methodologies. Contrary to our expectations, neither I-TASSER nor PSIPRED predicted gross tertiary structural anomalies due to the substitution, despite being situated between two conserved cysteine residues; the pathogenicity is therefore assumed to lie in the nature of the amino acid properties as opposed to consequential protein misfolding. The location of the p.Asp92 residue at the helical N-termini may explain the discrepancy between the predicted Grantham scores and the functional data obtained following yeast modelling; leucine–tyrosine interactions are reported to act as stabilisers within alpha helices (Padmanabhan and Baldwin 1994) meaning the p.Asp92Tyr substitution (with a higher GD score) may therefore be less deleterious than the p.(Asp92Gly) substitution harboured by our patient. Moreover, the location of the substitution may also be important in capping the positive helical dipole, and replacement with a non-polar residue such as glycine would fail to provide the same charge stabilization. There was slight discordance between the helix predictions from

I-TASSER and PSIPRED (Fig. 2b, c) but on closer inspection of the discordant residues, there was low confidence in the predictions.

Mutations in *SDHD* and other *SDHx* genes have been implicated not only in primary metabolic dysfunction, but also as drivers of neoplastic transformation in various tumour types. There is a wealth of information in the literature describing the involvement of *SDHx* gene mutations in cases of hereditary and sporadic cancers including head and neck paraganglioma, pheochromocytoma and gastrointestinal stromal tumours (Miettinen and Lasota 2014). In the context of hereditary cancer, each somatic cell harbours one heterozygous germline mutation either inherited from a parent or occurring *de novo*. This single loss-of-function allele, alone, is insufficient to cause neoplastic transformation but if a "second hit" affects the wild-type allele, the loss of SDH activity disrupts ATP production. The inability of SDH to metabolise succinate causes a build-up of substrate, with elevated succinate levels stabilizing HIF1α. This in turn creates a pseudo-hypoxic state, prompting a switch to glycolytic respiration consistent with neoplasia (Hanahan and Weinberg 2011; Pollard et al. 2005). The metabolic stalling due to SDH dysfunction also acts to inhibit multiple 2-oxoglutarate-dependent histone and DNA demethylase enzymes resulting in widespread histone and DNA methylation, further adding to the tumorigenic burden of these already respiratory-deficient cells (Xiao et al. 2012).

To date, mutations reported in the SDHx genes are loss of function, either as tumour suppressors or in metabolic enzymes. The mutation harboured by our patient transcends these fields in that, although manifesting as a primary metabolic condition in our case, the p.Asp92 residue is recognised as a Dutch founder HNPGL mutation, p.(Asp92Tyr). Given the established link between tumorigenesis and this residue, further functional investigations were undertaken to determine whether the p.(Asp92Gly) variant—associated with primary metabolic dysfunction—was as deleterious, or indeed more so, than the founder HNPGL mutation. Functional investigations were supportive of a deleterious effect, Western blotting of patient muscle homogenates revealed a reduction in the steady-state levels evident for not only SDHD, but also for SDHA. This was supported by one-directional BN-PAGE, which confirmed a decrease in fully assembled complex II, consistent with the hypothesis that an inability to anchor the unstable complex within the mitochondrial membrane triggers the recycling of intermediates to prevent aggregation. This turnover is seen in other cases of mitochondrial complex dysfunction and prevents accumulation and aggregation of assembly intermediates and surplus complex subunits (Alston et al. 2012).

To assess the pathogenic role of the novel p.(Asp92Gly) SDHD substitution, we carried out a series of experiments in yeast devoid of *SDH4*, the yeast *SDHD* orthologue. The use of ethanol or glucose as a carbon source tested the strains' ability to rely upon either OXPHOS or fermentation for ATP synthesis. The SDHD residue p.Asp92 shows high evolutionary conservation and corresponds to p.Asp98 in yeast. Given that a germline mutation involving the same amino acid has been reported as a cause of paraganglioma [p.(Asp92Tyr)], two mutant alleles—$sdh4^{D98G}$ and $sdh4^{D98Y}$—were constructed to compare the phenotypes associated with the different substitutions. Consistent with the reduction of SDHD steady-state levels and fully assembled complex II found in our patient, the p.(Asp92Gly) mutation was detrimental to both oxidative growth and succinate dehydrogenase activity in yeast. Contrariwise, the p.(Asp98Tyr) HNPGL-associated substitution did not affect oxidative growth and showed a mild, albeit significant, reduction of SDH activity. Altogether the results obtained in the yeast model provide compelling functional evidence supporting the pathogenic role of the p.(Asp92Gly) mutation and show that this substitution conveys a more severe phenotype than the founder HNPGL *SDHD* mutation, this finding is not unique as other PGL-associated *SDHD* mutations were found to cause a milder phenotype when modelled in yeast (Panizza et al. 2013). Whilst our modelling suggests that the well-characterised p.(Asp92Tyr) *PGL* mutation is associated with what might be considered a mild phenotype in yeast, the phenotype in question is not a primary metabolic one and indeed it is only associated with oncogenesis in tandem with a second mutation, which is often a large-scale deletion or other null allele.

There were no reports of potential *SDHD*-associated cancers in the immediate family although further information from extended family members was unavailable. We previously reported inherited recessive *SDHB* mutations in association with a paediatric primary mitochondrial phenotype and this case also lacked a history of hereditary cancer (Alston et al. 2012). It is unclear whether germline carriers of the p.(Asp92Gly) *SDHD* mutation are at elevated risk of HNPGL and despite no tumours having been reported in the family, it is the opinion of their clinicians that surveillance was advisable and is ongoing.

Left ventricular non-compaction is a rare form of cardiomyopathy characterised by abnormal trabeculations in the left ventricle and associated with either ventricular hypertrophy or dilation. In some patients, LVNC arises from a failure to complete the final stage of myocardial morphogenesis, but this is not a satisfactory explanation for all cases, particularly those associated with congenital heart defects or arrhythmias. LVNC is genetically heterogeneous with many cases remaining genetically undiagnosed, but metabolic derangements are common and this form of cardiomyopathy is typical of Barth Syndrome, a disorder

of mitochondrial cardiolipin typically accompanied by neutropenia (Chen et al. 2002) and has also been observed in other mitochondrial disorders including those due to mutations in mtDNA (Pignatelli et al. 2003).

In conclusion, our case further expands the clinical and genetic heterogeneity associated with isolated complex II deficiency and demonstrates that sequencing analysis of all SDH subunits and assembly factors should be undertaken for patients in whom an isolated succinate dehydrogenase defect has been identified.

Acknowledgments This work was supported by grants (to RWT and RM) from The Wellcome Trust Centre for Mitochondrial Research (096919Z/11/Z), the Medical Research Council (UK) Centre for Translational Muscle Disease Research (G0601943), The Lily Foundation and the UK NHS Highly Specialised Commissioners which funds the "Rare Mitochondrial Disorders of Adults and Children" Diagnostic Service in Newcastle upon Tyne (http://www.newcastle-mitochondria.com). CLA is the recipient of a National Institute for Health Research (NIHR) doctoral fellowship (NIHR-HCS-D12-03-04). The views expressed are those of the authors and not necessarily those of the NHS, the NIHR or the Department of Health.

References

Adzhubei IA, Schmidt S, Peshkin L, Ramensky VE, Gerasimova A, Bork P, Kondrashov AS, Sunyaev SR (2010) A method and server for predicting damaging missense mutations. Nat Methods 7:248–249. doi:10.1038/nmeth0410-248

Alston CL, Davison JE, Meloni F, van der Westhuizen FH, He L, Hornig-Do HT, Peet AC, Gissen P, Goffrini P, Ferrero I, Wassmer E, McFarland R, Taylor RW (2012) Recessive germline SDHA and SDHB mutations causing leukodystrophy and isolated mitochondrial complex II deficiency. J Med Genet 49:569–577. doi:10.1136/jmedgenet-2012-101146

Birch-Machin MA, Taylor RW, Cochran B, Ackrell BA, Turnbull DM (2000) Late-onset optic atrophy, ataxia, and myopathy associated with a mutation of a complex II gene. Ann Neurol 48:330–335

Bonneaud N, Ozier-Kalogeropoulos O, Li GY, Labouesse M, Minvielle-Sebastia L, Lacroute F (1991) A family of low and high copy replicative, integrative and single-stranded *S. cerevisiae/E. coli* shuttle vectors. Yeast 7:609–615. doi:10.1002/yea.320070609

Bradford MM (1976) A rapid and sensitive method for the quantitation of microgram quantities of protein utilizing the principle of protein–dye binding. Anal Biochem 72:248–254

Chen R, Tsuji T, Ichida F, Bowles KR, Yu X, Watanabe S, Hirono K, Tsubata S, Hamamichi Y, Ohta J, Imai Y, Bowles NE, Miyawaki T, Towbin JA (2002) Mutation analysis of the G4.5 gene in patients with isolated left ventricular noncompaction. Mol Genet Metab 77:319–325

Ghezzi D, Goffrini P, Uziel G, Horvath R, Klopstock T, Lochmuller H, D'Adamo P, Gasparini P, Strom TM, Prokisch H, Invernizzi F, Ferrero I, Zeviani M (2009) SDHAF1, encoding a LYR complex-II specific assembly factor, is mutated in SDH-defective infantile leukoencephalopathy. Nat Genet 41:654–656. doi:10.1038/ng.378

Gietz RD, Schiestl RH (2007) Quick and easy yeast transformation using the LiAc/SS carrier DNA/PEG method. Nat Protoc 2:35–37. doi:10.1038/nprot.2007.14

Goffrini P, Ercolino T, Panizza E, Giache V, Cavone L, Chiarugi A, Dima V, Ferrero I, Mannelli M (2009) Functional study in a yeast model of a novel succinate dehydrogenase subunit B gene germline missense mutation (C191Y) diagnosed in a patient affected by a glomus tumor. Hum Mol Genet 18:1860–1868. doi:10.1093/hmg/ddp102

Gorman GS, Schaefer AM, Ng Y, Gomez N, Blakely EL, Alston CL, Feeney C, Horvath R, Yu-Wai-Man P, Chinnery PF, Taylor RW, Turnbull DM, McFarland R (2015) Prevalence of nuclear and mitochondrial DNA mutations related to adult mitochondrial disease. Ann Neurol 77:753–759. doi:10.1002/ana.24362

Hanahan D, Weinberg RA (2011) Hallmarks of cancer: the next generation. Cell 144:646–674. doi:10.1016/j.cell.2011.02.013

Hensen EF, Siemers MD, Jansen JC, Corssmit EP, Romijn JA, Tops CM, van der Mey AG, Devilee P, Cornelisse CJ, Bayley JP, Vriends AH (2011) Mutations in SDHD are the major determinants of the clinical characteristics of Dutch head and neck paraganglioma patients. Clin Endocrinol Oxf 75:650–655. doi:10.1111/j.1365-2265.2011.04097.x

Ho SN, Hunt HD, Horton RM, Pullen JK, Pease LR (1989) Site-directed mutagenesis by overlap extension using the polymerase chain reaction. Gene 77:51–59

Horscroft JA, Murray AJ (2014) Skeletal muscle energy metabolism in environmental hypoxia: climbing towards consensus. Extrem Physiol Med 3:19. doi:10.1186/2046-7648-3-19

Jackson CB, Nuoffer JM, Hahn D, Prokisch H, Haberberger B, Gautschi M, Haberli A, Gallati S, Schaller A (2014) Mutations in SDHD lead to autosomal recessive encephalomyopathy and isolated mitochondrial complex II deficiency. J Med Genet 51:170–175. doi:10.1136/jmedgenet-2013-101932

Jarreta D, Orus J, Barrientos A, Miro O, Roig E, Heras M, Moraes CT, Cardellach F, Casademont J (2000) Mitochondrial function in heart muscle from patients with idiopathic dilated cardiomyopathy. Cardiovasc Res 45:860–865

Jones DT (1999) Protein secondary structure prediction based on position-specific scoring matrices. J Mol Biol 292:195–202. doi:10.1006/jmbi.1999.3091

Kaiser C, Michaelis S, Mitchel A (1994) Methods in yeast genetics: a laboratory course manual, 1994, ed edn. Cold Spring Harbor Laboratory Press, Cold Spring Harbor

Kirby DM, Thorburn DR, Turnbull DM, Taylor RW (2007) Biochemical assays of respiratory chain complex activity. Methods Cell Biol 80:93–119. doi:10.1016/s0091-679x(06)80004-x

Ma YY, Wu TF, Liu YP, Wang Q, Li XY, Ding Y, Song JQ, Shi XY, Zhang WN, Zhao M, Hu LY, Ju J, Wang ZL, Yang YL, Zou LP (2014) Two compound frame-shift mutations in succinate dehydrogenase gene of a Chinese boy with encephalopathy. Brain Dev 36:394–398. doi:10.1016/j.braindev.2013.06.003

Manning NJ, Olpin SE, Pollitt RJ, Webley J (1990) A comparison of [9, 10-3H] palmitic and [9, 10-3H] myristic acids for the detection of defects of fatty acid oxidation in intact cultured fibroblasts. J Inherit Metab Dis 13:58–68

Miettinen M, Lasota J (2014) Succinate dehydrogenase deficient gastrointestinal stromal tumors (GISTs)—a review. Int J Biochem Cell Biol 53:514–519. doi:10.1016/j.biocel.2014.05.033

Ng PC, Henikoff S (2003) SIFT: predicting amino acid changes that affect protein function. Nucleic Acids Res 31:3812–3814

Nijtmans LG, Henderson NS, Holt IJ (2002) Blue native electrophoresis to study mitochondrial and other protein complexes. Methods 26:327–334. doi:10.1016/s1046-2023(02)00038-5

Ohlenbusch A, Edvardson S, Skorpen J, Bjornstad A, Saada A, Elpeleg O, Gartner J, Brockmann K (2012) Leukoencephalopathy with accumulated succinate is indicative of SDHAF1 related complex II deficiency. Orphanet J Rare Dis 7:69. doi:10.1186/1750-1172-7-69

Olpin SE, Manning NJ, Carpenter K, Middleton B, Pollitt RJ (1992) Differential diagnosis of hydroxydicarboxylic aciduria based on release of $3H_2O$ from [9, 10-3H] myristic and [9, 10-3H] palmitic acids by intact cultured fibroblasts. J Inherit Metab Dis 15:883–890

Olpin SE, Manning NJ, Pollitt RJ, Clarke S (1997) Improved detection of long-chain fatty acid oxidation defects in intact cells using [9, 10-3H] oleic acid. J Inherit Metab Dis 20:415–419

Oyedotun KS, Lemire BD (2001) The quinone-binding sites of the *Saccharomyces cerevisiae* succinate–ubiquinone oxidoreductase. J Biol Chem 276:16936–16943. doi:10.1074/jbc.M100184200

Padmanabhan S, Baldwin RL (1994) Helix-stabilizing interaction between tyrosine and leucine or valine when the spacing is *i*, $i + 4$. J Mol Biol 241:706–713. doi:10.1006/jmbi.1994.1545

Pagliarini DJ, Calvo SE, Chang B, Sheth SA, Vafai SB, Ong SE, Walford GA, Sugiana C, Boneh A, Chen WK, Hill DE, Vidal M, Evans JG, Thorburn DR, Carr SA, Mootha VK (2008) A mitochondrial protein compendium elucidates complex I disease biology. Cell 134:112–123. doi:10.1016/j.cell.2008.06.016

Panizza E, Ercolino T, Mori L, Rapizzi E, Castellano M, Opocher G, Ferrero I, Neumann HP, Mannelli M, Goffrini P (2013) Yeast model for evaluating the pathogenic significance of SDHB, SDHC and SDHD mutations in PHEO–PGL syndrome. Hum Mol Genet 22:804–815. doi:10.1093/hmg/dds487

Parfait B, Chretien D, Rotig A, Marsac C, Munnich A, Rustin P (2000) Compound heterozygous mutations in the flavoprotein gene of the respiratory chain complex II in a patient with Leigh syndrome. Hum Genet 106:236–243

Pettersen EF, Goddard TD, Huang CC, Couch GS, Greenblatt DM, Meng EC, Ferrin TE (2004) UCSF Chimera—a visualization system for exploratory research and analysis. J Comput Chem 25:1605–1612. doi:10.1002/jcc.20084

Pignatelli RH, McMahon CJ, Dreyer WJ, Denfield SW, Price J, Belmont JW, Craigen WJ, Wu J, El Said H, Bezold LI, Clunie S, Fernbach S, Bowles NE, Towbin JA (2003) Clinical characterization of left ventricular noncompaction in children: a relatively common form of cardiomyopathy. Circulation 108:2672–2678. doi:10.1161/01.cir.0000100664.10777.b8

Pollard PJ, Briere JJ, Alam NA, Barwell J, Barclay E, Wortham NC, Hunt T, Mitchell M, Olpin S, Moat SJ, Hargreaves IP, Heales SJ, Chung YL, Griffiths JR, Dalgleish A, McGrath JA, Gleeson MJ, Hodgson SV, Poulsom R, Rustin P, Tomlinson IP (2005) Accumulation of Krebs cycle intermediates and over-expression of HIF1alpha in tumours which result from germline FH and SDH mutations. Hum Mol Genet 14:2231–2239. doi:10.1093/hmg/ddi227

Renkema GH, Wortmann SB, Smeets RJ, Venselaar H, Antoine M, Visser G, Ben-Omran T, van den Heuvel LP, Timmers HJ, Smeitink JA, Rodenburg RJ (2014) SDHA mutations causing a multisystem mitochondrial disease: novel mutations and genetic overlap with hereditary tumors. Eur J Hum Genet. doi:10.1038/ejhg.2014.80

Skladal D, Halliday J, Thorburn DR (2003) Minimum birth prevalence of mitochondrial respiratory chain disorders in children. Brain 126:1905–1912. doi:10.1093/brain/awg170

Tavtigian SV, Deffenbaugh AM, Yin L, Judkins T, Scholl T, Samollow PB, de Silva D, Zharkikh A, Thomas A (2006) Comprehensive statistical study of 452 BRCA1 missense substitutions with classification of eight recurrent substitutions as neutral. J Med Genet 43:295–305. doi:10.1136/jmg.2005.033878

Taylor RW, Birch-Machin MA, Schaefer J, Taylor L, Shakir R, Ackrell BA, Cochran B, Bindoff LA, Jackson MJ, Griffiths P, Turnbull DM (1996) Deficiency of complex II of the mitochondrial respiratory chain in late-onset optic atrophy and ataxia. Ann Neurol 39:224–232. doi:10.1002/ana.410390212

Xiao M, Yang H, Xu W, Ma S, Lin H, Zhu H, Liu L, Liu Y, Yang C, Xu Y, Zhao S, Ye D, Xiong Y, Guan KL (2012) Inhibition of alpha-KG-dependent histone and DNA demethylases by fumarate and succinate that are accumulated in mutations of FH and SDH tumor suppressors. Genes Dev 26:1326–1338. doi:10.1101/gad.191056.112

Yang J, Yan R, Roy A, Xu D, Poisson J, Zhang Y (2014) The I-TASSER suite: protein structure and function prediction. Nat Methods 12:7–8. doi:10.1038/nmeth.3213

JMG Online First, published on October 27, 2017 as 10.1136/jmedgenet-2017-104822

ORIGINAL ARTICLE

A novel de novo dominant mutation in *ISCU* associated with mitochondrial myopathy

Andrea Legati,[1] Aurelio Reyes,[2] Camilla Ceccatelli Berti,[3] Oliver Stehling,[4] Silvia Marchet,[1] Costanza Lamperti,[1] Alberto Ferrari,[3] Alan J Robinson,[2] Ulrich Mühlenhoff,[4] Roland Lill,[4,5] Massimo Zeviani, Paola Goffrini,[3] Daniele Ghezzi[1]

► Additional material is published online only. To view please visit the journal online (http://dx.doi.org/10.1136/jmedgenet-2017-104822).

[1]Molecular Neurogenetics Unit, Foundation IRCCS Neurological Institute Besta, Milan, Italy
[2]Medical Research Council Mitochondrial Biology Unit, University of Cambridge, Cambridge, UK
[3]Department of Chemistry, Life Sciences and Environmental Sustainability, University of Parma, Parma, Italy
[4]Department of Medicine, Institut für Zytobiologie und Zytopathologie, Philipps-Universität, Marburg, Germany
[5]Unit of Metabolism, LOEWE Zentrum für Synthetische Mikrobiologie SynMikro, Marburg, Germany

Correspondence to
Dr Paola Goffrini, Department of Chemistry, University of Parma, Life Sciences and Environmental Sustainability, Viale delle Scienze 11/A, 43124 Parma, Italy; paola.goffrini@unipr.it and Dr Daniele Ghezzi, Molecular Neurogenetics, Istituto Nazionale Neurologico C. Besta, Milan 20126, Italy; daniele.ghezzi@istituto-besta.it

AL and AR contributed equally.

Received 18 May 2017
Revised 16 August 2017
Accepted 22 August 2017

To cite: Legati A, Reyes A, Ceccatelli Berti C, *et al*. *J Med Genet* Published Online First: [please include Day Month Year]. doi:10.1136/jmedgenet-2017-104822

ABSTRACT

Background Hereditary myopathy with lactic acidosis and myopathy with deficiency of succinate dehydrogenase and aconitase are variants of a recessive disorder characterised by childhood-onset early fatigue, dyspnoea and palpitations on trivial exercise. The disease is non-progressive, but life-threatening episodes of widespread weakness, metabolic acidosis and rhabdomyolysis may occur. So far, this disease has been molecularly defined only in Swedish patients, all homozygous for a deep intronic splicing affecting mutation in *ISCU* encoding a scaffold protein for the assembly of iron–sulfur (Fe-S) clusters. A single Scandinavian family was identified with a different mutation, a missense change in compound heterozygosity with the common intronic mutation. The aim of the study was to identify the genetic defect in our proband.

Methods A next-generation sequencing (NGS) approach was carried out on an Italian male who presented in childhood with ptosis, severe muscle weakness and exercise intolerance. His disease was slowly progressive, with partial recovery between episodes. Patient's specimens and yeast models were investigated.

Results Histochemical and biochemical analyses on muscle biopsy showed multiple defects affecting mitochondrial respiratory chain complexes. We identified a single heterozygous mutation p.Gly96Val in *ISCU*, which was absent in DNA from his parents indicating a possible de novo dominant effect in the patient. Patient fibroblasts showed normal levels of ISCU protein and a few variably affected Fe-S cluster-dependent enzymes. Yeast studies confirmed both pathogenicity and dominance of the identified missense mutation.

Conclusion We describe the first heterozygous dominant mutation in *ISCU* which results in a phenotype reminiscent of the recessive disease previously reported.

INTRODUCTION

Iron–sulfur (Fe-S) clusters are prosthetic groups found in several mitochondrial, cytosolic and nuclear enzymes, which play a role in fundamental cellular processes, such as respiration, DNA synthesis and repair, ribosome biogenesis and iron metabolism. In eukaryotes, the biogenesis of Fe-S clusters is performed by two main multiprotein machineries, the ISC (iron–sulfur cluster assembly) machinery localised in mitochondria and the CIA (cytosolic iron–sulfur protein assembly) machinery localised in the cytosol.[1 2] Fe-S clusters are found in almost all living organisms, and the most common stoichiometric species include [2Fe-2S], [3Fe-4S] and [4Fe-4S] structures in which the Fe ions are co-ordinated, for example, by cysteine thiol groups or histidine residues.

The ISC machinery is involved in the biogenesis of Fe-S proteins in mitochondria enzymes as well as in the cytosol and nucleus. The current understanding of the molecular mechanism of mitochondrial Fe-S protein biogenesis has been worked out in both yeast and human cells. The ISC machinery comprises 18 known proteins that perform several steps of Fe-S cluster synthesis, transfer and insertion into recipient proteins including subunits of the mitochondrial respiratory chain (MRC) complexes I, II and III, mitochondrial aconitase (mACO) and lipoic acid synthase (LIAS).[3] De novo synthesis of the [2Fe-2S] cluster is accomplished on the scaffold protein ISCU. This reaction requires the cysteine desulfurase NFS1 with its stabilising partners ISD11/LYRM4 and ACP1, frataxin/FXN as an iron donor and/or regulator of cysteine desulfurase activity, and the ferredoxin FDX2 (MIM 614585) as an electron donor for sulfur reduction.[4 5] Conflicting results have been published regarding the role of FDX1 (MIM 103260) in this process.[6 7] All these ISC proteins form a dynamic complex with ISCU. Dissociation of the preformed Fe-S cluster from the ISCU scaffold and transfer to intermediate carriers, for example the monothiol glutaredoxin GLRX5 (MIM 609588), is mediated by a dedicated Hsp70-Hsp40 chaperone system (HSC20/HSP70).[8] The transiently GLRX5-bound [2Fe-2S] cluster is inserted into [2Fe-2S] targets or used for [4Fe-4S] cluster synthesis by ISCA1-ISCA2-IBA57. Finally, the cluster is inserted into target apoproteins with the help of factors including IND1 (MIM 613621), NFU1 (MIM 608100) and BOLA3 (MIM 613183). A different targeting mode has been suggested, based on interactions of the adaptable HSC20/HSPA9 scaffold complex with LYR motifs of SDHAF1 for complex II,[9] with LYRM7 for complex III or directly with Fe-S cluster subunits of complex I.[10]

Recessive mutations in *ISCU* have been described in patients presenting myopathy with severe exercise intolerance and myoglobinuria (MIM 255125). A homozygous intronic transversion (c.418+382G>C or IVS5 +382G>C) was initially reported in patients from northern Sweden, with

associated deficiencies of succinate dehydrogenase and aconitase in skeletal muscle.[11 12] The mutation causes the retention of an 'extra exon', leading to marked reduction of *ISCU* mRNA and protein in patient muscle. The splicing defect was shown to be selective for muscle tissue, thus explaining the muscle-specific phenotype of this disorder.[13] Later, compound heterozygosity for the common intronic mutation and a missense c.149G>A/p.G50E substitution was found in two brothers with Swedish/Finnish origin. These boys had a more severe phenotype than patients homozygous for the intronic mutation, with progressive and severe muscle weakness, muscle wasting and heart involvement.[14]

Contrary to the muscular phenotype of *ISCU* mutant patients, mutations in other components of the core Fe-S assembly complex cause neurological diseases (eg, Friedreich's ataxia, MIM 229300, due to *FXN* mutations) or multisystem disorders (eg, combined oxidative phosphorylation deficiency 19, MIM 615595, due to *ISD11*/*LYRM4* mutations).

We report here a patient with myopathy, lactic acidosis and combined MRC complex deficiency, caused by a de novo heterozygous missense pathological variant in *ISCU*.

METHODS

Histochemical and biochemical studies in skeletal muscle

Muscle morphology and histochemistry, respiratory chain activities of complexes I to IV and pyruvate dehydrogenase complex (PDHC) assays were performed as previously described.[15–17] Histochemical staining of iron using Prussian blue colour was performed as previously described.[18]

Genetic analysis

Genomic DNA was extracted from peripheral blood by standard methods. Whole exome sequencing (WES) and variants filtering were performed as previously described.[19] Variants identified by WES were validated by Sanger sequencing. For deep sequencing of parental DNAs, the PCR products were processed with Nextera XT DNA sample preparation kit (Illumina). Sequencing was performed on an Illumina MiSeq instrument.

RNA was extracted from skin fibroblasts, and 1 µg was used as template for RT-PCR to obtain full-length cDNA. *ISCU* transcript was amplified by PCR and run through a 1% agarose gel in order to detect potential splicing alterations. PCR products were also sequenced in order to confirm genomic variants and unmask potential events of nonsense-mediated decay.

Cell culture and biochemical analysis of fibroblast samples

Fibroblasts obtained from skin biopsy were grown in 1 g/L glucose DMEM-F14 (Euroclone) supplemented with 20% fetal bovine serum (FBS), 1% uridine, 1% L-glutamine and 0.2% sodium pyruvate.

For enzyme activity measurements, cells were treated with digitonin in order to separate a cytosolic cell fraction from a crude mitochondria-containing organellar fraction.[20] Biochemical assays were essentially performed as described.[16] Analysis of steady-state protein levels by immunoblotting was carried out by common methods, using a 6%–20% sodium dodecyl sulfate polyacrylamide (SDS-PA) gradient gel. Blocked membranes were probed with primary antibodies (online supplementary table S1), and antigens were visualised by horseradish peroxidase (HRP) coupled secondary reagents and a chemiluminescence reaction.

Yeast studies

Details on yeast strains, media, cloning procedures and vectors[21 22] as well as on generation of mutant allele and construction of mutant strains[23–25] are reported in the online supplementary data

Complex II (succinate dehydrogenase (SDH)) and complex IV (cytochrome c oxidase (COX)) specific activities were measured on a mitochondrial-enriched fraction prepared as previously described.[26 27] Aconitase activity was measured in whole-cell extracts.[28] In vivo radiolabelling of yeast cells with $^{55}FeCl_3$ (ICN) and measurement of ^{55}Fe-incorporation into Fe-S proteins by immunoprecipitation and scintillation counting were performed as described.[29] Antibodies against c-Myc were obtained from Santa-Cruz. The green fluorescent protein (GFP) based reporter assay for determination of *FET3* promoter strength was described previously.[29] The iron content was determined by a colorimetric assay, essentially as described before.[30 31]

Bioinformatics and structural analysis tools

The effect of the p.(Gly96Val) substitution on ISCU function was predicted using the in silico tools (ie, SIFT, Polyphen2 and EVmutation), all running recommended parameters. All images of the *Escherichia coli* IscU-IscS (PDB ID:3LVL) complex were made by using Visual Molecular Dynamics viewer.[32] The evaluation of the impact of the mutated residue and the protein–protein interaction analysis were performed by using Swiss PDB viewer,[33] and FirstGlance in Jmol (http://www.jmol.org)

RESULTS

Case report

The patient is a 23-year-old Italian male, first child from non-consanguineous parents, born at term after a normal pregnancy by caesarean delivery. He has a healthy younger brother. He started walking at 18 months, but he always presented some walking difficulties, with frequent falls. Parents reported easy fatigability since the first years of life. At 7 years of age, the neurological examination showed bilateral ptosis not associated with ophthalmoparesis, muscle hypotonia and wasting, and absent deep tendon reflexes. No obvious weakness was present, but marked exercise intolerance was reported. Neither cognitive impairment nor other central nervous system (CNS) involvements were noticed. The brain nuclear magnetic resonance (NMR) and the EEG were normal. Electromyography showed myopathic changes in all tested muscles. Creatine kinase (CK) level was slightly increased (about 300 U/L; normal values, n.v.:<180), lactate acid was high in blood (4.6 mmol/L; n.v.: 0.4–2.2). He showed leucopenia (2.94×10^3/µL; n.v.: 5–14) and anaemia (haemoglobin 10.9 g/dL; n.v. 13–16) with microcythemia (72.9; n.v. 80–99); a bone marrow biopsy performed at 7 years was normal. No heart involvement was present: echocardiogram and ECG were both normal. Over time, his clinical conditions worsened and he started presenting episodes of profound exercise intolerance and weakness, with partial recovery of muscle weakness between episodes in about 2 weeks. During these episodes, the patient was unable to walk, and showed tachycardia; neither breathing shortness nor dysphagia was noticed. At the neurological examination at 17 years of age, he presented predominantly distal limb weakness with muscle hypotrophy; deep tendon reflexes were absent. He was able to stand up from a chair and walk, but was unable to run. No signs of CNS involvement were present; CK level remained high (about 1700 U/L). The disease has since been slowly progressive, punctuated by episodes of acute weakness, with preserved cognitive function and no other signs of CNS involvement.

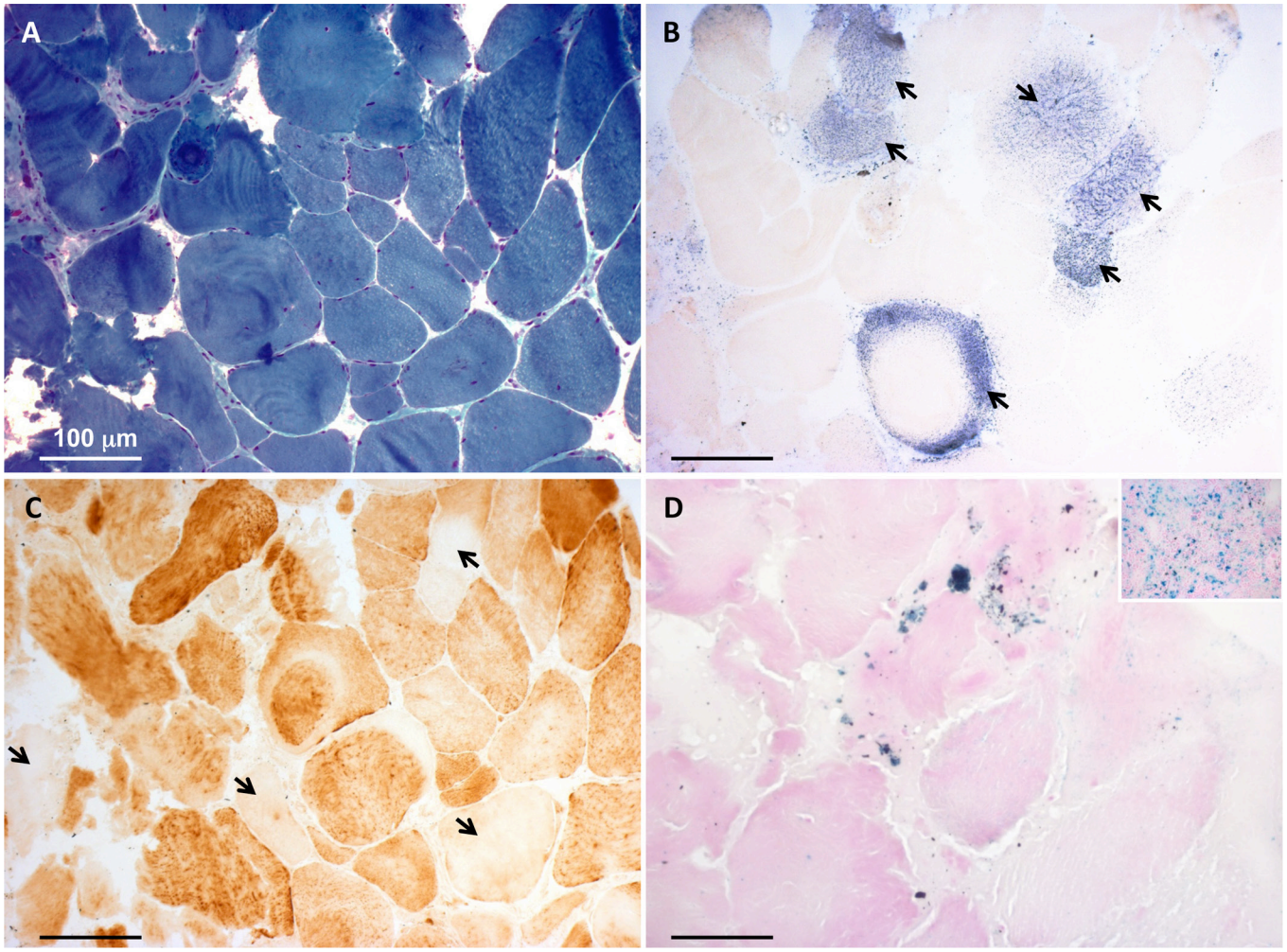

Figure 1 Histochemical analysis of the patient's muscle biopsy. (A) Gomori trichrome stain showing fibre size variability. (B) Strongly reduced histochemical activity of succinate dehydrogenase. Few fibres showed succinate dehydrogenase-positive staining (arrows). (C) Cytochrome c oxidase (COX) staining showing scattered fibres with severe reduction of histochemical COX activity (arrows). (D) Perls staining demonstrating punctuate accumulation of iron in the patient's muscle fibres. Inset is a positive control (spleen) for the Prussian blue reaction. Bars correspond to 100 µm.

Histochemical and biochemical analyses in skeletal muscle

A first muscle biopsy was performed at 8 years of age. At the histological examination, fibre size variability was present. The main feature was a severe reduction of the histochemical reaction for both COX and SDH, not associated with ragged red fibres. The biochemical examination showed severe decrease of all the MRC complexes (I, II, III, IV), with strong increase in citrate synthase (CS) activity (online supplementary figure S1A). A second muscle biopsy was performed at 22 years, confirming the histological and histochemical findings (figure 1A-C). At this age, the reduction in the MRC complex activities was still present, yet normal CS activity was observed (online supplementary figure S1B). Furthermore, the activity of PDHC was reduced (PDH/CS: 1.8, normal values: 2.5–5.0). After the genetic identification of the *ISCU* variant (see below), we carried out histological analysis for the presence of iron deposits in the muscle biopsy by Perls staining. We found Perls-positive material in numerous patient's fibres, whereas no such material was detected in control muscle biopsies, indicating iron overload in ISCU-mutant muscle (figure 1D).

Genetic studies

Genetic alterations linked to mitochondrial DNA were ruled out: no mutation was detected by sequencing and no evidence of depletion or deletion was observed by Southern blot analysis of mitochondrial DNA from muscle. We performed WES on genomic DNA from the proband. After filtering steps to exclude common SNPs (frequency >0.5%), we selected genes with two compound heterozygous or one homozygous variant, according to a predicted recessive mode of inheritance. Then we focused on genes encoding proteins with mitochondrial localisation. Two entries were found: *MTIF2* (translation initiation factor IF-2, mitochondrial) and *PDPR* (pyruvate dehydrogenase phosphatase regulatory subunit). However, the two missense variants in *MTIF2* were in cis, on the same paternal allele, whereas the two variants in *PDPR* were not confirmed by Sanger sequencing, being probably due to the presence of a pseudogene. No hemizygous variant, suggestive of an X-linked transmission, was detected. A deep analysis of the heterozygous variants, prioritising genes associated with mitochondrial myopathies, highlighted a single variant in *ISCU*, a c.287G>T (NM_213595.2) predicted to cause the amino acid substitution p.G96V (figure 2A). This nucleotide change was not reported in public variant databases (dbSNP, EVS, ExAC (August 2016)); the substitution affected a highly conserved residue (figure 2B) and gave high scores of pathogenicity, according to several bioinformatics tools. This variant was confirmed by Sanger sequencing in the proband but was not present in the parents' blood DNA,

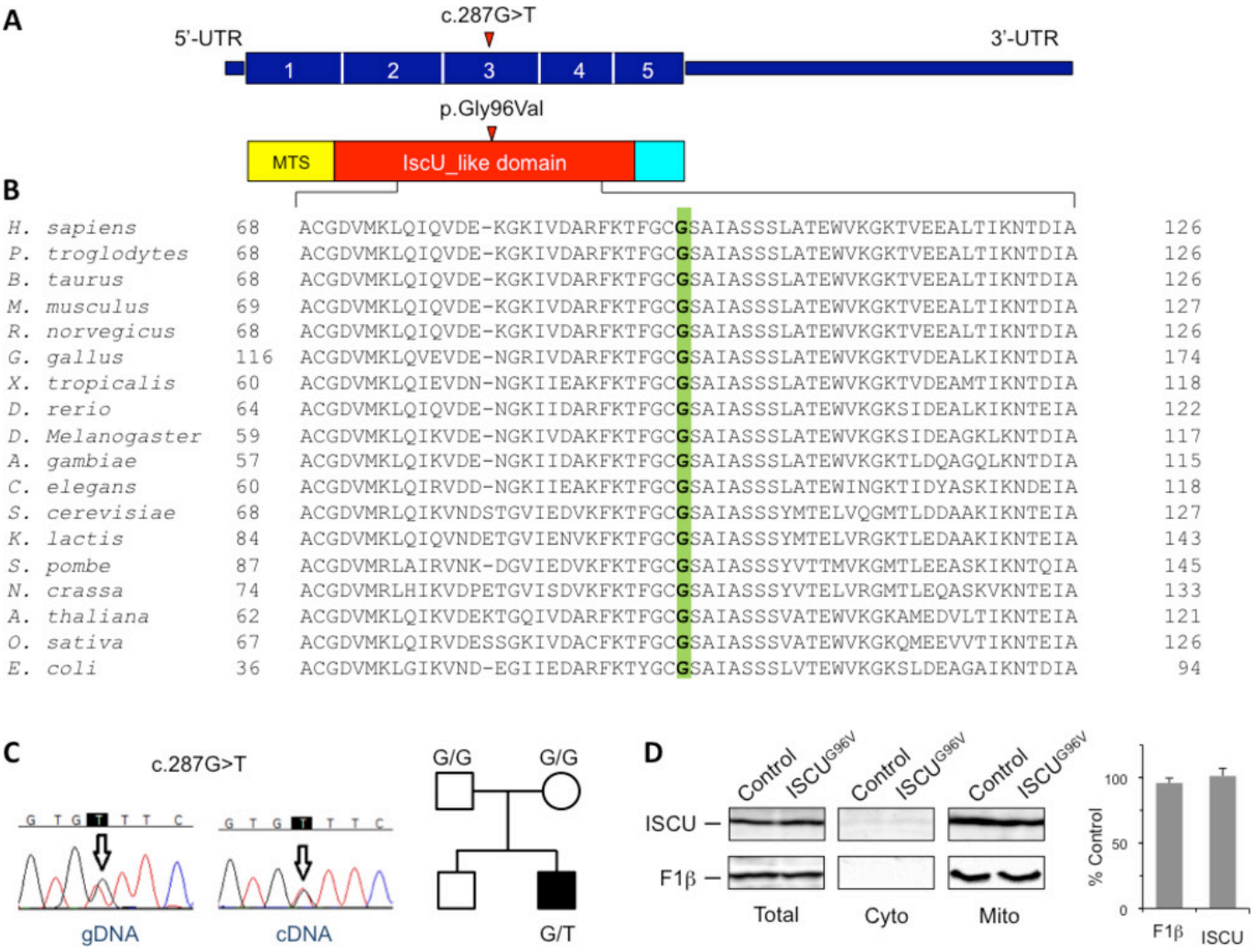

Figure 2 Identification and characterisation of an *ISCU* mutation. (A) Schematic representation of the *ISCU* cDNA (NM_213595.2) and ISCU protein with the nucleotide/amino acid change identified in this study. The functional IscU-like domain is in red; the mitochondrial targeting sequence (MTS) is in yellow. (B) Phylogenetic conservation of the amino acid residue (Gly96, in green) affected by the missense mutation identified in the patient. (C) Electropherograms of the genomic region (gDNA) and transcript (cDNA) harbouring the *ISCU* mutation, and pedigree. (D) Immunoblot analysis of ISCU^{G96V} mutant protein expression and subcellular localisation. Control and patient fibroblasts were harvested by trypsination, permeabilised by digitonin treatment, and separated into a cytosolic and a mitochondria-containing membrane fraction. Total cell lysates as well as cytosolic and crude mitochondrial fractions were subjected to sodium dodecyl sulfate polyacrylamide gel electrophoresis (SDS-PAGE) and analysed for ISCU and ATP synthase F1β subunit (mitochondrial marker) steady-state protein levels (left panel). Chemiluminescence signals of ISCU and F1β in total lysate samples were quantified, and values obtained from patient fibroblasts were expressed relative to control cells (right panel). Error bars indicate the SDs (n=3). UTR, untranslated region.

indicating a de novo event (figure 2C, online supplementary figure S2): the parental DNA samples were analysed also by deep sequencing to exclude very low level of the variant, suggestive of germinal mosaicism. All the *ISCU* coding regions were well covered by WES. We then screened our patient and his parents for the intronic region encompassing the common mutation present in all the previously described *ISCU* mutant patients but no variant was identified.

To exclude that WES could have missed the presence of another deep intronic variant affecting the splicing or a 'non-exonic' variant impairing mRNA transcription/stability, we further investigated patient's specimen at the transcriptional level. No aberrant mRNA *ISCU* species was observed in PCR products obtained from fibroblast RNA, and their sequencing showed a biallelic expression, suggested by the presence of overlapping peaks corresponding to G and T nucleotides in position c.287 (online supplementary figure S2).

Characterisation of patient's fibroblasts

The amount of ISCU protein in patient's fibroblasts was similar to controls, indicating that the mutant protein is normally synthesised, imported into mitochondria and stable (figure 2D). In line with previous reports showing that the biochemical phenotype associated with mutant ISCU is very much attenuated, fibroblasts harbouring the *ISCU*^{G96V} mutation showed hardly any defect in activities or protein amounts for a number of mitochondrial Fe-S dependent enzymes including mACO, LIAS (as indicated by the presence of lipoate cofactor (Lip) on pyruvate and ketoglutarate dehydrogenase E2 subunits), ferrochelatase and respiratory chain complexes I, II and III (online supplementary figure S3A-F). A minor defect was observed in complex IV, in line with the muscle biopsy analyses, and in the activity of cytosolic aconitase (IRP1). Analysis of steady-state levels of cytosolic/nuclear Fe-S proteins as a measure for maturation-dependent stability

revealed no general alteration of their cellular abundance (online supplementary figure S3G-H). However, we observed a severe deficiency of the base-excision DNA repair enzyme NTHL1, a [4Fe-4S] protein, and a slight decrease in protein levels of the CIA factor IOP1 containing 2 [4Fe-4S] clusters. Taken together, our analyses indicate that the presence of the *ISCU*^{G96V} mutation does not have a strong impact on Fe-S cluster assembly in patient's cultured fibroblasts.

Yeast model

To assess the pathogenic role of the substitution p.Gly96Val identified in the patient, we performed studies in a yeast model, by introducing the analogous amino acid substitution (G97V) in the *Saccharomyces cerevisiae* orthologue of *ISCU*, the yeast gene *ISU1*. *ISU1* has a paralogue, *ISU2*, arising from a recent gene duplication. The double deletion mutant *isu1*Δ*isu2*Δ is unviable, thus indicating the essential role of these proteins in the biogenesis of Fe-S clusters, which is in turn indispensable for yeast cell survival.[34] The double deletion mutant *isu1*Δ*isu2*Δ, harbouring the centromeric pFL38 plasmid (*URA3* marker) with the wild-type (wt) *ISU1* to allow viability, was additionally transformed with pFL39 centromeric plasmids (*TRP1* marker) containing either the mutant allele *isu1*^{G97V}, a wt copy of *ISU1,* or no gene.

The different strains were plated on 5-fluoroorotic acid containing medium to select for cells that have lost the pFL38/*ISU1* plasmid. The strain expressing *isu1*^{G97V} as the sole *ISU1* gene was able to grow on glucose at rates similar to strains carrying the wt *ISU1*, while the empty pFL39 did not support growth (figure 3A). This result indicates that glycine 97 is not essential for the function of the Isu1 protein. However, growth of the strain expressing the *isu1*^{G97V} variant was severely retarded on non-fermentable carbon sources (figure 3A), highlighting a deleterious effect of the G97V mutation on mitochondrial function.

To test whether the G97V mutation acts as a dominant trait, the *isu1*Δ*isu2*Δ/*isu1*^{G97V} and the *isu1*Δ*isu2*Δ/*ISU1* strains were transformed with either the pGL38 empty vector (as a control) or pFL38/*ISU1* thus obtaining the heteroallelic strain *isu1*Δ*isu2*Δ/*ISU1*/*isu1*^{G97V} and the homoallelic strain *isu1*Δ*isu2*Δ/*ISU1*/*ISU1*. Growth on non-fermentable carbon sources was clearly reduced in the heteroallelic strain compared with the homoallelic wt strain, and also to the strain transformed with the empty vector and expressing a single copy of *ISU1 (isu1*Δ*isu2*Δ/*ISU1)*. These results indicate that the G97V mutation behaves as dominant (figure 3B). The measurement of the cell

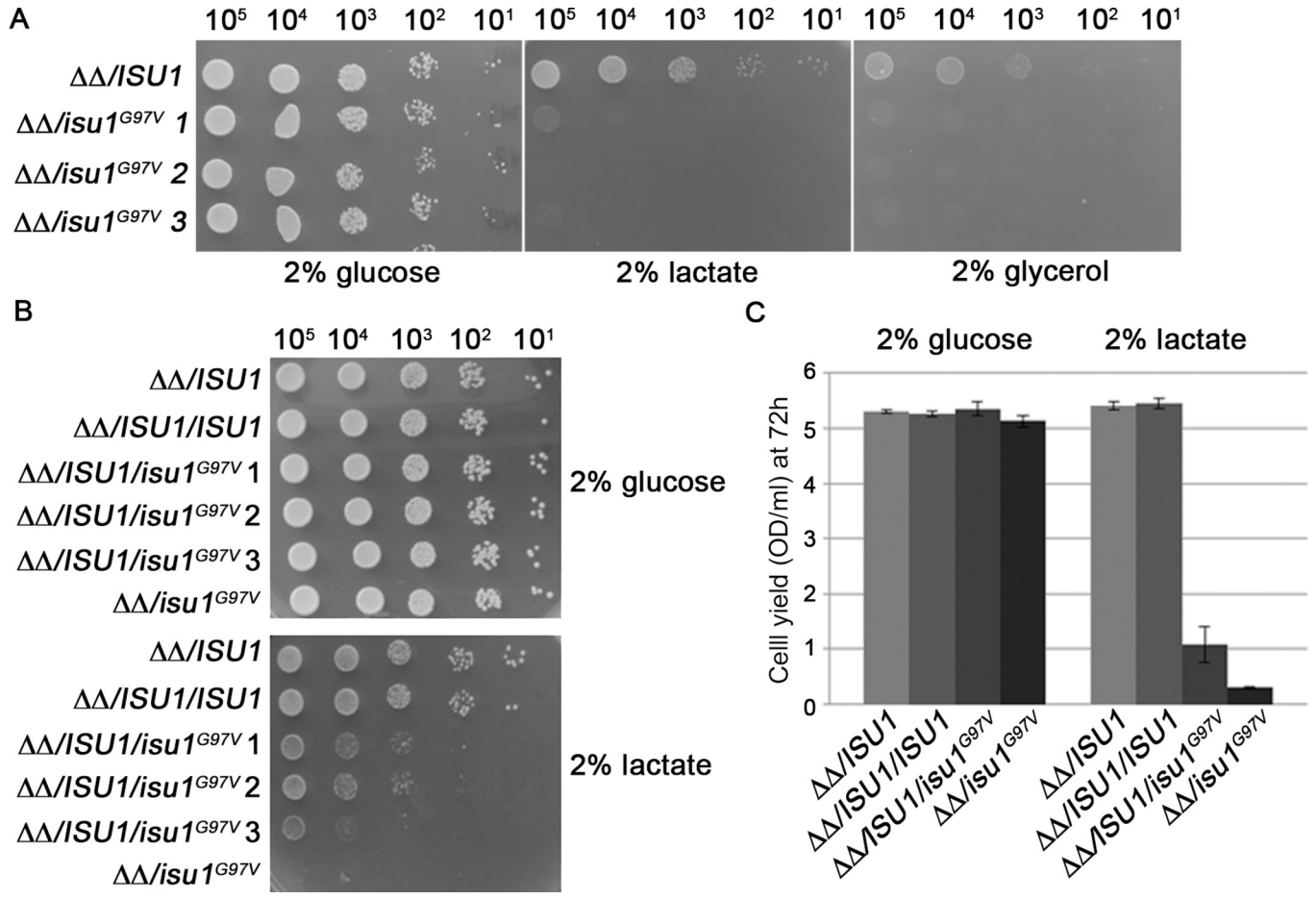

Figure 3 Growth analysis of mutant yeast strains. (A) The strain *isu1*Δ*isu2*Δ harbouring plasmid pFL39 with the wild-type *ISU1* gene or the mutant allele *isu1*^{G97V} was analysed for growth on various media. Equal amounts of serial dilutions of cells from exponentially grown cultures were spotted onto yeast nitrogen base (YNB) medium plus 2% glucose, 2% lactate or 2% glycerol. The growth was scored after 3 days of incubation at 28°C. (B) The strains *isu1*Δ*isu2*Δ/*ISU1* and *isu1*Δ*isu2*Δ/*isu1*^{G97V} were transformed with pFL38/ISU1 or with the empty vector. Equal amounts of serial dilutions of cells from exponentially grown cultures were analysed for growth on YNB medium plus 2% glucose or 2% lactate after 4 days of incubation at 28°C. (C) Cell yield was calculated by growing cells on liquid medium containing glucose or lactate and measuring the optical density at 600 nm after 72 hours of growth. Error bars indicate the SDs (n=3).

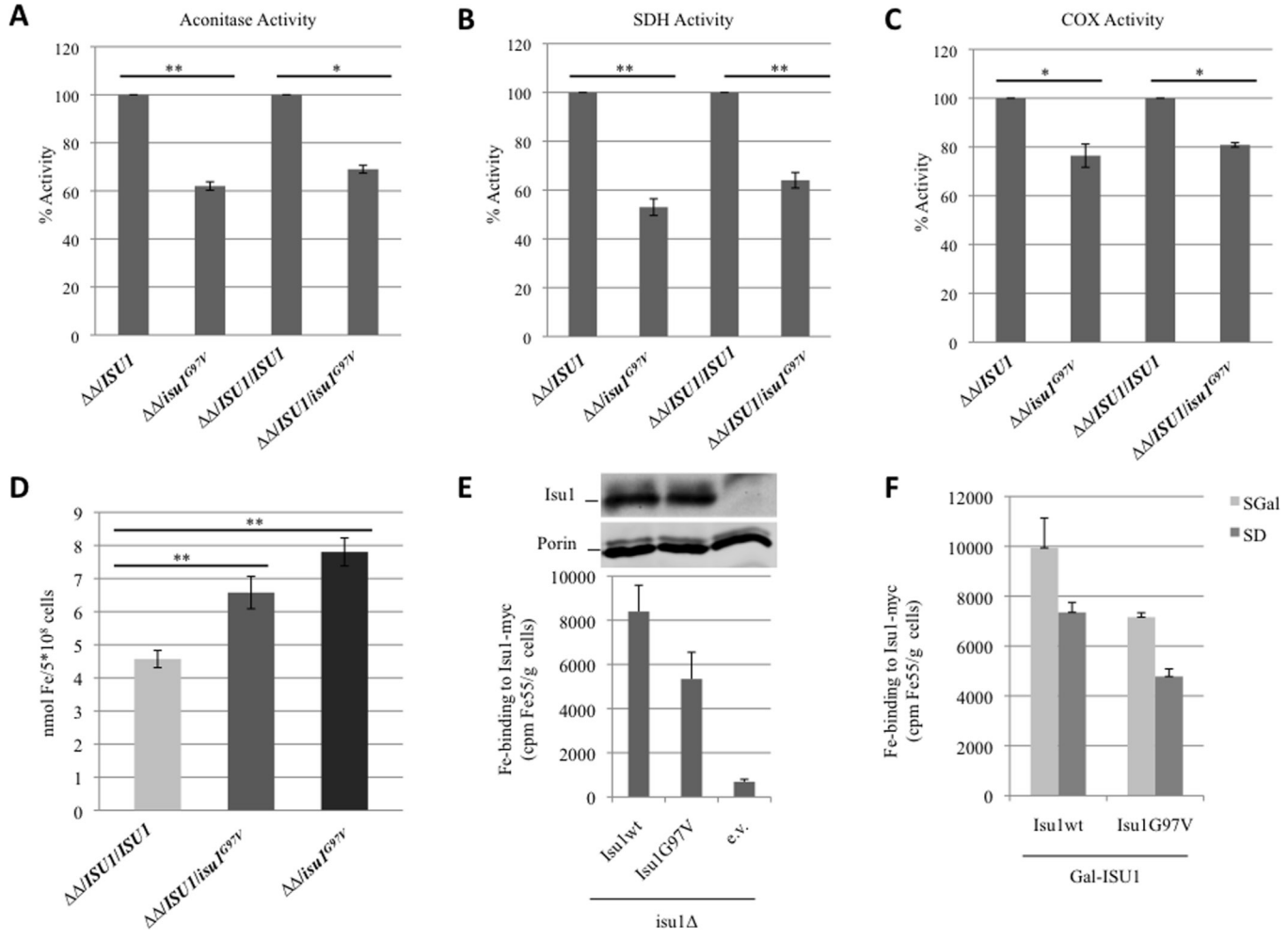

Figure 4 Measurement of enzyme activities and iron content in yeast. (A) Aconitase activity was measured in whole-cell extracts from cells grown exponentially at 28°C in yeast nitrogen base (YNB) medium plus 0.6% glucose. (B and C) Succinate dehydrogenase activity and cytocrome c oxidase activities were measured in a mitochondria-enriched fraction obtained from cells grown as described before. The values for *isu1*Δ*isu2*Δ/*isu1*^{G97V} and *isu1*Δ*isu2*Δ/*ISU1*/*isu1*^{G97V} strains are expressed as percentage of the activities obtained in the strains *isu1*Δ*isu2*Δ/*ISU1* and *isu1*Δ*isu2*Δ/*ISU1*/*ISU1*. (D) Cellular iron content was quantified in cells grown up to early stationary phase in YNB 0.2% glucose and 2% galactose medium. *<0.05 (unpaired two-tailed t-test), **<0.01 (unpaired two-tailed t-test). (E) *Gal-ISU1*/*isu2*Δ cells and *isu1*Δ cells expressing Myc-tagged Isu1 were radiolabelled with ^{55}Fe and ^{55}Fe incorporation into Isu1-Myc was determined by immunoprecipitation with α-Myc antibodies followed by scintillation counting. Wild-type cells harbouring the empty vector (e.v.) served as control. Isu1-myc protein levels in *isu1*Δ cells were determined by immunostaining with α-Myc antibodies. Porin (Por1) served as a loading control. (F) *Gal-ISU1*/*isu2*Δ cells expressing Isu1 from vector pFL39 and the reporter plasmid pFET3-GFP were cultivated in SD or SGal medium supplemented with 50 µM ferric ammonium citrate. At an optical density=0.5, the GFP-specific fluorescence emission of whole cells was determined. Error bars indicate the SDs (n=3).

yield in liquid cultures confirmed what observed in the spot assay analysis (figure 3C).

To investigate if the G97V mutation affects mitochondrial Fe-S protein biogenesis, we measured the biochemical activities of two Fe-S cluster-containing enzymes: aconitase and complex II. These activities were reduced in both the *isu1*Δ*isu2*Δ/*isu1*^{G97V} and the heteroallelic strain *isu1*Δ*isu2*Δ/*ISU1*/*isu1*^{G97V} (figure 4A and B) indicating an impairment in Fe-S cluster biogenesis in *isu1*^{G97V}-containing yeast cells. The activity of complex IV which contains two heme centres was also partially reduced (figure 4C). Finally, we evaluated the cellular iron content by a colorimetric assay and found a twofold increase in the mutant compared with wt strain (figure 4D) consistent with a defective core ISC machinery.[35]

To further investigate the impact of the G97V mutation on Isu1 function, we measured the ability of mutant versus wt Isu1 protein to assemble a Fe-S cluster in vivo.[36] To this end, we used the strain *Gal-ISU1*/*isu2*Δ, in which *ISU2* is deleted and *ISU1* is under the control of the *GAL1-10* promoter. The levels of Isu1 can be downregulated by growing the cells in the presence of glucose.[37] *Gal-ISU1*/*isu2*Δ cells were transformed with pRS426-TDH3 vectors encoding Myc-tagged *ISU1*^{wt} or *isu1*^{G97V}. To estimate Fe-S cluster binding of Isu1, cells were radiolabelled with ^{55}Fe, and the incorporation of radioactivity into Isu1^{G97V} or Isu1^{wt} was measured by immunoprecipitation and scintillation counting (figure 4E,F). As shown in figure 4F (darker bars), the mutant protein showed a 30% reduction in the ^{55}Fe binding capacity; this reduction is consistent with the mutant growth defect displayed on respiratory carbon sources. A decrease was also evident when *isu1*^{G97V} was expressed in *isu1*Δ cells or when *Gal-ISU1*/*isu2*Δ cells were depleted by growth in galactose-containing medium, conditions in which endogenous wt Isu1 and Isu2 are present, thus mimicking the heteroallelic condition (figure 4F, light grey bars, and figure 4E). This result showed that the Isu1^{G97V} mutant protein is slightly impaired

in its ability to incorporate Fe into Fe-S clusters in vivo. The alterations observed in mutant strains were not due to a reduced amount of the mutant Isu1^{G97V} protein since its abundance was similar to the wt form (figure 4E). Furthermore, *Gal-ISU1/isu2*Δ cells expressing *isu1*^{G97V} from vector pFL39 displayed a twofold increase of the iron-dependent *FET3* promoter on both glucose and galactose-containing medium (online supplementary figure S4). A deregulated iron homeostasis is a hallmark of cells with defective core ISC machinery and explains the increased iron levels in cells expressing *isu1*^{G97V}.

In silico pathogenicity prediction and structural modelling

In silico predictions, by using different tools, were used to evaluate the potential effect of the Gly96Val substitution on ISCU structure and interaction with its protein partners. ISCU interacts with NFS1, yet the 3D structure of the human NFS1-ISCU complex is hitherto unknown. Instead, we used the reported crystal structure of the *E. coli* IscS-IscU complex formed by an IscS dimer which binds two IscU at opposite ends of IscS.[38] Notably a similar, yet unusual monomeric structure has been recently described for the IscS human orthologue NFS1.[39] Human Gly$_{96}$ which corresponds to Gly$_{64}$ in *E. coli*[38] is located in a flexible loop, at the beginning of the helix α1, next to the potential Fe-S cluster-co-ordinating Cys$_{95}$ residue (Cys$_{63}$ in *E. coli*).[40] We analysed the possible interactions of Gly$_{64}$ with IscS/NFS1 by using First Glance in Jmol. The glycine backbone could establish hydrophobic interaction with IscS Met$_{315}$ that is located inside a stretch (YVEGESLLMAL) highly conserved from *E. coli* to human. Although both glycine and valine are hydrophobic residues, the greater steric hindrance of the valine side chain could interfere with the IscS-IscU interaction (figure 5A). Moreover, the loop encompassing residues 62–64 (GCG) of IscU is opposite to Glu$_{311}$ and Ser$_{312}$ on IscS, and we suggest that the valine slightly disturbs these hydrophilic residues (figure 5A). The substitution Gly96Val could therefore prevent the correct orientation of the adjacent cysteine side chain, thus interfering with the Fe co-ordination and explaining the defective ISCU function (figure 5B).

DISCUSSION

ISCU (Isu1-2 in yeast) is an essential scaffold protein for the biosynthesis of Fe-S clusters. Recessive hypomorphic *ISCU* alleles have been associated with isolated myopathy[11 12] or skeletal and cardiac myopathy[14] in humans. Here, we report a heterozygous, de novo dominant *ISCU* variant, G96V, causing congenital myopathy in a single patient. The following considerations provide evidence that this variant exerts a deleterious, dominant effect on Fe-S-dependent enzyme activities. First, we observed striking

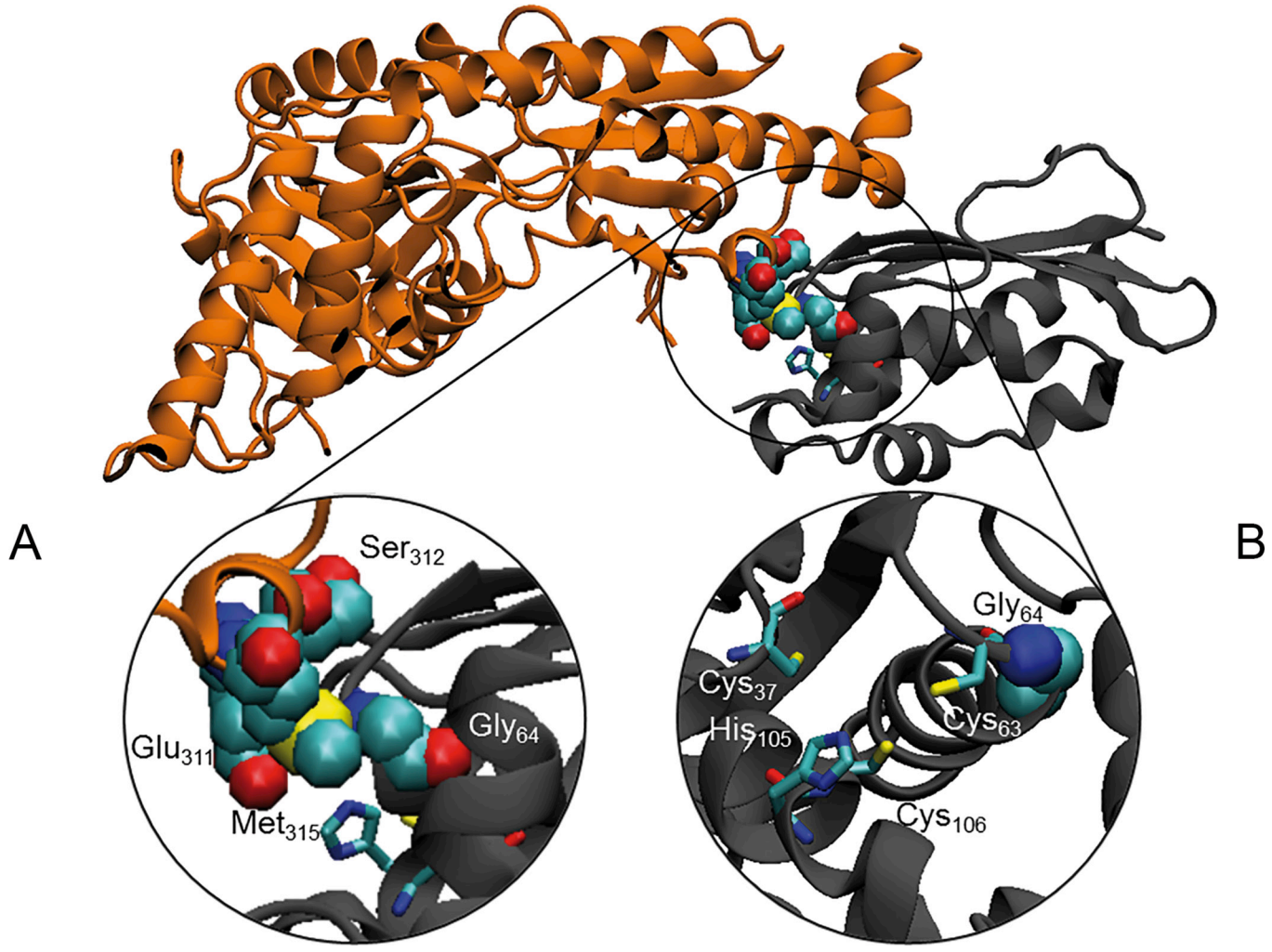

Figure 5 In silico structural analysis. (A) Ribbon diagram of the *Escherichia coli* IscS (coloured in grey)-IscU (coloured in orange) complex (PDB ID: 3lvl). Close view of the Gly64 of IscU and Glu311, Ser312 and Met315 of IscS represented in Van der Waals and coloured by type. (B) Residues supposed to be involved in the co-ordination of the 2Fe-2S are represented as sticks.

clinical, histological, histochemical and biochemical abnormalities affecting skeletal muscle, which define a mitochondrial myopathy similar to that reported in *ISCU* recessive mutations, including partial depletion of SDH and COX histochemical reactions, generalised reduction of the MRC complex activities, and accumulation of iron deposits. Similar to recessive *ISCU* cases, our patient displayed isolated myopathy with fluctuating, waxing and weaning episodes of profound muscle weakness, in the context of a congenital myopathy with moderately high CK and no involvement of extramuscular organs, including the CNS. Second, the mutation was absent in both healthy parents, supporting its sporadic occurrence in the proband, and was the only gene defect related to mitochondrial myopathies identified by WES. Third, analysis of the corresponding genetic defect in yeast suggested a Fe-S protein biogenesis defect, including defects in OXPHOS and the cellular iron regulon. The effects were dominant, since both the monoallelic and the heteroallelic genotypes were associated with the phenotype.

While our yeast studies suggest that $Isu1^{G97V}$ is functionally impaired by itself, what might then be the reason for the observed dominance of both the human $ISCU^{G96V}$ and corresponding yeast $Isu1^{G97V}$ mutations? ISCU, as the scaffold protein for the de novo synthesis of Fe-S clusters within mitochondria, interacts with a number of other ISC proteins during Fe-S biosynthesis, although the stoichiometry of these interactions is controversial. Similar to the bacterial structure, the mammalian ISC complex was proposed to be composed of two NFS1 and two ISCU subunits,[4 41] with a central NFS1 dimer and two molecules of ISCU at each end of the NFS1 dimer. Recently, a $[FXN^{42–210}]_{24}$-$[NFS1]_{24}$-$[ISD11]_{24}$-$(ISCU)_{24}$ complex model was proposed,[40] but it was obtained by overexpressing human proteins in *E. coli* and it is probably not relevant in vivo. We think that the functional impairment of ISCU by the G96V mutation may be caused by structural changes, as suggested by our in silico analyses. For instance, the orientation of the potential Fe-S cluster-co-ordinating Cys95 adjacent to Gly96 could be altered by replacement of the helix-breaking glycine residue, with a negative outcome on protein function in Fe-S cluster assembly. Moreover, the mutated protein structure may become stiffer, thus negatively affecting the interactions with its other partner ISC proteins, notably NFS1. The altered interaction between NFS1 and the mutant ISCU could in turn affect the assembly/function of the entire ISC biosynthetic complex. In support of this view stands the observation that the $ISCU^{G96V}$ mutant protein is stable and not degraded, and its amount is similar to that of $ISCU^{wt}$ in patient's fibroblasts. In addition, the dominant effect may be caused by the intermediate formation of an ISCU holodimer which, according to in vitro reconstitution studies, is the product of the ISC biosynthetic complex.[5 42] In the homodimer, the mutated Gly_{96} residue in one ISCU monomer would likely directly face the other wt ISCU monomer because of the bridging character of [2Fe-2S] cluster binding. This could lead to the observed dominant negative effect of the mutated ISCU on wt ISCU proteins. This might also be the reason why we observed less radiolabelled ^{55}Fe bound to yeast $Isu1^{G97V}$ compared with the wt protein. Interestingly, the dominant-negative behaviour of the G97V mutation differs from the recessive effect reported for the G50E mutation in both yeast and humans, which can be ascribed to haploinsufficiency of the G50E allele.[43]

Although ubiquitous, the $ISCU^{G96V}$ variant produces a clinically detectable effect only in one critical tissue, skeletal muscle, in line with the purely myopathic presentation of the common $ISCU^{IVS5+382G>C}$ splicing variant already reported in Swedish patients. Similar to our results, no evident mitochondrial phenotype in fibroblasts has been previously reported in cases with ISCU-related recessive disease.[14 44–46] The molecular mechanisms that make skeletal muscle exquisitely sensitive to partial ISCU impairment warrant further investigation in patient-derived cells and, possibly, animal models. A tissue-specific splicing of *ISCU* was proposed for the common $ISCU^{IVS5+382G>C}$ mutation to explain the skeletal muscle phenotype,[13] but this hypothesis cannot be applied for either the p.G96V or the p.G50E missense variants, which are equally associated with muscle-specific dysfunction. The structural alterations and impaired interactions with partner proteins caused by the p.G96V could have tissue-specific effects which explain the muscle involvement. A greater sensitivity of *ISCU*-mutant myoblasts to oxidative stress,[45] and exercise-induced oxidative damages in muscle,[47] may also account for the muscular phenotype. Nevertheless, tissue specificities for many of the mitochondrial diseases due to defective nuclear-encoded genes with housekeeping functions are currently poorly understood and hardly predictable.

The multiple biochemical defects of MRC activities observed in our patient were expected for complexes I, II and III which contain Fe-S clusters. A defect was also seen for the Fe-S cluster-free complex IV, which harbours Cu^{2+} and Fe-containing heme *a*/*a3* as redox centres. In principle, this may be due to a defect in the Fe-S protein ferrochelatase catalysing the last step of heme biosynthesis.[48] However, strong complex IV defects are also seen on depletion of *ISCA1*, *ISCA2* and *IBA57* in both human and yeast cells.[49 50] These ISC proteins are specific for mitochondrial [4Fe-4S] protein maturation, yet are not involved in the assembly of the [2Fe-2S] cluster on human ferrochelatase. Moreover, we observed a complex IV impairment in the mutant yeast model despite the yeast orthologue enzyme is devoid of a Fe-S cluster. Nevertheless, complex IV defects are common secondary effects of an impairment of Fe-S protein biogenesis.[6 49] A complex IV deficiency (19%–28% residual activity) was also reported in the two siblings with the most severe *ISCU*-related phenotype, and a partial reduction was found in five subjects with the Swedish-type myopathy.[14] This may be due to a downstream damaging effect linked to impairment of complexes I, II and III or to the hampered formation of MRC supercomplexes. In addition to the biochemical defects, the histochemical analysis was peculiar, with a quite specific pattern of SDH and COX deficiency; this was suggested to be a pathognomonic finding of a myopathy related to Fe-S cluster.[9] However, in patients with mutations in *FXN*, the picture is different, with mainly COX negative fibres and nearly normal SDH staining.[51] Other Fe-S diseases are rare and usually present as neurological disorders with minimal myopathic signs, while little is known about their muscle features. Collectively, the histochemical pattern in muscle biopsy seems specific for ISCU myopathy.

In conclusion, we report the first heterozygous dominant mutation in *ISCU*; notably, this alteration resulted in a similar phenotype as the recessive *ISCU* disease previously described. Our finding stresses the importance of a deep analysis of WES data that may include, for sporadic cases, any mode of transmission. Moreover, our study confirms that recessive and dominant mutations in the same gene may lead to the same disease, as already reported for other mitochondrial disorders (eg, *DNM1L* mutations).

Acknowledgements We are grateful to Ileana Ferrero for stimulating discussions, Joanna Poulton for providing patient's fibroblasts, the contribution of the Core Facility 'Protein Spectroscopy and Protein Biochemistry' of Philipps-Universität Marburg, and R. Rösser for excellent technical support. We acknowledge the 'Cell lines and DNA Bank of Paediatric Movement Disorders and Neurodegenerative Diseases' of the Telethon Network of Genetic Biobanks (grant GTB12001J) and the Eurobiobank Network for supplying biological specimens.

Contributors AL carried out the molecular biology experiments; AR carried out WES; CCB performed yeast studies under the supervision of PG; OS performed experiments in patient's fibroblasts; SM carried out the histochemical analysis; CL provided the clinical report; AF performed structural analysis; AJR provided bioinformatics management of the WES data; UM performed yeast studies under the supervision of RL; RL, MZ, PG and DG organized the experimental set-up and wrote the manuscript; all authors read and approved the manuscript.

Funding This work was supported by the TelethonItaly [GrantGGP15041]; the Pierfranco and Luisa Mariani Foundation; the MRC7QQR [201572020] grant; the ERC advanced grant [FP77322424]; the NRJ Foundation7Institut de France; the E7Rare project GENOMIT. RL acknowledges generous financial support from Deutsche Forschungsgemeinschaft [SFB 987 and SPP 1927] and the LOEWE program of state Hessen.

Competing interests None declared.

Patient consent Obtained.

Ethics approval Ethical Committee of the Fondazione IRCCS Istituto Neurologico 'Carlo Besta', Milan, Italy.

Provenance and peer review Not commissioned; externally peer reviewed.

Data sharing statement Values of the biochemical activities reported in the graphs are available upon request.Images of the histochemical stainings are available upon request. The complete list of the variants found by WES in the proband is available upon request.

REFERENCES

1 Lill R, Hoffmann B, Molik S, Pierik AJ, Rietzschel N, Stehling O, Uzarska MA, Webert H, Wilbrecht C, Mühlenhoff U. The role of mitochondria in cellular iron-sulfur protein biogenesis and iron metabolism. *Biochim Biophys Acta* 2012;1823:1491–508.
2 Rouault TA. Biogenesis of iron-sulfur clusters in mammalian cells: new insights and relevance to human disease. *Dis Model Mech* 2012;5:155–64.
3 Stehling O, Lill R. The role of mitochondria in cellular iron-sulfur protein biogenesis: mechanisms, connected processes, and diseases. *Cold Spring Harb Perspect Biol* 2013;5:a011312.
4 Schmucker S, Martelli A, Colin F, Page A, Wattenhofer-Donzé M, Reutenauer L, Puccio H. Mammalian frataxin: an essential function for cellular viability through an interaction with a preformed ISCU/NFS1/ISD11 iron-sulfur assembly complex. *PLoS One* 2011;6:e16199.
5 Webert H, Freibert SA, Gallo A, Heidenreich T, Linne U, Amlacher S, Hurt E, Mühlenhoff U, Banci L, Lill R. Functional reconstitution of mitochondrial Fe/S cluster synthesis on Isu1 reveals the involvement of ferredoxin. *Nat Commun* 2014;5:5013.
6 Sheftel AD, Stehling O, Pierik AJ, Elsässer HP, Mühlenhoff U, Webert H, Hobler A, Hannemann F, Bernhardt R, Lill R. Humans possess two mitochondrial ferredoxins, Fdx1 and Fdx2, with distinct roles in steroidogenesis, heme, and Fe/S cluster biosynthesis. *Proc Natl Acad Sci U S A* 2010;107:11775–80.
7 Shi Y, Ghosh M, Kovtunovych G, Crooks DR, Rouault TA. Both human ferredoxins 1 and 2 and ferredoxin reductase are important for iron-sulfur cluster biogenesis. *Biochim Biophys Acta* 2012;1823:484–92.
8 Ye H, Jeong SY, Ghosh MC, Kovtunovych G, Silvestri L, Ortillo D, Uchida N, Tisdale J, Camaschella C, Rouault TA. Glutaredoxin 5 deficiency causes sideroblastic anemia by specifically impairing heme biosynthesis and depleting cytosolic iron in human erythroblasts. *J Clin Invest* 2010;120:1749–61.
9 Maio N, Ghezzi D, Verrigni D, Rizza T, Bertini E, Martinelli D, Zeviani M, Singh A, Carrozzo R, Rouault TA. Disease-Causing SDHAF1 Mutations Impair Transfer of Fe-S Clusters to SDHB. *Cell Metab* 2016;23:292–302.
10 Maio N, Kim KS, Singh A, Rouault TA. A Single Adaptable Cochaperone-Scaffold Complex Delivers Nascent Iron-Sulfur Clusters to Mammalian Respiratory Chain Complexes I-III. *Cell Metab* 2017;25:945–53.
11 Mochel F, Knight MA, Tong WH, Hernandez D, Ayyad K, Taivassalo T, Andersen PM, Singleton A, Rouault TA, Fischbeck KH, Haller RG. Splice mutation in the iron-sulfur cluster scaffold protein ISCU causes myopathy with exercise intolerance. *Am J Hum Genet* 2008;82:652–60.
12 Olsson A, Lind L, Thornell LE, Holmberg M. Myopathy with lactic acidosis is linked to chromosome 12q23.3-24.11 and caused by an intron mutation in the ISCU gene resulting in a splicing defect. *Hum Mol Genet* 2008;17:1666–72.
13 Nordin A, Larsson E, Thornell LE, Holmberg M. Tissue-specific splicing of ISCU results in a skeletal muscle phenotype in myopathy with lactic acidosis, while complete loss of ISCU results in early embryonic death in mice. *Hum Genet* 2011;129:371–8.
14 Kollberg G, Tulinius M, Melberg A, Darin N, Andersen O, Holmgren D, Oldfors A, Holme E. Clinical manifestation and a new ISCU mutation in iron-sulphur cluster deficiency myopathy. *Brain* 2009;132:2170–9.
15 Sciacco M, Bonilla E. Cytochemistry and immunocytochemistry of mitochondria in tissue sections. *Methods Enzymol* 1996;264:509–21.
16 Bugiani M, Invernizzi F, Alberio S, Briem E, Lamantea E, Carrara F, Moroni I, Farina L, Spada M, Donati MA, Uziel G, Zeviani M. Clinical and molecular findings in children with complex I deficiency. *Biochim Biophys Acta* 2004;1659:136–47.
17 Uziel G, Garavaglia B, Di Donato S. Carnitine stimulation of pyruvate dehydrogenase complex (PDHC) in isolated human skeletal muscle mitochondria. *Muscle Nerve* 1988;11:720–4.
18. Stevens A. Pigments and minerals. In: Bancroft JD, Stevens A, eds. *Theory and practice of histological techniques*. Edinburgh: Churchill Livingstone, 1990:245–67.
19 Legati A, Reyes A, Nasca A, Invernizzi F, Lamantea E, Tiranti V, Garavaglia B, Lamperti C, Ardissone A, Moroni I, Robinson A, Ghezzi D, Zeviani M. New genes and pathomechanisms in mitochondrial disorders unraveled by NGS technologies. *Biochim Biophys Acta* 2016;1857:1326–35.
20 Biederbick A, Stehling O, Rösser R, Niggemeyer B, Nakai Y, Elsässer HP, Lill R. Role of human mitochondrial Nfs1 in cytosolic iron-sulfur protein biogenesis and iron regulation. *Mol Cell Biol* 2006;26:5675–87.
21 Bonneaud N, Ozier-Kalogeropoulos O, Li GY, Labouesse M, Minvielle-Sebastia L, Lacroute F. A family of low and high copy replicative, integrative and single-stranded S. cerevisiae/E. coli shuttle vectors. *Yeast* 1991;7:609–15.
22 Sambrook J, Russel DW. *Molecular cloning: a laboratory manual*. Cold Spring Harbor: Cold Spring Harbor Laboratory Press, 2001.
23 Brachmann CB, Davies A, Cost GJ, Caputo E, Li J, Hieter P, Boeke JD. Designer deletion strains derived from Saccharomyces cerevisiae S288C: a useful set of strains and plasmids for PCR-mediated gene disruption and other applications. *Yeast* 1998;14:115–32.
24 Gietz RD, Schiestl RH. Quick and easy yeast transformation using the LiAc/SS carrier DNA/PEG method. *Nat Protoc* 2007;2:35–7.
25 Ho SN, Hunt HD, Horton RM, Pullen JK, Pease LR. Site-directed mutagenesis by overlap extension using the polymerase chain reaction. *Gene* 1989;77:51–9.
26 Barrientos A, Fontanesi F, Díaz F. Evaluation of the mitochondrial respiratory chain and oxidative phosphorylation system using polarography and spectrophotometric enzyme assays. *Curr Protoc Hum Genet* 2009;Chapter 19:Unit19.3.
27 Soto IC, Fontanesi F, Valledor M, Horn D, Singh R, Barrientos A. Synthesis of cytochrome c oxidase subunit 1 is translationally downregulated in the absence of functional F1F0-ATP synthase. *Biochim Biophys Acta* 2009;1793:1776–86.
28 Patil VA, Fox JL, Gohil VM, Winge DR, Greenberg ML. Loss of cardiolipin leads to perturbation of mitochondrial and cellular iron homeostasis. *J Biol Chem* 2013;288:1696–705.
29 Molik S, Lill R, Mühlenhoff U. Methods for studying iron metabolism in yeast mitochondria. *Methods Cell Biol* 2007;80:261–80.
30 Almeida T, Marques M, Mojzita D, Amorim MA, Silva RD, Almeida B, Rodrigues P, Ludovico P, Hohmann S, Moradas-Ferreira P, Côrte-Real M, Costa V. Isc1p plays a key role in hydrogen peroxide resistance and chronological lifespan through modulation of iron levels and apoptosis. *Mol Biol Cell* 2008;19:865–76.
31 Tamarit J, Irazusta V, Moreno-Cermeño A, Ros J. Colorimetric assay for the quantitation of iron in yeast. *Anal Biochem* 2006;351:149–51.
32 Humphrey W, Dalke A, Schulten K. VMD: visual molecular dynamics. *J Mol Graph* 1996;14:33–8.
33 Guex N, Peitsch MC. SWISS-MODEL and the Swiss-PdbViewer: an environment for comparative protein modeling. *Electrophoresis* 1997;18:2714–23.
34 Schilke B, Voisine C, Beinert H, Craig E. Evidence for a conserved system for iron metabolism in the mitochondria of Saccharomyces cerevisiae. *Proc Natl Acad Sci U S A* 1999;96:10206–11.
35 Garland SA, Hoff K, Vickery LE, Culotta VC. Saccharomyces cerevisiae ISU1 and ISU2: members of a well-conserved gene family for iron-sulfur cluster assembly. *J Mol Biol* 1999;294:897–907.
36 Mühlenhoff U, Gerber J, Richhardt N, Lill R. Components involved in assembly and dislocation of iron-sulfur clusters on the scaffold protein Isu1p. *Embo J* 2003;22:4815–25.
37 Gerber J, Neumann K, Prohl C, Mühlenhoff U, Lill R. The yeast scaffold proteins Isu1p and Isu2p are required inside mitochondria for maturation of cytosolic Fe/S proteins. *Mol Cell Biol* 2004;24:4848–57.
38 Shi R, Proteau A, Villarroya M, Moukadiri I, Zhang L, Trempe JF, Matte A, Armengod ME, Cygler M. Structural basis for Fe-S cluster assembly and tRNA thiolation mediated by IscS protein-protein interactions. *PLoS Biol* 2010;8:e1000354.
39 Cory SA, Van Vranken JG, Brignole EJ, Patra S, Winge DR, Drennan CL, Rutter J, Barondeau DP. Structure of human Fe-S assembly subcomplex reveals unexpected cysteine desulfurase architecture and acyl-ACP-ISD11 interactions. *Proc Natl Acad Sci U S A* 2017;114:E5325–E5334.
40 Gakh O, Ranatunga W. Smith DY4th, Ahlgren EC, Al-Karadaghi S, Thompson JR, Isaya G. Architecture of the Human Mitochondrial Iron-Sulfur Cluster Assembly Machinery. *J. Biol. Chem* 2016;291:21296–321.
41 Stiban J, So M, Kaguni LS. Iron-Sulfur Clusters in Mitochondrial Metabolism: Multifaceted Roles of a Simple Cofactor. *Biochemistry* 2016;81:1066–80.

42 Freibert SA, Goldberg AV, Hacker C, Molik S, Dean P, Williams TA, Nakjang S, Long S, Sendra K, Bill E, Heinz E, Hirt RP, Lucocq JM, Embley TM, Lill R. Evolutionary conservation and in vitro reconstitution of microsporidian iron-sulfur cluster biosynthesis. *Nat Commun* 2017;8:13932.
43 Saha PP, Kumar SK, Srivastava S, Sinha D, Pareek G, D'Silva P. The presence of multiple cellular defects associated with a novel G50E iron-sulfur cluster scaffold protein (ISCU) mutation leads to development of mitochondrial myopathy. *J Biol Chem* 2014;289:10359–77.
44 Sanaker PS, Toompuu M, Hogan VE, He L, Tzoulis C, Chrzanowska-Lightowlers ZM, Taylor RW, Bindoff LA. Differences in RNA processing underlie the tissue specific phenotype of ISCU myopathy. *Biochim Biophys Acta* 2010;1802:539–44.
45 Crooks DR, Jeong SY, Tong WH, Ghosh MC, Olivierre H, Haller RG, Rouault TA. Tissue specificity of a human mitochondrial disease: differentiation-enhanced mis-splicing of the Fe-S scaffold gene ISCU renders patient cells more sensitive to oxidative stress in ISCU myopathy. *J Biol Chem* 2012;287:40119–30.
46 Holmes-Hampton GP, Crooks DR, Haller RG, Guo S, Freier SM, Monia BP, Rouault TA. Use of antisense oligonucleotides to correct the splicing error in ISCU myopathy patient cell lines. *Hum Mol Genet* 2016;25:ddw338–5187.
47 Powers SK, Jackson MJ. Exercise-induced oxidative stress: cellular mechanisms and impact on muscle force production. *Physiol Rev* 2008;88:1243–76.
48 Dailey HA, Finnegan MG, Johnson MK. Human ferrochelatase is an iron-sulfur protein. *Biochemistry* 1994;33:403–7.
49 Sheftel AD, Wilbrecht C, Stehling O, Niggemeyer B, Elsässer HP, Mühlenhoff U, Lill R. The human mitochondrial ISCA1, ISCA2, and IBA57 proteins are required for [4Fe-4S] protein maturation. *Mol Biol Cell* 2012;23:1157–66.
50 Gelling C, Dawes IW, Richhardt N, Lill R, Mühlenhoff U. Mitochondrial Iba57p is required for Fe/S cluster formation on aconitase and activation of radical SAM enzymes. *Mol Cell Biol* 2008;28:1851–61.
51 Nachbauer W, Boesch S, Reindl M, Eigentler A, Hufler K, Poewe W, Löscher W, Wanschitz J. Skeletal muscle involvement in friedreich ataxia and potential effects of recombinant human erythropoietin administration on muscle regeneration and neovascularization. *J Neuropathol Exp Neurol* 2012;71:708–15.

A novel de novo dominant mutation in *ISCU* associated with mitochondrial myopathy

Andrea Legati, Aurelio Reyes, Camilla Ceccatelli Berti, Oliver Stehling, Silvia Marchet, Costanza Lamperti, Alberto Ferrari, Alan J Robinson, Ulrich Mühlenhoff, Roland Lill, Massimo Zeviani, Paola Goffrini and Daniele Ghezzi

J Med Genet published online October 27, 2017